UNIVERSITAT DE BARCELONA

Nanostructured systems for therapeutic treatment of neurodegenerative diseases

Sistemas nanoestructurados en el abordaje terapéutico de enfermedades neurodegenerativas

Elena Sánchez López

UNIVERSITAT DE BARCELONA

FACULTAT DE FARMACIA I CIÈNCIES DE L'ALIMENTACIÓ

Nanostructured systems for therapeutic treatment of neurodegenerative diseases

Sistemas nanoestructurados en el abordaje terapéutico de enfermedades neurodegenerativas

Elena Sánchez López

2017

UNIVERSITAT DE BARCELONA

PROGRAMA DE DOCTORAT

Recerca, Desenvolupament i Control de Medicaments

Nanostructured systems for therapeutic treatment of neurodegenerative diseases

Memòria presentada per Elena Sánchez López per a optar al títol de Doctor per la Universitat de Barcelona

Directoras

Dra. María Luisa García López Dra. Mª Antònia Egea Gras

Doctoranda

Elena Sánchez López

Tutora

Dra. María Luisa García López

ELENA SÁNCHEZ LÓPEZ, 2017

A mis padres,

Por animarme siempre a hacer aquello que me hiciera feliz,

Sin ellos este reto no hubiera sido posible.

Está demostrado que aerodinámicamente es imposible que el abejorro pueda volar, por su tamaño, su peso y la forma de su cuerpo. Solo que él no lo sabe.

INDEX

INDEX

ACKNOWLEDGEMENTS

ACKNOWLEDGEMENTS

This work has been carried out during the last 4 years and I would like to thank everyone who has been part of it during this time because even sometimes it was hard to keep going everyone mentioned here (and some of them who I don't have space for) has contributed somehow to this thesis.

Primeramente, quiero agradecer a la Sección Departamental de Fisicoquímica del Departamento de Farmacia y Tecnología Farmacéutica y Fisicoquímica por acogerme con los brazos abiertos y hacer que este departamento sea como una segunda casa para mí (aun no sé como me habéis aguantado tanto tiempo).

Agradecer a la Dra. Maria Luisa García porque sin su empeño en sacar todo adelante esta tesis no hubiera sido posible. Porque no podía encontrar un mejor referente que me animara a seguir adelante, te admiro profundamente y tienes todo mi cariño y devoción. A las Dras. Maria Antonia Egea y Marta Espina, por estar siempre apoyándome y dándome ánimos, sin vosotras estas publicaciones no hubieran sido posibles. Especialmente a mi co-directora Maria Antonia Egea, por todos sus ánimos y apoyo incondicional especialmente en los primeros pasos de esta tesis. A la Dra. Marta Espina, porque hablar con ella me proporciona la tranquilidad que a mí me falta. A la Dra. Ana Calpena, por su constante optimismo que supone una dosis extra de energía cada vez que charlamos. Agraïr a la Fiden l'experiència treballant a la seva Farmàcia on desde la primera semana tant tu com la Alba em vàreu fer sentir com a casa.

Gracias de todo corazón a todos mis compañeros del laboratorio de nanopartículas con los que he ido creciendo a nivel personal y profesional. A los que me enseñaron hace años, Fany, Veva y Eli, no os imagináis cuanto llegué a aprender de vosotras. A aquellos con los que empecé: Alexander, Guadalupe, Helen y Gladys, por hacer más llevaderos los experimentos de caracterización de las formulaciones que implicaban horas y horas de laboratorio. Sin su alegría todo hubiera sido muy diferente. A los compañeros actuales; Roberto (siento tener toda la poyata llena de material cada vez que llegas), Camille (gracias especialmente por estar conmigo en Londres), Marcelle (aún nos quedan muchas tardes de ir a patinar por Diagonal), Maria, Martha, Ana, Paulina (por tu alegría y tus ánimos constantes a nivel personal y profesional) y Amanda (gracias por estar a mi lado

codo con codo en lo personal y lo profesional aunque tuvieras pesadillas con los experimentos), porque cada uno de ellos es como un granito de arena en este trabajo. A todos los estudiantes que han contribuido con su tiempo en esta investigación, especialmente Sergi, Nuria y Markel, agradeceros vuestras ganas de aprender y vuestro tiempo sin el cual todo hubiera sido muchísimo más complicado.

Gràcies a tot el professorat de la Secció de Fisicoquímica que no forma part del grup de recerca, especialment a les Dres. Busquets, Cajal, Montero i Ortiz per fer que els migdies que mengem a la biblioteca siguin un descans i no una continuació de la feina així com per el seu interés sobre el transcurs d'aquesta tesi. Agraïr també les seves preguntes i interés constant al Dr. Doménech, Dra. Girona, Dr. Estelrich, Dra. Prat i Dra. Muñoz. Gràcies també al personal tècnic, Montse Sánchez, pel seguiment i ajuda de les comandes

del laboratori així com per saludar-me amb un somriure cada dia. Gracias también a Malika por preguntar como va todo cada vez que me ve corriendo por los pasillos.

Segon però no menys important, agrair a membres d'altres departaments de la Facultat, especialment al Dr. Camins, del Departament de Farmacologia, Química Terapèutica i Toxicologia, l'oportunitat de treballar amb el seu model experimental d'Alzheimer així com per els seus ànims i energies permititnt-me col·laborar al seu grup de recerca. Y no podía faltar una de las personas más importantes de esta tesis, Miren Ettcheto, con quien he aprendido todo lo que sé sobre el manejo de los ratones. Porque el trabajo contigo es más llevadero y divertido aunque nos estresemos mutuamente. Agradecer también especialmente a Oriol por ayudarnos con los experimentos de comportamiento así como los días de curva de glucosa e insulina.

À Dra. Amélia Dias da Silva por em Portugal me receber de braços abertos e me fazer sentir em família desde o primeiro momento em que cheguei à bela cidade de Vila Real. Obrigada por toda a sua paciência e por todos os ensinamentos transmitidos sobre culturas celulares. Ao Raul, por todas essas horas dedicadas às experiencias de citometria o meu agradecimento especial e, também por todo o seu apoio, o do Nelson e o do Jorge durante a minha estadia fora do meu país. Muito obrigada a todas as pessoas que conheci naquele belo lugar, em especial à Véronique e à Shwetta. Não consigo imaginar melhores pessoas do que as que tive o prazer de conhecer, conviver e trocar ideias mais ou até menos profundas! Especialmente a minha princesa Veronik, porque Vila Real não será o mesmo

sem você. Queria ainda acrescentar o meu profundo agradecimento à Dra. Eliana Souto pela sua inestimável ajuda durante esta tese.

Very kind acknowledgements to Dr. Francesca Cordeiro for letting me work with your team in London bringing me the opportunity to learn a lot of new things as well as improving my English. I would like to thank each one of the members of her group, Ben, Ljuban and Lies, which make me feel welcome there. I want to give special mention to Nivi for being there listening to me and showing me the immunohistochemistry experiments and to Jon thank you for your support and for giving a special meaning to lab work. Also, I would like to thank all the people I met in London, specially Andrea and Alice, for cheering me up during my first month because it was a really hard time. Finally but not less important, thank you Silvia for becoming my London sister, you have become a friend forever and it would be impossible to imagine London without you.

También agradecer a los Laboratorios Reig Jofré y especialmente al Dr. Enric Jo la oportunidad de realizar unas prácticas en el Centro de excelencia de Liofilización para llevar a cabo los estudios con nanopartículas. Mi más sincero agradecimiento al Dr. Sasha Nikolik por la confianza depositada en mí así como por el trato recibido en este tiempo. Gracias a él y a todos los miembros del departamento, Laia, Gloria, Ana y Rafa, por hacerme sentir parte del grupo así como por compartir vuestros conocimientos conmigo y por la ayuda prestada en estos últimos meses.

Moltes gràcies a tot el personal dels serveis científico-tècnics que han sigut un gran suport per aquesta investigació. Especialment, el David Bellido, per la seva ajuda en la quantificació de fàrmacs mitjançant l'espectometria de masses, a la Esther Miralles i la Eva del Álamo per la seva orientació amb l'HPLC i a Yolanda Muela per la seva ajuda amb la visualització i contatje de les partícules mitjançant microscopia electrónica de transmissió.

A todos aquellos amigos que me habéis apoyado a lo largo de estos 4 años, épocas mejores y peores así como cada uno de los baches que este Doctorado ha conllevado agradeceros de todo corazón que hayáis estado allí. A mis amigas del colegio, Irene, Claudia y Patricia, por estar siempre ahí escuchándome aun cuando a veces no tengan ni idea de lo que hablo pero aguantarme mis interminables dolores de cabeza y apoyarme en las buenas y en las malas.

A Ale, porque sabes que una parte de esta investigación también es tuya; siempre me has animado con tus gestos de admiración a seguir trabajando. A mi mejor amigo, Rubén López, quien siempre está a mi lado tirando de mí cuando yo no puedo (hasta para subir montañas), agradecerte todo lo que haces por mí aun cuando a veces solo haga que protestar así como tu preocupación constante. A Marc, porque pese a que a veces no hemos sido las mejor personas ninguno de los dos, nunca me has dejado de lado y siempre que he necesitado nunca has tenido un no por respuesta. A mis amigas de la carrera, especialmente Cris, Eva y Noemí por compartir esta experiencia conmigo y ayudarme siempre en todo lo que podéis ya sea colaborando con experimentos o escuchándome durante horas y horas. A mis compañeros de los diferentes pisos Silverio, Pau, Oscar y Camille, doy gracias a que la casualidad me llevara a conoceros, especialmente a Silverio porque con tu trabajo constante en tu doctorado me has servido como inspiración y ejemplo a seguir.

Finalmente pero no menos importante, a cada uno de los miembros de mi familia. A mis tíos, Ignacio, Ernesto, David, Montse, Flora, Leandro, Bene e Isabel, por preguntar en cada reunión familiar como va todo y hacer un seguimiento de mi vida sino a través mío a través de mis padres. A mis primos, Laia, Jana, Eric, Rubén y Arantxa, porque ya sea con vuestra alegría o con vuestros conocimientos me inspiráis para dar lo mejor de mí. A mis abuelas, a la yaya Tarsida y sobretodo a la yaya Pepita por su alegría contagiosa y ganas de vivir que pasan de generación en generación. Y mi eterno amor y agradecimientos a mis padres, quienes han estado conmigo a lo largo de todos los baches de mi vida así como en este doctorado, siempre conmigo en mis malos humores y mis decepciones sin quejarse nunca, sois una inspiración y no podría imaginar tener un mejor referente en cuanto a valores personales y profesionales.

Agradecer también a todas aquellas personas que a lo largo de estos años han pasado por mi vida y que no he podido mencionar en esta sección porque esta tesis está formada por granitos de arena que cada persona ha aportado y que me han ayudado a finalizar esta etapa.

Agradecer a la Universidad de Barcelona por la oportunidad de hacer uso de sus instalaciones para esta investigación así como a las universidades de Tras-ós-Montes e

Alto Douro y al University College of London, donde se realizaron las estancias predoctorales. Agradecer también al proyecto MAT (MAT 2014-59134).

Gracias a la Fundación Pere i Pons por permitirme disfrutar de su ayuda para estancias predoctorales. Mi más profundo agradecimiento al Ministerio de Economía y Competitividad por permitirme disfrutar de la beca de formación de personal investigador (BES-2012-056083) así como la ayuda para la realización de estancias predoctorales en Inglaterra.

ABBREVIATION LIST

ABBREVIATION LIST

ACh	Acetylcholine
AChE	Acetylcholinesterase
AChEI	Acetylcholinesterase inhibitors
AD	Alzheimer's disease
Aβ	beta-amyloid
APCs	Antigen presenting cells
APP/PS1	APPswe/PS1De9
BACE-1	β-secretase 1
BBB	Blood brain barrier
BCSFB	blood–CSF barrier
BRB	Blood retinal barrier
CAM	Chorioallantoic membrane
CNS	Central nervous system
COX	Cyclooxygenase
DoE	Design of experiments
DLS	Dynamic light scattering
DXI	Dexibuprofen
EE	Entrapment efficiency
EMA	European drug agency
FDA	Food and drug administration
FTIR	Fourier-transformed infrared spectroscopy
HSA	Human serum albumin
IBU	Ibuprofen
IOP	Intraocular pressure

MDSCs	Myeloid-derived suppressor cells
MEM	Memantine
NFTs	Neurofibrillary tangles
NNDs	Neurodegenerative diseases
NOS	Nitric oxide synthase
NTs	Neurotransmitters
NMDAR	N-methyl-D-aspartate receptors
NPs	Nanoparticles
NSAIDs	Non-steroidal anti-inflammatory drugs
PBCA	Poly(butyl cyanoacrylate)
PEG	Polyethylenglycol
PGs	Prostaglandins
PI	Polydispersity index
PLA	Poly(lactic) acid
PLGA	Poly-(D,L)lactic-co-glycolic acid
PVA	Polyvinyl alcohol
RES	Reticulum endothelial system
RGCs	Retinal ganglion cells
ROS	Reactive oxygen species
RPE	Retinal pigment epithelium
TEM	Transmission electron microscopy
T_g	Glass transition temperature
XRD	X-Ray diffraction
WHO	World health organization
ZP	Zeta potential

1. INTRODUCTION

1. INTRODUCTION

1.1 BACKGROUND

Neurodegenerative diseases (NDDs) show high prevalence with a trend of a progressively growing incidence, especially in aging societies (1). The pathologic term *neurodegeneration* refers to a heterogeneous group of progressively evolving central nervous system (CNS) and brain diseases. It is an "umbrella" term indicating gradual structural neuronal loss with functional consequences due to the abnormal accumulation of misfolded and dysfunctional proteins within the complex nervous system (1).

Among all, Alzheimer's disease (AD) is the most common form of dementia and it is strictly related with the increasing age population. According to recent studies, up to 70% of the dementias occurring in older adults are attributed in whole or in part to AD (2). According to the Alzheimer's Association, 13% of people over 65 years suffer from this disease in developed countries, where it is the fifth leading cause of death in patients at this age. The World Health Organization (WHO) estimates that the overall projected dementia prevalence in global population will quadruple in the next decades, reaching 114 million patients by 2050 (3). In this sense, either the development of effective drugs or increase their availability developing drug delivery systems are a crucial issue. Additionally, patient's compliance of the approved drugs able to delay and decrease the neurodegeneration rates improving the symptomatology is also a matter of relevance.

Several authors reported similarities between brain and eye structures and there is a very close relationship between eye diseases such as glaucoma, and AD (4, 5). So far, it has been shown that the same hallmarks of AD correlate with glaucoma such as the Aβ and neurofibrillary tangles deposition on the retina of glaucomatous patients. Furthermore, the retina possess the blood-retinal-barrier (BRB) which is similar to the brain blood-brain barrier (BBB). Both of them show a highly restricted transport of molecules due to the tight junctions. According to this assumption, drug delivery strategies such as nanoparticles (NPs) useful for the transport across the BBB would also work out across the BRB. Additionally, some surgical procedures or diseases could induce ocular inflammation and an inflammatory process are also involved in AD. Therefore, NSAIDs could be useful for the treatment of both AD and ocular inflammation (6). In the case of

AD, NSAIDs permeation coefficient across the BBB is extremely low and encapsulation of the drug into NPs would be a suitable approach to overcome this issue. In the case of ocular inflammation, the drugs administered topically undergo a high clearance effect due to the tear film and a suitable vehicle containing the drug would help to increase the amount of drug retained, decrease enzyme inactivation and ameliorate the side effects cause by the drug blood circulation.

1.2 BRAIN NEURODEGENERATIVE DISEASES

1.2.1 THE CENTRAL NERVOUS SYSTEM

The central nervous system (CNS) consists on the brain and the spinal cord. The retina, optic nerve, olfactory nerves and olfactory epithelium are nowadays considered to be part of the CNS because they connect directly with the brain tissue without intermediate nerve fibres. This system controls thought processes, guides movement, and registers sensations throughout the body (7).

Brain structures

The brain is divided in three different parts: forebrain, midbrain and hindbrain.

The **forebrain** is constituted by the cortex, thalamus, and hypothalamus (part of the limbic system). The brain cortex is the largest part of the human brain, associated with higher brain functions such as thought and action. At the same time, the cerebral cortex is divided into four *lobes* (Figure 1), each one associated with different tasks:

1 The frontal lobe: associated with reasoning, planning, speech, movement, emotions, and problem solving.
2 The parietal lobe: associated with movement, orientation, recognition, perception of stimuli.
3 The occipital lobe: associated with visual processing.
4 The temporal lobe: associated with perception and recognition of auditory stimuli, memory, and speech.

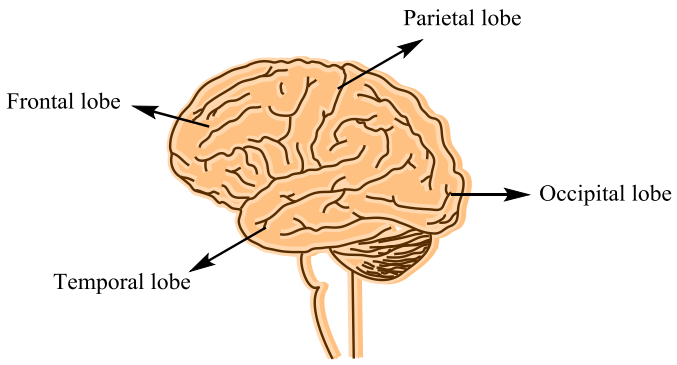

Figure 1. Subdivisions of the brain cortex

The **midbrain** is divided in tectum and tegmentum.

The cerebrum is divided in two hemispheres (left and right) connected by a group of axons called *corpus callosum*. The cerebrum is formed by nerve cells which form the grey surface and underneath white nerve fibres carry signals between this cells and other parts of the body. The **limbic system** contain the thalamus, hypothalamus, amygdala, and hippocampus.

- **Thalamus:** a large mass of grey matter deeply situated in the forebrain. It has both sensory and motor functions. Almost all sensory information enters this structure where neurons send that information to the overlying cortex. Axons from every sensory system (except olfaction) synapse here as the last relay site before the information reaches the cerebral cortex.

- **Hypothalamus:** is involved in functions including homeostasis, emotion, thirst, hunger, circadian rhythms, and control of the autonomic nervous system. In addition, it controls the pituitary.

- **Amygdala:** located in the temporal lobe, is involved in memory, emotion, and fear. It is just beneath the surface of the front, medial part of the temporal lobe where it causes the bulge on the surface called the uncus.

- **Hippocampus:** the portion of the cerebral hemispheres in basal medial part of the temporal lobe. This part of the brain is important for learning and memory and for converting short-term memory to more permanent memory, and for recalling spatial relationships.

The **hindbrain** is made of cerebellum, pons and medulla. The cerebellum also possess two hemispheres and has a highly folded surface. It is associated with regulation of movement, posture and balance. Underneath the limbic system is the brain stem. This structure is responsible for basic vital life functions such as breathing, heartbeat, and blood pressure (7).

Brain barriers

Brain cells can be divided in two groups: neurons or nerve cells, that perform all the communication and processing within the brain, and neuroglia (glial cells, such as

astrocytes, oligodendrocytes, microglia, and ependymal cells) which support and protect the neurons.

There are three main barriers between blood and brain:

The **blood–brain barrier** (BBB) is a dynamic structure which main function is the separation of the circulatory system from the CNS and protect the later from potentially harmful chemicals, toxins and infections (8). It is a highly selective semipermeable membrane barrier created at the level of the cerebral capillary endothelial cells by the formation of structures named as tight junctions around these capillaries, that do not exist in normal circulation. This barrier is a unique regulatory system of brain capillaries that protects the brain environment by preventing most molecules in the blood stream from entering the central nervous system (CNS) and maintains the correct homeostasis (9). The BBB possess a high surface area (20 m^2) and a length of 600 km (10). This is a highly specialized barrier and is the main obstacle for drug transport to the brain; therefore, the development of systems able to cross the BBB is of high relevance. Mainly, the BBB exerts three different functions (11):

- Protects the brain against blood compounds due to the tight junctions restricting the transport of compounds except for oxygen, glucose, amino acids and other essential nutrients. This is the main problem in the use of pharmaceutical compounds to treat CNS disorders due to its inability to cross the BBB and reach the target site.

- Selective transport from the capillary cells to the brain parenquima by a facilitate transport or active diffusion ATP-dependent mechanism.

- Metabolism of specific blood compounds to the CNS.

Drug transport to the brain is highly conditioned by this barrier and, therefore, for the physicochemical characteristics of the compound (12). The main factors affecting drug transport across the BBB are shown in Table 1 being some of the optimum characteristics of compounds able to cross the BBB are the following ones:

- The compounds should be unionised

- The log P value should be around 2

- The molecular weight must be less than 400 Da
- Cumulative numbers of hydrogen bonds should not go beyond 8 or 10

Table 1. Main factors affecting the transport of compounds across the BBB (12).

Factors influencing drug transport across the BBB	
- Concentration gradient	- Affinity for receptors
- Molecular weight	- Cerebral blood flow
- Lipophilicity	- Metabolism by other tissues
- Sequestration by other cells	- Clearance rate
- Flexibility and conformation	- Cellular enzymatic stability
- Molecular charge	- Affinity for efflux proteins

Unfortunately, the same mechanism that protect the brain from intrusive factors also frustrates therapeutic interventions (8). The selective permeability of the BBB mainly favours the transport of small, lipophilic compounds. Therefore, large molecules such as neuropeptides, antibiotics or hydrophilic drugs are not able to cross this barrier (13).

However, in some conditions such as hypoxia or isquemia, the normal functioning of the BBB is compromised increasing the permeability of macromolecules and compounds that would be usually restricted. Considering this, different strategies to overcome the BBB for drug administration had been developed, such as the use of some drugs in order to open the thigh junctions, increase the drug cell internalization with specific proteins or nasal administration of the drug in order to arrive directly to the brain (14).

The **blood–CSF barrier** (BCSFB) lies at the choroid plexuses in the ventricles of the brain where tight junctions are formed between the plexus epithelial cells; the choroid plexus secretes CSF.

The arachnoid barrier: The brain is surrounded by the arachnoid membrane which lies under the duramater. Tight junctions between cells of the inner layer of the arachnoid

form an effective seal. The transport across the arachnoid membrane is not an important route for the entry of solutes into brain.

The BBB hinders most drugs from entering the CNS from the blood stream, leading to the difficulty of delivering drugs to the brain via the circulatory system for the treatment of brain diseases (15). The main mechanisms to cross this barrier are shown in figure 2.

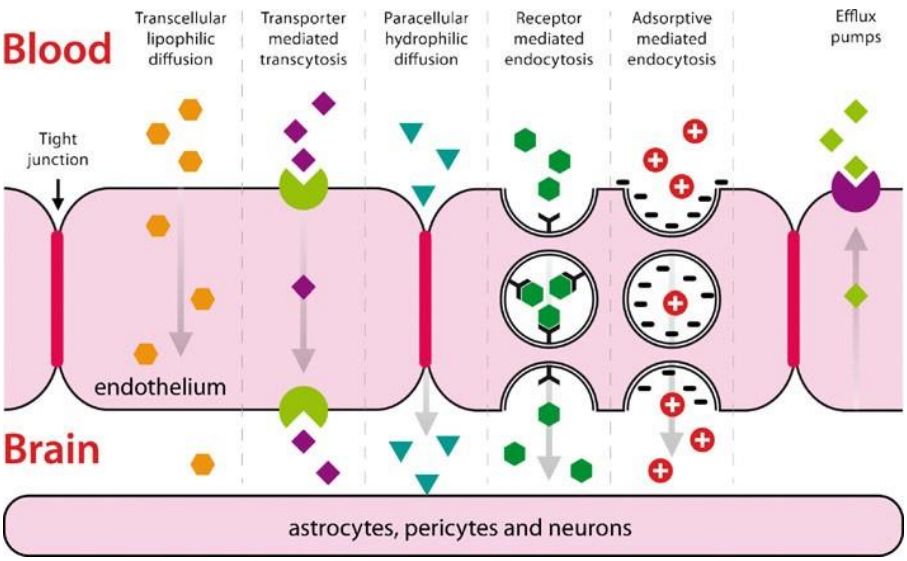

Figure 2. Drug transport across BBB (from (15))

Different strategies have been carried out to facilitate of drug delivery to the brain (Figure 3) such as avoiding the barrier by using direct drug delivery by injection to the brain or cerebrospinal fluids or the nasal route (14). Also intrathecal or intraventricular drug administrations are sometimes used but it's slow and ineffective brain delivery make unavoidable to find alternatives routes for brain delivery. Other strategies are using the transport pathways of the BBB modifying the drug properties or designing ligands that are able to attach to the transport receptors like insulin or transferrin. Modifying the BBB functions constitutes another useful approach; these functions can be modulated using strategies such as opening the tight junctions by hyperosmolar mannitol in patients with brain tumors or inhibiting the efflux pump. However, this strategy should be well-evaluated since it could cause serious adverse effects.

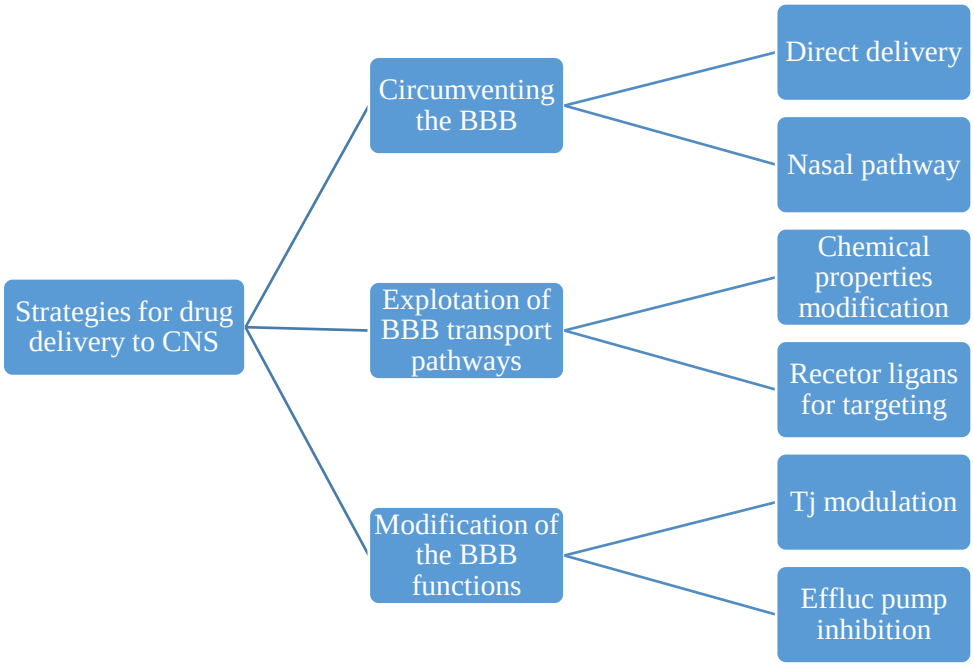

Figure 3. Mechanism for drug delivery to CNS (modified from (14))

1.2.2 ALZHEIMER'S DISEASE

AD is named after a German physician, Alois Alzheimer. In the early 20th century, Alois Alzheimer, a doctor at the state asylum in Frankfurt, studied a patient; Auguste D. She was a 51-year-old woman with symptoms of cognition and language deficits, auditory hallucinations, delusions, paranoia and aggressive behaviour. After the death of the patient 5 years later, Alois Alzheimer, in collaboration with Emil Kraepelin, carried out the post-mortem examination of the brain and observed her brain exhibited arteriosclerotic changes, senile plaques, and neurofibrillary tangles (16). They published the observations and in 1910, Kraepelin coined the term 'Alzheimer's disease' – a term still used to refer to the most common cause of senile dementia (17).

Pathogenic Mechanism of Alzheimer's Disease

Amyloid beta hypothesis

The amyloid cascade hypothesis suggests that the Amyloid beta (Aβ) peptides are the main event in AD pathogenesis thus triggering neurotoxicity and neurodegeneration processes. It is well known that Aβ peptide is derived from proteolysis of APP, an integral transmembrane protein which can be found in neurons and glial cells (3). In humans, APP

is processed into smaller peptide fragments, one of which is Aβ. This cleavage is carried out by α, β, and γ-secretase enzymes (Figure 4).

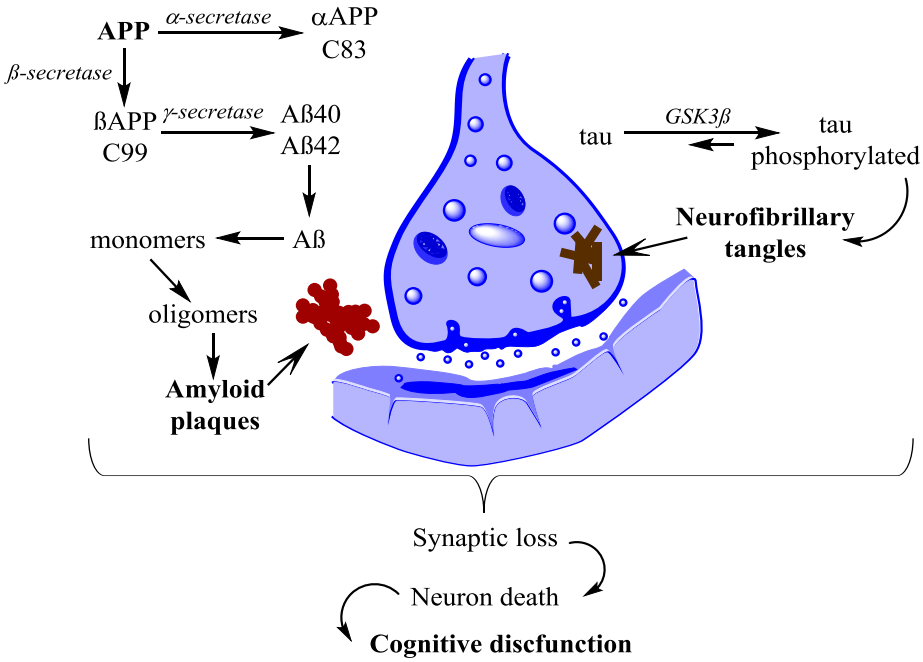

Figure 4. Amyloid β and tau hypothesis of Alzheimer's disease.

Under physiological conditions, APP is catabolized by the α-secretase to produce a soluble sAPPα fragment, which remains in the extracellular space, and a carboxy-terminal 83-amino acid (C_{83}) fragment, which is anchored in the plasma membrane. sAPPα is involved in the regulation of neuronal excitability, improving synaptic plasticity, learning, and memory, and increasing neuronal resistance to oxidative and metabolic stresses (18). As can be observed in Figure 4, in a neuropathological situation such as Alzheimer's disease, APP is first preferentially cleaved by β-secretase 1 (BACE). BACE processes APP producing sAPPβ and a 99-amino acid membrane-bound fraction (C_{99}). Afterwards, γ-secretase processes the C_{99} fragment thus resulting on the generation of $Aβ_{1-40}$ or $Aβ_{1-42}$ peptides, thought to be responsible for senile plaque formation. This senile plaques would be responsible of AD pathology (3). In addition, excessive extracellular Aβ may also presumably lead to increased Tau phosphorylation and the formation of neurofibrillary tangles (NFTs) (3).

Cholinergic hypothesis

Impairment in the cholinergic function is of critical importance in AD especially the brain areas dealing with learning, memory, behaviour and emotional responses that include the neocortex and the hippocampus. Brain atrophy is the most obvious clinical finding in AD in which the levels of acetylcholine (ACh), a neurotransmitter responsible for the conduction of electrical impulses between nerve cells, are decreased due to its rapid hydrolysis by acetylcholinesterase (AChE) enzyme. According to *amyloid hypothesis* AChE produces secondary non-cholinergic functions including promotion in Aβ deposition as senile plaques/neurofibrillary tangles in the brain of effected individuals (19). In this hypothesis, deficiency of a critical brain neurotransmitter (NTs), ACh, was observed either due to decreased production of NT or amplified AChE activity. This decreased level of the NT causes impairment of the cholinergic neurotransmission leading to the loss of intellectual abilities. This hypothesis generally implies that the cholinergic augmentation will improve the cognition in AD (17).

Tau hypothesis

Tau proteins, abundantly in neurons of the CNS, stabilize the microtubules (17). However, Tau protein can be altered and hyperphosphorilated. Eventually, this hyperphosphorylated tau forms neurofibrillary tangles inside nerve cell bodies. The formation of neurofibrillary tangles results in disintegration of microtubules, collapsing the neuron's transport system. This may lead to malfunctions in biochemical communication between neurons and later results in the death of the cells. This is one of the expected reasons for the deposition of the plaques in the brain (17).

Neuroinflammation hypothesis

Neuroinflammation is a blanket term used to describe immune response in neurodegenerative diseases. It involves the activation of glial cells, especially microglia and astrocytes. Under physiological conditions, microglial cells have a phagocytic function. However, in AD, activated microglia secrete a large number of molecules. Such substances, among which are proinflammatory cytokines, prostaglandins, reactive oxygen species (ROS), and nitric oxide synthase (NOS), contribute to a chronic state of perpetual stress. This vicious circle increases Aβ thus leading to more neuroinflammation (Figure 5) causing neuronal death.

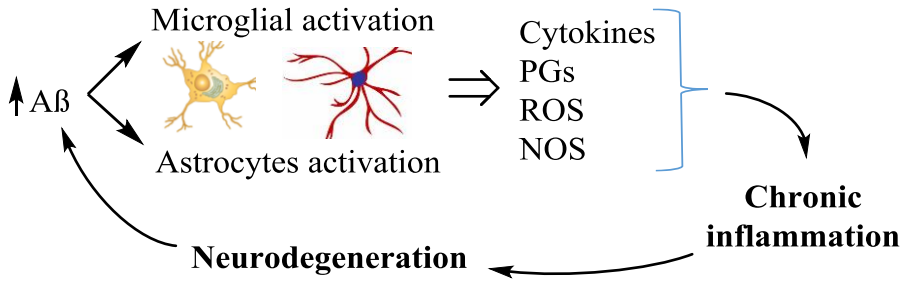

Figure 5. Neuroinflammation hypothesis in AD

Alzheimer's disease treatment

Nowadays, there are only five drugs in the market for AD treatment, which are divided in two different families: acetylcholinesterase inhibitors (AChEI) and N-methyl-D-aspartic acid receptor (NMDAR) antagonists (Figure 6).

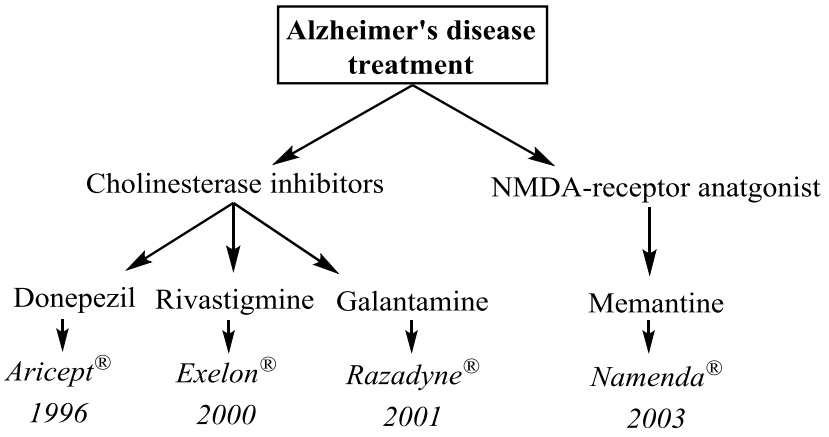

Figure 6. Drugs currently approved for Alzheimer's disease.

Acetylcholinesterase inhibitors

It has been demonstrated that AcChE plays an important role in Aβ-aggregation during the early stages of senile plaque formation. The mechanism of action of these group is based on the increasing of the cholinergic transmission trough the inhibition of the AchE enzyme (hydrolyses acetylcholine) thus enhancing cholinergic transmission in the synaptic cleft and therefore increasing the cognitive ability of patients with AD (19). Tacrine was the first drug of this group used for AD but it's hepatotoxic effect led to it's withdrawal from the market (19). Chemical modifications to decrease Tacrine adverse effects were carried out leading to the currently approved drugs (donepezil, rivastigmine and galantamine).

Although these drugs are safer, they are also less efficient than the former. Therefore, there has been a continuous research related with synthesis of more potent and highly efficacious cholinesterase inhibitors by modifying the main template moieties of available cholinesterase inhibitors for AD management (19).

NMDA receptor antagonists: Memantine

N -methyl- d -aspartate (NMDA) receptor is essential for controlling synaptic plasticity and stimulation (20). However, since overstimulation of the N -methyl- d -aspartate (NMDA) receptor by glutamate is implicated in neurodegenerative disorders, memantine (MEM), an N-Methyl-D-aspartate receptor (NMDAR) moderate antagonist that reduces excitotoxicity by blocking this inotropic receptor has been approved for AD (21). MEM was approved as a therapeutic drug for moderate-to-severe AD by the European drug Agency and by the USA Food and Drug Administration (EMA and FDA, respectively) (22). Clinical evidence supports the efficacy of MEM on overall cognitive, functional, behavioural and global outcomes and it has been shown that MEM slows down clinical progression of AD over time (23).

MEM is a low-to-moderate affinity antagonist of NMDA receptors, therefore, it prevents tonic activation of the N-methyl- D-aspartate (NMDA) subtype of glutamate receptors to avoid calcium-induced excitotoxicity, thus contributing to the pathogenesis of AD (24), (25). Acting as an NMDA receptor antagonist, MEM can block the excitotoxicity evoked by the pathogenesis of AD and other neurodegenerative processes. However, NMDA receptors are not only involved in the excitotoxicity of neurons but are also critical glutamate receptors that mediate the learning and memory functions of the brain (24). NMDA receptor is blocked in a voltage- dependent manner by Mg^{+2}. In a physiological situation, NMDA receptors are activated only following depolarization of the postsynaptic membrane which physiologically follows AMPA receptor stimulation relieving Mg^{+2} blockade. During pathological activation, NMDA receptors are activated by lower concentrations of glutamate but for much longer periods of time. The voltage-dependency of Mg^{+2} is so pronounced that it also leaves the NMDA channel upon moderate depolarisation under pathological conditions (Figure 7). Producing a tonic activation of the receptor by glutamate (25). MEM acts overlapping the site where magnesium binds, therefore, it’s effects is exerted only when an excitation is produced (26).

Additionally, it has been suggested that MEM also acts as inhibitor of a novel translation initiation mechanism, the internal ribosome entry site (IRES), blocking the expression of APP and tau protein and thereby relieving the symptoms of AD (24). This mechanism may be responsible for the reduction of Aβ production and tauopathies in AD patients. (24).

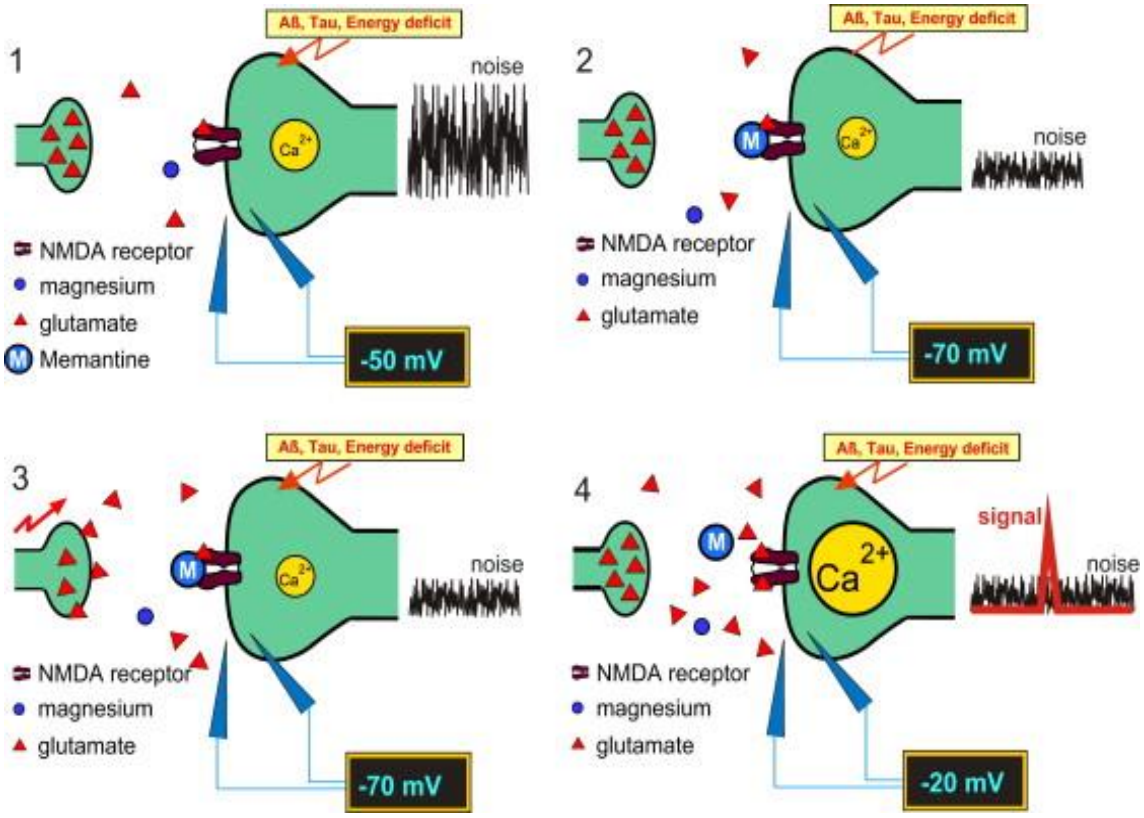

Figure 7. Mechanism of action of memantine in AD (from (27)).

NSAIDs and Dexibuprofen: an alternative strategy for AD

However, it has been shown that none of the drugs approved by the FDA actually represents a cure for AD, since its effects are only palliative and its efficacy decrease with time. Several studies confirm that the long-term treatment with non-steroidal anti-inflammatory drugs (NSAIDs) such as ibuprofen (IBU), reduce the risk of AD, delay disease onset, ameliorate symptomatic severity, and slow cognitive decline (28, 29).

However, an important clinical limitation of ibuprofen, and in general of NSAIDs clinical administration, are the gastrointestinal adverse effects. These adverse effects include gastric irritation, toxicity and gastric ulcers.

These adverse effects can be partially reduced by the use of the active enantiomer, dexibuprofen (DXI), which is twice more potent than the former (30). DXI, the (S)-ibuprofen,

has been assessed on a short-term treatment by Jin and co-workers (28) using animal models of AD achieving successful results.

In clinical studies for inflammation associated with rheumatoid arthritis, this enantiomer demonstrates to cause less side effects than the racemic mixture being a good candidate to prevent AD. However, the typical secondary effects associated with NSAIDs (such as gastric toxicity) still appeared in human trials and it's probability increases with long-term administration (30, 31, 32). In addition, due to the low water solubility of DXI, this drug exhibits many *in vivo* limitations like incomplete release, poor bioavailability, food interactions, and high inter-subject variability (33).

1.3 OCULAR NEURODEGENERATIVE AND INFLAMMATORY DISORDERS

1.3.1 THE EYE

The eye is one of the smallest and most complex organs of the organism. It is a sphere of 2.5 cm of diameter and possesses a volume of 6.5 ml. Each ocular tissue has a different structure that plays a necessary function in enabling visual perception. The eyes constitute less than 0.05% of the total body weight, therefore each ocular tissue is compact and only several cell layers thick. Furthermore, the eye is a part of the central nervous system and possess some barriers in order to keep the systemic circulation separated from ocular tissues (34).

Some authors divide the eye in three different layers. The corneoscleral coat (composed by cornea and sclera), the uvea (composed of choroid, ciliary body and iris) and the neural layer (retina) (35). The eye ends in an optic nerve, which transmits the electronic signals that the retina had transformed. However, inside each layer there are several barriers and structures (Figure 8).

The **cornea** is the first barrier of the eye and is associated with the tear film providing a transparent protective structure. The tear film maintains a proper refractive index as well as corneal smoothness, both indispensable for the vision. Furthermore, corneal transparency is due to different factors such as avascularity, the regularity and smoothness of the covering epithelium and the regular arrangement of the stroma components. In addition, the cornea is mainly protected from autoimmunity by the lack of blood and lymphatic vessels (36). The limited diffusion across this tissue and limited capacity of the lacrimal lake result in a low bioavailability of 1–7% for the majority of the approved drugs and much lower bioavailability for other compounds, including macromolecules (34). Moreover, protective function of the cornea against pathogens involves different components such as keratocytes, corneal fibroblasts, langerhans cells (dendritic cells) and immunoglobulins (IgG and IgA). It has been demonstrated that injury or infections to the cornea triggers an immune reaction which leads to recruitment of polymorphonuclear cells, lymphocytes, and fibroblasts following the release of chemotactic factors such as IL-8 and cationic antimicrobial protein of 37 kD from corneal epithelium (37). According to some authors the cornea is composed of five layers (35, 38) whereas others such as

Kanwar et al. (2011), divide it into 3 layers (epithelial, stromal and endothelial) and others in 6 layers (37, 39). Here, six corneal layers would be explained since it help to a better understanding of this eye structure. The **corneal epithelium** which contains multilayered non keratinized epithelial cells with tight junctions preventing tears to enter in the intercelullar space. In this layer, dendritic cells (antigen presenting cells, APCs) could be founded, which combined with the avascularity are crucial factors for corneal grafting due to the particular immunity. **Bowman's layer or anterior lamina** is made by collagen fibrils type I that maintain corneal shape and form a boundary between the stroma and the epithelium. **Corneal stroma** or **substantia propia**, is made of keratinocytes connected by gap junctions to the neighbor cells as well as fibroblasts, neural tissue and Schwann cells. The stroma account for the 95% of corneal thickness and is comprised mainly by collagen I fibrils which provide mechanical strength to this structure. Limiting with the stroma the **Dua's layer** could be found. This part of the cornea is an acellular membrane which physiological role remains yet to be studied. **Posterior limiting lamina** or **descemet's membrane** is an amorphous membrane situated after Dua's layer. **The corneal endothelium** separates the cornea from the aqueous filled anterior chamber and has limited permability to ion flux being thus necessary to maintain osmotic pressure (35, 38).

The border between the cornea and the sclera is the **limbus** (35). It is highly vascularized and possess a reservoir of pluripotent stem cells (39). It finishes in the **sclera**, an opaque avascular tissue of viscoelastic nature composed by fibroblasts, which segregates a collagen matrix. The sclera has three layers: lamina fusca, stroma and episclera (35). This opaque tissue also possess a barrier to diffusion of molecule being the permeability descending as molecular weight of the molecule increases (34).

The **conjunctiva** is a thin highly vascularized mucosing secreting tissue and is reflected into the eye as a thin transparent tissue on the sclera and extends up to the limbus. It provides elasticity and facilitates motion of the eye balls and lids (39).

The **uveal tract** it's an eye structure consisting on the iris, ciliary body and choroid. The **iris** is surrounded by the aqueous humor and separates the anterior and posterior chambers. It has a rich blood supply and extensive anastomoses with veins draining to the ciliary body. Iris capillaries are less permeable to a variety of solutes than normal somatic vessels being essential for the blood ocular barrier. It is comprised of three layers (endothelium, stroma and epithelium) and has an aperture in front of the lens called the

pupil, which helps to regulate the amount of light passing through the retina. The **ciliary body** secretes the aqueous humor and the blood supply is received from the ciliary arteries. It is located anterior to the iris and involved in three different functions: secretion of aqueous humor, adjustment to lens focus and drainage of aqueous humor from the eye. The **choroid** is a vascular pigmented connective tissue focused on nourishing retinal layers (35, 39).

The **crystalline lens** are transparent, avascular and biconvex covered in the anterior part by aqueous humor and of vitreous humor on the posterior part. They control metabolic subtracts exchange and waste as well as light entry into the eye and its refraction. While the lens blocks the most ultraviolet light in the wavelength range from 300 to 400 nm, the cornea blocks shorter wavelengths. The lens consist on four different parts: the capsule, epithelium, cortex and nucleus. The capsule is an strong elastic membrane which encapsulate the lens and provides structural support. Capsule membrane utility is to avoid direct contact between the lens and the surrounding ocular tissues and fluids and provide a barrier for microbial attack as well as be a reservoir for growth factors, Growth factors release made differentiation of lens cells. Below the capsule, the epithelium can be found. The epithelium is a monolayer only present on the anterior part of the lens. Next to the lens epithelium is present the cortex which contains a high amount of water. It also contains tightly packed fibers. The core of the lens is formed by deposition of old cells and is the denser part of the cells.

The **retina** is the inner layer of the eye and converts images to neural impulses transmitted to the brain trough the optic nerve. It constitutes itself a barrier to molecules being the diffusion of a compound with a molecular weight of larger than 76 kDa is severely limited (34). The retina is organized into layers with the photoreceptors in the outermost layer, interneurons in the middle, and the retinal ganglion cells in the innermost layer (34). The retinal pigment epithelium (RPE) is formed by cells that maintain retina as well as photoreceptor's cells health. The RPE is responsible for forming the blood-retina-barrier (BRB), which sequesters retinal antigens and keeps the systemic immune system from entering the retinal space (36). In this layer is where the visual cells (cons and rods) are located. The cons are the photoreceptors and present a single cell layer situated on the outer retinal part. It continuous trough bipolar cells (connective neurons) until retinal ganglion cells (RGCs) originating the ganglion cells layer continuing as a long axon to the optic nerve (38). The **BRB** separates the neurosensory retina from the systemic

circulation and is subdivided into the inner and outer barriers (Figure 8). The inner blood–retinal barrier possesses the retinal vasculature, which supplies the inner retina, and is composed of the tight junctions between the endothelium of the retinal vasculature. The outer blood–retinal barrier is comprised of RPE, which lies between the photoreceptors and the choriocapillaries (34).

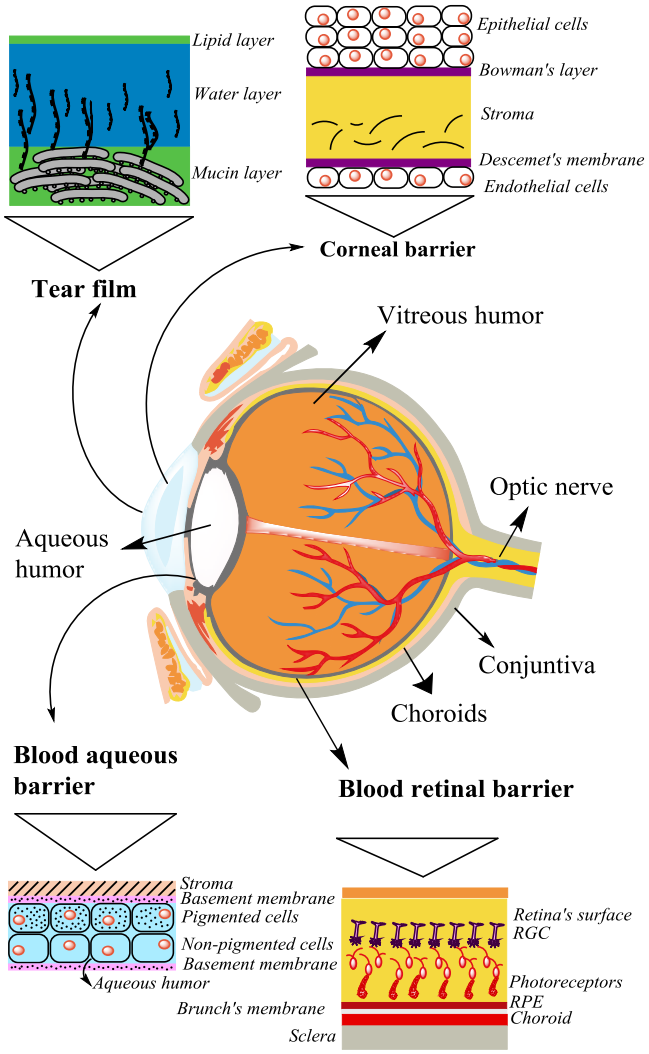

Figure 8. Eye barriers (from (40))

The **optic nerve** marks the beginning of the short canal through which leaves the eyeball to be enveloped by the meninges. It is a fiber-tract within the central nervous system which carries the vascular system for the inner retinal layers, the central retinal artery and vein (38).

The eye is also divided in two different chambers: anterior chamber (behind the cornea and in front of the iris and lens), which contains the aqueous humor, posterior chamber

(behind the iris and in front of the lens) and vitreous humor (between the lens and the retina). The **aqueous humor** is continuously formed from the plasma by the epithelial cells of the ciliary body being transparent and slightly alkaline. It contains less protein, albumin and γ-globulins than plasma but it has glucose, lactic acid, ascorbic acid and immunoglobulin G. This chamber provides oxygen to the cornea and lens and removes it's waste products (39). The posterior chamber is filled with a transparent gel-like fluid which covers the space between lens and retina called **vitreous humor**. It is composed mainly of water and the minority part of the gel is formed by hyaluronic acid, collagen fibronectin, fibrillin and opticin. Although the vitreous is essentially acellular, there are some hyalocytes which possess the immunophenotipic characteristics of bone marrow-derived macrophages (35).

1.3.2 OCULAR NEURODEGENERATIVE DISEASES: GLAUCOMA

Glaucoma is a multi-factorial neurodegenerative disease and is the second leading cause of blindness worldwide (41). The outcome of glaucoma is neuroretinal damage which, when mediated by the amino acid glutamate, is accompanied by a prominent inflammatory response. Remarkably, however, the retinal response to glutamate damage appears to be one of enhanced neuroprotection mediated by recruitment of myeloid-derived suppressor cells (MDSCs) (42). Although the exact mechanism of glaucoma pathology is debatable the disease induces damage to optic nerve axons thus resulting in progressive loss of retinal ganglion cells (RGCs) (43, 44). Elevated intraocular pressure presently remains the only clinically modifiable risk factor for glaucoma and, therefore, traditional therapeutic strategies seek to reduce elevated intraocular pressure (IOP). However, it is recognized that IOP modulation alone is not enough for the treatment of glaucoma due to a growing recognition that patients with well-controlled IOP can continue to suffer vision loss (45). This observation, coupled with results suggesting that some existing IOP modulating agents such as bromoimide can elicit neuroprotective effects in RGCs over and above their IOP modulatory effects, (46) reason the use of neuroprotective therapies for the treatment of glaucoma (47). In addition, an increasing number of studies have reported similarities between the mechanisms of cell death in glaucoma and AD because they both can be characterized by dysregulation of neurotrophic growth factors, caspase activation, and glutamate excitotoxicity (3).

Moreover, evidence is emerging to suggest that both conditions can be managed via NMDAR antagonists such as MEM (48).

Memantine in glaucoma treatment

MEM is a neuroprotective agent approved for the treatment of AD that acts by inhibiting NMDA induced glutamate excitotoxicity that may also play a role in RGC death in glaucoma (45). Although preclinical data previously suggested a potential clinical benefit of orally administered MEM for the treatment of glaucoma (49), the efficacy of this administration route is limited as recently demonstrated in failing to meet its primary endpoint in a phase III clinical trial (50,51).

MEM acts on the excessive NMDA receptor activity without disrupting normal activity through its action with the intracellular Mg^{2+} blocking site as a low-affinity, uncompetitive open-channel blocker with a relatively rapid off-rate (52). Recent assays developed with monkeys fed with MEM showed no IOP improvement caused by the drug (53). However, MEM demonstrated to increase RGCs survival (54).

Since 2001, MEM has undergone several preclinical and clinical trial for glaucoma (55, 56). The majority of the preclinical studies showed drug efficacy after glaucoma induction in different animal models creating robust evidence of the excitotoxicity involvement on glaucoma disease (57),(58),(45). However, human clinical trials with the drug failed and to date, several hypotheses have been proposed to explain the reasons for the MEM failure in clinical trials. One of the most accepted is that the endpoints of the study were not clear enough and it could be possible that with better parameters definition the drug would achieved statistical significance (50).

1.3.3 OCULAR INFLAMMATORY DISEASES

Inflammation is the manifestation of vascular and cellular response of the host tissue to an injury. Injury to the tissue may be inflicted by physical or chemical agents, invasion of pathogens, ischemia, and excessive (hypersensitivity) or inappropriate (autoimmunity) operation of immune mechanisms. Inflammation facilitates the immune response and the subsequent removal of antigenic material and damaged tissue. As soon as the injury is recognized, the mechanisms to localize and clear foreign substances and damaged tissues are initiated. Further the response is amplified by activation of inflammatory cells and

production of chemical mediators like acidic lipids e.g. prostaglandins (PGs), thromboxane's, leukotrienes; vasoactive amines and cytokines. Acidic lipids are produced in the arachidonic cascade. Arachidonic acid is released from the phospholipid component of the cell membrane by the action of phospholipase A2. The arachidonic acid produced enters either the cyclooxygenase or lipoxygenase pathway. Activation of cyclooxygenase pathway results in formation of PGs and thromboxanes, while the lipoxygenase pathway yields eicosanoids (hydroxyeicosatetraenoic acid and leukotrienes). Ocular actions of PGs are manifested in three ways (59).

Firstly, they act the IOP. PGE1 and E2 increase the IOP by local vasodilation and increased permeability of blood aqueous barrier. On the other hand PGF2 lowers the IOP which is attributed to increased uveoscleral outflow. Secondly, they act on iris smooth muscle to cause miosis. Thirdly, PGs cause vasodilation and increase the vascular permeability resulting in increased aqueous humour protein concentration. Corticosteroids, the potent anti-inflammatory agents elicit their action by blocking the enzyme phospholipase A2 to inhibit arachidonic acid production, thereby preventing the synthesis of all the PGs, thromboxanes and eicosanoids. On the other hand non-steroidal anti-inflammatory drugs (NSAIDs) exert their anti-inflammatory action by inhibiting the enzymes cyclooxygenase (COX 1 and COX2) (59).

Dexibuprofen in corneal inflammation

Inflammation is a non-specific response of the body against injuries from the external environment, acting as a defense mechanism to isolate and destroy the triggering agent, as well as to repair the damaged tissues. Ocular inflammation is one of the most prevalent diseases in ophthalmology. It can affect any part of the eye or the surrounding tissues. Corticosteroids are commonly used as anti-inflammatory drugs in the treatment of ocular inflammation but they induce serious adverse effects when administered continuously (60). The main alternatives to corticosteroids in the treatment of inflammation are NSAIDs (61). In the field of ophthalmology, Ibuprofen (IBU) has been receiving particular attention in recent years due to its anti-inflammatory activity although it possesses an elevated number of adverse effects that limit its use (30).

Drugs administered onto the ocular mucosa are known to suffer absorption via conjunctiva and nasolacrimal duct, easily reaching the systemic circulation (62, 63). Drugs, such as ibuprofen (IBU), may induce adverse side effects that can be minimized

by the use of the active enantiomer – dexibuprofen (DXI), which is twice more potent and has less side effects than IBU (31). Gastric and epigastric pain, nausea and vomiting have been the most frequent side effects reported in randomized clinical trials in patients treated with DXI. Effects of this drug in the central nervous system (CNS) were less common than the use of racemic IBU (32). The racemic mixture was also responsible for a higher gastric toxicity than the S(+) isomer (31). Moreover, the safety, tolerability and equivalent efficacy between DXI and the double dose of IBU was confirmed by comparing the oral uptake of both drugs for osteoarthritis treatment in a clinical study (32, 64).

1.3.4 THE EYE AS A WINDOW TO THE BRAIN: GLAUCOMA AND AD

Several well-defined neurodegenerative conditions that affect the brain and spinal cord have manifestations in the eye, and ocular symptoms often precede conventional diagnosis of such CNS disorders. Furthermore, various eye-specific pathologies share characteristics of other CNS pathologies (65). Beyond the fact that major brain diseases manifest within the eye, several diseases that are unique to the eye display characteristics of neurodegenerative disorders. Such overlap is probably explained by the similarities between the eye and the brain in terms of tissue structure and interactions with the immune system (65).

The eye is also surrounded by an array of blood–ocular barriers that share structures, characteristics and mechanisms with the CNS gating system. For example, the inner BRB is composed of non-fenestrated endothelial cells that are firmly connected by tight junctions and surrounded by astroglial and Müller cell endfeets, and thus strongly resembles the BBB. The anterior chamber of the eye is filled with aqueous humor, a fluid enriched with anti-inflammatory and immunoregulatory mediators that is reminiscent of the cerebrospinal fluid circulating around brain and spinal cord parenchyma’s (65). The light that enters the eye is captured by photo-receptor cells in the outermost layer of the retina, which initiates a cascade of neuronal signals that eventually reach the RGCs, the axons of which form the optic nerve. These axons extend to the lateral geniculate nucleus in the thalamus and the superior colliculus in the midbrain, from which information is further relayed to the higher visual processing centers that enable us to perceive images.

Despite their diverse morphology (65). RGCs display the typical properties of CNS neurons, and generally comprise a cell body, dendrites and an axon.

The axons of many RGCs are collected to form the optic nerve. Like insult to other CNS axons, insult to the optic nerve results in retrograde and anterograde degeneration of the severed axons, scar formation, myelin destruction, and the creation of a neurotoxic environment that involves oxidative stress, deprivation of neurotrophic factors, excitotoxic levels of NTs, and abnormal aggregation of proteins and debris. Such a hostile milieu often results in death of neighboring neurons that were spared in the initial damage a phenomenon that is termed secondary degeneration (65).

These two organs share functional building blocks in the form of neurons and axons, as well as common degenerative and regenerative processes, and unique mechanisms of crosstalk with the immune system (65). Pathological accumulation of amyloid-β (Aβ) and phosphorylated tau (p-tau)—the classic manifestations of AD in the brain—has also been reported in the eyes of patients with AD and in the eyes of transgenic mouse models of this disease of the CNS. Aβ and p-tau, the major pathological features of AD, have also been detected in patients with glaucoma, and are thought to have a role in neuronal death and progression of vision loss in this disease (65). It has also been found epidemiological support for RGC atrophy in AD. Compared with healthy individuals, patients with AD displayed narrowing of retinal veins, reduced retinal blood flow and RGC numbers (65).

In addition, nowadays the understanding of AD has been expanded to include extracerebral manifestations such as ocular processes. Some studies investigating retinal changes in AD animal models have shown that AD double-transgenic mice possess altered processing of APP and accumulation of Aβ peptides in neurons of retinal ganglion cell layer (RGCL). Moreover, apoptotic cells were also detected in the RGCL. This processes are correlated correlated with local inflammation, retinal ganglion cell degeneration, and functional deficit (66). Intraocular pressure is slightly elevated but no significant differences have been found yet (67). Therefore, mice models of AD show evidence of molecular, functional and morphological degenerative changes in the retina. Thus, the pathophysiological changes of retinas in AD patients are possibly resembled by AD transgenic models thus showing the strong connection between the two diseases (68).

Given the various associations and similarities between the eye and the brain, to test whether therapies that are beneficial in brain disorders could alleviate diseases of the eye (and viceversa) is tempting. Indeed, approaches that reduce Aβ load and improve cognitive performance in models of AD and, to some extent, patients, have proved successful in decreasing visual deficits and reducing RGC loss in mouse models (65).

1.4 POLYMERIC NANOPARTICLES AS DRUG DELIVERY SYSTEMS

Drug delivery systems represent an interesting approach in order to increase the therapeutic efficacy of the drugs. In addition, these systems would provide an advantage over traditional strategies for long-term treatments since the therapeutic posology of the patients would be more spaciated due to the prolonged drug released achieved. Since the drug would be released slowly and focussed on the target site, drug delivery systems would decrease drug side effects. These systems could improve the transport across the BBB and BRB as well as increase the mucoadhesion on the topically administered drugs. There are several types of drug delivery systems such as liposomes, lipid nanoparticles (NPs) or polymeric NPs.

Among all, biodegradable NPs constitute one of the most studied drug delivery systems. These colloidal systems, with a particles size ranged between 10 and 1000 nm, are able to increase drug bioavailability and reducing its toxicity. In these group, polymeric NPs are nanostructured systems formed by natural or synthetic polymer chains with a matrix or vesicular structure (Figure 9). Nanosphere systems composed of a matrix structure where the drug can be adsorbed, entrapped or solved into the polymeric matrix. Nanocapsules are vesicular systems made of a polymeric membrane which contains an inner liquid core. The drug can be either solved into the core of the nanocapsule or adsorbed on the surface.

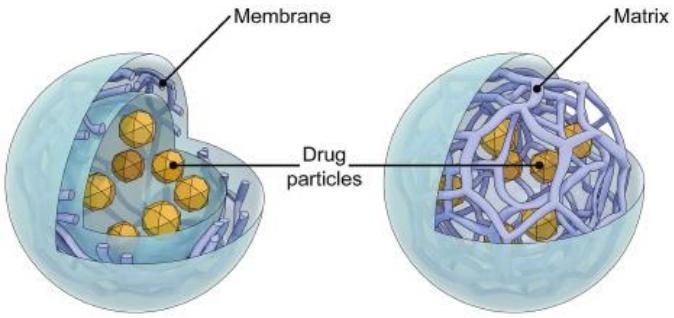

Figure 9. Polymeric biodegradable nanoparticles a) nanocapsules vs b) nanospheres, figure from (69).

Among these two types of polymeric biodegradable NPs, nanospheres have been considered as an important drug release system allowing a controlled drug release and increasing it's bioavailability on the target site. Among all the polymers, nanosystems formed by a polymeric matrix of poly-(D,L)-lactic-co-glycolic acid (PLGA) are approved by the European and American drug agencies (EMA and FDA, respectively) and have been widely used as a biomaterial in medical prostheses and surgical sutures (70). More recently, PLGA has been used in the development of colloidal carriers for controlled release of drugs, due to its biocompatibility, biodegradability and non-toxicity (71). Furthermore, compared to natural polymers, these synthetic polymers demonstrate higher reproducibility, are easily formulated and allow the control and prediction of the degradation kinetics (72). These polymers possess several advantages such as biocompatibility, biodegradability and non-toxicity, which constitutes an ideal carrier for long-term administration treatments. Additionally, polyethylene glycol (PEG) chains surrounded the NPs in order to increase it's mucoadhesivity and transport across the BBB (73). In this way, biodegradable NPs could constitute a suitable alternative as drug delivery systems for AD (2).

On the other hand, for ocular drug delivery purposes, polymeric NPs would protect the drug from inactivation by the enzymes present in the tear film or corneal epithelium, to facilitate its transcorneal penetration prolonging its stay in the precorneal area, and to avoid undesired adverse effects, polymeric NPs have been proposed (74). Among other, strategies, PEG-coating on PLGA NPs offer several advantages. These are firstly attributed to the enhanced contact time of the particles with the corneal surface by the interaction with the mucin. NPs interact with the mucus layer of the tear film either by electrostatic, hydrophobic and hydrogen bonding, or by their physical retention in the mucin network (75). Griffiths et al. (75) demonstrated that such retention in the mucin network is dependent on the hydrophobic surface of the particles, which could be overcome by coating them with PEG. On the other hand, the hydrophobic entrapment could be minimized as long as the nanoparticles were adequately surfaced with such hydrophilic PEG layers and depicted negative electrical charge (75). Therefore, the accumulation of the NPs in the conjunctival sac, as well as, the ability of the particles to penetrate in the first layers of the corneal epithelium contribute to enhance drugs' bioavailability (76). In addition, PEGylation contributes to maintain the particles in circulation for a longer time, thus avoiding their recognition by the reticuloendothelial

system (RES) (77).

Pharmacological agents delivery is compromised by the eye structures, which act a barrier such as the corneal epithelium and endothelium, the sclerocorneal parenchyma, the inner and outer blood–retinal barriers, and the retinal inner limiting membrane. Lipophilic drugs penetrate trough transcellular route whereas hydrophilic drugs pass through the paracellular route. The endothelium is a membrane one cell layer with large intracellular junctions that offers no permeation resistance toward hydrophilic drugs but may offer some resistance toward lipophilic drugs. Conjunctiva is slightly more permeable than the sclera and the sclera is approximately more permeable than the cornea. The choroidal vasculature contributes to drug clearance from the eye and, thus, constitutes another barrier to overcome during drug permeation from the eye surface to the retina and vitreous. Although systematically administered drugs can reach the choroid membrane, drug delivery into the retina or the vitreous body is difficult to achieve through conventional methods because of the presence of the blood aqueous barrier and the inner and outer BRB in those structures. Direct intravitreal injection of drugs into the vitreous cavity is employed to achieve higher drug concentrations in the vitreous and the retina. However, repeated injections are required to maintain drug concentrations at an effective therapeutic level over a certain period of time because the half-life of drugs in the vitreous is relatively short (78).

Ophthalmic delivery of normal molecules is considered to be difficult due to different factors:

a) the large size of some macromolecules limits diffusion and renders topical therapies highly inefficient
b) eye tissue barriers, such as the BRB, limit the penetration of applied pharmacotherapies to the target site
c) The small size of the eye and presence of many distinct tissues makes targeting necessary.

In general, only ~1–5% of an applied drug is absorbed into the eye, and most of that, typically, is absorbed into the anterior segment. Adequate therapy with eyedrops requires either the provision of a sufficient peak magnitude so that the effect extend for a useful period of time or more frequent applications of a lower dose. An optimal formulation of

topical ocular agents is very important from the point of view of comfort, safety, and ocular bioavailability, requiring optimization of pH, osmolality, solubility, stability, and, for most multidose formulations, preservative effectiveness. For this reason, ophthalmic drug delivery technology must evolve alongside the significant market growth of biopharmaceutical therapies (76, 77).

1.4.1 NANOPARTICLE PREPARATION METHODS

Numerous methods available for producing nanoparticles have been developed on the last years. Depending on the physicochemical characteristics of a drug, it is now possible to choose the best method of preparation and the best polymer to achieve an efficient entrapment of the drug (81). NPs preparation methods can be classified into two main categories according to whether the formulation requires a polymerization reaction or is achieved directly from a macromolecule or preformed polymer. In this case, this work will focus on preparation methods with preformed polymers (Figure 10).

Emulsification/solvent evaporation

This preparation method consists of a first step where the polymer solution previously solved in an organic solvent is emulsified using high-energy homogenization into an aqueous phase and a second step based the solvent evaporation and induction of the polymer precipitation as nanospheres. NPs size can be modified adjusting the stirring rate, the dispersing agent, the temperature and the viscosity and type of organic solvent. The main disadvantage of this method is that it can only be applied to liposoluble drugs (81).

Solvent displacement and interfacial deposition

These methods are based on spontaneous emulsification of the organic internal phase containing the dissolved polymer into the aqueous external phase (81).

- ***Solvent displacement*** involves the precipitation of a preformed polymer from an organic solution and the diffusion of the organic solvent in the aqueous medium in the presence or absence of a surfactant. It can form nanospheres or nanocapsules. Polymer deposition on the interface between the water and the organic solvent, caused by fast diffusion of the solvent, leads to the instantaneous formation of a colloidal suspension (81).

- ***Interfacial deposition:*** in this method, the polymer deposits on the interface between the disperse oil droplets and the aqueous phase, forming nanocapsules. An aqueous solution is used as the dispersing medium. This mixture is injected slowly into a stirred aqueous medium, resulting in the deposition of the polymer in the form of nanoparticles (81).

Emulsification/solvent diffusion

This method was proposed in the literature based on the use of organic solvents, and then it was adapted to the following salting-out procedure. The encapsulating polymer is dissolved in a partially water-soluble solvent such as propylene carbonate and saturated with water to ensure the initial thermodynamic equilibrium of both liquids. In fact, to produce the precipitation of the polymer and the consequent formation of nanoparticles, it is necessary to promote the diffusion of the solvent of the dispersed phase by dilution with an excess of water when the organic solvent is partly miscible with water or with another organic solvent in the opposite case. Subsequently, the polymer-water saturated solvent phase is emulsified in an aqueous solution containing stabilizer, leading to solvent diffusion to the external phase and the formation of nanospheres or nanocapsules, according to the oil-to-polymer ratio. Finally, the solvent is removed by evaporation according to its boiling point (81).

Salting-out

This method is based on the separation of a water-miscible solvent from aqueous solution via a salting-out effect. The salting-out procedure can be considered as a modification of the emulsification/solvent diffusion. Polymer and drug are initially dissolved in a solvent such as acetone, which is subsequently emulsified into an aqueous gel containing the salting-out agent and a colloid. This oil/water emulsion is diluted with a sufficient volume of water or aqueous solution to enhance the diffusion of acetone into the aqueous phase, thus inducing the formation of nanospheres. Both the solvent and the salting-out agent are then eliminated by cross-flow filtration. Salting out does not require an increase of temperature and, therefore, may be useful when heat-sensitive substances have to be processed. The greatest disadvantages are exclusive application to lipophilic drugs and the extensive nanoparticle washing steps (81).

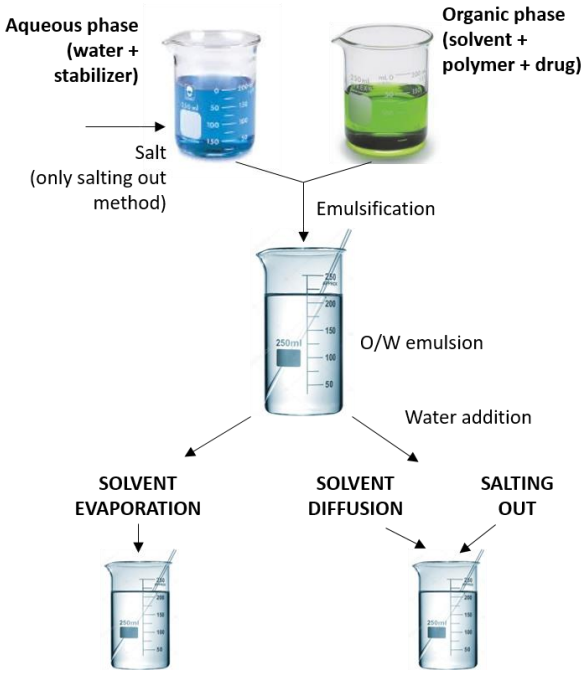

Figure 10. Preparation methods of polymeric nanoparticles (Modified from (82))

1.4.2 NANOPARTICLES FOR BRAIN DRUG DELIVERY

An ideal nanocarrier for brain drug delivery is one which delivers the drug efficiently cross the BBB with selective targeting and protects the drug from enzymatic degradation. Furthermore, a good carrier should achieve long circulation time, prevent efflux transport, possess low immunogenicity and good biocompatibility and bioavailability (8). In this sense, polymeric NPs demonstrated to be a useful vehicle to enhance drug delivery into the brain by increasing the transport across the BBB (83). However, it is still unclear the mechanism of transport of these NPs across the barrier and it is hypothesized that some of the following possibilities can be involved (8):

- An increased retention of the nanoparticles in the brain blood capillaries combined with an adsorption to the capillary walls could create a higher concentration gradient that would enhance the transport of drug across the endothelial cell layer and as a result its delivery to the brain.
- A general surfactant effect characterized by the solubilization of endothelial cell membrane lipids that would lead to membrane fluidisation and enhanced drug permeability through the BBB.

- The nanoparticles could lead to an opening of the tight junctions between the endothelial cells. The drug could then permeate through the tight junctions either in free form or together with the nanoparticles in bound form.
- The nanoparticles may be endocytosed by the endothelial cells followed by the release of the drug within these cells and its delivery to the brain.
- The nanoparticles with bound drugs could be trans- cytosed through the endothelial cell layer.
- The Polysorbate-80 used as the coating agent could inhibit the efflux system, especially P-glycoprotein (Pgp)

The uptake of nanoparticles is dependent on their physicochemical characteristics such as size and surface charge. Mean nanoparticles size is determinant due to the fact that is particles smaller than 200 nm are internalized by clarithrin mediated endocytosis whereas larger particles undergo caveolae-mediated transport. Recent investigations report that small nanoparticles tend to accumulate in brain tissue in a higher concentration than nanoparticles larger than 200 nm (8). Surface charge of the nanoparticles is also a crucial issue since cationic nanoparticles undergo adsorptive-mediated endocytosis favoring their transport but they are rapidly opsonized and cleared from the circulation by the RES (8). However, it has been shown that NPs with high positive ZP lead to BBB toxicity. Therefore, due to safety reasons, the majority of the formulations for brain delivery possess negative surface charge (84).

As can be observed in Table 2, for the purpose of developing polymeric nanoparticles three types of materials are being predominantly used: poly(alky cyanoacrylates) such as poly(butyl cyanoacrylate) (PBCA) which is the fastest degrading material, poly(lactic acid) (PLA) or its copolymer poly(lactide-co-glycolide) (PLGA), and human serum albumin (HSA) (85). In addition, PEGylation leads to the so-called stealth effect that is characterized by a significant reduction in liver uptake and increase in blood circulation time and distribution into other organs and tissues (85).

1.4.3 NANOPARTICLES FOR OCULAR DRUG DELIVERY

A colloidal carrier system may be applied in liquid form like eye-drop solutions or other administration form such as implants or intravitreal administration. In the case of eye-drops, upon their interaction with the glycoproteins of the cornea and conjunctiva can form a precorneal depot resulting in prolonged release of the drug. In addition, nanotechnology-based drug delivery is also very efficient in crossing membrane barriers, such as the BRB in the eye. Drug delivery based on nanotechnology can function as excellent systems for chronic ocular diseases requiring frequent drug administration or for drugs which are unable to be retained on the eye due to their physicochemical characteristics (63). In these sense, several authors develop different types of polymeric nanoparticles using biodegradable polymers such as PLGA, PLGA-PEG, Eudragit or gelatin in order to encapsulate a wide variety of drugs either hydrophilic or hydrophobic (Table 3).

Table 2. Polymeric nanoparticles for brain drug delivery (modified from (85))

Polymer and surfactant	Drug	Preparation method	Average size (nm)	Zeta potential (mV)	Entrapment efficiency (%)	Model to assess therapeutic efficacy	Administration route	Ref
BSA with Cyclodextrin	Tacrine	Coacervation	177.4 ± 18.0	-10.0 ± 0.9	88 ± 9	-	Intranasal	(86)
Chitosan with P80	Tacrine	Spontaneous emulsification	41.0 ± 7.0	34.7 ± 1.5	13.4 ± 0.2	Biodistribution in Wistar rats	Intravenous	(87)
PLGA with PEG	Donepezil	Double emulsion w/o/w	Ranged from 174 ± 12.0 to 240 ± 16	Ranged from -20.5 to -11	Ranged from 52.5 to 60.5	$A\beta_{1-40}$ and $A\beta_{1-42}$ fibrils, PCR, ELISA and immunostaining	-	(88)
PLGA with P80	Donepezil	Solvent-emulsification diffusion method	89.7 ± 6.4	-36.0 ± 1.1	88.7 ± 2.5	Biodistribution in Wistar rats	Intravenous	(89)
Chitosan	Donepezil	Ionic crosslinking	Ranged from 150 to 200	-	Ranged from 92 to 96	Biodistribution and safety on Sprague–Dawley rats	Intranasal	(90)
PLGA with P80 and P188	Rivastigmine tartrate	Modified nanoprecipitation	135.6 ± 4.2	23.6 ± 1.2	74.5 ± 0.7	Scopolamine-induced amnesic mice	Intravenous	(91)
PBCA	Rivastigmine tartrate	Emulsion polymerization	146.8 ± 2.7	-13.9 ± 0.6	57.3 ± 0.9	Scopolamine-induced amnesic mice	Intravenous	(91)
Chitosan	Rivastigmine hydrochloride	Ionic gelation	164.4 ± 5.0	45.3 ± 6.2	73.6 ± 3.3	Biodistribution in Wistar rats	Intranasal	(92)

Chitosan with P80	Rivastigmine tartarate	Spontaneous emulsion	45.5 ± 1.3	35.1 ± 1.5	85.3 ± 3.1	Biodistribution in mice	Intravenous	(93)
PLGA with P80	Galantamine	Nanoemulsion templating	21.5 ± 0.3	−11.2 ± 0.9	98	In vitro AcCE inhibition	-	(94)
Chitosan with P80	Galantamine	Ionic gelation	190.0 ± 1.2	31.6 ± 9.8	23.34	Biodistribution in rats	Intranasal	(95)
PBCA with P80	Nerve growth factor	Ionic polymerization	250 ± 30	-	23.34	scopolamine-induced amnesia in rats	Intravenous	(96)
PLA with PEG	NAP- peptide B6	Solvent-emulsion diffusion	118.3 ± 7.8	-22.7 ± 0.9	51.2 ± 3.5	Aβ injection in mice	Intravenous	(97)
PLGA and trimethyl chitosan	Coenzyme Q10	Nanoprecipitacion	146.7 ± 5.1	21 ± 2.9	99.9	APP/PS1 transgenic mice	Intravenous	(98)
PLGA with an aptamer	Curcumin	Solvent-emulsion diffusion	168	-	-	In vitro uptake studies	-	(99)
PLGA	Tarenflurbil	Solvent-emulsion diffusion	169.87	-30.0	64.11 ± 2.21	-	Intranasal	(100)
PLGA with PVA	Quercetin	Double emulsion-solvent evaporation	100-150	-	-	APP/PS1 mice	Intravenous	(101)

Table 3. Polymeric nanoparticles for glaucoma and ocular inflammation

Polymer and surfactant	Drug	Preparation method	Average size (nm)	Zeta potential (mV)	Entrapment efficiency (%)	Ocular disease	Animal model	Administration route	Ref
Gelatin (collagen) with cyclodextrin	Pilocarpine	Desolvation technique	Ranged from 425 to 312	Ranged from -8.4 to -4.7	Ranged from 44 to 54	High IOP	-	-	(102)
Gelatin (collagen) with cyclodextrin	Hydrocortisone	Desolvation technique	Ranged from 154 to 224	Ranged from -6.1 to -12.5	Ranged from 35 to 45	High IOP	-	-	(102)
Poly-ε-caprolactone	Flurbiprofen	Solvent emulsion-diffusion	188.4±1.3	-16.4±0.1	85.5±1.4	Cornel inflammation	Pig	Eye-drops	(103) (104)
Methyl–methacrylate and chlorotrimethyl–ammonioethyl methacrylate)	Methylprednisolo-ne acetate	quasiemulsion solvent diffusion tech-	-	-	-	Uveitis	Rabbits	Eye-drops	(105)
Polybutylcyanoacrylate	Progesterone	Emulsion-polymeritzation	-	-	98.8 ± 0.8	-	Albino rabbits	Eye-drops	(106)
Chitosan	Dorzolamide	Ionic gelation	300 ± 5	-	-	Glaucoma	-	Eye-drops	(107)
Chitosan (CS)-sodium alginate (ALG)	Gatifloxacin	Coacervation	347.0	+38.6	79.63	Bacterial infections	-	Eye-drops	(108)
Eudragit RS100 and RL100 and Ttween80	Cloricromene	Quasi-emulsion solvent diffusion	Ranged from 154.3 to 48.7	Ranged from +27.6 to +8.2	-	uveitis	-	Eye-drops	(109)

PLGA-PEG with POD peptide	Flurbiprofen	Solvent displacement	219.9 ± 1.2	30.2 ± 1.4	70.3 ± 5.6	Ocular inflammation	Albino rabbit	Eye-drop	(110)
PLGA	Pranoprofen	Solvent displacement	350	-7.4	80.0	Ocular inflammation	Albino rabbit	Eye-drop	(111)
PLGA	Carprofen	Solvent displacement	189.50 ± 1.67	–22.80 ± 0.66	74.70 ± 0.95	Ocular inflammation	Albino rabbit	Eye-drop	(112)
PLGA	Aleanolic and ursolic acid	Solvent displacement	< 225	- 27	77	Ocular inflammation	Albino rabbit	Eye-drop	(113)
PLGA-PEG and Tween80®	Melatonin	Solvent displacement	400	- 8.2	78.20 ± 2.93	Glaucoma	Albino rabbit	Eye-drop	(114)

1 OBJECTIVES

2. OBJECTIVES

The aim of this research is the development and characterisation of biodegradable polymeric NPs able to cross the BBB and the BRB in order to efficiently deliver the drug for the treatment of AD and glaucoma, respectively. Since these systems could be also applicable for corneal inflammatory diseases, a secondary objective would be the development of these NPs for corneal inflammation treatment.

The specific objectives of the study are the following ones:

- Development of PEGylated biodegradable NPs encapsulating the drug Memantine and Dexibuprofen separately by double emulsion and solvent-displacement technique, respectively.

- Characterize the physicochemical properties of these formulations in terms of size, polydispersity index, surface charge, encapsulation efficiency and stability at different temperatures.

- Obtain a sustained drug release increasing, at the ocular level, the permeation rate against the free drug.

- Obtain solid evidence trough *in vitro* and *in vivo* studies that the developed system were non-cytotoxic, non-irritating after topical administration and were able to cross the BBB.

- *In vivo* studies with New Zealand rabbits to prove that DXI loaded PLGA-PEG NPs were suitable for ocular inflammation treatment

- Demonstrate that MEM-PLGA-PEG NPs were effective for glaucoma in an *in vivo* rat glaucoma model.

- Obtain solid evidence that both DXI and MEM PLGA-PEG NPs were suitable for AD treatment after oral administration with a double transgenic model of AD.

3. RESULTS

3. RESULTS

The results obtained through the different analyzes carried out in the present research allowed to generate four scientific publications, in the form of articles. Two of them are published and the other two are under revision.

3.1 Memantine loaded PLGA PEGylated Nanoparticles for Alzheimer's disease: in vitro & in vivo characterization, *Journal of Nanobiotechnology*, submitted (Impact factor: 4.946)

3.2 New potential strategies for Alzheimer's disease prevention: pegylated biodegradable dexibuprofen nanospheres administration to APPswe/PS1dE9, *Nanomedicine: Nanotechnology, Biology and medicine*, 3 (2017) 1171–1182. Doi: 10.1016/j.nano.2016.12.003 (Impact factor: 5.720)

3.3 Memantine loaded PEGylated biodegradable nanoparticles for the treatment of glaucoma, *Small*, (2017), 1-12. Doi: 10.1002/smll.201701808 (Impact factor: 8.643)

3.4 PEGylated PLGA nanospheres optimized by design of experiments for ocular administration of dexibuprofen—in vitro, ex vivo and in vivo characterization, *Colloids and Surface B: Biointerfaces*, 145 (2016) 241–250. Doi: 10.1016/j.colsurfb.2016.04.054 (Impact factor: 3.887)

3.1 MEMANTINE LOADED PLGA PEGYLATED NANOPARTICLES FOR ALZHEIMER'S DISEASE: *IN VITRO* & *IN VIVO* CHARACTERIZATION

Elena Sánchez-López, Miren Ettcheto, Maria Antonia Egea, Marta Espina, Ana Cristina Calpena, Antoni Camins, Nuria Carmona, Amelia M. Silva, Eliana B. Souto, Maria Luisa García

Memantine loaded PLGA PEGylated Nanoparticles for Alzheimer's disease: in vitro & in vivo characterization

*Journal of Nanobiotechnology (*Submitted)

Memantine loaded PLGA PEGylated Nanoparticles for Alzheimer's disease: *in vitro* & *in vivo* characterization

Elena Sánchez-López[1,2*], Miren Ettcheto[3,4], M. Antonia Egea[1,2], Marta Espina[1,2], Ana Cristina Calpena[1,2], Antoni Camins[3,4] , Nuria Carmona[1], Amélia M. Silva[5,6], Eliana B. Souto[7,8], M. Luisa García[1,2]

[1] Department of Pharmacy, Pharmaceutical Technology and Physical Chemistry, Faculty of Pharmacy, University of Barcelona, 08028, Barcelona, Spain

[2] Institute of Nanoscience and nanotechnology (IN2UB). Faculty of Pharmacy, University of Barcelona, 08028 Barcelona, Spain

[3] Networking Research Centre of Neurodegenerative Disease (CIBERNED), Instituto de Salud Juan Carlos III, Madrid

[4] Department of Pharmacology and Therapeutic Chemistry. Faculty of Pharmacy, University of Barcelona, 08028 Barcelona, Spain

[5] Department of Biology and Environment, School of Life and Environmental Sciences (ECVA, UTAD), University of Trás-os-Montes and Alto Douro, Quinta de Prados, 5001-801 Vila Real, Portugal

[6] Centre for Research and Technology of Agro-Environmental and Biological Sciences, University of Trás-os-Montes and Alto Douro, CITAB-UTAD, 5001-801 Vila Real, Portugal

[7] Department of Pharmaceutical Technology, Faculty of Pharmacy, University of Coimbra (FFUC), Polo das Ciencias da Saúde Azinhaga de Santa Comba, 3000-548 Coimbra, Portugal

[8] REQUIMTE/LAQV, Group of Pharmaceutical Technology, Faculty of Pharmacy, University of Coimbra, Portugal

* Corresponding author:

esanchezlopez@ub.edu

Pharmacy, Pharmaceutical Technology and Physical Chemistry

University of Barcelona

Abstract

Memantine was loaded in biodegradable polylactic-co-glycolic (PLGA) nanoparticles, produced by double emulsion method and surface-coated with polyethylene glycol (PEGylated). MEM-PEG-PLGA nanoparticles (NPs) were aimed to target the blood-brain barrier (BBB) upon oral administration for the treatment of Alzheimer's disease. The production parameters were optimized by design of experiments (DoE). MEM-PEG-PLGA NPs showed a mean particle size below 200 nm (152.6 ± 0.5 nm), monomodal size distribution (polydispersity index, PI< 0.1) and negative surface charge (-22.4 mV). Physicochemical characterization of NPs confirmed that the crystalline drug was dispersed inside the PLGA matrix. MEM-PEG-PLGA NPs were found to be non-cytotoxic on the tested brain cell lines (bEnd.3 and astrocytes). Memantine followed a slower release profile from the NPs against the free drug solution, allowing to reduce drug administration frequency *in vivo*. Nanoparticles were able to cross BBB both *in vitro* and *in vivo*. Behavioral tests carried out on transgenic APPswe/PS1dE9 mice demonstrated a more efficient memory impairment reduction when using MEM-PEG-PLGA NPs in comparison to the free drug solution. Histological studies confirmed that MEM-PEG-PLGA NPs reduced β-amyloid plaques and the associated inflammation characteristic of Alzheimer's disease.

Keywords: Memantine; Nanoparticles; Alzheimer's disease; Brain targeting; APPswe/PS1dE9 mice; β-amyloid plaques; bEnd.3; astrocytes

Abbreviations: Alzheimer's disease, AD; β-amyloid, Aβ; Memantine, MEM; poly(lactic-co-glycolic acid), PLGA; Food and Drug administration, FDA; nanoparticles, NPs; poly(ethylene glycol), PEG; polyvinyl alcohol (PVA); Mean average size, Z-AVE; polydispersity index, PI; zeta potential, ZP; encapsulation efficiency, EE; transmission electron microscopy, TEM; Akaike's information criterion, AIC; permeability across cell monolayer, P_e; APPswe/PS1dE9 mice, APP/PS1.

Background

Alzheimer's disease (AD) is the most prevalent neurodegenerative disorder amongst patients over 65 years old [1]. Memantine hydrochloride (MEM), a low-affinity voltage-dependent uncompetitive antagonist to glutamatergic N-methyl-D-aspartate (NMDA) receptors, is the only drug approved both in Europe and in the United States for moderate and severe degrees of the disease.

The clinical applications of nanoparticles (NPs) have proven enormous advantages for targeting and delivery of drugs, in particular, for the management of AD since current therapeutic strategies are compromised by the tight junctions and endothelial cells of the blood-brain-barrier (BBB) [2]. Nanoparticles, with an average size below 200 nm, may represent an alternative for prolonged drug delivery across the BBB, given their capacity for endocytic transport [3, 4]. While a number of polymers have already been used in the production of NPs, polyesters such as poly D,L-(lactic-*co*-glycolic) acid (PLGA), have been extensively applied for controlled drug delivery, including brain targeting [5, 6]. PLGA, which has been approved by the Food and Drug Administration, is one of the most successful biodegradable polymers because it undergoes hydrolysis to produce lactic and glycolic acid easily cleared from the body [7]. In addition, advanced drug delivery systems based on PLGA NPs have recently demonstrated to be potential alternatives for the treatment neurodegenerative diseases [8]. A limitation on the use of PLGA NPs in drug delivery is, however, their fast uptake and clearance from the reticuloendothelial system (RES). To overcome the RES clearance, surface coating of NPs with poly (ethylene glycol) (PEG) has been recommended, an approach that has demonstrated to reduce NPs' clearance significantly *in vivo* [9]. In addition, it has also been proven that such surface coating may increase NPs targeting and uptake through the BBB [10]. Loading MEM in PEG-PLGA NPs with a matrix structure is expected to prolong the drug's circulation half-life compared to non-coated PLGA NPs, due to the presence of mobile and flexible PEG chains on their surface.

While MEM was found to improve patients' cognition, global functioning behavior and stage of dementia in comparison to placebo groups, results obtained from meta-analysis of AD monotherapy translate its limited clinical benefits (i.e. the assessment scores were not statistically significant between treated and non-treated groups) [11]. In addition, despite being well-tolerated, MEM requires daily administration by the patients which, combined with the poor drug compliance, may also reduce the rates of successful treatment.

A sustained release formulation, based on PLGA NPs for oral administration, has been proposed to assure that the drug remains on the target site until the next patients' intake of the medicine. MEM-PEG-PLGA NPs are expected to contribute to a time-stable dose on the brain, prolonging drug release, reducing administration frequency and decreasing the adverse-side effects. Comparing to other routes, and for chronic treatment schedules, oral administration offers comfort and improves patient's compliance. Recent studies have demonstrated the added-value of loading drugs in PLGA NPs to enhance their oral bioavailability [12, 13]. PEG surfacing PLGA NPs have enhanced mucus permeating properties, therefore contributing to increase the drug's bioavailability after oral administration [14].

In the present work, we report the development of a physicochemically stable, sustained-release MEM-PEG-PLGA NPs formulation, for the treatment of AD. Developed MEM-PEG-PLGA NPs are reported to be a non-invasive approach for brain targeting of MEM, with minimal adverse-side effects. The physicochemical stability of MEM after loading in PLGA NPs has been characterized by drug-polymer interaction studies, and by in vitro release profile. Cell viability was studied in two different cell lines, mapping the *in vitro* transport across the BBB. Transgenic and non-transgenic mice were orally treated with MEM-PEG-PLGA NPs and compared with the results obtained after treatment with free drug solution. Brain and plasma drug concentrations were measured, whilst behavioural test and histological studies were undertaken to elucidate the therapeutic efficacy of MEM-PEG-PLGA NPs against free drug, for brain delivery.

Materials and Methods

Materials

PLGA-PEG Resomer® RGP d 5055 was obtained from Boehringer Ingelheim, Germany and memantine (MEM) was purchased from Capotchem (Hangzhou, China). Water filtered through Millipore MilliQ system was used for all the experiments and all the other reagents were of analytical grade.

Production and Physicochemical Characterization of Nanoparticles

MEM loaded NPs were produced by a modified double emulsion method described elsewhere [15, 16]. Briefly, a predetermined amount of PLGA-PEG was dissolved in ethyl acetate (EA) forming the organic phase. Aqueous phase (w_1) was obtained by dissolving MEM in deionized water. Sonication energy was applied to form the primary emulsion (w_1/o). The w_1/o emulsion was then dispersed in 2 ml of deionized water containing PVA. Secondary emulsion ($w_1/o/w_2$)

was formed with ultrasound energy [17]. A volume of 2 ml of PVA (0.3%) were then added, under magnetic stirring, to stabilize the colloidal system. Solvent was evaporated and NPs were washed by centrifugation at 15000 r.p.m. during 20 min. The loading of NPs with rhodamine followed the same procedure. Empty NPs were prepared using the same approach but without addition of drug into the inner water phase [18].

Mean average size (Z-AVE) and polydispersity index (PI) of NPs were determined by photon correlation spectroscopy (PCS) using a ZetaSizer Nano ZS (Malvern Instruments). Measurements were carried out by triplicate at 180º in 10 mm diameter cells at a temperature of 25ºC. Zeta potential (ZP) was calculated from electrophoretic mobility as described elsewhere [19, 20].

Drug concentration was determined indirectly. Previously to the analysis, the non-loaded drug was separated from NPs by filtration/centrifugation at 14000 r.p.m. (Mikro 22 Hettich Zentrifugen, Germany) using an Amicon® Ultra 0.5 centrifugal filter device (Amicon Millipore Corporation, Ireland). The encapsulation efficiency (EE) was calculated by the difference between the total amount of drug and the free drug, present in the filtered fraction, using Equation /1/:

$$EE\ (\%) = \frac{\text{Total amount of MEM – Free MEM}}{Total\ amount\ of\ MEM} \qquad /1/$$

The quantification of MEM was performed in multiple reaction monitoring (MRM) mode using an ion trap mass spectrometer equipped with an atmospheric pressure electrospray ionization ion source, positive mode. The HPLC system was an Agilent 1100 series (Agilent Technologies, USA) coupled with a Brucker Ion Trap SL (Brucker Daltonics GmbH, Germany). MEM was separated on a reversed phase column (Kinetex de 2.6 μm 50 x 2.1 (Phenomenex) using methanol 0.1% formic acid in water 55:45 (v/v) as mobile phase. The flow rate was 1 ml/min at 45ºC [21].

Design of Experiments

Design of experiment (DoE) was used to optimize the developed formulation. Series of independent parameters and their influence on NPs properties were studied, determining the effects and interactions between factors. The effect of a factor x (E_x), was calculated using Equation /2/:

$$E_x = \frac{\Sigma x(+) - \Sigma x(-)}{n/2} \qquad /2/$$

where $\Sigma x(+)$ stands for the sum of the factors at their highest level (+1), $\Sigma x(-)$ is the sum of the factors at their lowest level (−1), and *n/2* is the half of the number of measurements. Interactions between factors (factor 1: factor 2) were also calculated. To estimate an interaction between two factors, the effect of the first factor at the lowest level of the second factor has to be calculated and subtracted it from the effect of the first factor at the highest level of the second factor.
For the study of the sonication parameters (Table 1) and concentration compounds (Table 2) two independent full factorial designs were performed. The mean size (Z-AVE), PI and ZP of the NPs were studied and the effects and interactions between factors were calculated. According to the composite design matrix generated by Statgraphics Plus 5.1 software, a total of 16 experiments (8 factorial points, 6 axial points and two replicated center points) were required for each design. The studied experimental responses were the result of the individual influence and the interaction of the three independent variables.

Nanospheres characterization and interaction studies

Morphology of the optimized formulation of MEM loaded NPs was determined by transmission electron microscopy (TEM), performed on a JEOL 1010 microscope (Akishima, Japan). The physical state and chemical interactions between drug and polymers were studied by thermal and x-ray diffraction analyses. For the interaction studies, NPs were washed by centrifugation and dried to constant weight previous to carry out the analysis. MEM thermal properties were studied by thermogravimetric (TG) analysis and differential thermal analysis (DTA) on a TASC 414/3 (Netsch, Thermal Analysis). Temperature ranged from 25ºC to 600ºC at 10ºC /min and AlO_3 pan was used as a reference. All experiments were carried out under nitrogen flow. Thermograms were obtained by differential scanning calorimetry (DSC) on a Mettler TA 4000 system (Greifensee, Switzerland) equipped with a DSC 25 cell. Samples were weighed (Mettler M3 Microbalance) in perforated aluminium pans and heated under a flow nitrogen at a rate of 10ºC/min. X-Ray diffraction (XRD) was used to analyse the amorphous versus crystalline status of the samples. Compounds were sandwiched between polyester films and exposed to CuK" radiation (45 kV, 40 mA, $\lambda = 1.5418$ Å) in the range (2θ) from 2º to 60º with a step size of 0.026º and a measuring time of 200 s per step. Fourier-transformed infra-red (FTIR) spectra of different

compounds were obtained using a Thermo Scientific Nicolet iZ10 with an ATR diamond and DTGS detector.

Storage stability

The stability of MEM-PEG-PLGA NPs stored at three different temperatures (4ºC, 25ºC and 38ºC) was studied by light backscattering using Turbiscan®Lab operated at constant temperature. For this purpose, a glass measurement cell was filled with 20 ml of sample. The light source is a pulsed near infrared light and was received by a backscattering detector at an angle of 45° from the incident beam. Backscattering data were acquired once a month for 24 h at intervals of 1 h. In addition to this technique, morphometric parameters (Z-AVE, PI and ZP) were also measured.

***In vitro* drug release**

In vitro drug release of MEM-PEG-PLGA NPs was studied against free MEM in PBS, in a bulk equilibrium direct dialysis bag technique under sink conditions for 36 h (n=6). Briefly, a volume of 5 ml of each formulation was placed directly into a dialysis bag (cellulose membrane, 12-14 kDa, size 3,20/32'' diameter, Iberlabo) and each bag was placed on 150 ml of isotonic phosphate-buffered saline (PBS) 0.1 M, pH 7.4 at 37ºC. At predetermined intervals, 1 ml of sample was withdrawn from the stirred release medium and simultaneously replaced with 1 ml of fresh buffer at the same temperature. AIC was determined as an indicator of the suitability of the model for a given dataset. The model associated to the smallest AIC value is considered as giving the best fit of the set of data [19].

Cell culture

Cells were thawed, grown, maintained and regularly observed under a microscope. Two cell lines were used, namely, mouse microvascular endothelial cells (bEnd.3) and astrocytes from brain rat cortex. Primary cultures of astrocytes were obtained from bank GAIKER-IK4 culture. The bEnd.3 cells were maintained in their specific culture medium, DMEM + 10% FBS [21]. Cells and corresponding culture medium were tempered at 37ºC, 1 ml of cells was diluted in 9 ml of medium and the cell suspension was centrifuged at 4ºC for 5 minutes at a speed of 130 *g*. The supernatant was removed and the cells were re-suspended in culture medium. Cells were seeded

in 75 cm^2 flasks and kept in an incubator at 37ºC, an atmosphere of 5% CO_2 and a relative humidity of 95%. Once removed and washed, the cells were seeded with fresh medium.

Cytotoxicity studies

Alamar blue reduction was used as a parameter for cell viability. This assay is based on that viable and metabolically active cells reduce resazurin to resorufin, which is released into the culture medium. This conversion is intracellular, facilitated by oxidoreductases of mitochondrial, microsomal and cytosolic origin. In a toxic event, where a loss of cell viability and proliferation occurs, the cells that comprise the epithelial tissue lose the ability to reduce resazurin. Therefore, resazurin reduction ratio is directly proportional to the number of viable cells. Absorbance was determined at λ of 570 nm and 620 nm, reduced and oxidized form, respectively [22]. Data were analysed by calculating the percentage of Alamar blue reduction and expressed as percentage of control (untreated), as reported before [23].

***In vitro* transport across the BBB**

In vitro BBB models have become a standard tool for estimating the ability of drugs to bypass the BBB at the early stage of drug development. In the present work, endothelial cell-based models were optimized by co-culturing the endothelial cells with astrocytes in Transwell systems, as shown in Figure 1. Polycarbonate transwell inserts were used with a semipermeable membrane of 0.4 μm pore. For co-culture experiments (Figure 1), endothelial cells were seeded in the apical part of the inserts. A semipermeable filter was placed, and in the basolateral compartment cells from primary cultures of rat astrocytes were added.

[Please insert Figure 1 about here]

Figure 1. Representation of the blood-brain barrier model to assess in vitro transport of nanoparticles.

Trans-epithelial electrical resistance study

The brain vasculature is characterized by endothelial cells with strong tight junctions that limit paracellular diffusion of hydrophilic molecules selectively, according to their charge and size. When the movement of ions across the monolayer is restricted due to the proper functioning of the barrier, an electric potential gradient on both sides is generated. Transepithelial electrical resistance (TEER) is an indicator of cell confluence, monolayer integrity and the formation of tight junctions between cells. Thus, TEER manual measurements were taken daily until a steady state was reached, employing epithelial EVOM2 voltmeter connected to a pair of electrodes STX2. The system operates with two electrodes, which can be applied directly to the inserts. To calculate TEER of each insert, Equation /3/ was used and values are expressed in $\Omega \cdot cm^2$.

$$TEER = \left[\Omega_{Cell\ monolayer} - \Omega_{Filter\ (without\ cells)}\right] \times [Filter\ Surface] \qquad /3/$$

Co-culture experiments were carried out in 24-well plates. Inserts were removed and placed in new media plates with Hanks and 0.5% bovine serum albumin (BSA). Apical media was removed, washed with Hanks and MEM-PEG-PLGA NPs were added (dissolved in 0.5% BSA Hanks) in the apical part of the inserts and left for one hour. Furthermore, to verify that MEM-PEG-PLGA NPs did not compromise membrane integrity, a compound with low paracellular permeability, Lucifer yellow (LY), was added at the end of the study. Membrane integrity (with LY) was determined calculating the permeability coefficient by using the clearance principle which allows a permeability value independent of concentration.

***In vivo* studies**

Male APPswe/PS1dE9 and C57BL/6 mice were used for the *in vivo* studies. APP/PS1 animals co-express a Swedish (K594M/N595L) mutation of a chimeric mouse/human APP (Mo/HuAPP695swe), together with the human exon-9-deleted variant of PS1 (PS1-dE9), allowing these mice to secrete elevated amounts of human Aβ peptide [24]. The animals were kept under controlled temperature, humidity and light conditions with food and water provided *ad libitum*. Mice were treated in accordance with the European Community Council Directive 86/609/EEC and the procedures established by the *Departament d'Agricultura, Ramaderia i Pesca of the Generalitat de Catalunya*. Every effort was made to minimize animal suffering and to reduce the number of animals used. Sixty 6 month-old animals, divided into six groups, were

used for the present study, with at least 10 WT and 10 APP/PS1 transgenic mice, per group. Mice were treated for two months with MEM at therapeutic dose (30 mg/kg/day) and MEM-PEG-PLGA NPs were administered. NPs volume was calculated for each animal previously weighted and was administered on a drinking bottle. Afterwards, NPs drinking bottle was replaced by untreated water for 24 hours. Following *in vivo* testing, the animals were sacrificed and at least 6 mice in each group were used for histological studies [25].

Nanoparticles brain distribution

Fluorescent PEG-PLGA NPs were developed applying double emulsion method. Three WT mice were used for each group, administering 300 µl of Rho NPs. After 24 hours this time, mice were sacrificed and brains were extracted and fixed in paraformaldehyde. After 48 hours, brains were removed, placed in a 30% sucrose solution and stored at -80ºC. Brains were sliced at 40 µm by using a cryostat. Samples were washed trice with PBS for 5 minutes and stained with Hoetsch for 15 min. After that, samples were washed with PBS-Triton (0.5% V/V) trice for 5 min. Brain sections were mounted into jellified slides and observed at confocal microscope (Leica Microsystems Heidelberg GmbH) using DAPI and TRITC filters for Hoestch and Rhodamine, respectively. Images were processed using Fiji Plugin for ImageJ and maximum intensity projection was applied.

Previously to the study of the therapeutic effects, drug at steady state levels was quantified in order to confirm drug amount into target tissue after MEM NPs administration. Moreover, drug was also quantified on plasma. Blood samples were extracted from the facial vein and samples were centrifuged during 20 min at 2000 r.p.m. adding EDTA (10 µl K_2EDTA 18 mg/ml) to avoid blood coagulation. Mice were sacrificed by cervical dislocation and immediately brains were removed and preserved at -80ºC. Amantadine was added as internal standard and MEM extraction was carried out using organic solvents (*t*-butyl methyl ether and diethyl ether–chloroform for brain and blood samples, respectively). Solvents were evaporated under nitrogen flow and samples were reconstituted with methanol [26, 27]. Samples were analysed as described previously (section NPs production). The analyses were carried out using the parent to daughter combinations of *m*/*z* 180 > 163 (MEM) and *m*/*z* 152 > 135 (amantadine) [21].

Morris water Maze

The Morris water maze (MWM) test was conducted in a circular tank filled with water at 21 ± 2 °C and divided into four equal quadrants. A white platform was submerged below the water surface in the middle of the northeast quadrant. The behavioural data were acquired and analysed using a computerized video tracking system. The procedure of the behaviour assessment consisted of a six-day navigation testing session and a probe trail. Mice received five trials per day for six successive days continuing with the same drug regime. Animals were placed into the maze facing the tank wall at water-level. They were allowed to swim freely for 60 s to seek the invisible platform and allowed to remain there for 10 s. If a mouse failed to find the platform, it was guided to it and left there for 30 s. The probe trial was performed the day after the last training test. In the probe test, the hidden platform was removed, and the mice were released from the southwest quadrant and allowed to swim for 60 s. Results were calculated individually for each animal [28].

Immunohistochemistry studies

Mice were anesthetized with sodium pentobarbital and perfused with 4% paraformaldehyde in 0.1M phosphate buffer (PBS) after the probe trial. Brains were stored in 4% paraformaldehyde at 4ºC overnight then dehydrated in 30% phosphate-buffered sucrose solution for cryoprotection. Samples were preserved at -80ºC and coronal sections of 20 μm were obtained by a cryostat (Leica Microsystems, Wetzlar, Germany). Sections were incubated overnight at 4°C with the rabbit anti-GFAP (1:2,000; Dako, Glostrup, Denmark) primary antibody, and sequentially incubated for 2h with Alexa Fluor 594 goat anti-rabbit antibody at room temperature (1:500; Invitrogen, Eugene, OR, USA). Staining of β-Amyloid plaques was performed using Thioflavin S (ThS 0.002%, Sigma-Aldrich) to compare β-amyloid plaque density among different treatment groups. Sections were counterstained with 0.1 μg/ml Hoechst 33258 (Sigma-Aldrich, St Louis, MO, USA) and rinsed afterwards with PBS 0.1M [29]. ThS-stained β-amyloid plaques were visualized using a fluorescence microscope with a fluorescence filter (BX41 Laboratory Microscope, Melville, NY-Olympus America Inc). For each image, the proportion of total image area covered by fluorescently stained β-amyloid plaques was quantified. For each mouse, four fields per section with the highest density of plaques were chosen as representative and were averaged [30].

Statistical analysis

All of the data are presented as the mean ± S.D. Two-way ANOVA followed by Tukey post hoc test was performed for multi-group comparison. Student's *t*-test was used for two-group comparisons. Statistical significance was set at $p < 0.05$ by using GraphPad Prism version 5.00 for Windows, GraphPad Software, San Diego California USA.

Results and discussion

Optimization of NPs' parameters

Double emulsion evaporation method was chosen for the production of PLGA NPs due to its suitability for the loading of hydrophilic drugs, such as MEM. Since the mean particle size is a critical parameter to assure that NPs are absorbed in the gastrointestinal tract and achieve the BBB, the aim of the factorial design was to produce MEM-PEG-PLGA NPs with a mean size 100 and 200 nm. Since MEM is insoluble in ethyl acetate, this organic solvent has been used for the preparation of $w_1/o/w_2$ emulsions, allowing the retention of the drug in the inner aqueous phase. From preliminary studies, the addition of small amount of polyvinyl alcohol (PVA, 0.3%) after the second emulsification process was shown to contribute to the decrease of the mean size of NPs from 264.6 nm (with a bimodal distribution) down to 220.1 nm (with a monomodal distribution, $PI < 0.1$). These results were attributed to the delay of the solvent diffusion to the outer aqueous phase upon addition of the aqueous PVA solution, limiting the risk of droplets agglutination and polymer precipitation [18]. The results obtained from the full factorial designed performed for the selection of the appropriate sonication parameters (i.e. wave amplitude and sonication time) are shown in Table 1.

[Please insert Table 1 about here]

Table 1. Values of the matrix of a factorial design of sonication parameters and measured responses. Bold values correspond to the optimized formulation of MEM loaded NPs.

Factorial design demonstrates that the interaction between 1st and 2nd sonication times increased the mean size of NPs. As a consequence, a lower 1st sonication time was chosen to obtain NPs smaller than 200 nm. High amplitudes, around 38%, are mandatory to obtain small and

monodispersed NPs (Figure 2a) [18]. As shown in Figure 2b, amplitude was a significant parameter regarding particles surface charge, establishing a trend where increasing the amplitude causes a slight increase of the negative charge and, subsequently, the creation of more stable particles. Therefore, the maximum amplitude (F9, Table 1) would be applied.

[Please insert Figure 2 about here]

Figure 2. DoE of sonication parameters **A)** Surface plot of MEM-PLGA-PEG NPs PI and **B)** Pareto's chart of the effect of sonication parameters on ZP.

The optimized concentration parameters of the formulation compounds have also been studied (Table 2). The increase of the polymer concentration caused the increase of both z-AVE and PI (Figure 3a). Indeed, the higher the viscosity of the inner aqueous phase of the primary emulsion (w_1/o), the less efficient is the reduction of the emulsion droplet size during the second emulsification step ($w_1/o/w_2$) [15, 16]. The higher the PVA concentration, the smaller the NPs obtained (Figure 3a). These results suggest that the optimized PVA concentration should be able to ensure enough surfactant molecules to cover the interface between the organic phase and the external aqueous phase, improving the protection of the droplets from coalescence [16].

[Please insert Table 2 about here]

Table 2. Values of the matrix of a factorial design of concentration parameters and measured responses. Bold values correspond to the optimized formulation of MEM loaded NPs.

[Please insert Figure 3 about here]

Figure 3. DoE of concentration parameters; A) Surface plot of MEM –PLGA-PEG NPs z-AVE and B) Effect of compounds concentration on ZP.

Pareto's chart (Figure 3b) shows that MEM concentration influenced the surface electrical charge of NPs significantly. MEM has an amine group which can easily be protonated and decrease negative surface charge caused by the polymer [31],[32].

However, while high MEM concentrations negatively affect the particles stability, a statistically significant relationship between EE and MEM concentration was established. According to the factorial design data, a suitable formulation was achieved with a minimum concentration of

polymer (10 mg/ml), an upper-intermediate drug concentration (9 mg/ml) and a maximum amount of PVA (7.5 mg/ml)
(F7, Table 2). After ultracentrifugation at 15000 r.p.m. for 20 min of the optimized formulation, NPs kept their size properties (z-AVE of 152.6 ± 0.5 nm and PI 0.043 ± 0.009), although ZP was more negative (-22.4 ± 0.5 mV), which was attributed to the removal of surfactant molecules from the surface of the particles. Detailed structure of MEM-PEG-PLGA NPs was further characterized by TEM, which confirmed the spherical shape and smooth surface of NPs (Figure 4).

[Please insert Figure 4 about here]

Figure 4. MEM-PLGA-PEG NPs transmission electron microscopy and size distribution obtained by dynamic light scattering.

Characterization of NPs and interaction studies

In vitro and *in vivo* drug release profiles are highly dependent on the physical state of the drug inside the NPs. TG and DTA were therefore used to study the interaction between MEM and polymers. As shown in Figure 5a, the presence of the anhydrous form of the drug was identified therefore MEM was shown to be stable at low temperatures [32]. TG profile of MEM exhibited a weight loss starting at 290ºC, and finishing at 354ºC, which correspond to the complete degradation of drug. DTA showed an onset of endothermic event at 280ºC followed by a maximum at 352ºC being these results similar to those obtained by DSC. A thermal decomposition of MEM was shown to occur in two steps, corresponding the latter to a final oxidative degradation.

[Please insert Figure 5 about here]

Figure 5. MEM thermogravimetric and differential thermal analysis.

DSC curves of MEM, PVA, PEG-PLGA, MEM-PEG-PLGA NPs, and physical mixture of MEM are depicted in Figure 6. PVA exhibits two endothermic peaks, corresponding to the melting (192.86ºC) and decomposition (318.61ºC) events, respectively. PEG-PLGA onset transition temperature (T_g) takes place around 44.50ºC. PLGA without PEG chains exhibited a T_g around 54.18ºC. The presence of PEG chains produced a decrease of the T_g values, attributed to the plasticizing effect based on the reduction of the attractive forces among the polymer chains.

MEM displayed a melting transition followed by decomposition between 190ºC and 322ºC, exhibiting a thermal event comprising both phenomena. DSC analysis of MEM-PEG-PLGA NPs displayed an endothermic event corresponding to the T_g of the polymer occurring at 50.56ºC. The increasing of the T_g of the polymer has been attributed to the incorporation of an alkaline drug, which causes interactions between the carboxylic groups of the polymer.

[Please insert Figure 6 about here]

Figure 6. MEM-PLGA-PEG NPs differential scanning calorimetry analysis.

Results from XRD studies are shown in Figure 7a. Drug powder diffraction pattern showed sharp crystalline peaks, whereas PEG-PLGA showed an amorphous profile. MEM-PEG-PLGA NPs displayed a profile similar as PEG-PLGA, but a slight attenuated peak corresponding to the drug was also observed. The surfactant displayed a semi-crystalline pattern, not present in the formulation. This fact demonstrates the effectiveness of the centrifugation process, confirmed by FTIR analysis (Figure 7b). This suggests that the surfactant acts only as adjuvant in the NPs production, stabilizing the freshly prepared particles while it is not entrapped in the polymer because it was effectively removed by centrifugation. This property is relevant since a high surfactant concentration may induce toxicity by establishing an interconnected network with the polymer [33].

FTIR analysis (Figure 7b) does not show any evidence of chemical interaction or strong bond formation between MEM and PEG-PLGA or between NPs and surfactant. The stretching band of the polymer carbonyl groups (C=O) was observed at 1740 cm^{-1}, whereas the first polymer bands are due to C-O PLGA-PEG bonds [34]. The bond at 2950 cm^{-1} clearly indicates the presence of C-H (ethylene glycol). PVA exhibits a number of absorption peaks at 2900, 1324, 843 and 1084 and 3237 cm^{-1} due to C-H stretching, C-H bending and C-O stretching, which are not depicted in the profile obtained for MEM-PEG-PLGA NPs. Around 3000 cm^{-1} MEM showed the amine corresponding peak associated with N-H stretching bond. As reported by other authors, the peak at 1648 cm^{-1} indicates presence of C-O group attached to –NH [35].

[Please insert Figure 7 about here]

Figure 7. MEM-PLGA-PEG NPs interaction studies **A)** X-Ray diffraction and **B)** Fourier transformed infra-red analysis.

Storage stability

Stability of the developed NPs at different temperatures (4ºC, 25ºC and 38ºC) was also monitored. Samples stored at 4ºC and 25ºC remained visually unchanged during the first 6 months of storage. Samples stored at 38ºC were completely transparent and unstable by the end of the first month because of the degradation of the polymer induced by higher temperatures (Figure 8a).

Samples stored at 4ºC and 25ºC kept their ZP and size parameters (z-AVE and PI) for 6 months. No statistically significant differences were found between formulations stored at 4ºC and at 25ºC. Backscattering profiles at both temperatures were similar to those obtained by the end of the first month, but NPs stored at 25ºC showed a slight decrease of the light scattered percentage corresponding to the bottom of the sample, which was not observed at 4ºC (Figures 8b and 8c). This result was attributed to a slight NPs sedimentation process being preferential the particles' storage at 4ºC.

[Please insert Figure 8 about here]

Figure 8. Backscattering profile of MEM-PLGA-PEG NPs stored for 6 months; A) 38ºC, B) 25ºC and C) 4ºC.

***In vitro* drug release**

In vitro drug release was analysed against a drug solution in PBS (free MEM). Free MEM release was faster than the observed for MEM-PEG-PLGA NPs (Figure 9). The optimized formulation showed an immediate release (*burst* release) attributed to the non-loaded MEM fraction which is weakly bound to the NPs' surface, because of the PEG coating [36]. After this initial phase, the drug displayed a sustained release diffusing slowly from the polymeric matrix into the release medium. Akaike's information criterion (AIC) for hyperbola adjustment was 64.97 for MEM-loaded NPs and 86.8 for free drug. Parameters corresponding to hyperbola adjustment were analysed. K_d, equilibrium dissociation constant, expressed in concentration, corresponding to MEM-PEG-PLGA NPs was almost twice (0.74 for drug loaded NPs and 0.38 for the free drug)

than K_d obtained for the free drug, confirming the slower release of the drug from the colloidal system.

[Please insert Figure 9 about here]

Figure 9. In vitro release profile of MEM from PBS solution or MEM-PLGA-PEG NPs. Mean parameters were obtained adjusting data to hyperbola equation.

Cytotoxicity studies

Cell viability of MEM-PEG-PLGA NPs was measured in bEnd.3 (brain endothelial cells) and rat astrocyte primary cultures. These cells form the BBB and, for this reason together they are considered as a suitable model to test nanoparticles cytotoxicity. Following the incubation for 24 h, MEM-PEG-PLGA NPs did not show any measurable toxic effect (Figure 10). These results confirm that the developed particles are biocompatible with both endothelial glial brain cells. In addition, the slight amount of PVA that could remain after centrifugation process did not induce any toxicity nor influenced the normal growth of both epithelial cell lines within the assessed doses.

[Please insert Figure 10 about here]

Figure 10. Cell viability assessment using Alamar blue on brain cell lines.

***In vitro* transport across the BBB**

Results show that 40 % of the initial MEM-PEG-PLGA NPs were retained by the cell membrane of the *in vitro* model within one hour of incubation, whereas only 30% of the initial MEM was found inside the barrier. Drug permeability coefficient (P_e) in this model was 0.933. This fact indicates that NPs retained in this tissue would be able, either to achieve a slow drug release from there, or to partially cross through it and release the drug into the basolateral media. TEM images demonstrate that the part of MEM-PEG-PLGA NPs achieving the BBB remained spherical and non-aggregated with an average size below 200 nm (Figure 11). Similar results were obtained in other tissues, such as cornea in which NPs composed of different biodegradable polymers penetrate the first layers of the epithelium [37].

In addition, Lucifer Yellow (LY) was used as control at the end of the study, showing that these systems do not cause disruption of the BBB as no increase of paracellular passage of LY was observed (P_e<1 in all the experiments).

[Please insert Figure 11 about here]

Figure 11. TEM pictures of MEM-PEG-PLGA-NPs on the basolateral compartment of the BBB transport model after one hour of incubation.

***In vivo* transport across the BBB**

To tackle the NPs uptake and visualize them in the target tissue *in vivo*, MEM was replaced by Rhodamine 6G (Rho, 0.2% w/V) in the formulation. EE was measured indirectly by spectrophotometric methods at $\lambda_{525\ nm}$ (linear range 0.1-5 μg/ml). Results showed that PLGA-PEG NPs were able to load 6.69 μg/ml of Rho inside the NPs. Mean size (149.7 ± 0.6 nm) and PI (PI < 0.1) of Rho NPs were similar to those obtained by MEM-PEG-PLGA NPs. NPs surface charge was also negative (-11.5 mV). Qualitative evidence from confocal microscopy studies of mice treated with Rhodamine NPs showed that Rho loaded NPs were able to reach the brain upon oral administration. These results were also in agreement with those obtained from the *in vitro* studies. Absorption of Rho loaded NPs by GI were confirmed by other authors, demonstrating also an improvement of the absorption of hydrophilic drugs [38].

[Please insert Figure 12 about here]

Figure 12. Rho-loaded NPs brain distribution. **(a)** Rho-NPs on hippocampus (left part corresponding to Hoetsch nucleus staining) **(b)** Rho NPs on cortex (left part corresponding to Hoetsch nucleus staining).

In order to ascertain that the drug was able to efficiently reach the target tissue, quantification of the drug into the brain was also carried out. MEM concentration on the brain after achieving steady state levels (three weeks after drug administration) was measured administering NPs in alternate days. Brain concentration of MEM and of other aminoadamantane drugs was shown to be higher than the recorded plasma levels [39]. Particularly, in mice, MEM was reported to be between 2 and 9 times higher in brain than in plasma [40]. Mice treated for 3 weeks with MEM-PEG-PLGA NPs showed an average ratio brain/plasma of 111. Specifically, plasma

concentration was around 883.02 ng/ml. This may correlate with the burst release obtained *in vitro*. Brain levels were higher than those obtained in plasma (around 133.47 µg/ml) and to those described previously for free MEM.

These results demonstrate that the developed MEM-PEG-PLGA NPs were able to be absorbed by the gastrointestinal tract and efficiently deliver the drug across the BBB, being able to reach the hippocampus section of the brain, more effectively than the free drug. NPs would be absorbed by the gastrointestinal tract, and attributed to the fraction from the burst release observed *in vitro*. The remaining NPs would be able to cross to systemic circulation and, because of the PEG coating, protein adsorption and decrease liver uptake would be suppressed. In addition, PEG would increase NPs contact and penetration on the BBB [41].

Morris water maze test

The effects of MEM treatment on the animal's behaviour were assessed with the MWM test (Figure 13). The overall ANOVA for the training days revealed both a genotype (APP/PS1 against WT showed significant differences, $p < 0.01$) and a drug effect (treated vs untreated APP/PS1 mice) on mice spatial learning capacities. Escape latency on the test day results are shown in Figure 13a. Untreated APP mice showed a significant increase on scape latency compared to MEM loaded NPs group ($p < 0.01$). Moreover, no significant differences were found between WT and APP/PS1 mice treated with NPs, indicating that NPs indeed have therapeutic effects. NPs APP/PS1 mice revealed an improvement on spatial learning memory when compared with free MEM (no statistically significant differences).

[Please insert Figure 13 about here]

Figure 13. Morris water maze results on the probe trail. A) Escape latency and B) Representative swimming path of transgenic mice. Data represent mean ± SD; *$p < 0.05$, **$p < 0.01$, ***$p < 0.001$, ****$p<0.0001$.

As shown in Figure 13b, MEM-loaded NPs groups followed a more direct path until platform, than the rest of transgenic groups. As expected, significant differences were obtained with APP/PS1 untreated group and MEM-loaded NPs ($p<0.01$). Regarding time percentage in the platform quadrant (data not shown), APP/PS1 mice treated with MEM-loaded NPs presented an average of 37.22% of the time, whereas transgenic mice treated with MEM spend a 24.72% of

the time revealing that oral MEM-loaded NPs restore cognition more effectively than the free drug.

Immunohistochemistry

The formation of Aβ plaques, which is a pathologic hallmark of AD, could be observed by Thioflavin-S staining. Several studies confirmed that MEM decrease the number of amyloid plaques, therefore, histological studies to observe plaque development would be of great relevance. Figure 14 shows the results corresponding to amyloid plaques counting of WT and APP/PS1 mice. WT groups did not develop β-amyloid plaques. APP/PS1 mice treated with NPs developed some plaques, for which the levels were significantly lower than those obtained for the rest of transgenic groups ($p<0.001$), thus including MEM free groups.

[Please insert Figure 14 about here]

Figure 14. Amyloid plaques counting. Data represent mean ± SD; *$p < 0.05$, **$p < 0.01$, ***$p < 0.001$.

Figure 15 depicts the microscopic images after immunohistochemically staining of insoluble β-plaque development. APP untreated mice showed a greater plaque development. Moreover, plaques were surrounded by a high inflammatory state characteristic of AD. MEM-PEG-PLGA NPs groups showed fewer plaques and also inflammation degree was lower than the rest of transgenic groups [42]. These results are in agreement with behavioural assays, indicating that MEM restored cognition by decreasing insoluble amyloid plaques and the inflammatory response associated with AD.

[Please insert Figure 15 about here]

Figure 15. Immunohistochemically (cortex) staining of amyloid plaques (green) and GFAP (red) of WT and APP/PS1 mice (untreated, MEM free and MEM loaded NPs). Bar reference equivalent to 100 μm.

Conclusions

In this study, factorial design allowed to obtain NPs with an average size lower than 200 nm and PI <0.1, characteristic of monodispersed systems, suitable to be absorbed by the gastrointestinal tract and release the drug across the BBB. The optimized formulation was obtained by adding 7.5 mg/ml of surfactant, a low polymer concentration and a high drug amount. NPs were washed by ultracentrifugation process and effective surfactant elimination was demonstrated both by XRD and FTIR since no PVA bands were observed in the NPs profile. This suggests that the surfactant only acts as an adjuvant in the NPs production, stabilizing the colloidal suspension and it is not entrapped in the polymer since it was effectively removed by centrifugation. This is an increase outcome since a high surfactant amount may induce toxicity by establishing an interconnected network with the polymer. MEM-PEG-PLGA NPs raised the T_g of the polymer, thus confirming the drug loading within the particles. Moreover, no evidence of strong bond or chemical interaction between drug and polymer was found. MEM-PEG-PLGA NPs did not show the drug melting and decomposition process observed in the physical mixture, confirming that the drug loaded into NPs was in the form of either a molecular dispersion or in a solid solution.
MEM-PEG-PLGA NPs showed to be physically stable upon 6 months storage both at 25ºC and 4ºC, being preferable 4ºC storage due to a slight NPs sedimentation process observed in the backscattering profile. The developed formulation presented a slow *in vitro* release profile at 37ºC against free drug both fitting to hyperbola equation. This could be due to a first fast drug release (burst effect) provided by the drug accumulated onto the NPs surface, followed by a released caused by the drug entrapped into the polymeric matrix.
The *in vitro* and *in vivo* results for brain drug levels showed clear evidence that the developed systems provide a sustained delivery of the drug into the target tissue. The developed colloidal systems increase drug amount into the target organ and confirm the suitability of the NPs for oral administration attributed to the bioadhesive polymer properties. Moreover, reduced administration frequency (on alternate days) demonstrated to be adequate to achieve brain therapeutic concentrations of drug. Behavioural and histological studies of APP/PS1 and WT mice treated with NPs in alternate days showed a better effect of NPs groups against free MEM treatment improving both learning capacities and β-amyloid brain plaques on APP/PS1 animals. This can be attributed to the sustained release obtained with MEM-PEG-PLGA NPs that provide a stable drug amount into the target organ.

In summary, MEM-PEG-PLGA NPs could be a promising alternative towards a better treatment of AD patients since NPs have demonstrated to be capable to provide a more effective treatment than free MEM.

Acknowledgements

This work was supported by the Spanish Ministry of Science and Innovation (MAT 2014-59134-R projects). MLG, ACC, ME, MAE and ESL belong to 2014SGR-1023 and AC and ME belong to 2014SGR 525. The first author, ESL, acknowledges the support of the Spanish Ministry for the PhD scholarship FPI-MICINN (BES-2012-056083) and Agustí Pere i Pons Institution. We also acknowledge the Portuguese Foundation for Science and Technology under the projects M-ERA-NET-0004/2015, UID/AGR/04033/2013 and UID/QUI/50006/2013, receiving financial support from FCT/MEC through national funds, and co-financed by FEDER, under the Partnership Agreement PT2020.

None of the authors have any competing interests in the manuscript.

References

[1] Y. Nakamura, S. Kitamura, A. Homma, K. Shiosakai, D. Matsui, Efficacy and safety of memantine in patients with moderate-to-severe Alzheimer's disease: results of a pooled analysis of two randomized, double-blind, placebo-controlled trials in Japan, Expert opinion on pharmacotherapy, 15 (2014) 913-925.

[2] C. Roney, P. Kulkarni, V. Arora, P. Antich, F. Bonte, A. Wu, N.N. Mallikarjuana, S. Manohar, H.F. Liang, A.R. Kulkarni, H.W. Sung, M. Sairam, T.M. Aminabhavi, Targeted nanoparticles for drug delivery through the blood-brain barrier for Alzheimer's disease, Journal of controlled release : official journal of the Controlled Release Society, 108 (2005) 193-214.

[3] F. Gamisans, F. Lacoulonche, A. Chauvet, M. Espina, M.L. Garcia, M.A. Egea, Flurbiprofen-loaded nanospheres: analysis of the matrix structure by thermal methods, International journal of pharmaceutics, 179 (1999) 37-48.

[4] P. Calvo, B. Gouritin, H. Chacun, D. Desmaele, J. D'Angelo, J.P. Noel, D. Georgin, E. Fattal, J.P. Andreux, P. Couvreur, Long-circulating PEGylated polycyanoacrylate nanoparticles as new drug carrier for brain delivery, Pharmaceutical research, 18 (2001) 1157-1166.

[5] Q. Cai, L. Wang, G. Deng, J. Liu, Q. Chen, Z. Chen, Systemic delivery to central nervous system by engineered PLGA nanoparticles, American journal of translational research, 8 (2016) 749-764.

[6] S. Jose, S. Sowmya, T.A. Cinu, N.A. Aleykutty, S. Thomas, E.B. Souto, Surface modified PLGA nanoparticles for brain targeting of Bacoside-A, European journal of pharmaceutical

sciences : official journal of the European Federation for Pharmaceutical Sciences, 63 (2014) 29-35.

[7] Y. Xu, C.S. Kim, D.M. Saylor, D. Koo, Polymer degradation and drug delivery in PLGA-based drug-polymer applications: A review of experiments and theories, Journal of biomedical materials research. Part B, Applied biomaterials, (2016).

[8] C. Fornaguera, N. Feiner-Gracia, G. Caldero, M.J. Garcia-Celma, C. Solans, Galantamine-loaded PLGA nanoparticles, from nano-emulsion templating, as novel advanced drug delivery systems to treat neurodegenerative diseases, Nanoscale, 7 (2015) 12076-12084.

[9] Z.J. Huo, S.J. Wang, Z.Q. Wang, W.S. Zuo, P. Liu, B. Pang, K. Liu, Novel nanosystem to enhance the antitumor activity of lapatinib in breast cancer treatment: Therapeutic efficacy evaluation, Cancer science, 106 (2015) 1429-1437.

[10] L.J. Cruz, M.A. Stammes, I. Que, E.R. van Beek, V.T. Knol-Blankevoort, T.J. Snoeks, A. Chan, E.L. Kaijzel, C.W. Lowik, Effect of PLGA NP size on efficiency to target traumatic brain injury, Journal of controlled release : official journal of the Controlled Release Society, 223 (2016) 31-41.

[11] S. Matsunaga, T. Kishi, N. Iwata, Memantine monotherapy for Alzheimer's disease: a systematic review and meta-analysis, PloS one, 10 (2015) e0123289.

[12] G. Joshi, A. Kumar, K. Sawant, Bioavailability enhancement, Caco-2 cells uptake and intestinal transport of orally administered lopinavir loaded PLGA nanoparticles, Drug delivery, (2016) 1-31.

[13] S. Zhu, S. Chen, Y. Gao, F. Guo, F. Li, B. Xie, J. Zhou, H. Zhong, Enhanced oral bioavailability of insulin using PLGA nanoparticles co-modified with cell-penetrating peptides and Engrailed secretion peptide (Sec), Drug delivery, 23 (2016) 1980-1991.

[14] L. Inchaurraga, N. Martin-Arbella, V. Zabaleta, G. Quincoces, I. Penuelas, J.M. Irache, In vivo study of the mucus-permeating properties of PEG-coated nanoparticles following oral administration, European journal of pharmaceutics and biopharmaceutics : official journal of Arbeitsgemeinschaft fur Pharmazeutische Verfahrenstechnik e.V, 97 (2015) 280-289.

[15] F.T. Meng, G.H. Ma, W. Qiu, Z.G. Su, W/O/W double emulsion technique using ethyl acetate as organic solvent: effects of its diffusion rate on the characteristics of microparticles, Journal of controlled release : official journal of the Controlled Release Society, 91 (2003) 407-416.

[16] A. Lamprecht, N. Ubrich, M. Hombreiro Perez, C. Lehr, M. Hoffman, P. Maincent, Influences of process parameters on nanoparticle preparation performed by a double emulsion pressure homogenization technique, International journal of pharmaceutics, 196 (2000) 177-182.

[17] M.F. Zambaux, F. Bonneaux, R. Gref, P. Maincent, E. Dellacherie, M.J. Alonso, P. Labrude, C. Vigneron, Influence of experimental parameters on the characteristics of poly(lactic acid) nanoparticles prepared by a double emulsion method, Journal of controlled release : official journal of the Controlled Release Society, 50 (1998) 31-40.

[18] U. Bilati, E. Allemann, E. Doelker, Sonication parameters for the preparation of biodegradable nanocapsules of controlled size by the double emulsion method, Pharmaceutical development and technology, 8 (2003) 1-9.

[19] G. Abrego, H.L. Alvarado, M.A. Egea, E. Gonzalez-Mira, A.C. Calpena, M.L. Garcia, Design of nanosuspensions and freeze-dried PLGA nanoparticles as a novel approach for ophthalmic delivery of pranoprofen, Journal of pharmaceutical sciences, 103 (2014) 3153-3164.

[20] T. Andreani, L. Miziara, E.N. Lorenzon, A.L. de Souza, C.P. Kiill, J.F. Fangueiro, M.L. Garcia, P.D. Gremiao, A.M. Silva, E.B. Souto, Effect of mucoadhesive polymers on the in vitro performance of insulin-loaded silica nanoparticles: Interactions with mucin and biomembrane models, European journal of pharmaceutics and biopharmaceutics : official journal of Arbeitsgemeinschaft fur Pharmazeutische Verfahrenstechnik e.V, 93 (2015) 118-126.

[21] A.A. Almeida, D.R. Campos, G. Bernasconi, S. Calafatti, F.A. Barros, M.N. Eberlin, E.C. Meurer, E.G. Paris, J. Pedrazzoli, Determination of memantine in human plasma by liquid chromatography-electrospray tandem mass spectrometry: application to a bioequivalence study, Journal of chromatography. B, Analytical technologies in the biomedical and life sciences, 848 (2007) 311-316.

[22] T. Andreani, C.P. Kiill, A.L. de Souza, J.F. Fangueiro, L. Fernandes, S. Doktorovova, D.L. Santos, M.L. Garcia, M.P. Gremiao, E.B. Souto, A.M. Silva, Surface engineering of silica nanoparticles for oral insulin delivery: characterization and cell toxicity studies, Colloids and surfaces. B, Biointerfaces, 123 (2014) 916-923.

[23] J.F. Fangueiro, T. Andreani, M.A. Egea, M.L. Garcia, S.B. Souto, A.M. Silva, E.B. Souto, Design of cationic lipid nanoparticles for ocular delivery: development, characterization and cytotoxicity, International journal of pharmaceutics, 461 (2014) 64-73.

[24] R. Minkeviciene, P. Banerjee, H. Tanila, Memantine improves spatial learning in a transgenic mouse model of Alzheimer's disease, The Journal of pharmacology and experimental therapeutics, 311 (2004) 677-682.

[25] I. Pedros, D. Petrov, M. Allgaier, F. Sureda, E. Barroso, C. Beas-Zarate, C. Auladell, M. Pallas, M. Vazquez-Carrera, G. Casadesus, J. Folch, A. Camins, Early alterations in energy

metabolism in the hippocampus of APPswe/PS1dE9 mouse model of Alzheimer's disease, Biochimica et biophysica acta, 1842 (2014) 1556-1566.
[26] A. Nagakura, Y. Shitaka, J. Yarimizu, N. Matsuoka, Characterization of cognitive deficits in a transgenic mouse model of Alzheimer's disease and effects of donepezil and memantine, European journal of pharmacology, 703 (2013) 53-61.
[27] H. Steuer, A. Jaworski, B. Elger, M. Kaussmann, J. Keldenich, H. Schneider, D. Stoll, B. Schlosshauer, Functional characterization and comparison of the outer blood-retina barrier and the blood-brain barrier, Investigative ophthalmology & visual science, 46 (2005) 1047-1053.
[28] C. Zhang, X. Wan, X. Zheng, X. Shao, Q. Liu, Q. Zhang, Y. Qian, Dual-functional nanoparticles targeting amyloid plaques in the brains of Alzheimer's disease mice, Biomaterials, 35 (2014) 456-465.
[29] D. Porquet, P. Andres-Benito, C. Grinan-Ferre, A. Camins, I. Ferrer, A.M. Canudas, J. Del Valle, M. Pallas, Amyloid and tau pathology of familial Alzheimer's disease APP/PS1 mouse model in a senescence phenotype background (SAMP8), Age, 37 (2015) 9747.
[30] K.K. Cheng, C.F. Yeung, S.W. Ho, S.F. Chow, A.H. Chow, L. Baum, Highly stabilized curcumin nanoparticles tested in an in vitro blood-brain barrier model and in Alzheimer's disease Tg2576 mice, The AAPS journal, 15 (2013) 324-336.
[31] S.K. Sonkusare, C.L. Kaul, P. Ramarao, Dementia of Alzheimer's disease and other neurodegenerative disorders--memantine, a new hope, Pharmacological research, 51 (2005) 1-17.
[32] E. Vega, M.A. Egea, A.C. Calpena, M. Espina, M.L. Garcia, Role of hydroxypropyl-beta-cyclodextrin on freeze-dried and gamma-irradiated PLGA and PLGA-PEG diblock copolymer nanospheres for ophthalmic flurbiprofen delivery, International journal of nanomedicine, 7 (2012) 1357-1371.
[33] S.K. Sahoo, J. Panyam, S. Prabha, V. Labhasetwar, Residual polyvinyl alcohol associated with poly (D,L-lactide-co-glycolide) nanoparticles affects their physical properties and cellular uptake, Journal of controlled release : official journal of the Controlled Release Society, 82 (2002) 105-114.

[34] A. Parra, M. Mallandrich, B. Clares, M.A. Egea, M. Espina, M.L. Garcia, A.C. Calpena, Design and elaboration of freeze-dried PLGA nanoparticles for the transcorneal permeation of carprofen: Ocular anti-inflammatory applications, Colloids and surfaces. B, Biointerfaces, 136 (2015) 935-943.

[35] M.V. Lokhande, M. Kumar Gupta, N.G. Rathod, Structural Elucidation of Process Related Impurity in Memantine Hydrochloride Bulk Drug by GCMS, NMR and IR Techniques, Int J Med Pharm Sci, 3 (2013) 107-114.

[36] M. Gajendiran, V. Gopi, V. Elangovan, R.V. Murali, S. Balasubramanian, Isoniazid loaded core shell nanoparticles derived from PLGA-PEG-PLGA tri-block copolymers: in vitro and in vivo drug release, Colloids and surfaces. B, Biointerfaces, 104 (2013) 107-115.

[37] A. Vasconcelos, E. Vega, Y. Perez, M.J. Gomara, M.L. Garcia, I. Haro, Conjugation of cell-penetrating peptides with poly(lactic-co-glycolic acid)-polyethylene glycol nanoparticles improves ocular drug delivery, International journal of nanomedicine, 10 (2015) 609-631.

[38] S. Zhu, S. Chen, Y. Gao, F. Guo, F. Li, B. Xie, J. Zhou, H. Zhong, Enhanced oral bioavailability of insulin using PLGA nanoparticles co-modified with cell-penetrating peptides and Engrailed secretion peptide (Sec), Drug delivery, 23 (2016) 1980-1991.

[39] M.B. Hesselink, B.G. De Boer, D.D. Breimer, W. Danysz, Brain Penetration and in Vivo Recovery of NMDA Receptor Antagonists Amantadine and Memantine: A Quantittative Microdialysis Study, Pharm Res, 16 (1999) 637-642.

[40] S. Samnick, S. Ametamey, K.L. Leenders, P. Vontobel, G. Quack, C.G. Parsons, H. Neu, P.A. Schubiger, Electrophysiological study, biodistribution in mice, and preliminary PET evaluation in a rhesus monkey of 1-amino-3-[18F]fluoromethyl-5-methyl-adamantane (18F-MEM): a potential radioligand for mapping the NMDA-receptor complex, Nuclear medicine and biology, 25 (1998) 323-330.

[41] I. Cacciatore, M. Ciulla, E. Fornasari, L. Marinelli, A. Di Stefano, Solid Lipid Nanoparticles as a Drug Delivery System for the Treatment of Neurodegenerative Diseases, Expert Opin Drug Deliv, 5247 (2016) 1121-1131.

[42] S.L. Valles, P. Dolz-Gaiton, J. Gambini, C. Borras, A. Lloret, F.V. Pallardo, J. Viña, Estradiol or Genistein Prevent Alzheimer's Disease-Associated Inflammation Correlating with an Increase PPAR Gamma Expression in Cultured Astrocytes, Brain Res, 1312 (2010) 138-144.

Table 1. Values of the matrix of a factorial design of sonication parameters and measured responses. Bold values correspond to the optimized formulation of MEM loaded NPs.

	Amplitude		1st sonication time		2nd sonication time		Z_{av} (nm)	PI	ZP (mV)	EE (%)
	Coded level	(%)	Coded level	(s)	Coded level	(s)				
Factorial points										
F1	-1	25.0	-1	20.0	-1	120.0	390.4 ± 2.2	0.213 ± 0.039	-6.73 ± 0.04	3.46
F2	1	35.0	-1	20.0	-1	120.0	249.7 ± 4.7	0.069 ± 0.022	-6.33 ± 0.49	9.59
F3	-1	25.0	1	40.0	-1	120.0	184.6 ± 0.7	0.125 ± 0.023	-6.43 ± 0.45	42.57
F4	1	35.0	1	40.0	-1	120.0	227.0 ± 2.6	0.057 ± 0.019	-6.72 ± 0.33	36.89
F5	-1	25.0	-1	20.0	1	240.0	243.0 ± 0.9	0.194 ± 0.012	-6.72 ± 0.24	7.43
F6	1	35.0	-1	20.0	1	240.0	248.1 ± 1.9	0.053 ± 0.037	-6.48 ± 0.15	14.69
F7	-1	25.0	1	40.0	1	240.0	258.7 ± 4.5	0.198 ± 0.011	-6.35 ± 0.33	22.63
F8	1	35.0	1	40.0	1	240.0	206.4 ± 1.2	0.061 ± 0.045	-6.67 ± 0.30	2.88
Axial points										
F9	**1.68**	**38.4**	**0**	**30.0**	**0**	**180.0**	**222.4 ± 2.4**	**0.033 ± 0.011**	**-5.63 ± 0.37**	**39.12**
F10	-1.68	21.6	0	30.0	0	180.0	162.6 ± 0.4	0.262 ± 0.012	-6.83 ± 0.37	39.36
F11	0	30.0	1.68	47.0	0	180.0	226.7 ± 4.4	0.236 ± 0.011	-6.49 ± 0.25	19.94
F12	0	30.0	-1.68	13.0	0	180.0	196.8 ± 2.5	0.103 ± 0.056	-6.47 ± 0.55	43.10
F13	0	30.0	0	30.0	1.68	281.0	239.8 ± 0.7	0.056 ± 0.020	-5.77 ± 0.47	23.39
F14	0	30.0	0	30.0	-1.68	79.0	382.6 ± 5.2	0.221 ± 0.011	-5.93 ± 0.21	33.95
Center points										
F15	0	30.0	0	30.0	0	180.0	220.1 ± 5.6	0.059 ± 0.019	-5.36 ± 0.03	24.01
F16	0	30.0	0	30.0	0	180.0	222.1 ± 3.6	0.062 ± 0.021	-5.36 ± 0.11	23.23

Table 2. Values of the matrix of a factorial design of concentration parameters and measured responses. Bold values correspond to the optimized formulation of MEM loaded NPs.

	$C_{PLGA-PEG}$		C_{MEM}		C_{PVA}		Z_{av} (nm)	PI	ZP (mV)	EE (%)
	Coded level	(mg/ml)	Coded level	(mg/ml)	Coded level	(mg/ml)				
Factorial points										
F1	-1	10	-1	3	-1	2.5	270.0 ± 2.4	0.081 ± 0.002	-13.4 ± 0.93	50.45
F2	1	30	-1	3	-1	2.5	450.1 ± 6.6	0.306 ± 0.022	-8.27 ± 0.16	60.84
F3	-1	10	1	9	-1	2.5	230.1 ± 3.2	0.034 ± 0.026	-2.95 ± 0.23	98.98
F4	1	30	1	9	-1	2.5	369.3 ± 3.4	0.287 ± 0.028	-3.33 ± 0.13	98.76
F5	-1	10	-1	3	1	7.5	324.4 ± 3.8	0.188 ± 0.009	-9.79 ± 0.27	57.74
F6	1	30	-1	3	1	7.5	287.8 ± 4.6	0.139 ± 0.029	-7.84 ± 0.25	72.07
F7	**-1**	**10**	**1**	**9**	**1**	**7.5**	**177.9 ± 2.9**	**0.034 ± 0.030**	**-3.81 ± 0.44**	**81.23**
F8	1	30	1	9	1	7.5	223.4 ± 0.6	0.063 ± 0.007	-3.88 ± 0.17	84.87
Axial points										
F9	1.68	37	0	5	0	5	260.4 ± 1.6	0.102 ± 0.018	-8.85 ± 0.53	66.08
F10	-1.68	3	0	5	0	5	147.1 ± 0.7	0.032 ± 0.007	-4.96 ± 0.17	69.52
F11	0	20	1.68	11	0	5	204.3 ± 2.5	0.081 ± 0.018	-3.86 ± 0.27	52.84
F12	0	20	-1.68	1	0	5	238.8 ± 0.7	0.077 ± 0.013	-14.5 ± 0.45	55.33
F13	0	20	0	5	1.68	9.2	199.0 ± 2.1	0.071 ± 0.027	-5.59 ± 0.19	57.27
F14	0	20	0	5	-1.68	0.8	272.2 ± 2.1	0.103 ± 0.033	-3.26 ± 0.19	65.65
Center points										
F15	0	20	0	5	0	5	213.1 ± 0.4	0.023 ± 0.024	-6.03 ± 0.27	72.61
F16	0	20	0	5	0	5	211.7 ± 0.3	0.034 ± 0.023	-5.96 ± 0.16	40.92

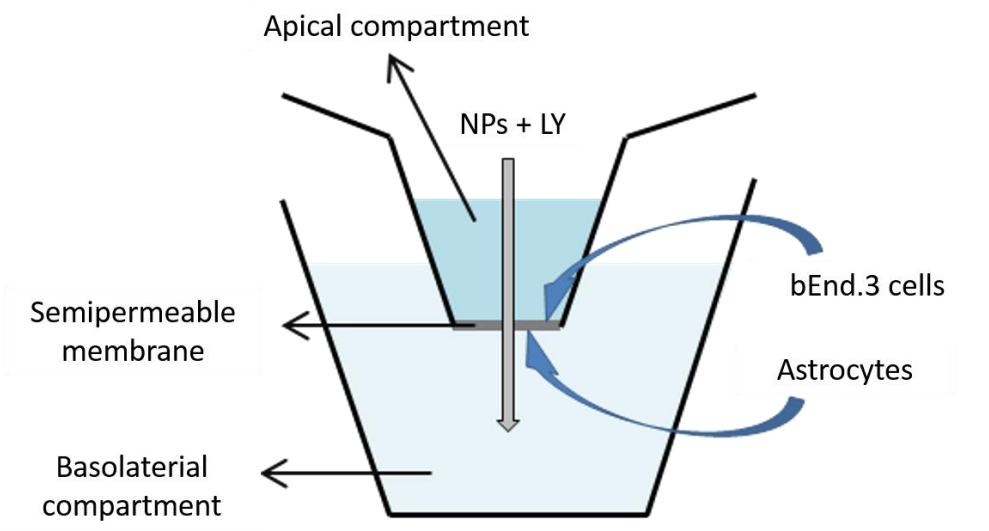

Figure 1. Representation of the blood-brain barrier model to assess *in vitro* transport of nanoparticles.

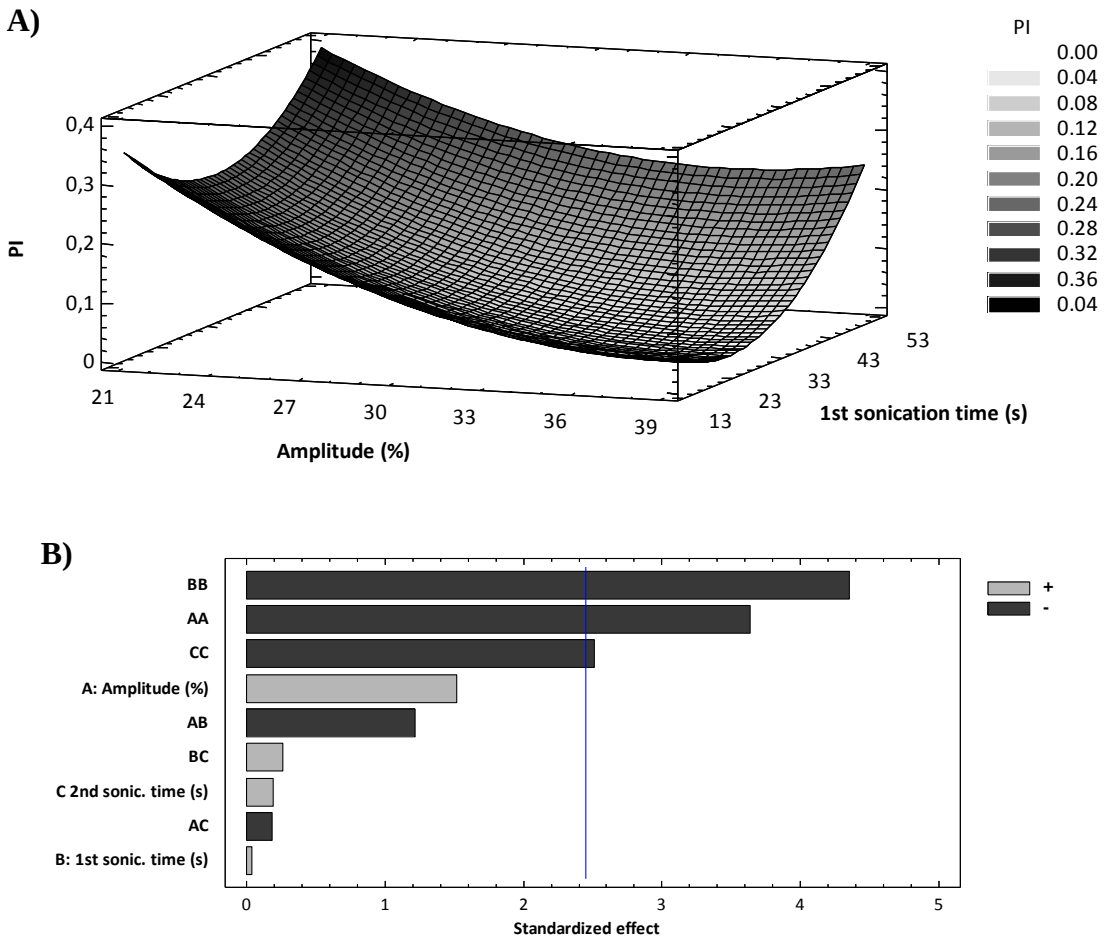

Figure 2. DoE of sonication parameters **A)** Surface plot of MEM-PLGA-PEG NPs PI and **B)** Pareto's chart of the effect of sonication parameters on ZP

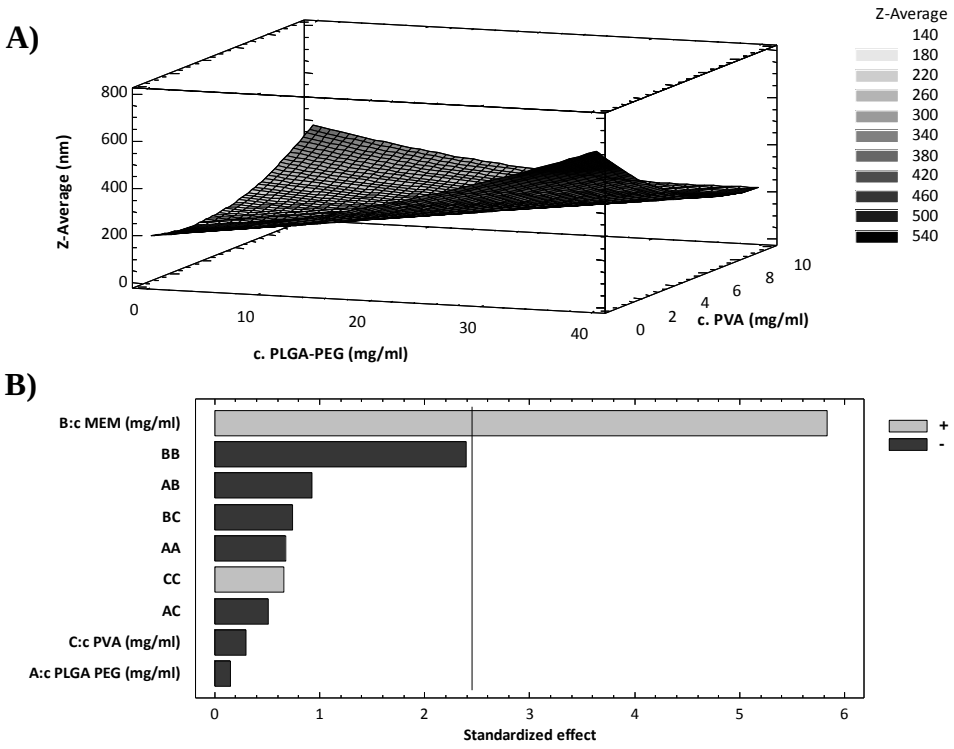

Figure 3. DoE of concentration parameters; A) Surface plot of MEM –PLGA-PEG NPs z-AVE and B) Effect of compounds concentration on ZP.

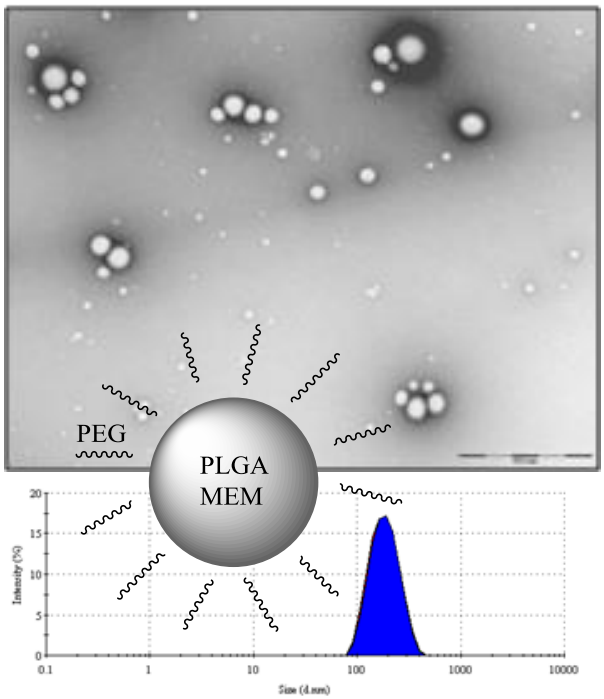

Figure 4. MEM-PLGA-PEG NPs transmission electron microscopy and size distribution obtained by dynamic light scattering.

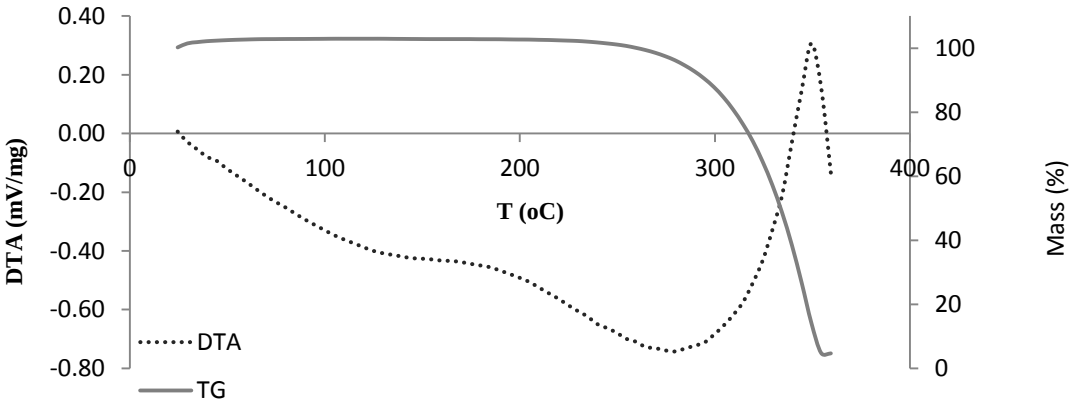

Figure 5. MEM thermogravimetric and differential thermal analysis.

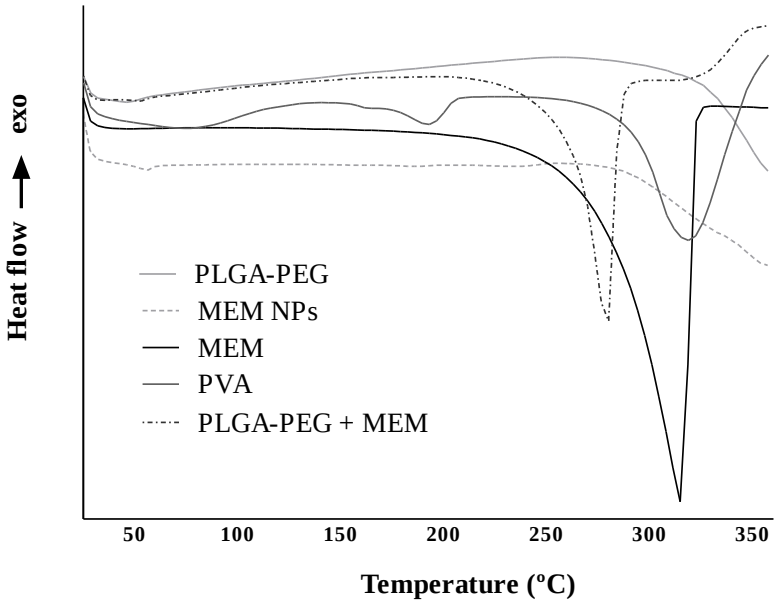

Figure 6. MEM-PLGA-PEG NPs differential scanning calorimetry analysis.

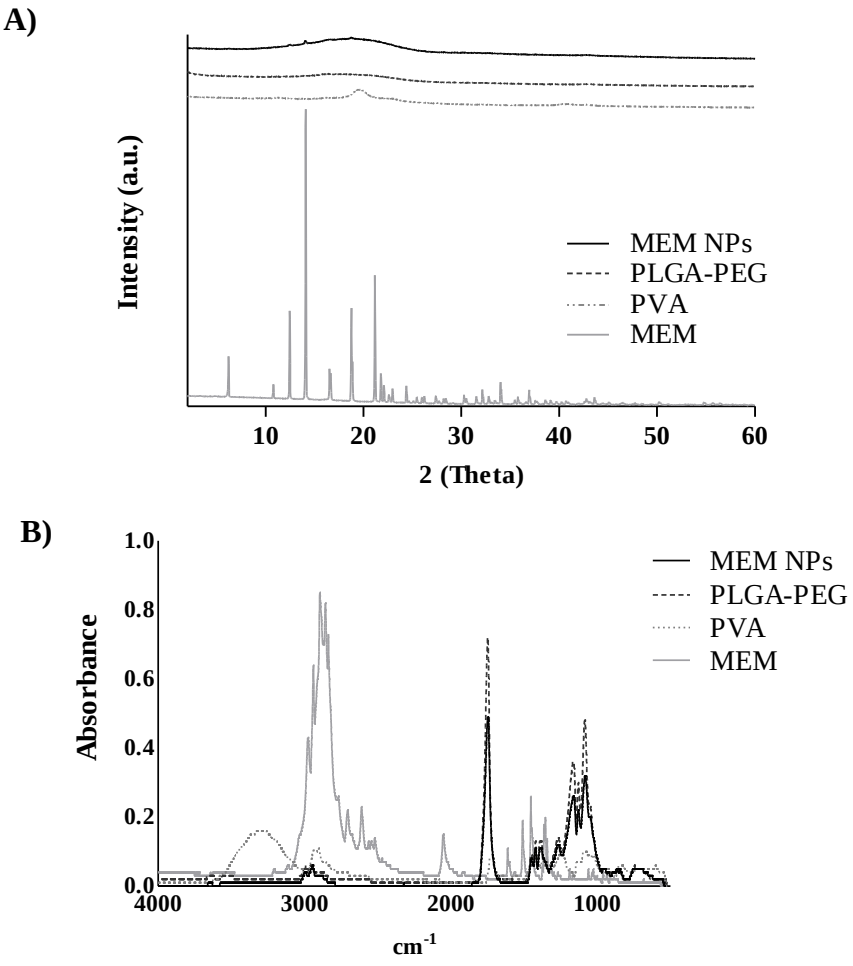

Figure 7. MEM-PLGA-PEG NPs interaction studies **A)** X-Ray diffraction and **B)** Fourier transformed infra-red analysis

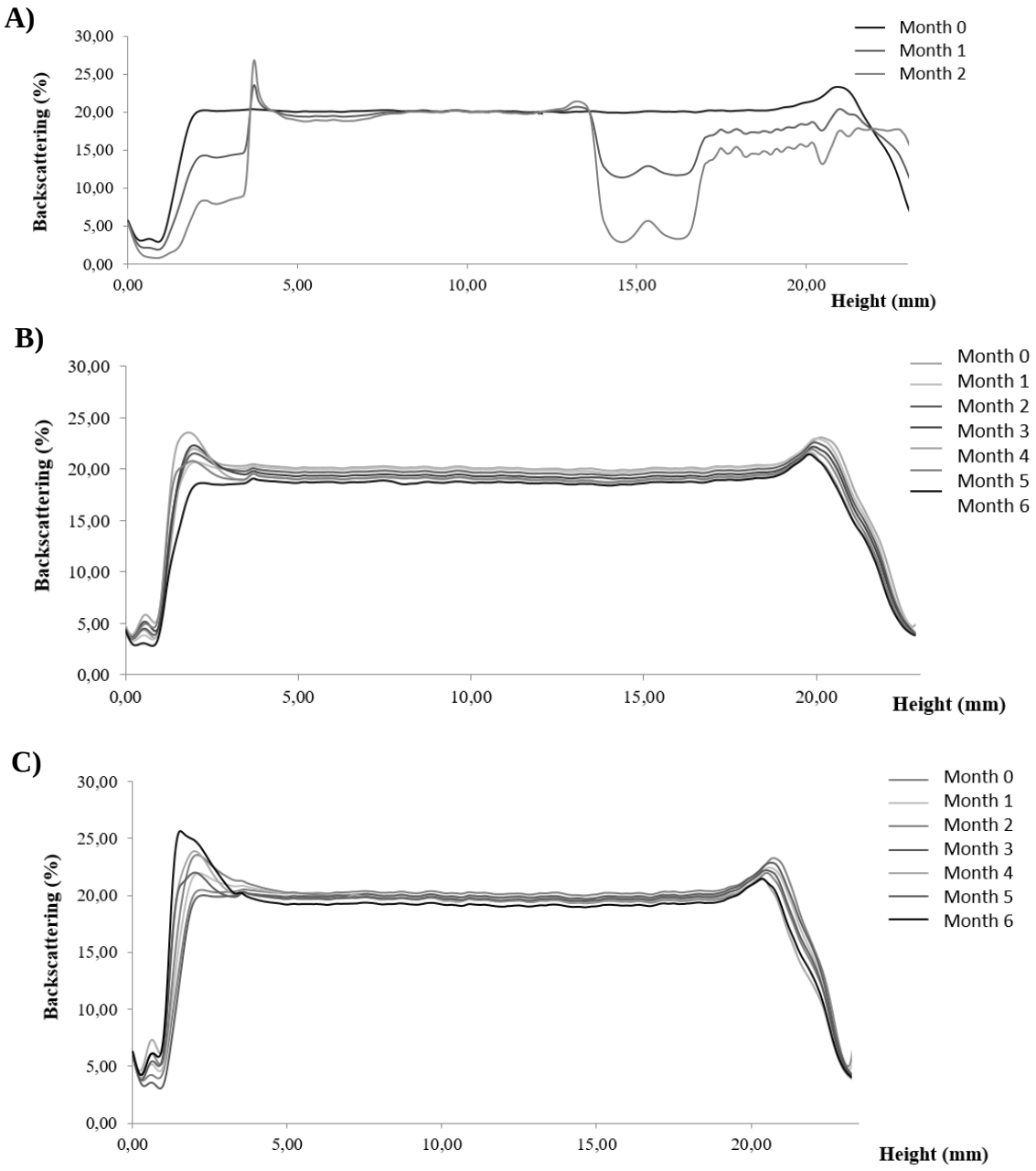

Figure 8. Backscattering profile of MEM-PLGA-PEG NPs stored for 6 months; A) 38ºC, B) 25ºC and C) 4ºC.

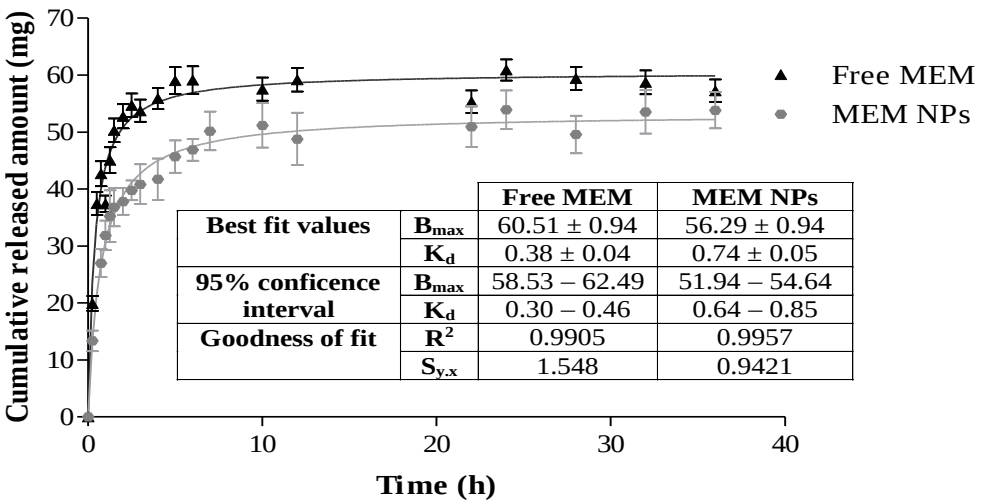

		Free MEM	MEM NPs
Best fit values	B_{max}	60.51 ± 0.94	56.29 ± 0.94
	K_d	0.38 ± 0.04	0.74 ± 0.05
95% conficence interval	B_{max}	58.53 – 62.49	51.94 – 54.64
	K_d	0.30 – 0.46	0.64 – 0.85
Goodness of fit	R^2	0.9905	0.9957
	$S_{y.x}$	1.548	0.9421

Figure 9. *In vitro* release profile of MEM from PBS solution or MEM-PLGA-PEG NPs. Mean parameters were obtained adjusting data to hyperbola equation.

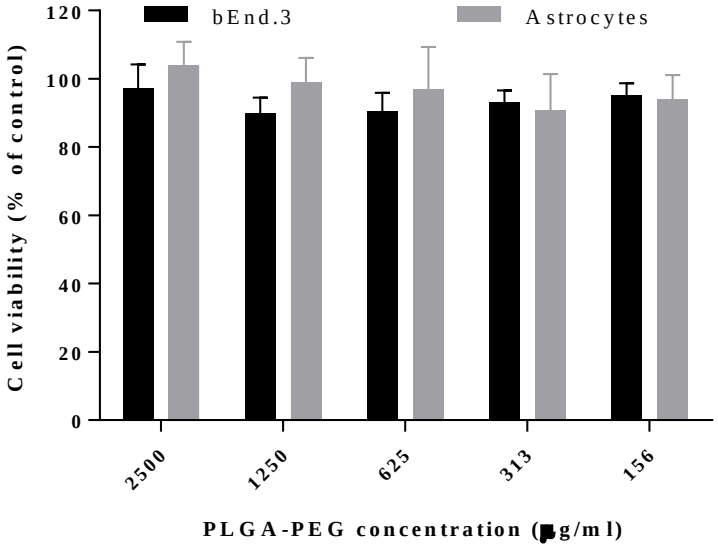

Figure 10. Cell viability assessment using Alamar blue on brain cell lines.

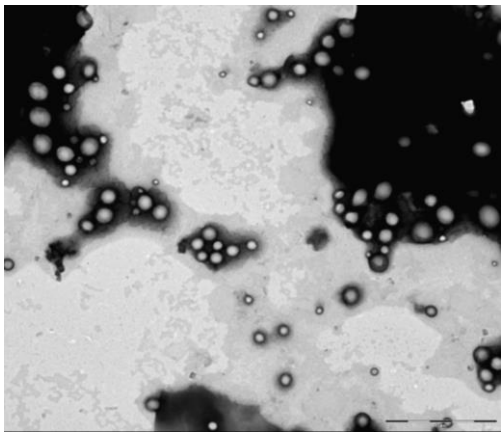

Figure 11. TEM pictures of MEM-PEG-PLGA-NPs on the basolateral compartment of the BBB transport model after one hour of incubation.

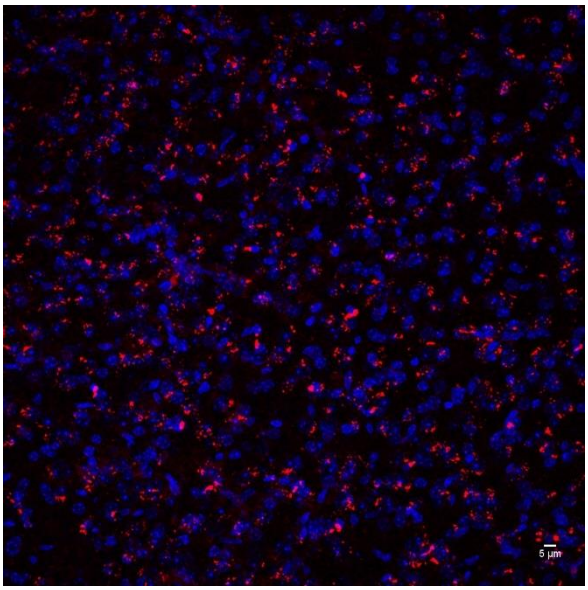

Figure 12. Confocal microscopy image of brain section of WT mice treated with oral Rho-loaded NPs.

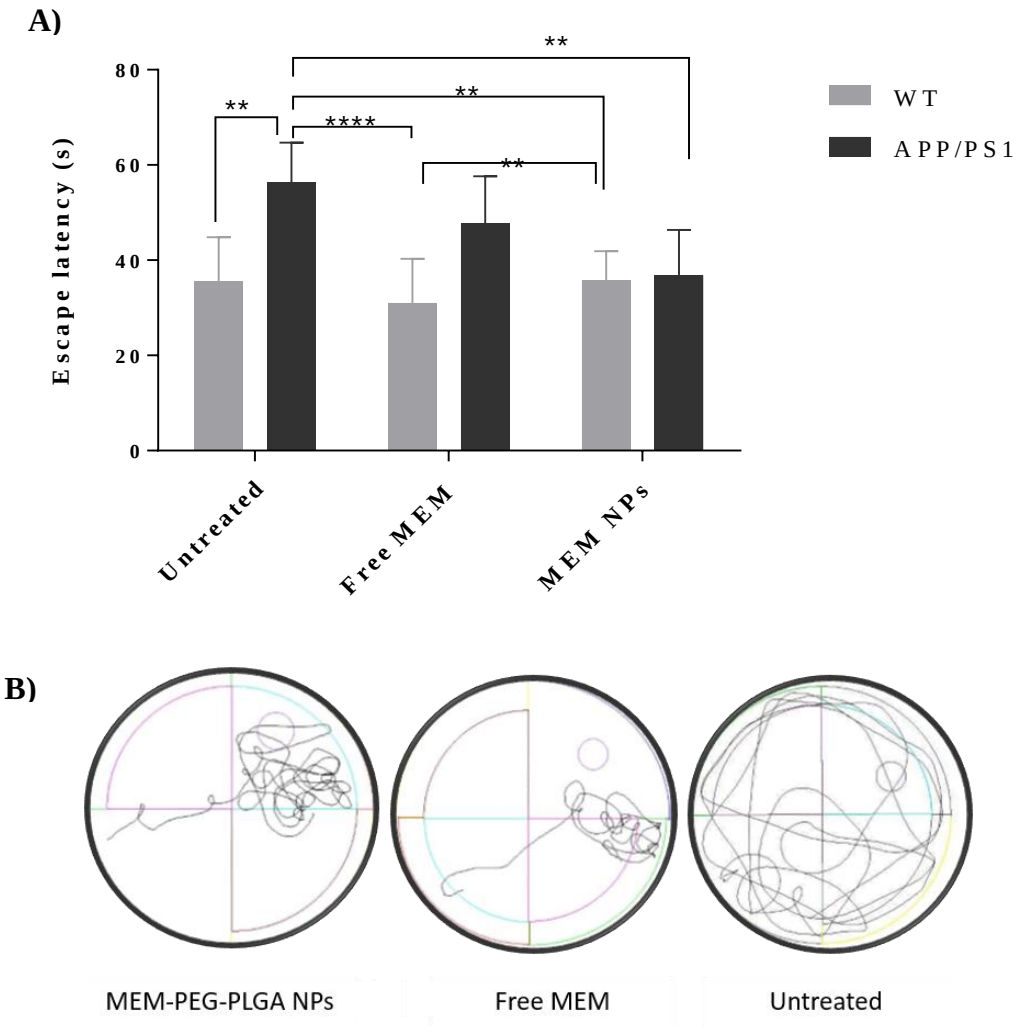

Figure 13. Morris water maze results on the probe trail. **A)** Escape latency and **B)** Representative swimming path of transgenic mice. Data represent mean ± SD; *p < 0.05, **p < 0.01, ***p < 0.001, ****p<0.0001.

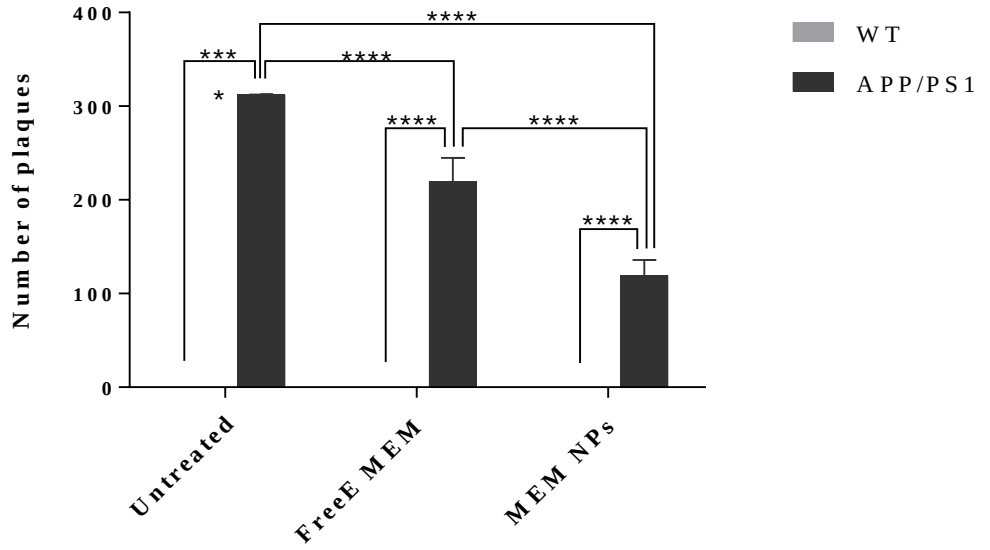

Figure 14. Amyloid plaques counting. Data represent mean ± SD; *p < 0.05, **p < 0.01, ***p < 0.001

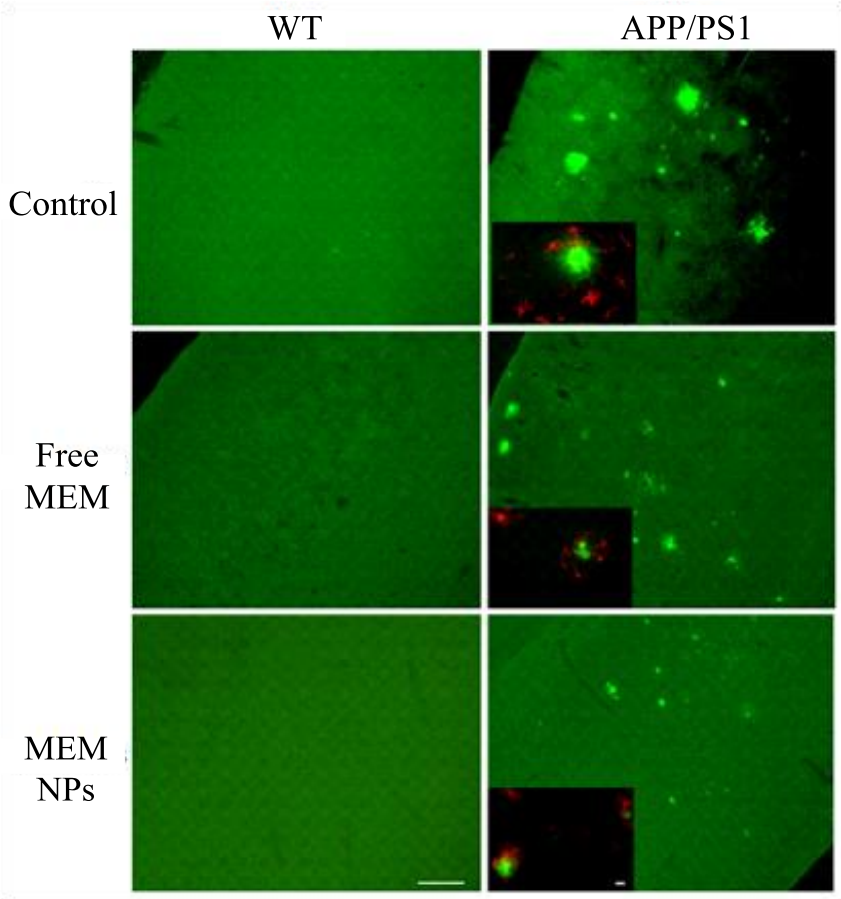

Figure 15. Immunohistochemically (cortex) staining of amyloid plaques (green) and GFAP (red) of WT and APP/PS1 mice (untreated, MEM free and MEM loaded NPs). Bar reference equivalent to 100m.

3.2. NEW POTENTIAL STRATEGIES FOR ALZHEIMER'S DISEASE PREVENTION: PEGYLATED BIODEGRADABLE DEXIBUPROFEN NANOSPHERES ADMINISTRATION TO APPSWE/PS1DE9

Elena Sánchez-López, Miren Ettcheto, Maria Antonia Egea, Marta Espina, Ana Cristina Calpena, Jaume Folch, Antoni Camins, Maria Luisa García

Nanomedicine: Nanotechnology, Biology and Medicine. 13 (2017) 1171 -1182

Doi: 10.1016/j.nano.2016.12.003

BASIC SCIENCE

Nanomedicine: Nanotechnology, Biology, and Medicine
13 (2017) 1171 –1182

Original Article

nanomedjournal.com

New potential strategies for Alzheimer's disease prevention: pegylated biodegradable dexibuprofen nanospheres administration to APPswe/PS1dE9

Elena Sánchez-López, MD[a,b], Miren Ettcheto, MD[c,d], Maria Antonia Egea, PhD[a,b], Marta Espina, PhD[a,b], Ana Cristina Calpena, PhD[a,b], Jaume Folch, PhD[d,e], Antoni Camins, PhD[c,d], Maria Luisa García, PhD[a,b,*]

[a]*Department of Pharmacy and Pharmaceutical Technology and Physical Chemistry, Faculty of Pharmacy, University of Barcelona*
[b]*Institute of Nanoscience and Nanotechnology (IN2UB), Faculty of Pharmacy, University of Barcelona*
[c]*Department of Pharmacology and Therapeutic Chemistry, Faculty of Pharmacy, University of Barcelona*
[d]*Biomedical Research Networking Center in Neurodegenerative Diseases (CIBERNED), Madrid, Spain*
[e]*Biochemistry unit, Faculty of Medicine and Health Sciences, University Rovira i Virgili, Reus Tarragona, Spain*

Received 24 May 2016; accepted 6 December 2016

Abstract

Dexibuprofen loaded pegylated poly(lactic-co-glycolic) nanospheres prepared by solvent diffusion method were designed to increase Dexibuprofen brain delivery reducing systemic side effects. Nanospheres exhibited a mean particle size around 200 nm (195.4 nm), monomodal population and negative surface charge. Drug loaded nanospheres showed a sustained release profile, allowing to modify the posology *in vivo*. Nanospheres were non-toxic neither in brain endothelial cells nor astrocytes and do not cause blood–brain barrier disruption. Nanospheres were able to partially cross the cells barrier and release the drug after co-culture *in vitro* experiments, increasing Dexibuprofen permeation coefficient. Behavioral tests performed in APPswe/PS1dE9 mice (mice model of familial Alzheimer's disease) showed that nanospheres reduce memory impairment more efficiently than the free drug. Developed nanospheres decrease brain inflammation leading to β-amyloid plaques reduction. According to these results, chronical oral Dexibuprofen pegylated poly(lactic-co-glycolic) nanosystems could constitute a suitable strategy for the prevention of neurodegeneration.

Key words: Nanoparticles; Nanospheres; PLGA-Peg; Dexibuprofen; Blood–Brain barrier; Alzheimer's disease

Currently, Alzheimer's disease (AD) is a multifactorial and incurable neurodegenerative condition highly prevalent in old age.[1] It is widely accepted that brain increase in β-amyloid (Aβ) levels, mainly Aβ42, and TAU phosphorylation are the main markers of the disease. Thus, approximately 25 years ago Hardy et al[2] proposed the "amyloid cascade hypothesis", where Aβ42 was primarily responsible of neuronal damage in AD. However, it has been demonstrated that Aβ42 cannot completely explain

the process of neuronal loss in AD because drugs developed against Aβ42 do not improve all the related disease symptomatology. Thus, alternative hypothesis had been developed, among them, the neuroinflammatory hypothesis where AD could be considered as a chronic brain inflammatory process. Neuroinflammatory responses are characteristic of pathologically affected tissue in neurodegenerative disorders such as Parkinson disease, epilepsy and AD.[3] Several evidences have been found indicating that increased peripheral inflammation leads to more neurodegeneration and accelerated disease progression in animal models.[4]

Inflammation occurs in vulnerable regions of the AD brain, with increased expression of acute phase proteins and proinflammatory cytokines, which are hardly evident in a normal brain. Glial cells (microglia and astrocytes) are responsible for the inflammatory reaction through the generation of inflammatory mediators stimulated by Aβ42 oligomers and plaques containing dystrophic neurites. Chronically activated glial cells can contribute to neuronal dysfunction and cell death through the release of highly toxic products.[5]

Several studies confirm that the long-term treatment with non-steroidal anti-inflammatory drugs (NSAIDs) such as ibuprofen, reduce the risk of AD, delay disease onset, ameliorate symptomatic severity, and slow cognitive decline.[3,6] However, an important clinical limitation of ibuprofen, and in general of NSAIDs clinical administration, are the gastrointestinal adverse effects. These can be reduced by the use of the active enantiomer, dexibuprofen (DXI), which is twice more potent than the former.[7] DXI has been assessed on short-term treatment by Jin and co-workers[3] on animal models of AD achieving successful results. In clinical studies, this enantiomer demonstrates to cause less side effects than the racemic mixture being therefore a good candidate to prevent AD. However, the typical secondary effects associated with NSAIDs (such as gastric toxicity) still appeared in human trials and would increase with long-term administration.[7–9] In addition, due to the low water solubility of DXI, this drug exhibits many *in vivo* limitations like incomplete release, poor bioavailability, food interactions, and high inter-subject variability.[10] Side effects caused by continuous DXI administration could be overcome by the use of the drug encapsulated on nanostructured systems. To carry the drug across the blood–brain-barrier (BBB), facilitate its posology and avoid undesired side effects, polymeric nanoparticles (NPs) have been proposed.

Biodegradable polymers such as poly(lactic-co-glycolic acid) (PLGA) had been approved by the Food and Drug Administration (FDA) and used as colloidal carriers for drug controlled release.[11,12] Among other carriers, PLGA possess several advantages such as its biocompatibility, biodegradability and non-toxicity. Furthermore, these synthetic polymers demonstrate higher reproducibility, are easily formulated and allow the control and prediction of the degradation kinetics.[13] Coating of PLGA NPs with poly(ethylene glycol) (PEG) represents an improvement since it increase particles circulation avoiding their recognition by the reticuloendothelial system.[14]

The main goal of this work was the development of a formulation for brain delivery of DXI, based on nanospheres (NSs) composed of PLGA surrounded by PEG chains (DXI-PLGA-PEG NSs). The suitability of DXI-PLGA-PEG NSs to treat and prevent inflammation associated with AD has been demonstrated. *In vitro* studies of NSs transport across the BBB were undertaken and *in vivo* effectivity of the developed NSs on transgenic mice for AD were carried out.

Methods

PLGA-PEG 5% Resomer® was obtained from Evonik Corporation (Birmingham, USA) and the active compound *S*-(+)-Ibuprofen (dexibuprofen) was purchased from Amadis Chemical (Hangzou, China). Water filtered through Millipore MilliQ system was used for all the experiments and all the other reagents were of analytical grade.

Nanospheres production

NSs were prepared by solvent displacement method described elsewhere.[15] NSs mean size (Z_{av}) and polidispersity index (PI) of DXI loaded PLGA-PEG NSs were determined by photon correlation spectroscopy (PCS) using a ZetaSizer Nano ZS (Malvern Instruments). Measurements were carried out by triplicate at angles of 180° in 10 mm diameter cells at 25 °C. Zeta potential (ZP) was calculated from electrophoretic mobility.[16]

The encapsulation efficiency (EE) of DXI in the NSs was determined indirectly. The non-entrapped DXI was separated using filtration/centrifugation. DXI was measured by HPLC method as is described on previous publications.[17]

Design of experiments

Design of experiments (DoE) was applied to optimize formulation parameters using a full factorial design.[18] Series of independent parameters and their influences in DXI loaded NSs were studied, determining the effects and interactions between factors.[19]

As can be observed on Table 1, concentration of each formulation compound and pH of the aqueous phase were used as independent variables and Z_{av}, PI and ZP of the NSs were studied.

Nanospheres characterization

To visualize the optimized DXI loaded NSs, negative staining was carried out with uranyl acetate (2%) on copper grids activated with UV light. NSs morphology was determined by transmission electron microscopy (TEM), performed on a JEOL 1010 microscope (Akishima, Japan).

Storage stability

DXI loaded NSs stability at 4, 25 and 38 °C was assessed studying light backscattering and transmission profiles by using Turbiscan®Lab. For this purpose, a glass measurement cell was filled with 20 ml of sample. The radiation source was a pulsed near infrared light and was received by a transmission and backscattering detectors at an angles of 90 and 45° from the incident beam, respectively. Data were acquired once a month for 24 h at 1 h intervals.

Table 1
Design of experiments of DXI loaded NSs.

	Independent variables								Dependent varibales			
	c. PLGA (mg/ml)	PEG	c. PVA (mg/ml)		c. DXI (mg/ml)		pH		Z_{av} (nm)	PI	ZP (mV)	EE (%)
Factorial points												
F1	1	7.5	-1	12.0	-1	1.5	-1	3.8	212.6 ± 1.0	0.166 ± 0.016	-11.1 ± 0.3	91.06
F2	1	7.5	1	18.0	-1	1.5	1	5.3	193.8 ± 1.0	0.057 ± 0.013	-12.3 ± 0.5	81.22
F3	-1	4.5	-1	12.0	1	4.5	1	5.3	170.2 ± 1.0	0.055 ± 0.010	-6.3 ± 0.7	90.81
F4	-1	4.5	1	18.0	1	4.5	1	5.3	166.4 ± 1.3	0.074 ± 0.021	-9.9 ± 0.9	99.99
F5	-1	4.5	-1	12.0	-1	1.5	1	5.3	161.6 ± 0.7	0.085 ± 0.001	-9.0 ± 0.3	88.13
F6	-1	4.5	1	18.0	1	4.5	-1	3.8	168.5 ± 1.1	0.091 ± 0.032	-8.4 ± 0.6	97.73
F7	1	7.5	-1	12.0	1	4.5	1	5.3	192.4 ± 1.0	0.052 ± 0.019	-8.3 ± 1.7	94.38
F8	1	7.5	1	18.0	1	4.5	-1	3.8	222.1 ± 2.9	0.171 ± 0.066	-3.2 ± 4.3	97.99
F9	-1	4.5	-1	12.0	1	4.5	-1	3.8	103.2 ± 9.6	0.369 ± 0.547	-0.1 ± 0.3	95.40
F10	1	7.5	1	18.0	-1	1.5	-1	3.8	249.6 ± 5.3	0.205 ± 0.018	-17.1 ± 0.6	96.47
F11	-1	4.5	1	18.0	-1	1.5	-1	3.8	260.7 ± 11.0	0.314 ± 0.012	-12.5 ± 1.1	95.36
F12	-1	4.5	1	18.0	-1	1.5	1	5.3	163.9 ± 0.6	0.060 ± 0.018	-7.4 ± 0.8	92.78
F13	1	7.5	-1	12.0	-1	1.5	1	5.3	199.4 ± 10.4	0.203 ± 0.029	-11.7 ± 0.4	87.18
F14	1	7.5	1	18.0	1	4.5	1	5.3	293.6 ± 6.7	0.235 ± 0.039	-15.1 ± 0.9	96.82
F15	-1	4.5	-1	12.0	-1	1.5	-1	3.8	185.4 ± 1.3	0.053 ± 0.015	-8.6 ± 0.8	93.16
F16	1	7.5	-1	12.0	1	4.5	-1	3.8	196.5 ± 0.9	0.068 ± 0.006	-5.9 ± 0.5	93.04
Axial points												
F17	0	6	0	15.0	0	3.0	-1.68	3.2	181.3 ± 1.1	0.069 ± 0.027	-8.1 ± 3.7	97.94
F18	0	6	-1.68	10.0	0	3.0	0	4.5	177.8 ± 1.1	0.060 ± 0.009	-12.4 ± 0.5	95.23
F19	-1.68	3.5	0	15.0	0	3.0	0	4.5	196.9 ± 2.7	0.207 ± 0.014	-10.3 ± 0.5	94.35
F20	0	6	0	15.0	0	3.0	0	4.5	204.7 ± 4.1	0.151 ± 0.027	-9.4 ± 0.7	88.69
F21	0	6	1.68	20.0	0	3.0	0	4.5	310.7 ± 21.8	0.197 ± 0.046	-12.9 ± 0.5	96.42
F22	0	6	0	15.0	-1.68	0.5	0	4.5	214.7 ± 9.47	0.212 ± 0.052	-16.2 ± 0.3	81.75
F23	0	6	0	15.0	1.68	5.5	0	4.5	227.8 ± 17.7	0.224 ± 0.014	-11.7 ± 0.1	96.77
F24	1.68	8.5	0	15.0	0	3.0	0	4.5	230.4 ± 20.2	0.191 ± 0.032	-19.0 ± 0.6	99.20
F25	0	6	0	15.0	0	3.0	1.68	5.8	180.1 ± 4.7	0.073 ± 0.039	-11.9 ± 0.5	94.45
Central points												
F26	0	6	0	15.0	0	3.0	0	4.5	204.7 ± 0.4	0.151 ± 0.008	-9.4 ± 0.3	88.69
F27	0	6	0	15.0	0	3.0	0	4.5	172.6 ± 1.0	0.083 ±0.025	-8.8 ± 0.6	99.19

In vitro drug release

An inverse dialysis was performed under "sink conditions". This technique is based on the dispersion of the colloidal suspension in the dialysis medium (buffer solution) at 37 °C.[20] At predetermined time intervals, one sac containing 1 ml of sample was withdrawn from the stirred release medium and simultaneously replaced with 1 ml of fresh buffer at the same temperature.

Akaike's information criterion, AIC, was determined as an indicator of the model's suitability for a given dataset. The model associated to the smallest AIC value is considered as giving the best fit of the set of data.[19]

Cell culture

Different cell lines were cultured for *in vitro* studies: cells derived from rat pheochromocytoma (PC12), mouse microvascular endothelial cells (bEnd.3 cells) and primary glial cells from brain rat cortex (astrocytes). PC12 cells were obtained from Sigma-Aldrich®. Primary cultures of astrocytes were obtained from bank Gaiker-IK4 culture. Glial cells were from Sprague Dawley cerebral cortex of newborn rats. The endothelial cell line was maintained in its specific culture medium.[21]

Cytotoxicity studies

The dye Alamar Blue is widely used as indicator of cell viability.[22] Absorbance was determined at λ of 570 nm (reduced form) and 620 nm (oxidized form) after incubating the cells with DXI NSs at different concentrations for 24 h. Data were analyzed by calculating the percentage of Alamar blue reduction and expressed as percentage of control.[22,23]

In vitro transport across the BBB

In vitro BBB models have become a standard tool to estimate the ability of drugs to overcome this barrier.[24] For co-culture experiments, bEnd.3 cells were seeded in the apical part of polycarbonate transwell inserts. A semipermeable filter was placed and in the basolateral compartment cells from primary cultures of rat astrocytes were added at a density of $6 \cdot 10^4$ cells/ml.[25]

Trans-epithelial electrical resistance (TEER) manual measurements were taken daily until a steady state was reached. To calculate the TEER of each insert, (Eq. (1)) was applied and values are expressed in Ω · cm^2.

TEER ¼ ½Ω cell monolayer − Ω filter ðwithout cellsÞ] · filter surface ð1Þ

bEnd.3 cells were co-cultured on the apical part of the inserts placing astrocytes on the basolateral compartment. Inserts were removed and placed in new media plates with Hanks +0.5% bovine serum albumin (BSA). Apical media was removed, washed with Hanks and DXI loaded NSs were added in the apical part of the inserts and were left for one hour.

In order to verify that DXI loaded NSs do not cause membrane disruption, a low paracellular permeability compound was added and quantified at the end of the study, namely, Lucifer yellow (LY). Membrane integrity was also determined.

NSs quantification on the basolateral compartment was carried out measuring PEG chains on a Triple Quadrupole LC/MS/MS Mass Spectrometer in MRM with a positive mode. Source was a Turbo Spray a 400 °C and separation module was a UPLC Acquity. Mobile phase was composed of methanol: water (0.1% formic acid) and a gradient was applied. Mass variation was recorded at 710.8 and 89.10 Da. Proton nuclear magnetic resonance spectra (^{1}H–NMR) was used to confirm that PLGA-PEG DXI structure after crossing the barrier (supplementary material S1). The spectrum was recorded at 298 K on a Varian Inova 500 MHz spectrometer (Agilent Technologies, Santa Clara, CA, USA).[26]

Cellular uptake

Cellular internalization was measured by labeling the DXI NSs with Rhodamine. PC12 cells were cultured, collected, counted and then transferred to a 24-well plate and incubated overnight. Then the cell culture medium was replaced with medium containing Rho DXI NSs (2.5 mg/ml) and incubated for a predetermined times (5, 10, 15 and 30 min). After incubation, suspended NSs were removed and cells were washed trice with PBS to remove unbound NSs. Cell membranes were permeabilized by cell lysis solution and the fluorescence was read by spectrofluorometric methods.[27]

In vivo studies

Male APPswe/PS1dE9 (APP) and C57BL/6 mice age matched with the same background were used. APP/PS1 animals co-express a Swedish (K594 M/N595 L) mutation of a chimeric mouse/human APP (Mo/HuAPP695swe), together with the human exon-9-deleted variant of PS1 (PS1-dE9), allowing these mice to secrete elevated amounts of human Aβ peptide.[28] The animals were kept under controlled temperature, humidity and light conditions with food and water provided *ad libitum*. Mice were treated in accordance with the European Community Council Directive 86/609/EEC and the procedures established by the Department d'Agricultura, Ramaderia i Pesca of the Generalitat de Catalunya. Every effort was made to minimize animal suffering and to reduce the number of animals used. Forty animals of 6 month-old, divided into four groups were used for the present study.

Biodistribution studies

Biodistribution was determined with Rho DXI NSs and 300 µl were administered by oral gavage. After 24 h, animals were sacrificed and tissues were weighted, collected, and homogenized. DXI NSs extraction with methanol was carried out and fluorescence of Rhodamine was measured by fluorescence spectrometry at λ_{ex} 553 nm and λ_{em} 627 nm. Data were normalized with the negative control from mice treated with saline only.

Long-term treatment in vivo studies

Mice were treated for three months with DXI at therapeutic doses (50 mg/kg/day) and DXI loaded NSs were administered on alternate days.[28,29] NSs volume was calculated for each animal previously weighted and was administered on a drinking bottle. Afterwards, NSs drinking bottle was replaced by untreated water for 24 h. Following *in vivo* testing, the animals were sacrificed and at least 6 mice in each group were used for histological studies.[30]

Gastric damage

After treatment, mice were sacrificed and stomachs were removed, cut and rinsed with ice-cold distilled water. The ulcer index (UI) was determined.[31,32] The severity of the lesions was calculated as reported by other authors.[33] After scoring, the stomachs were frozen at −20 °C for 24 h. Samples were allowed to thaw at room temperature losing the surface mucosa from the underlying tissue. The mucosa was removed by scrapping with the edge of a microscope slide, freeze dried and weighted.[32]

Morris water maze

The Morris water maze (MWM) test was conducted in a circular tank. The water tank was colored white at a temperature of 21 ± 2 °C. A white platform was submerged in the middle of the northeast quadrant. Behavioral data were acquired and analyzed using a computerized video tracking system. The test procedure consisted of a six-day navigation testing with five trials per day and a probe trail. Animals were allowed to swim freely for 60 s to seek the platform and allowed to remain there for 10 s. If after 60 s a mouse was not able to find the platform, it was guided to it and left there for 30 s. The probe trail was performed the day after the last training test. This day, the hidden platform was removed, and the mice were released from the southwest quadrant and allowed to swim for 60 s. Results were calculated individually for each animal.[34]

Western blot analysis

Aliquots of hippocampus homogenate were analyzed using the Western blot method and normalized to GAPDH as previously described.[35] Measurements are expressed as arbitrary units.

Immunohistochemistry studies

To elucidate whether the differences in the cognitive behavior correlate with AD-related pathology on the brain, mice were anesthetized with sodium pentobarbital and perfused with 4% paraformaldehyde. Brains were stored at 4 °C overnight dehydrated in 30% phosphate-buffered sucrose solution. Samples were preserved at -80 °C and coronal sections of 20 µm were obtained by a cryostat (Leica Microsystems, Wetzlar, Germany).

Sections were incubated overnight at 4 °C with the rabbit antibodies against GFAP (1:2000; Dako, Glostrup, Denmark) and IBA-1 (1:1000, Wako) and sequentially incubated for 2 h with Alexa Fluor 594 goat anti-rabbit antibody at room temperature (1:500; Invitrogen, Eugene, OR, USA). Images were processed using ImageJ by comparing the different conditions and quantifying the integrated density.

Staining of β-Amyloid plaques was performed using Thioflavin S (ThS 0.002%, Sigma-Aldrich). Sections were counterstained with 0.1 µg/ml Hoechst 33,258 (Sigma-Aldrich, St Louis, MO, USA).[36] Samples were additionally stained with monoclonal anti-βA 1–42 (1:1000; Covance, USA) at 4 °C overnight.[37]

Samples were visualized using a fluorescence microscope (BX41 Laboratory Microscope, Melville, NY-Olympus America Inc). For each image, the proportion of total image area covered by fluorescently stained β-amyloid plaques was quantified. For each mouse, four fields per section with the highest density of plaques were chosen as representative and averaged.[38]

Statistical analysis

All of the data are presented as the mean ± S.D. Two-way ANOVA followed by Tukey *post hoc* test was performed for multi-group comparison. Student's *t* test was used for two-group comparisons. Statistical significance was set at $P<0.05$ by using GraphPad 5.00 Prism.

Results

Design of experiments

Design of experiments (DoE) was used to optimize formulation parameters in order to obtain small and monomodal DXI loaded NSs (Z_{av} b 200 nm, PI b0.1) able to cross the BBB. Regarding NSs size, polymer concentration and PVA amount are the factors presenting a significant relationship (P b 0.05). As is shown in Figure 1, *A*, increasing both polymer and surfactant concentration leads to higher NSs Z_{av}. The opposite effect was found regarding PI, were high polymer concentrations produced less NSs size dispersion. As can be observed in Table 1, ZP values are negative due to polymer negative charge. Subse- quently, higher polymer concentrations lead to more negative surface charge being NSs more stable (P b 0.05).[17] As is shown in Figure 1, *B*, this parameter is also affected by DXI concentration in an inverse relationship probably due to DXI masking of NSs surface charge. EE results show that as DXI amount increased, EE was also higher. This could be probably due to the great polymer entrapment capacity which is not reached at the studied concentrations and also to the PEG chains in which the drug remains adsorbed. The maximum EE was obtained when the pH of the aqueous phase was similar as the pK_a of the drug (DXI pK_a 4.65). However, this pH increases NSs PI (Figure 1, *C*).

With this trend, a formulation was optimized. Optimized DXI loaded NSs formulation contains 4.5 mg/ml of DXI, 7 mg/ml of polymer, a low PVA amount (10.0 mg/ml) and a pH of 3.8. NSs were centrifuged at 15000 r.p.m. for 30 min and observed by TEM (Figure 2) showing a round shape and a smooth surface.

In vitro release

DXI release data from the NSs were adjusted to hyperbola equation. Initial release corresponds to a burst effect, probably due to the drug adsorbed on NSs surface due to PEG chains.[39] DXI release from the NSs at 6 h achieves a maximum plateau (B_{max}) at 66.65 ± 1.27%, lower than free DXI. Dissociation constant (K_d), for DXI loaded NSs, which corresponds to the time where 50% of the drug is released, was 46.8 ± 3.0 min. These results suggest a faster release as more drug is encapsulated inside the NSs.[17] This would probably be due to

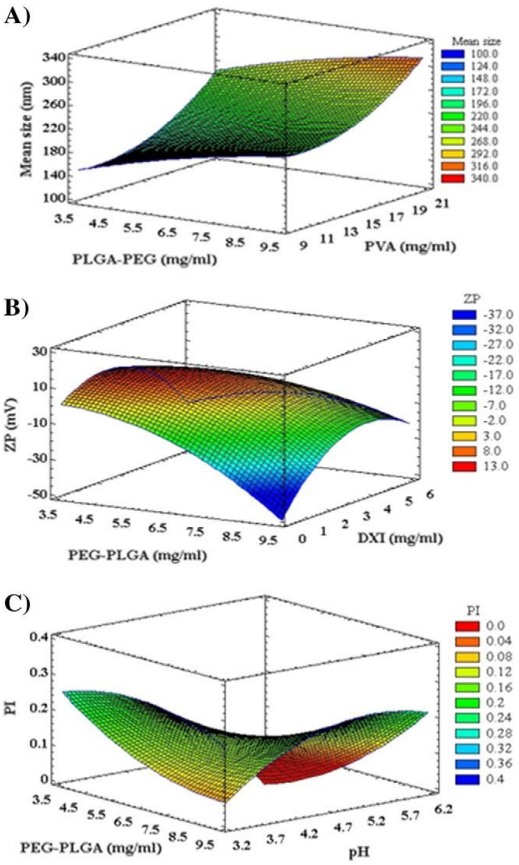

Figure 1. Surface response of DXI loaded NSs. (A) PLGA-PEG and PVA concentration influence on NSs mean size, (B) PLGA-PEG and DXI concentrations influence on NSs ZP and (C) PLGA-PEG concentration and pH influence on NSs PI.

the fact that after 6 h, the NSs are still achieving a sustained drug release whereas after 2 h free DXI was completely released.

Storage stability

Storage stability assays at different temperatures showed that DXI loaded NSs were stable for two months at 25 and at 4 °C. In Figure 3, *A* and *B*, backscattering and transmission profiles at each temperature could be observed. It could be noticed that samples are unstable within two months (differences of backscattering above 10%).[40] As was shown on previous publications, samples present high levels of instability at 38 °C at the end of the first month (Figure 3, *C*) due to polymer degradation processes.[17] These results are in agreement with those obtained by other authors for

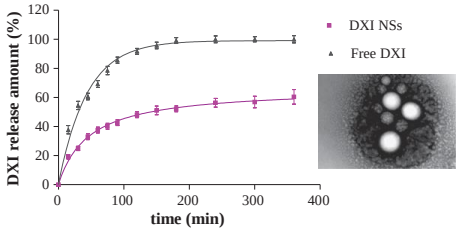

Figure 2. *In vitro* drug release of free DXI (adjusted to first order exponential kinetics) against DXI loaded NSs (adjusted to hyperbola equation) and NSs TEM.

Cytotoxicity assays

Cell viability was studied in both astrocytes and bEnd.3 cells prior to *in vitro* transport experiments. In addition, cytotoxicity was assessed in PC12 cell line.[41,42] As is shown in Figure 4, *A*, in all the cell lines assessed, cell viability was higher than 80%, thus meaning that DXI loaded NSs do not damage neither endothelial brain cells nor neuronal cells in any of the assessed concentrations. These results suggest that the development would be biocompatible with brain cells.[43]

In vitro BBB transport

Co-culture systems effectivity to predict the transport of drugs across the BBB has been demonstrated by other authors.[24] Graphical evidence of the NSs on the basolateral compartment after 1 h of incubation could be observed in Figure 4, *B*. In addition, H^1-NMR results show that both NSs peaks and DXI were present on the basolateral media (supplementary material S1).

According to LY used as a control, NSs at 2.5 mg/ml do not cause damage on the cells forming the BBB being able to preserve membrane integrity. 31.4% of the initial NSs remain inside the cells barrier. DXI was quantified on the basolateral and apical compartments, 28% of the drug was retained by the cells within one hour and drug endothelial permeability coefficient, P_e, was 0.99 cm/s.

Cellular uptake

In order to elucidate if the developed NSs would be able to be internalized by the cells, NSs were labeled fluorescent with Rhodamine (Rho). Fluorescence was measured after cell lysis at different times for both Rhodamine and DXI as is shown in Figure 4, *C*. DXI NSs were found to penetrate almost 100% after the first 5 min of incubation and therefore, DXI would be released inside the cells. In addition, a decreasing in free Rho uptake confirms that the cellular uptake was not due to the additional fluorescent coating.

Biodistribution studies

24 h after Rho DXI NSs administration by oral gavage, a considerable amount of NSs remain on the liver (supplementary material, S2). However, developed NSs were found also on the brain (0.37 mg/ml NSs/g tissue). PEGylation of PLGA NPs post-oral administration demonstrated to increase transport across the BBB.[44] PEGylated NPs have been reported to promote mucus penetration and increase drug half-life, in this case, after 24 h, NSs remain in the brain.[45] Despite this fact, accumulation can be observed on the liver probably due to the elimination route of the nanosystems *via* uptake of Kupffer cells.

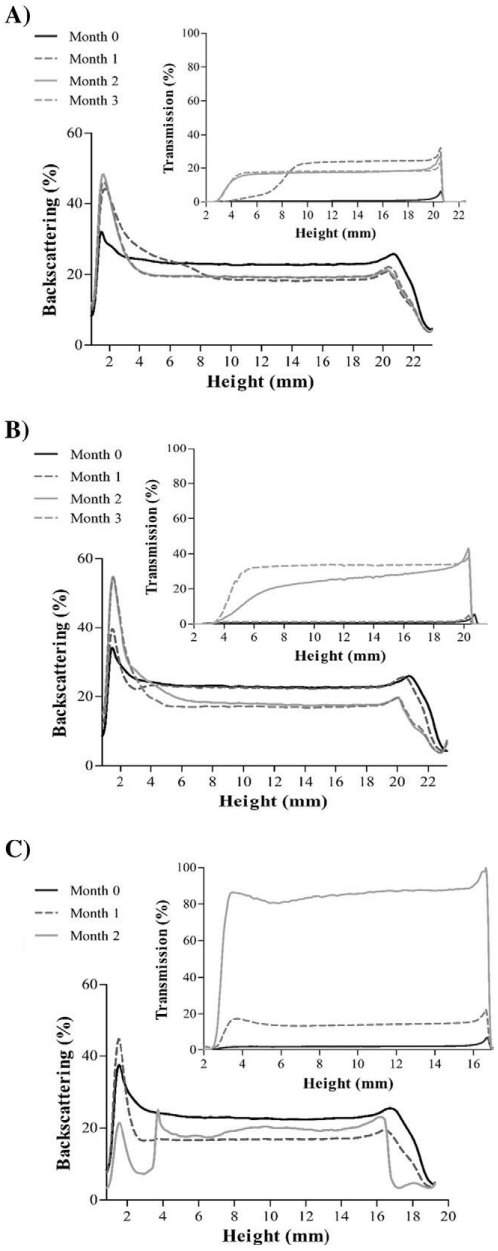

Figure 3. DXI loaded NSs backscattering and transmission profiles stored at different temperatures. (A) 4 °C, (B) 25 °C and (C) 38 °C.

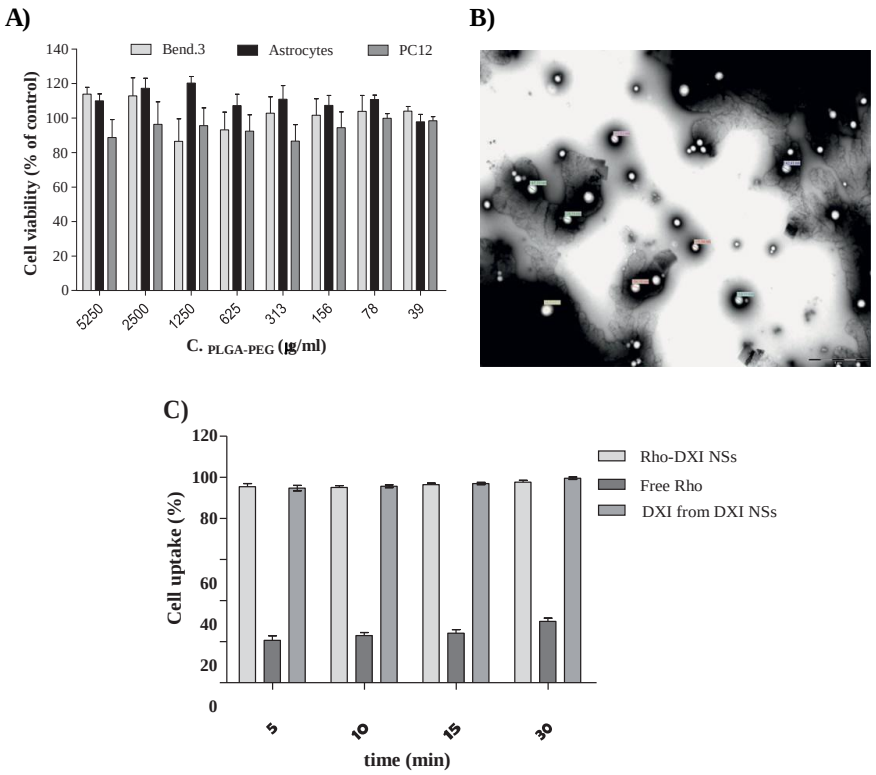

Figure 4. *In vitro* studies (A) Cell viability of DXI loaded NSs with different cell lines (bEnd.3, astrocytes, PC12), (B) TEM image of DXI loaded NSs on the basolateral media after one hour of *in vitro* blood–brain barrier transport assay and (C) Cellular uptake of Rhodamine labeled NSs at different times.

Morris water maze and Western blot analysis

The effect of DXI loaded NSs and free DXI on the spatial learning and memory deficits in APP mice were conducted using the MWM test.

Escape latency of all groups trough the training days is supplied as supplementary material (S3). A clear trend could be established toward mice learning where untreated and free DXI treated groups showed similar learning capacities whereas DXI loaded NSs group present an evolution more similar to WT groups. In Figure 5 results corresponding to the probe trail could be observed. In Figure 5, *A*, statistically significant differences were obtained regarding escape latency between transgenic groups treated either with free DXI or DXI loaded NSs compared with untreated APP animals. In addition, escape latency media corresponding to DXI loaded NSs was lower than the obtained for the free drug.

Regarding the percentage of time spend in the platform zone (Figure 5, *B*), DXI loaded NSs spend higher percentages on this area whereas transgenic control group show no tendency to find the platform. Significant differences were obtained compared with the untreated groups with DXI loaded NSs, whereas free DXI do not shown significant values. The number of times that the animals cross the platform zone is supplied as supplementary material S4. In this parameter, also significant differences are observed with DXI loaded NSs and untreated transgenic groups. The same tendency but without statistical differences was observed for the number of entries on the platform (supplementary material S5). Interestingly, our Western blot results, showed in Figure 5, *C* and *D*, demonstrated that DXI increases the levels of monophosphate response element-binding protein (p-CREB).

Gastric damage

As can be observed on Figure 6, *A*, DXI NSs did not shown significant differences on gastric damage compared with control group. Free drug produced an increase on stomach lesions compared with DXI NSs and control group. Similar results were obtained measuring the mucosal weight showing that free DXI produce significant differences against control group (Pb0.05) as can be observed on Figure 6, *B*.[32]

Immunohistochemistry studies

The formation of Aβ plaques, which is a pathologic hallmark of AD, could be observed by Thioflavin-S staining. Figure 6, *A* shows results corresponding to amyloid plaques counting of

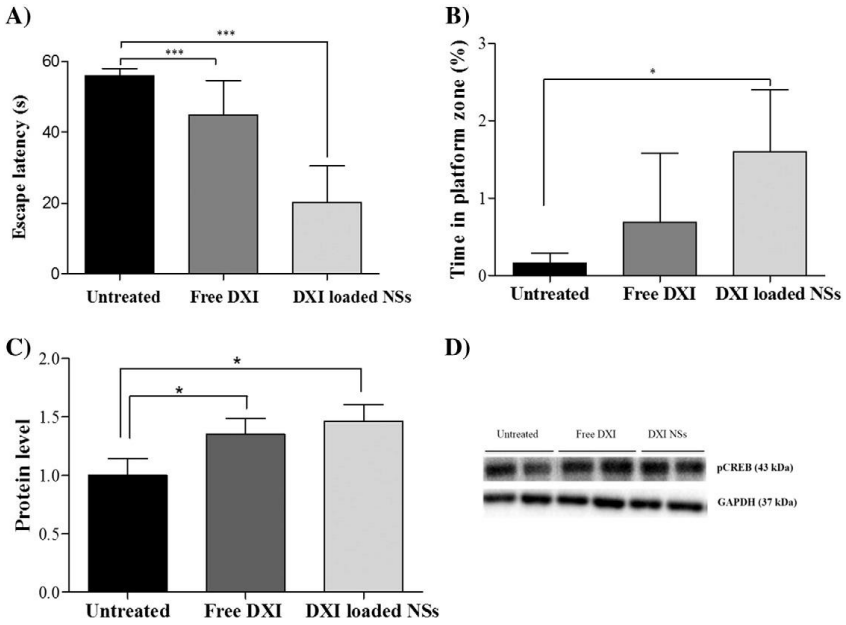

Figure 5. APP/PS1 mice results. (A) Morris water maze escape latency on the probe trial, (B) Morris water maze escape latency time in platform zone on the probe trial, (C) Mean pCREB levels and (D) representative Western blot of pCREB extracted from hippocampus.

APP/PS1 mice on brain cortex. ThS staining was negative for WT groups indicating the absence of fibrillar Aβ.[46] APP mice treated with DXI loaded NSs developed a certain number of plaques, which levels were significantly lower than those obtained for the rest of transgenic groups (*P*b0.001), including free DXI groups. In addition, as can be observed in Figure 6, *B*, plaques developed by free DXI or DXI loaded NSs groups were smaller than the untreated APP group.

Glial cells are the source of released cytokines, which are implicated in the formation of Aβ plaques on AD development.[47] GFAP reactive cells had been defined as an indicator for astrocyte activation and, as is shown in Figure 7, *A* and *C*, the number of reactive cells on the hippocampal brain sections of animals treated by DXI loaded NSs was lower than the untreated transgenic group. The same results, presented on Figure 7, *B* and *D*, were obtained regarding microglial activation (IBA1) showing DXI NSs significant differences (*P*b0.05) with the untreated transgenic groups. In addition, non-significant differences were obtained between DXI loaded NSs and DXI administered continuously.

Discussion

Current therapeutic strategies for AD, suggest that modulation or prevention of chronic neuroinflammation process could be a suitable target for AD prevention. In the present manuscript, we have demonstrated in APP/PS1 mice that DXI loaded NSs have a beneficial effect on key markers of AD namely Aβ plaque formation, glial activation and memory impairment.

The BBB is one of the most restrictive barriers of the body allowing only small molecules such as the developed NSs to cross it. With the purpose to achieve brain drug release upon oral administration, DoE was applied to establish useful trends in NSs behavior in order to obtain a suitable formulation. To obtain NSs Z_{av} below 200 nm with high EE, an intermediate PLGA-PEG concentration and a high drug amount were chosen. The optimized NSs showed EE N 99%, Z_{av} b 200 nm and a narrow monomodal population. The *in vitro* prolonged release of DXI from the NSs could contribute toward a decrease of the drug regime dosage and reduced side effects such as gastric toxicity, both improving patient adherence to the treatment.

Cytotoxicity studies confirm that the developed formulation does not affect cell viability neither on the cells of the BBB (bEnd.3 and astrocytes) or in neuronal cells (PC12). *In vitro* transport across the BBB experiments, show both DXI loaded NSs safety toward the BBB structure without compromising barrier's limited permeability and also suggest that the DXI NSs produced a prolonged release. These results, along with the *in vitro* drug release suggest that NSs would release the drug slowly and part of the NSs would cross the BBB during the first hours of administration, as is confirmed by H^1-RMN and TEM. Ibuprofen is reported by other authors[48] to be poorly distributed to the brain with P_{app} values oscillating between 0.31 and 0.41. To overcome this, optimized NSs would increase free drug P_e proving to be beneficial for brain delivery regarding free drug

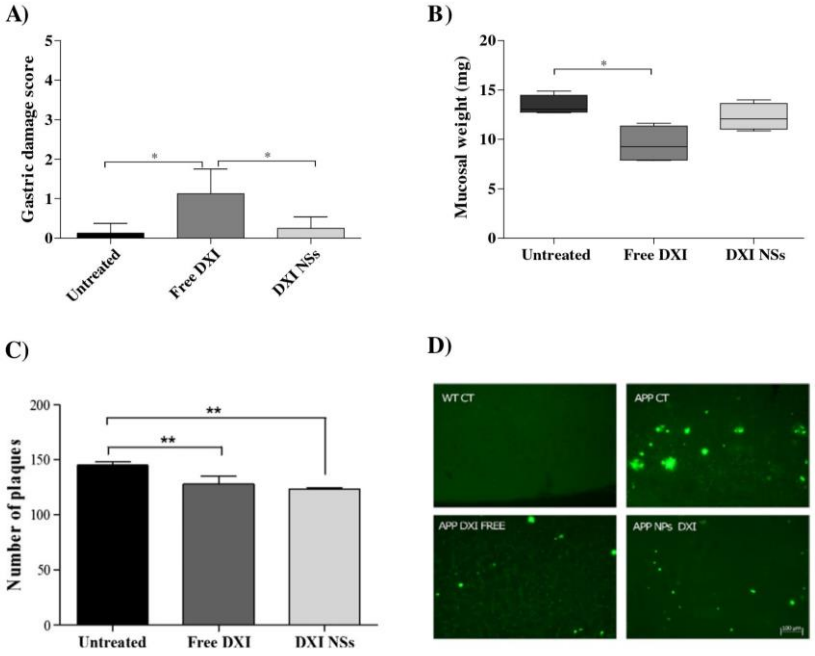

Figure 6. *In vivo* studies after DXI treatment. (A) Gastric damage score, (B) mucosal weight after freeze-drying, (C) mean counting of β-amyloid plaques in brain cortex after Th-S staining and (D) representative microscopic images of β-amyloid plaques.

formulation.[48,49] This could be due to the flexibility of PEG chains which act as a protective shield on the particles surface giving them the so-called stealth properties.[50] According to other authors, PEGylated PLGA NSs would enter later into the cells by claritin-mediated endocytosis.[50]

Biodistribution assays demonstrate that NPs are able to cross the BBB and remain in the brain 24 h after administration. Due to the higher surface area of the NPs and the increased mucoadhesitvity is probable that they are captured by the mucous layer of the GI tract and they are endocited and arrive to the brain *via* systemic circulation. High concentrations founded in the liver demonstrate that the elimination route would be *via* hepatic circulation. In addition, DXI NSs decrease gastric damage produced by the free drug.

In vivo experiments carried out comparing transgenic mice either without treatment or treated with the free drug or with DXI loaded NSs administered on alternate days showed that DXI NSs were more effective on spatial memory improvement than free DXI or untreated animals. In short, these results demonstrated that DXI loaded NSs could improve memory impairment compared to both free DXI and untreated transgenic groups. These positive results of DXI NSs against the free drug can be attributed to drug encapsulation and prolonged release into PEGylated NSs since PEGylation contributes to increase transport across the BBB.[50,51]

In brain cortex, DXI loaded NSs induce a significant amylogenesis decrease, which is one of the hallmarks of AD. Although the mechanism by which inflammation reduction inhibits amylogenesis has not been completely elucidated, a clear relationship is well known between Aβ plaques development and both astrocytes and microglial activation.[47] In the central nervous system, astrocytes and microglial cells are the main types of cells in the inflammatory response.[4] In a non-activated state (physiological conditions) glial cells are of great importance for neuronal plasticity processes and Aβ clearance and degradation. However, under certain conditions related to chronic stress, the role of glial cells may not be beneficial. Effectively, activation of glial cells induces morphologic changes, releasing cytokines, and neurotoxic agents that can worsen brain damage.[5] Interestingly, we demonstrated that brain glial activation in APP mice is prevented effectively by DXI loaded NSs administered on alternate days. These results are in agreement with those obtained for microglial inflammation reduction. Since Aβ42 oligomers and their precursor APP are potent glial activators, our data reinforce the potential chronic application of DXI loaded NSs in AD prevention. Obtained data indicate that DXI loaded NSs, prevent amylogenesis induced by neuroinflammatory processes by blocking cytokines release and glial activation.[47] These results are in accordance with behavioral assays, indicating that DXI restored cognition by

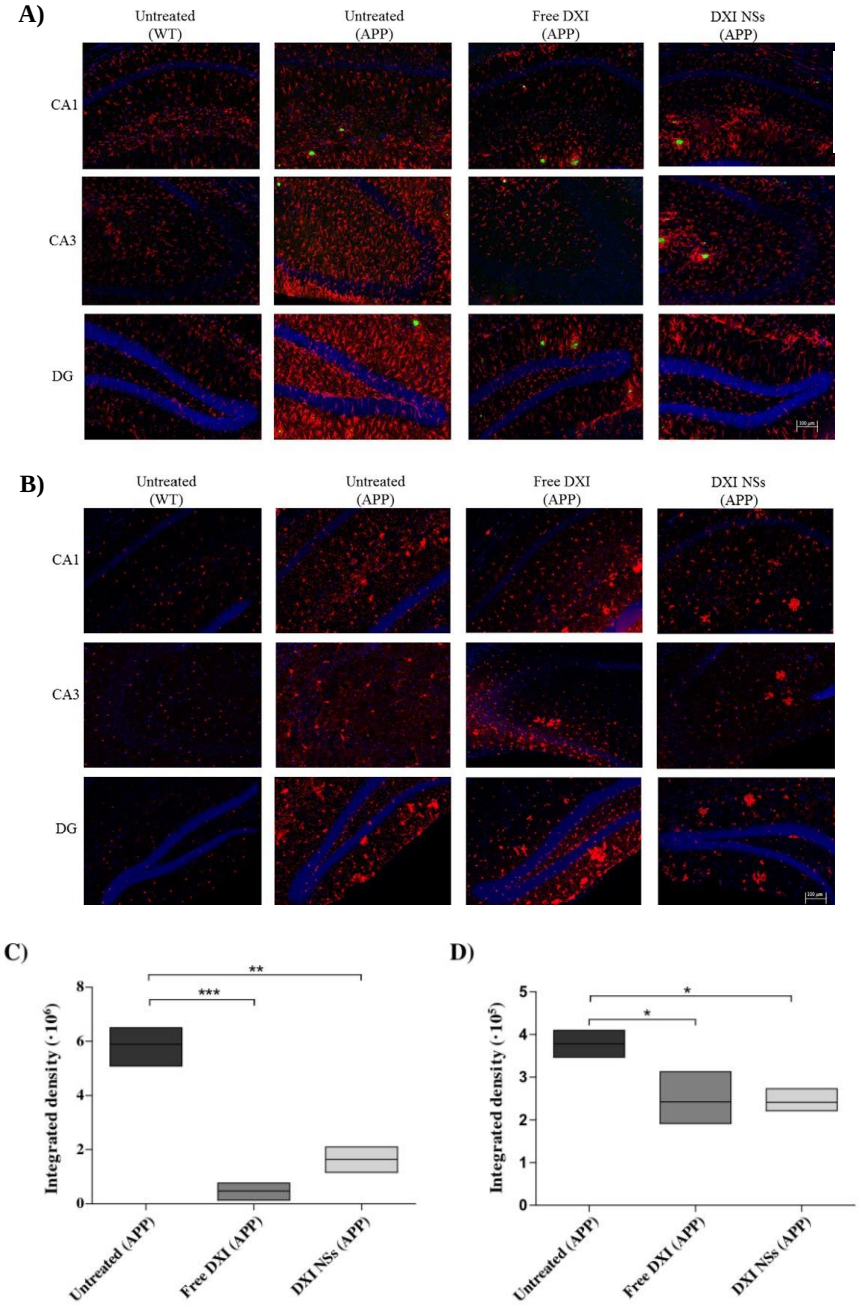

Figure 7. Detection of inflammatory markers on hippocampus subfields on APP/PS1 mice. (**A**) Immunostained for GFAP, ThS and Hoetsch, (**B**) immunostained for IBA-1 and Hoestch, (**C**) quantification of GFAP and (**D**) quantification of IBA-1.

inhibiting the neuroinflammatory response associated with AD thus decreasing insoluble amyloid plaques and interestingly at the molecular levels through the increase of p-CREB. These data are relevant because an increase in p-CREB levels leads to the transcription of memory-associated genes such as *c-fos, ARC, BDNF* that are involved in the process of learning and memory.[52]

In summary, the current study shows that treatment with DXI loaded NSs represent an improvement for AD neuropathological markers, mainly a significant reduction of brain Aβ accumulation, glial activation and improved cognitive performance in APP mice. In addition, DXI loaded NSs were safe for brain cells and suitable for oral administration. Pegylated NSs were capable of increasing drug permeability across the BBB without cause disruption of the barrier. Thus, we suggest that DXI loaded NSs could be a suitable and safe strategy for a chronic treatment for AD prevention.

Appendix A. Supplementary data

Supplementary data to this article can be found online at http://dx.doi.org/10.1016/j.nano.2016.12.003.

References

1. Folch J, Petrov D, Ettcheto M, Abad S, Sánchez-López E, García ML, et al. Current research therapeutic strategies for Alzheimer' s disease treatment. *Neural Plast* 2016;**2016**:1-15.
2. Hardy JA, Higgins A. Alzheimer's disease: the amyloid cascade hypothesis. *Perspective* 1992;**256**:184-5.
3. Jin DQ, Sung JY, Hwang YK, Kwon KJ, Han S-H, Min SS, et al. Dexibuprofen (S(+)-isomer ibuprofen) reduces microglial activation and impairments of spatial working memory induced by chronic lipopolysaccharide infusion. *Pharmacol Biochem Behav* 2008;**89**:404-11.
4. Wyss-coray T, Rogers J. Inflammation in Alzheimer disease — a brief review of the basic science and clinical literature. *Cold Spring Harb Perspect Biol* 2012:1-24, http://dx.doi.org/10.1101/cshperspect.a006346.
5. Rubio-Perez JM, Morillas-Ruiz JM. A review: inflammatory process in Alzheimer's disease, role of cytokines. *Sci World J* 2012;**2012**:1-15.
6. Tabet N, Feldmand H. Ibuprofen for Alzheimer's disease. *Cochrane Database Syst Rev* 2003;**2**.
7. Kaehler ST, Phleps W, Hesse E. Dexibuprofen: pharmacology, therapeutic uses and safety. *Inflammopharmacology* 2003;**11**:371-83.
8. Bonabello A, Galmozzi MR, Canaparo R, Isaia GC, Serpe L, Muntoni E, et al. Dexibuprofen (S(+)-isomer ibuprofen) reduces gastric damage and improves analgesic and antiinflammatory effects in rodents. *Anesth Pharmacol* 2003;**97**:402-8.
9. Phleps W. Overview on clinical data of dexibuprofen. *Clin Rheumatol* 2001;**20**:S15-21.
10. El-Houssieny BM, El-Dein EZ, El-Messiry HM. Enhancement of solubility of dexibuprofen applying mixed hydrotropic solubilization technique. *Drug Discov Ther* 2014;**8**:178-84.
11. Salem SA, Hwei NM, Bin Saim A, Ho CCK, Sagap I, Singh R, et al. Polylactic-co-glycolic acid mesh coated with fibrin or collagen and biological adhesive substance as a prefabricated, degradable, biocompatible, and functional scaffold for regeneration of the urinary bladder wall. *J Biomed Mater Res A* 2013;**101**(A):2237-47.
12. Graf N, Bielenberg DR, Kolishetti N, Muus C, Banyard J, Farokhzad OC, et al. αvβ3 integrin-targeted PLGA-PEG nanoparticles for enhanced anti-tumor efficacy of a Pt(IV) prodrug. *ACS Nano* 2012;**6**:4530-9.
13. Anderson JM, Shive MS. Biodegradation and biocompatibility of PLA and PLGA microspheres. *Adv Drug Deliv Rev* 2012;**64**:72-82.
14. Griffiths PC, Cattoz B, Ibrahim MS, Anuonye JC. Probing the interaction of nanoparticles with mucin for drug delivery applications using dynamic light scattering. *Eur J Pharm Biopharm* 2015;**97**:218-22.
15. Vega E, Gamisans F, García ML, Chauvet A, Lacoulonche F, Egea MA, et al. PLGA nanospheres for the ocular delivery of flurbiprofen: drug release and interactions. 2008;**97**:5306-17.
16. Vega E, Egea MA, Garduño-Ramírez ML, Garcia ML, Sánchez E, Espina M, et al. Flurbiprofen PLGA-PEG nanospheres: role of hydroxy-β-cyclodextrin on *ex vivo* human skin permeation and *in vivo* topical anti-inflammatory efficacy. *Colloids Surf B: Biointerfaces* 2013;**110**:339-46.
17. Sánchez-López E, Egea MA, Cano A, Espina M, Calpena AC, Ettcheto M, et al. PEGylated PLGA nanospheres optimized by design of experiments for ocular administration of dexibuprofen– *in vitro*, *ex vivo* and *in vivo* characterization. *Colloids Surf B: Biointerfaces* 2016;**145**:241-50.
18. Vega E, Egea M, Valls O, Espina M, Garcai M. Flurbiprofen loaded biodegradable nanoparticles for ophthalmic administration. 2006;**95**:2393-405.
19. Abrego G, Alvarado HL, Egea MA, Gonzalez-Mira E, Calpena AC, Garcia ML. Design of nanosuspensions and freeze-dried PLGA nanoparticles as a novel approach for ophthalmic delivery of pranoprofen. *J Pharm Sci* 2014;**103**:3153-64.
20. Levy MY, Benita S. Drug release from submicronized o/w emulsion: a new in vitro kinetic evaluation model. *Int J Pharm* 1990;**66**:29-37.
21. Bonakdar M, Wasson EM, Lee YW, Davalos RV. Electroporation of brain endothelial cells on chip toward permeabilizing the blood–brain barrier. *Biophys J* 2016;**110**:503-13.
22. Andreani T, Kiill CP, de Souza ALR, Fangueiro JF, Fernandes L, Doktorovová S, et al. Surface engineering of silica nanoparticles for oral insulin delivery: characterization and cell toxicity studies. *Colloids Surf B: Biointerfaces* 2014;**123**:916-23.
23. Fangueiro JF, Andreani T, Egea MA, Garcia ML, Souto SB, Silva AM, et al. Design of cationic lipid nanoparticles for ocular delivery: development, characterization and cytotoxicity. *Int J Pharm* 2014;**461**:64-73.
24. Cecchelli R, Berezowski V, Lundquist S, Culot M, Renftel M, Dehouck MP, et al. Modelling of the blood–brain barrier in drug discovery and development. *Nat Rev Drug Discov* 2007;**6**:650-61.
25. Burek M, Salvador E, Förster CY. *Concepts and Models for Drug Permeability Studies*. Woodhead publishing; 2016, http://dx.doi.org/10.1016/B978–0–08-100094-6.00019-5.
26. Vasconcelos A, Vega E, Pérez Y, Gómara MJ, García ML, Haro I, et al. Conjugation of cell-penetrating peptides with poly(lactic-co-glycolic acid)-polyethylene glycol nanoparticles improves ocular drug delivery. *Int J Nanomedicine* 2015;**10**:609-31.
27. Zhou Z, Badkas A, Stevenson M, Lee JY, Leung YK. Herceptin conjugated PLGA-PHis-PEG pH sensitive nanoparticles for targeted and controlled drug delivery. *Int J Pharm* 2015;**487**:81-90.
28. Minkeviciene R, Banerjee P, Tanila H. Memantine improves spatial learning in a transgenic mouse model of Alzheimer's disease. *J Pharmacol Exp Ther* 2004;**311**:677-82.
29. Bonabello A, Galmozzi MR, Canaparo R, Isaia GC, Serpe L, Muntoni E, et al. Dexibuprofen (S(+)-isomer ibuprofen) reduces gastric damage and improves analgesic and anti inflammatory effects in rodents. *Anesth Analg* 2003;**97**:402-8.
30. Pedrós I, Petrov D, Allgaier M, Sureda F, Barroso E, Beas-Zarate C, et al. Early alterations in energy metabolism in the hippocampus of APPswe/PS1dE9 mouse model of Alzheimer's disease. *Biochim Biophys Acta Mol basis Dis* 1842;**2014**:1556-66.
31. Chattopadhyay M, Kodela R, Duvalsaint PL, Kashfi K. *Gastrointestinal Safety, Chemotherapeutic Potential, and Classic Pharmacological*

Profile of NOSH-Naproxen (AVT-219) a Dual NO- and H 2 S-Releasing Hybrid; 20161-16, http://dx.doi.org/10.1002/prp2.224.
32. Best R, Lewis DA, Nasser N. The anti-ulcerogenic activity of the unripe plantain banana (Musa species). *Br J Pharmacol* 1984;**82**:107-16.
33. Li YH, Li J, Huang Y, Lü XW, Jin Y. Gastroprotective effect and mechanism of amtolmetin guacyl in mice. *World J Gastroenterol* 2004;**10**:3616-20.
34. Zhang C, Zheng X, Wan X, Shao X, Liu Q, Zhang Z, et al. The potential use of H102 peptide-loaded dual-functional nanoparticles in the treatment of Alzheimer's disease. *J Control Release* 2014;**192**:317-24.
35. Ettcheto M, Petrov D, Pedrós I, de Lemos L, Pallàs M, Alegret M, et al. Hypercholesterolemia and neurodegeneration. Comparison of hippocampal phenotypes in LDLr knockout and APPswe/PS1dE9 mice. *Exp Gerontol* 2015;**65**:69-78.
36. Porquet D, Andrés-Benito P, Griñán-Ferré C, Camins A, Ferrer I, Canudas AM, et al. Amyloid and tau pathology of familial Alzheimer's disease APP/PS1 mouse model in a senescence phenotype background (SAMP8). *Age (Omaha)* 2015;**37**:1-17.
37. Ettcheto M, Petrov D, Pedros I, Alva N, Carbonell T, Beas-Zarate C, et al. Evaluation of neuropathological effects of a high-fat diet in a presymptomatic Alzheimer's disease stage in APP/PS1 mice. *J Alzheimers Dis* 2016;**54**:233-51.
38. Cheng KK, Yeung CF, Ho SW, Chow SF, Chow AHL, Baum L. Highly stabilized Curcumin nanoparticles tested in an *in vitro* blood–brain barrier model and in Alzheimer's disease Tg2576 mice. *AAPS J* 2013;**15**:324-36.
39. Abrego G, Alvarado H, Souto EB, Guevara B, Halbaut L, Parra A, et al. Biopharmaceutical profile of pranoprofen-loaded PLGA nanoparticles containing hydrogels for ocular administration. *Eur J Pharm Biopharm* 2015;**231**:1-10.
40. Parra A, Mallandrich M, Clares B, Egea MA, Espina M, García ML, et al. Design and elaboration of freeze-dried PLGA nanoparticles for the transcorneal permeation of carprofen: ocular anti-inflammatory applications. *Colloids Surf B: Biointerfaces* 2015;**136**:935-43.
41. Asadpour E, Sadeghnia HR, Ghorbani A, Sedaghat M, Boroushaki MT. Oxidative stress-mediated cytotoxicity of zirconia nanoparticles on PC12 and N2a cells. *J Nanopart Res* 2016;**18**:14.
42. Yin T, Yang L, Liu Y, Zhou X, Sun J, Liu J. Sialic acid (SA)-modified selenium nanoparticles coated with a high blood–brain barrier permeability peptide-B6 peptide for potential use in Alzheimer's disease. *Acta Biomater* 2015;**25**:172-83.
43. Hu K, Shi Y, Jiang W, Han J, Huang S, Jiang X. Lactoferrin conjugated PEG-PLGA nanoparticles for brain delivery: preparation, characterization and efficacy in Parkinsons disease. *Int J Pharm* 2011;**415**:273-83.
44. Semete B, Booysen L, Kalombo L, Ramalapa B, Hayeshi R, Swai HS. Effects of protein binding on the biodistribution of PEGylated PLGA nanoparticles post oral administration. *Int J Pharm* 2012;**424**:115-20.
45. Griffin BT, Guo J, Presas E, Donovan M, Alonso MJ, O'Driscoll CM, et al. Pharmacokinetic, pharmacodynamic and biodistribution following oral administration of nanocarriers containing peptide and protein drugs. *Adv Drug Deliv Rev* 2016;**106B**:367-80.
46. Mckee AC, Carreras I, Hossain L, Ryu H, Klein WL, Oddo S, et al. Ibuprofen reduces aβ, hyperphosphorylated tau and memory deficits in Alzheimer mice. *Brain Res* 2008;**7**:225-36.
47. Lee YJ, Choi DY, Yun Y-P, Han SB, Oh KW, Hong JT. Epigallocatechin-3-gallate prevents systemic inflammation-induced memory deficiency and amyloidogenesis via its anti-neuroinflammatory properties. *J Nutr Biochem* 2013;**24**:298-310.
48. Novakova I, Subileau EA, Toegel S, Gruber D, Lachmann B, Urban E, et al. Transport rankings of non-steroidal antiinflammatory drugs across blood–brain barrier *in vitro* models. *PLoS One* 2014;**9**:1-14.
49. Parepally JMR, Mandula H, Smith QR. Brain uptake of nonsteroidal anti-inflammatory drugs: ibuprofen, flurbiprofen, and indomethacin. *Pharm Res* 2006;**23**:873-81.
50. Wohlfart S, Gelperina S, Kreuter J. Transport of drugs across the blood–brain barrier by nanoparticles. *J Control Release* 2012;**161**:264-73.
51. Zara GP, Cavalli R, Bargoni A, Fundarò A, Vighetto D, Gasco MR. Intravenous administration to rabbits of non-stealth and stealth doxorubicin-loaded solid lipid nanoparticles at increasing concentrations of stealth agent: pharmacokinetics and distribution of doxorubicin in brain and other tissues. *J Drug Target* 2002;**10**:327-35.
52. Ortega-Martínez SA. New perspective on the role of the CREB family of transcription factors in memory consolidation via adult hippocampal neurogenesis. *Front Mol Neurosci* 2015;**8**:1-12.

3.3. Memantine Loaded PEGylated Biodegradable Nanoparticles for the Treatment of glaucoma

Elena Sánchez-López, Maria Antonia Egea, Benjamin Davis, Li Guo, Marta Espina, Amelia M. Silva, Ana Cristina Calpena, Eliana B. Souto, Nniveditta Ravindran, Miren Ettcheto, Antoni Camins, Maria Luisa García, M. Francesca Cordeiro

Small. 2017, 1-12

Doi: 10.1002/smll.201701808

FULL PAPER
Nanoparticles
small
NANO MICRO
www.small-journal.com

Memantine-Loaded PEGylated Biodegradable Nanoparticles for the Treatment of Glaucoma

*Elena Sánchez-López, Maria Antonia Egea, Benjamin Michael Davis, Li Guo, Marta Espina, Amelia Maria Silva, Ana Cristina Calpena, Eliana Maria Barbosa Souto, Nivedita Ravindran, Miren Ettcheto, Antonio Camins, Maria Luisa García, and Maria Francesca Cordeiro**

Glaucoma is a multifactorial neurodegenerative disease associated with retinal ganglion cells (RGC) loss. Increasing reports of similarities in glaucoma and other neurodegenerative conditions have led to speculation that therapies for brain neurodegenerative disorders may also have potential as glaucoma therapies. Memantine is an *N*-methyl-D-aspartate (NMDA) antagonist approved for Alzheimer's disease treatment. Glutamate-induced excitotoxicity is implicated in glaucoma and NMDA receptor antagonism is advocated as a potential strategy for RGC preservation. This study describes the development of a topical formulation of memantine-loaded PLGA-PEG nanoparticles (MEM-NP) and investigates the efficacy of this formulation using a well-established glaucoma model. MEM-NPs <200 nm in diameter and incorporating 4 mg mL^{-1} of memantine were prepared with 0.35 mg mL^{-1} localized to the aqueous interior. In vitro assessment indicated sustained release from MEM-NPs and ex vivo ocular permeation studies demonstrated enhanced delivery. MEM-NPs were additionally found to be well tolerated in vitro (human retinoblastoma cells) and in vivo (Draize test). Finally, when applied topically in a rodent model of ocular hypertension for three weeks, MEM-NP eye drops were found to significantly ($p < 0.0001$) reduce RGC loss. These results suggest that topical MEM-NP is safe, well tolerated, and, most promisingly, neuroprotective in an experimental glaucoma model.

1. Introduction

Glaucoma is a multifactorial neurodegenerative disease and the second leading cause of vision loss worldwide.[1] Although the exact mechanism of glaucoma pathology is debatable,[2,3] the disease induces damage to optic nerve axons thus resulting in progressive loss of retinal ganglion cells (RGC). Elevated intraocular pressure presently remains the only clinically modifiable risk factor for glaucoma and, therefore, traditional therapeutic strategies seek to reduce elevated intraocular pressure (IOP). However, there are patients who suffer glaucoma and vision loss with normotensive IOP values.[4] Although it has been shown that there is some improvement in the course of the disease in normotensive glaucoma (NTG) patients by lowering the IOP, there is growing recognition that IOP reduction alone is not adequate in some patients who continue to lose vision despite well-controlled IOPs.[4,5] As a result, there

Dr. E. Sánchez-López, Prof. M. A. Egea, Prof. M. Espina, Prof. A. C. Calpena, Prof. M. L. García
Department of Pharmacy and Pharmaceutical Technology and Physical Chemistry
Faculty of Pharmacy
Institute of Nanoscience and Nanotechnology (IN2UB)
University of Barcelona
Barcelona 08028, Spain
Dr. E. Sánchez-López, M. Ettcheto, Prof. A. Camins
Biomedical Research and Networking Center in Neurodegenerative diseases (CIBERNED)
Madrid 28031, Spain
Dr. B. M. Davis, Dr. L. Guo, N. Ravindran, Prof. M. F. Cordeiro
Glaucoma and Retinal Neurodegeneration Research
Visual Neuroscience
UCL Institute of Ophthalmology
Bath Street, London EC1V 9EL, UK
E-mail: m.cordeiro@ucl.ac.uk
Prof. A. M. Silva
Department of Biology and Environment
School of Life and Environmental sciences (ECVA, UTAD)
and Centre for Research and Technology of Agro-Environmental and Biological Sciences (CITAB-UTAD)
University of Trás-os-Montes e Alto Douro
Quinta de Prados 5001-801, Vila Real, Portugal
Prof. E. B. Souto
Department of Pharmaceutical Technology
Faculty of Pharmacy
University of Coimbra (FFUC) and REQUIMTE/Group of Pharmaceutical Technology
Polo das Ciências da Saúde
Azinhaga de Santa Comba 3000-548, Coimbra, Portugal
M. Ettcheto, Prof. A. Camins
Department of Pharmacology, Toxicology and Therapeutic Chemistry
Faculty of Pharmacy
University of Barcelona
Barcelona 08028, Spain
Prof. M. F. Cordeiro
Western Eye Hospital
Imperial College Healthcare Trust
London, UK

DOI: 10.1002/smll.201701808

ADVANCED SCIENCE NEWS
www.advancedsciencenews.com

NANO MICRO small
www.small-journal.com

has been widespread research on IOP-independent neuroprotective strategies[6] for glaucoma patients.[7] Increasingly, there has been a recognition that similar mechanisms of cell death occur in glaucoma and Alzheimer's disease (AD), including dysregulation of neurotrophic growth factors, caspase activation, and glutamate excitotoxicity.[8] Therapies advocated in AD have also been suggested for glaucoma. One such treatment is the NMDA (*N*-methyl D-aspartate) receptor antagonists memantine (MEM).[9]

MEM is a neuroprotective agent approved by the FDA for the treatment of AD that acts by inhibiting NMDA-induced glutamate excitotoxicity; it may also prevent RGC death in glaucoma.[5] Although preclinical data previously suggested a potential clinical benefit of orally administered MEM for the treatment of glaucoma,[10] the efficacy of this route of MEM administration is limited, and may have contributed to the results of a phase III clinical trial in glaucoma which apparently failed in meeting its primary endpoint.[11,12]

A key challenge for MEM in glaucoma is the development of a safe and effective means of long-lasting delivery of MEM to the back of the eye.[13] Incorporation of MEM into a nanoparticle drug delivery systems could provide a strategy to enhance the efficacy of this agent by increasing concentrations in target retinal tissues whilst reducing the risk of side effects associated with systemic dosing regimens.[14] Nanocarriers have also been shown to enable loaded drug molecules to penetrate to posterior ocular tissues by promoting drug delivery across anterior ocular barriers including the lipidic tear film and corneal epithelial barrier and increasing drug residency time after eye drop instillation.[15–17] Poly(lactic-co-glycolic acid) or PLGA is presently the most widely used biocompatible and biodegradable polymer in the field of nanocarrier systems. It is FDA approved and is reported safe for the delivery of ophthalmic agents.[18] Moreover, polymeric PLGA nanoparticles (NPs) have been reported to facilitate the sustained delivery of other existing IOP-lowering agents to intraocular tissues.[17] Previously, PLGA has been covalently attached to hydrophilic polymers such as polyethylene glycol (PEG) due to its hydrophilicity and biocompatibility. This was found to enhance nanoparticle mucoadhesion by increasing residency time on the ocular surface.[19]

In this study, we sought to develop a novel biodegradable PLGA-PEG nanoparticle formulation of MEM which could be applied as an eye drop once a day. Topical administration is favored over subtenon or intravitreal implants owing to noninvasiveness, reduced risk of side effects, ability to self-administer and inherent socioeconomic costs.[13,20] Encapsulation of MEM in MEM-PLGA-PEG NPs was achieved using a double emulsion method. Stability, in vitro and ex vivo release of the constructed nanosystems were determined prior to assessing the neuroprotective activity of optimized formulations in a well-established rodent model of ocular hypertension.

1. Results

1.1. Preparation of a Homogeneous Nanoparticle Suspension of PLGA-PEG-Memantine Using the Double Emulsion Method

MEM-NP were developed using a double emulsion method using ethyl acetate as the organic solvent due to its partial water solubility and reduced toxicity compared to dichloromethane (class III and II, respectively according to ICH specifications).[21] Design of experiments (DoE) was used to obtain a suitable formulation for eye delivery studying the modifications of pH and composition of the two aqueous phases (w_1 and w_2). As shown in **Figure 1**A, smaller MEM-NP average size (Z_{av}) were obtained as the pH of the w_1 phase was similar to drug pK_a (10.7). A reduction in polydispersity index (PI) was also observed by maintaining w_1 under alkaline conditions thus favouring MEM-NP homogeneity (Figure 1B). Encapsulation efficiency (EE) was also found to be maximal (80.6%) at w_1 pH 11 and w_2 pH 6.5 (Figure 1C). EE values ≈80% were obtained with a 4.5 pH difference between the two phases, meaning the nanoparticles incorporated 4 mg mL^{-1} of memantine and this formulation was used in subsequent experiments (F6, **Table 1**).

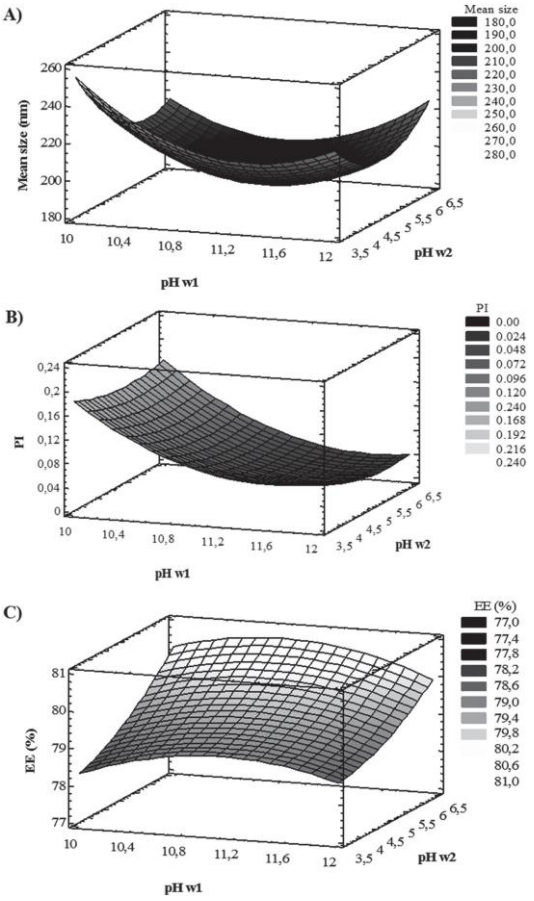

Figure 1. Characteristics of memantine-loaded nanoparticles in response to changes in pH of w_1 and w_2 phases. Results from DoE experiments regarding the influence of pH on double emulsion solvent evaporation method. The effect of pH on mean MEM-NP A) diameter, B) polydisper- sity (PI), and C) Encapsulation Efficiency (EE) was investigated.

ADVANCED SCIENCE NEWS
www.advancedsciencenews.com

NANO MICRO
www.small-journal.com

Table 1. Characteristics of memantine-loaded nanoparticles. Design of experiments matrix and results according to central factorial design to study pH influence of the inner and external water phases (MEM-NP prepared with 20 mg mL^{-1} PLGA-PEG and 5 mg mL^{-1} of MEM).

	pH w_1		pH w_2		Z_{av} [nm]	PI	ZP [mV]	EE [%]
Factorial points								
F1	12.0	+1	3.5	−1	234.0 ± 0.6	0.09 ± 0.02	−5.67 ± 0.28	78.45
F2	12.0	+1	6.5	+1	225.4 ± 1.2	0.04 ± 0.02	−5.65 ± 0.12	79.60
F3	12.0	+1	5.0	0	197.9 ± 3.64	0.03 ± 0.02	−5.17 ± 0.06	79.43
F4	10.0	−1	6.5	+1	221.3 ± 4.01	0.18 ± 0.02	−5.19 ± 0.16	80.81
F5	10.0	−1	3.5	−1	268.3 ± 4.83	0.21 ± 0.02	−5.87 ± 0.19	79.03
F6	**11.0**	**0**	**6.5**	**±1**	**193.1 ± 0.42**	**0.05 ± 0.01**	**−4.41 ± 0.15**	**80.64**
F7	11.0	0	3.5	−1	196.1 ± 3.33	0.04 ± 0.01	−4.39 ± 0.26	78.40
F8	10.0	−1	5.0	0	198.7 ± 3.03	0.12 ± 0.01	−4.82 ± 0.61	77.86
Center points								
F9	11.0	0	5.0	0	217.9 ± 1.5	0.11 ± 0.02	−5.03 ± 0.33	80.34
F10	11.0	0	5.0	0	219.5 ± 2.4	0.14 ± 0.01	−5.08 ± 0.24	79.99

Optimized MEM-NP were found to have a mean diameter <200 nm after centrifugation, a PI suggesting formulation homogeneity (0.078 ± 0.018), characteristic of the monodisperse systems (PI < 0.1) and a sufficiently negative zeta potential (ZP) to suggest the NP dispersion may be stable in solution (–26.5 mV, the negative charge increased after centrifugation due to PVA removal). Using dynamic light scattering,[22] particles were found to be monodisperse, with a mean diameter of 141.8 nm (Figure S1A,B, Supporting Information). Results were supported by transmission electron microscopy (TEM) observations, the structure of MEM NPs was distinct from the structure of crystalline memantine (**Figure 2**A,B). MEM-NP were found to be spherical and well dispersed with a mean diameter of 78.51 ± 11.01 nm (supplementary material Figure 3C). AFM results supported this observation with smooth spherical NPs with a mean horizontal and vertical distance of 89.8 and 98.08 nm respectively (Figure 2C,D). Differential scanning calorimetry (DSC) thermograms are shown in **Figure 3**A,B. The exotermic peak observed during the cooling process of the sample correspond to MEM NP freezing temperature. The freezing onset is –15.99 °C and after freezing and heated MEM NP showed a glass transition temperature (T_g) endotermic peak at 9.69 °C. Furthermore, MEM NP and empty NP were compared without the cooling process. The thermograms of MEM NP showed that the T_g (56.39°C) is slightly increased compared with empty NP (52.85 °C). The proton nuclear magnetic resonance (^{1}H-NMR) profile of MEM-NPs, empty nanoparticles and empty nanoparticles spiked with memantine are shown in Figure 3C. Here, D_2O was used as a solvent, with a reference peak ($\delta = 0$) from the methyl signal of trimethylsilyl propanoic acid (TMSP).[23] Compared to MEM-NP, or empty nanoparticles characteristic memantine peaks were observed in MEM-NP spectra (2.2, 1.4, and 0.9 ppm).[24] The profile of empty nanoparticles is comparable to that previously reported in the literature, with characteristic peaks of the lactic acid respectively.[25,26] As is shown in Figure 3B, one of the striking features is a large peak at 3.7 ppm due to the methylene groups of the MePEG.[22,23,27] Traces of ethyl acetate were observed in the sample, with peaks at 4.1 and 1.24 ppm corresponding to the ethyl quadruplet and methyl triplet of CH_2CH_3 respectively, Nevertheless, these traces are not able no cause ocular irritation.[23]

1.1. PLGA-PEG Nanocarriers Encapsulate Memantine and Demonstrate an Element of Sustained Release

The backscattering profile for MEM-NPs maintained at 25 °C for 24 h is shown in **Figure 4**. Except for peripheral peaks at the vial edges, a constant signal around 38% could be observed throughout the study without variations higher than 10% thus indicating good short-term stability of the formulation.[28] In vitro release of memantine fit well ($R^2 = 0.976$) to a single phase exponential association equation (Equation 1) liberating all memantine within 4 h with a half-life of 0.74 h (**Figure 5**). To assess the proportion of memantine that had been incorporated into the aqueous interior of the double emulsion compared to the surrounding hydrophobic (oil phase) milieu in vitro release from MEM-NPs was fit to a one-phase (Equation 1) or two-phase exponential association equation (Equations 1 and 2, respectively[29]) constraining the fast half-life as that for free memantine

$$Y = Y_0 + (P - Y_0)\left(1 - \exp(-K^* X)\right) \quad (1)$$

$$S_F = (P - Y_0)\, F\, 0.01$$

$$S_S = (P - Y_0)\,(100 - F)\, 0.01 \quad (2)$$

$$Y = Y_0 + S_F\left(1 - \exp(-K_F^* X)\right) + S_S\left(1 - \exp(-K_S^* X)\right)$$

ADVANCED SCIENCE NEWS
www.advancedsciencenews.com

NANO MICRO
www.small-journal.com

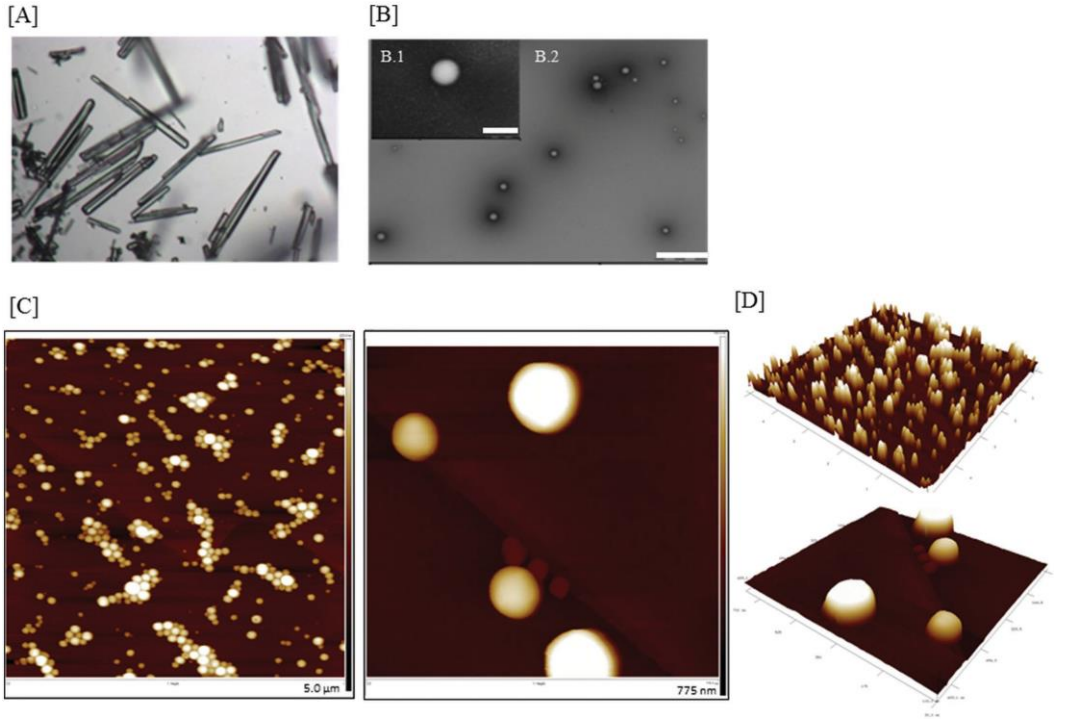

Figure 2. Transmission electron microscopy and Atomic force microscopy of MEM NP. A) Micrograph confirming the crystalline structure of free memantine, B) TEM micrograph illustrating the spherical structure of memantine-loaded nanoparticles (MEM-NP), scale bar of B.1) corresponding to 500 nm and B.2) 1 µm. C) 2D AFM microsgraph MEM NP, D) 3D analysis corresponding to the 2D micrographs.

components, respectively, and F describes the percentage of signal due to the fast phase.

The best fitting model was determined to be Equation 2 using an extra sum of squares F-test ($F = 45.41$, $p < 0.0001$), with a slow half-life of 6.0 h ($R^2 = 0.9828$). This result suggests a portion of the memantine contained within MEM-NPs has been successfully incorporated into the aqueous interior of the double emulsion. Using (Equation 2) the proportion of memantine in this slow release fraction was estimated to be 8.68% which equates to ≈0.35 mg mL^{-1} of the total incorporated memantine. As free memantine in solution was removed from MEM-NPs prior to conducting this assay, the fast release fraction is likely to be memantine rapidly liberated from the nanoparticle oil phase. This may explain why the greatest encapsulation of memantine was achieved at the pK of this drug where it has no overall charge and at its most lipophilic.

1.1. Ex Vivo Corneal and Scleral Permeation Studies

Ex vivo corneal and scleral permeation studies were carried out up to 6 h (Figure 5B,C). MEM-NP depicted a slower drug release on scleral tissue than on the cornea. The slope for corneal permeation was 6.64 ± 0.17 µg cm^2 h^{-1} whereas the slope for scleral permeation was 0.23 ± 0.01 µg cm^2 h^{-1}. Lag time (T_L) was almost null in both tissues, suggesting that MEM-NPs achieve the steady-state in the ocular tissue within a few minutes after its application.[30] The permeability coefficient (K_p) was 0.01 cm h^{-1} for cornea and 2.79·10^{-4} cm h^{-1} for scleral. On both cases, the parameter was highly influenced by P_2 ($K_p = P_1 \cdot P_2$). P_2 corresponds to the partition coefficient inside both tissues although, as demonstrated in previous publications, PLGA-PEG NP show significant corneal tropism, with a suggestion that memantine could be released slowly from within the cornea.[31] In addition, free drug retention in corneal tissue was 0.01 µg mg^{-1} whereas in sclera it was tenfold higher (0.11 µg mg^{-1}).

1.2. In Vitro Cytotoxicity and In Vivo Ocular Tolerance Assessment

In order to assess the safety of the produced MEM-NP, cell viability studies were carried out using retinoblastoma (Y-79) and keratinocytes (HaCaT) cells. As can be observed in **Figure 6**A, MEM-NP at 24 or 48 h of exposure did not cause a reduction in cell viability, whereas free memantine was found to be cytotoxic

ADVANCED SCIENCE NEWS
www.advancedsciencenews.com

NANO MICRO
www.small-journal.com

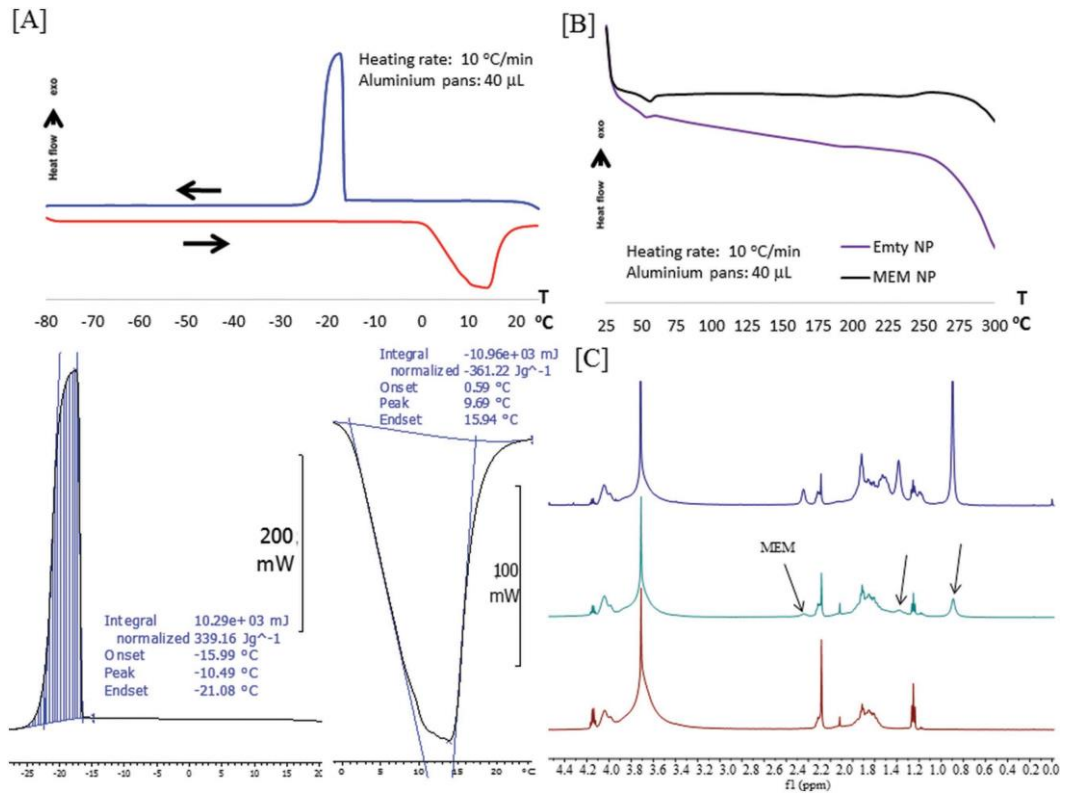

Figure 3. A) DSC curves starting at 25 °C (freezing until −80 °C and heating until 25 °C at 10 °C min^{-1}) and B) DSC curves of MEM NP and empty NP starting at 25 °C and heating until 300 °C (heating rate 10 °C min^{-1}). C) ^{1}H-NMR spectra of nanoparticles spiked with memantine, memantine-loaded nanoparticles, and empty nanoparticles.

at 50×10^{-6} M after 48 h ($p < 0.001$) but not 24 h of cell contact. The free drug also showed toxicity in retinoblastoma cells after short-term exposure (Figure 6B). These differences in exposure time and toxicity in different cell lines might be due to differences in cell metabolism. In contrast to the free drug, MEM-NP did not show toxicity in any of the assessed concentrations, with cell viability values greater than 80%, possibly related to the polymeric matrix slowing memantine release and reducing cell exposure to cytotoxic concentrations.

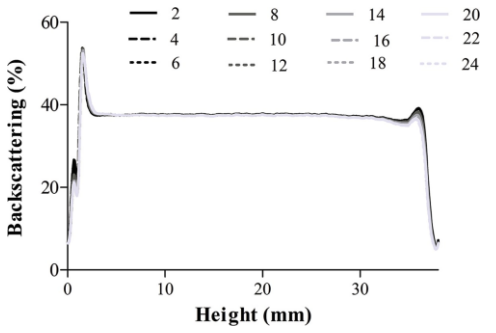

Figure 4. Backscattering profile of memantine-loaded nanoparticles demonstrates the formulation remains stable when stored at room temperature for 24 h.

In vitro ocular tolerance was assessed using the Hen's egg test chorioallantoic membrane (HET-CAM).[32] Addition of 0.9% saline solution to healthy membranes was used as a negative control which produced no adverse effects after 5 min. In contrast, application of a severe irritant (1 m sodium hydroxide) induced immediate and severe hemorrhages, which served as a positive control (**Figure 7**A). The application of 0.3 mL of free memantine onto the chorioallantoic membrane, induced small hemorrhages (Figure 7B) suggestive of mild irritation. In contrast instillation of the same volume and concentration of MEM-NPs was found to be well-tolerated and induced no detectable irritation (Figure 7C,D).[33] Upon completion of these in vitro tests, a tolerance assay was conducted in male albino rabbits. Similar to the in vitro result, MEM-NP had a low ocular irritation index (OII) and were therefore classified as nonirritant, whereas administration of free memantine was found to induce a degree of inflammation, and was therefore classified as slightly irritant.

ADVANCED SCIENCE NEWS
www.advancedsciencenews.com

NANO MICRO
www.small-journal.com

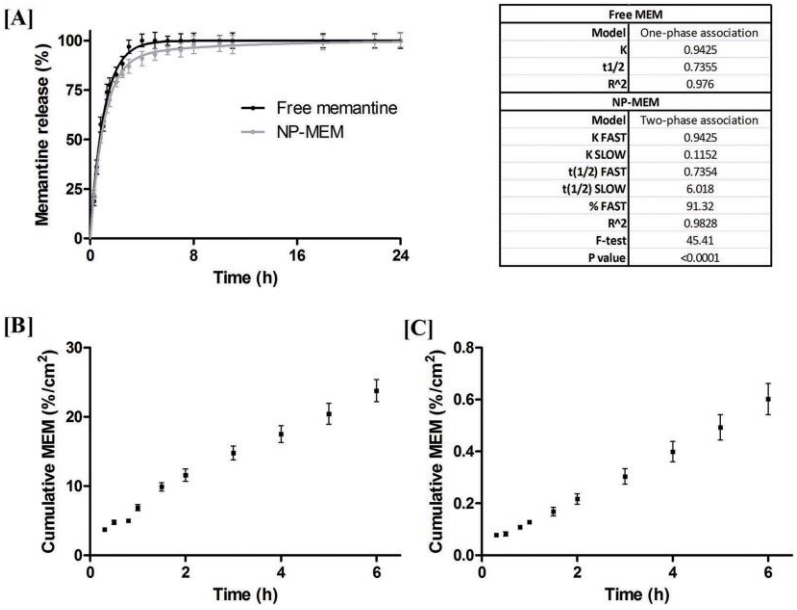

Free MEM	
Model	One-phase association
K	0.9425
t1/2	0.7355
R^2	0.976
NP-MEM	
Model	Two-phase association
K FAST	0.9425
K SLOW	0.1152
t(1/2) FAST	0.7354
t(1/2) SLOW	6.018
% FAST	91.32
R^2	0.9828
F-test	45.41
P value	<0.0001

Figure 5. In vitro release of memantine and ex vivo permeation assays. A) In vitro release of free memantine (MEM) versus memantine-loaded nanoparticles (MEM-NP) adjusted to the best fit kinetic models (single-phase exponential association (Equation 1) or two-phase exponential association (Equation 2) respectively. Ex vivo assessment of the B) corneal and C) scleral permeation of MEM-NPs.

1.1. MEM-NPs are Neuroprotective in a Rodent Model of Ocular Hypertension

After unilateral induction of the Morrison's ocular hypertension model in Dark Agouti (DA) rats, two drops of MEM-NP were administered daily for 3 weeks. Peak IOP was observed 1 d after surgery, and IOP elevation was sustained for at least 7 d (**Figure 8**A). The IOP profile was comparable between MEM-NP and ocular hypertension (OHT) control groups (20.59 ± 3.81 and 19.81 ± 0.93 mmHg, respectively) suggesting that MEM-NP therapy did not affect IOP.

Surviving RGC were visualised histologically in retinal flat mounts using the RGC specific nuclear-localized transcription factor Brn3a (Figure 8B). Quantification of RGC populations was completed using an automated script as previously described.[34] Global RGC density was significantly diminished in the untreated OHT group versus naïve controls ($p < 0.001$, Figure 8A). Treatment with MEM-NP was found to significantly protect against OHT induced RGC injury in this model ($p < 0.001$), suggesting it was neuroprotective in a nonIOP-dependent manner.

2. Discussion

In the present work, we developed a novel MEM-NP formulation using DoE in conjunction with a double emulsion method. MEM-NPs were found to be homogeneous with an average diameter <200 nm (141.8 nm) with high drug loading (4 mg mL^{-1}). Incorporated memantine was found to be localized at the particle surface and interior using in vitro release assays. As a single parameter cannot be used to adequately describe the sample distribution,[35] sub-200 nm particle size and spherical shape was confirmed using dynamic light scattering (DLS), TEM, and AFM investigations, suggesting this formulation would be unlikely to cause ocular irritation.[36] MEM NP were found to be well tolerated using a number of established in vitro and in vivo assays and these results suggest that topical MEM-NP is safe and well-tolerated formulation with neuroprotective activity in a well-established experimental model of glaucoma.

The MEM-NP formulation comprised a PLGA-PEG polymeric matrix which was synthesized using a modified double emulsion method. This technique was used due to its suitability for the encapsulation of hydrophilic compounds, minimizing the escape of these molecules from the aqueous core so increasing formulation stability, one of the main drawbacks of hydrophilic drug loading into liposomes.[21] The greatest memantine encapsulation efficiency was observed using pH values of w1 similar to memantine p*K*a (10.7, ChemAxon). A possible explanation for this observation is that memantine is most hydrophobic at its p*K*, maximizing solubility in the nanoparticle oil phase. This suggestion is supported by subsequent in vitro release assays which estimate that of the 4 mg mL^{-1} memantine incorporated into the formulation, 0.35 mg mL^{-1} was released slowly from nanoparticles (suggestive of encapsulation within the aqueous interior), while 3.65 mg mL^{-1} was released at a similar rate to free memantine. As unencapsulated

ADVANCED SCIENCE NEWS
www.advancedsciencenews.com

NANO MICRO
www.small-journal.com

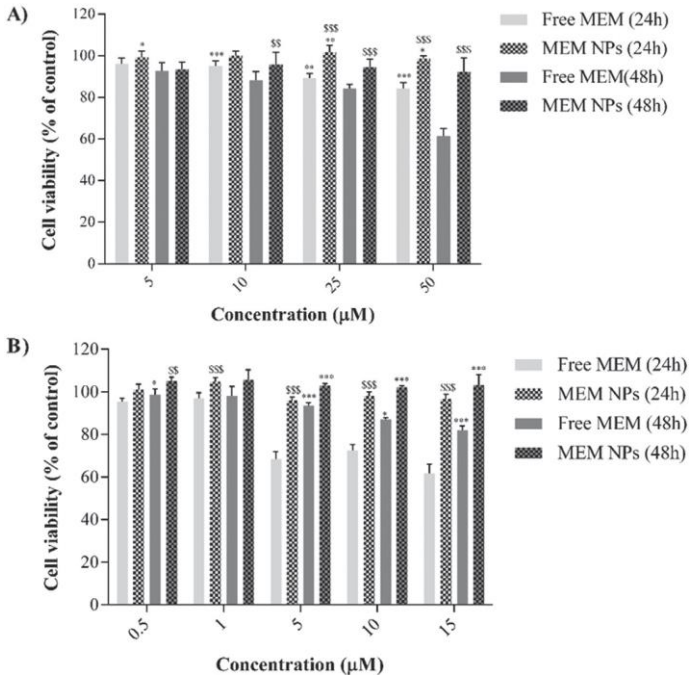

Figure 6. Memantine-loaded nanoparticles are well tolerated by epithelial and neuronal cultures in vitro. Cell viability was assessed using the Alamar blue viability assay with the A) keratinocyte cell line and B) retinoblastoma cells. Values are expressed as mean ± SD. Significant differences between free memantine (MEM) and MEM-NP at same exposure time and concentration are represented as $^{\$}p < 0.05$, $^{\$\$}p < 0.01$, and $^{\$\$\$}p < 0.001$ and $^{\$\$\$\$}p < 0.0001$. Significant differences between the exposure time with same formulation and concentration are represented as $p < 0.05$, $p < 0.01$, $p < 0.001$, and $p < 0.0001$.

memantine was removed from the formulation prior to in vitro assessment, we propose that the more rapidly released fraction was instead liberated from the lipophilic nanoparticle component. As a result, while 4 mg mL^{-1} of drug was incorporated into the formulation, 0.35 mg mL^{-1} of this material was incorporated within the aqueous nanoparticle core (the slower release fraction) and this may be the more relevant value to compare with other formulations. After confirming the release profile of the MEM-NPs, sclera and cornea of rabbits were used to investigate the permeation of formulated memantine across intraocular barriers. MEM-NP corneal penetration was found to be higher than scleral permeation but, interestingly, the amount of memantine found within scleral tissue could suggest that administration of MEM-NPs results in the formation of a drug reservoir in the sclera from which memantine diffuses into intraocular tissues.

DSC results supported encapsulation of MEM as a result of the increase in T_g observed on drug entrapment. The increasing of T_g of the polymer could be attributed to the incorporation of an alkaline drug, which causes interactions between the carboxylic groups of the polymer. In addition, results suggest that this formulation will be amenable to freeze-dried.[37] In vitro cell viability studies were performed demonstrating that MEM-NPs were better tolerated than free memantine by epithelial and neuronal cultures. Results

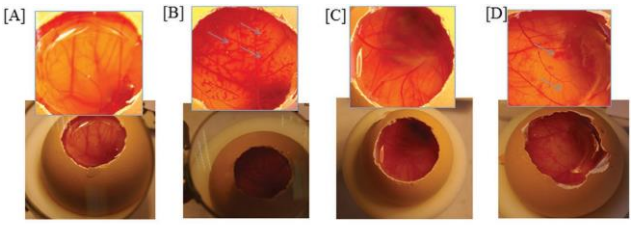

[E]

Formulation	Test	OII	Classification
Free MEM	HET-CAM	1.85 ± 0.15	Slightly irritant
	Draize	4.00 ± 1.00	Slightly irritant
MEM-NP	HET-CAM	0.13 ± 0.01	Non-irritant
	Draize	0.00 ± 0.00	Non-irritant

Figure 7. Ocular tolerance assessment of memantine and memantine-loaded nanoparticles. HET-CAM test results 5 minutes after exposure of 0.3 mL of A) 0.9% sodium cloride (negative control), B) 1m sodium hydroxide (positive control), C) memantine-loaded nanoparticles (MEM-NP), D) free memantine (MEM) memantine-loaded nanoparticles (MEM-NP). E) Classification of the ocular irritation potential in vitro and in vivo.

ADVANCED SCIENCE NEWS
www.advancedsciencenews.com

NANO MICRO
www.small-journal.com

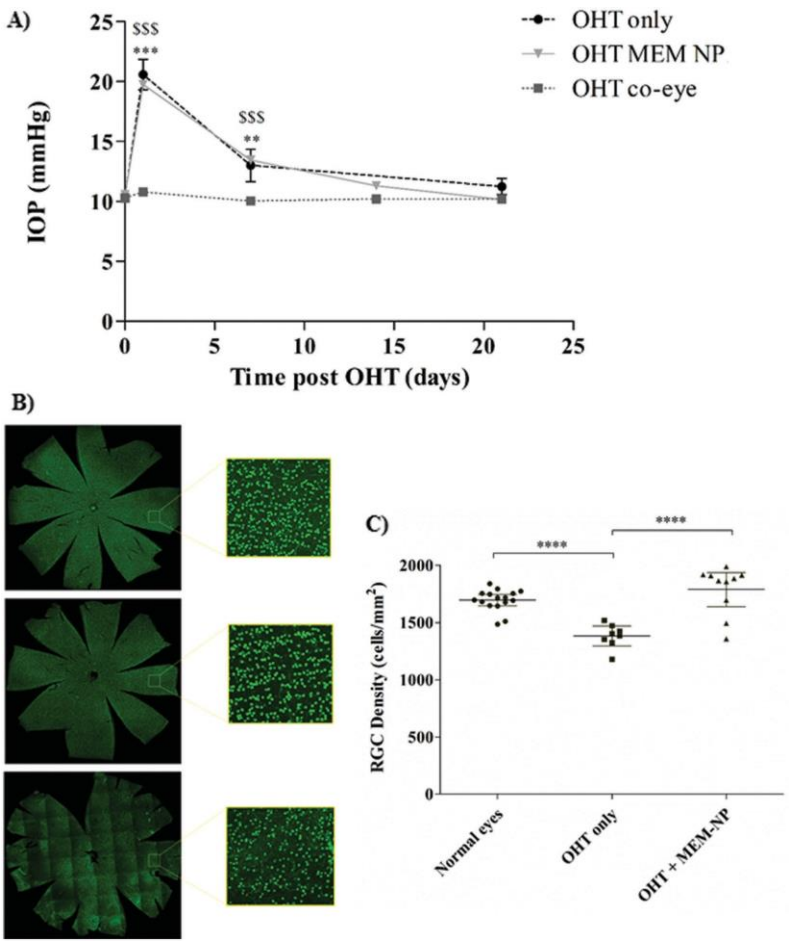

Figure 8. Topical administration of memantine-loaded nanoparticles protects RGC soma against ocular hypertension induced cell loss. A) IOP profiles of OHT only, OHT + MEM-NP, and OHT contralateral eyes. $p < 0.05$, significant differences between OHT and the coeye; $^{\$}p < 0.05$, significant differences between OHT and OHT MEM NPs. B) Comparable Brn3a labeled retinal flat mounts from contralateral eyes (top), OHT eyes treated with MEM- NPs (middle), and OHT only group (bottom). C) Whole retinal RGC density measurements indicate that while OHT induction caused a significant reduction in RGC density, RGC loss was mitigated by twice-daily administration of MEM-NPs (one-way ANOVA with Tukey post hoc test, $p < 0.0001$). Values are expressed as mean ± SE. Naive and OHT only Brn-3a whole retinal counts from DA rats were obtained from our previous work.[34]

from HET-CAM irritation tests were in agreement with in vitro observations, confirming not only the sensitivity of the in vitro test but also the nonirritant properties of the developed formulation and suitability for ocular administration.[29,32] These results are in accordance with those obtained by other groups working with PLGA-NPs for ocular applications.[33,34,38–40] We anticipate that encapsulation of memantine within the NP aqueous interior acts to slow memantine release and therefore reduces cell exposure to potentially cytotoxic concentrations of this agent.

Having established the tolerability of MEM-NPs, the neuroprotective effect of this formulation on RGC health was next assessed using an established in vivo rodent model of ocular hypertension. Quantitative assessment of RGC loss after three weeks of ocular hypertension induction was assessed using Brn3a immunofluorescence in conjunction with a previously described automatic image segmentation script.[34] Brn3a is a nuclear-restricted Pit-Oct-Unc (POU)-domain family transcription factor expressed exclusively by RGCs (97% of the total RGC population) in the rat retina which plays a role in differentiation, survival, and axonal elongation during development, thus providing an indirect indication of the functional state of the RGC.[41] As such, Brn3a several authors have previously used this marker to quantify RGC density in several rodent and mammalian glaucoma models.[41,42] Twice-daily topical administration of MEM-NPs

ADVANCED SCIENCE NEWS
www.advancedsciencenews.com

NANO MICRO
www.small-journal.com

for 3 weeks was found to significantly protect RGC soma from injury in this model in an IOP independent manner, suggestive of a neuroprotective effect. Although several animal models of glaucoma have been described, it is important to remember that they are imperfect and do not presently recreate all aspects of the human condition.[35,36,43–45] Despite this limitation, models such as the Morrison's ocular hypertension model used in this paper reproduce some aspects of the glaucoma, namely RGC loss in response to IOP elevation as the extent of IOP correlates with RGC loss and damage of RGC axons in untreated OHT eyes.[46]

RGC loss in the rodent model of ocular hypertension is reported to occur via a combination of primary and secondary degenerative processes.[34] Where, primary degeneration of RGCs occurs as a result of injury and secondary degeneration describes the loss of RGCs as a consequence of the primary insult, for example as a result of oxidative stress, inflammation, or excitotoxicity.[47] Glutamate excitotoxicity has previously been reported to play a role in RGC loss in the OHT model.[48] An attractive explanation for the neuroprotective effect of topically administered memantine nanoparticles in the OHT model could therefore be due to the well documented NMDA receptor antagonism of this agent.[49]

In addition to its effect on glutamate excitotoxicity, there are more recent reports that memantine can also lower amyloid beta peptide levels in vitro and in a transgenic murine model of AD.[50–52] Recent work by Ito et al. suggests that the mechanism of memantine mediated reduction in amyloid $\beta$is independent of α-,β-, or γ-secretase activity and instead influences amyloid precursor protein (APP) trafficking. Here, reduction of APP endocytosis results in the accumulation of a greater proportion of cellular APP at the plasma membrane where it is predominantly processed via the nonamyloidogenic pathway so reducing amyloid β production.[52] This is significant as there is growing evidence for the involvement of amyloid β accumula- tion in glaucoma pathology[53–55] and increasing recognition of mechanistic similarities between these neurodegenerative dis- orders.[50,51] In further support of this hypothesis, we recently demonstrated brimonidine-mediated RGC neuroprotection (an α2-adrenergic receptor agonist) in the OHT model were mediated in part by a reduction in amyloid β production and promotion of the nonamyloidogenic pathway.[55–57] Finally, as multiple studies now also link the progression of age-related macular degeneration (AMD) with amyloid β accumulation,[58] nonamyloidogenic promoting therapies such as, brimonidine and memantine may also provide useful therapies for the treatment of AMD.

Orally administered memantine has previously been tested in a Phase III clinical trial the treatment of primary open-angle glaucoma, however, the trial was reported to have failed to meet its primary endpoints.[11] To date, several hypotheses have been proposed to explain the reasons for its failure, including study endpoints that lacked sufficient power to identify a smaller but therapeutically relevant effect and insufficient treatment periods.[11] Owing to these study limitations and despite a high-profile failure, the use of noncompetitive NMDA antagonists for the treatment of glaucoma remains a promising therapeutic avenue for the development of novel glaucoma therapies.[59–61]

While some authors postulate that the use of more potent NMDA receptor antagonists such as bis(7)-tacrine may overcome the perceived limitations associated with the use of memantine for the treatment of glaucoma,[11] we postulate that by instead developing approaches to increase the concentration of memantine delivered to intraocular tissues via its incorporation into nanoparticles for local administration could provide an alternative strategy to achieve this goal.

To date, the majority of the preclinical studies examining memantine for the treatment of glaucoma, intraperitoneal,[54,55] subcutaneous,[62] or oral[63] administration routes were investigated. For studies involving oral administration in monkeys, doses of between 2 and 8 mg kg^{-1} day are reported,[64] while Alzheimer's disease patients are currently prescribed between 10 and 20 mg d^{-1}. The local administration of memantine permitted by our nanoparticle formulation resulted in localized dosing of ≈0.125 mg/rat/day. This reduced dosing in combination with localized administration would likely reduce the risk of systemic adverse effects associated with memantine therapy[65] while ensuring the delivery of therapeutically relevant concentrations of the drug to target tissues.

In this study, we demonstrated a novel PLGA-PEG nanocarrier for the delivery of therapeutically relevant concentrations to posterior ocular tissues using a rodent model of ocular hypertension. The biodegradable and mucoadhesive properties of PLGA-PEG nanoparticles are well documented and likely promoted memantine delivery to intraocular tissues through increasing precorneal drug residence.[19] Other groups have previously formulated memantine into nanoparticles. Prieto and colleagues developed Gantrez, a memantine-loaded poly(anhydride) nanoparticle formulation which possessed a similar diameter as our formulation but only contained 0.055 mg of memantine per mg of nanoparticles.[13] While the authors demonstrated sustained release of memantine from these formulations after subtenon and intravitreal injection in the rabbit, the authors did not investigate topical administration. While these results are of interest, invasive intraocular therapeutic administration is less desirable than noninvasive topical administration route.[66] More recently, lipoyl–memantine-loaded solid lipid nanoparticles[67] and memantine–pamonic acid nanocrystalline salts[68] have been described. Each of these formulations exhibited a sub-200 nm size and good homogeneity but only solubilized ≈0.1 mg mL^{-1} of lipoyl–memantine and 0.028 mg mL^{-1} of memantine–pamonic acid, respectively. To the authors' knowledge, neither of these formulations has been assessed as a glaucoma therapy.

1. Conclusion

This study describes a novel PLGA-PEG nanoparticle formulation that that incorporates 4 mg mL^{-1} of memantine with an 80% encapsulation efficiency of which 0.35 mg mL^{-1} was contained within the particles within the nanoparticle aqueous interior. This formulation was found to be better tolerated than free memantine by epithelial and neuronal cell cultures in vitro and was found to be neuroprotective through significant preservation of RGC density in a well-established rodent ocular hypertension model of glaucoma after twice-daily topical in vivo. In

ADVANCED SCIENCE NEWS
www.advancedsciencenews.com

NANO MICRO
www.small-journal.com

summary, we propose topical administration of memantine-loaded nanoparticles as a novel technique as a safe, noninvasive and effective strategy for the treatment of glaucoma.

1. Experimental Section

MEM-NP Preparation: MEM-NP were prepared by a modification of the double emulsion solvent evaporation technique.[69] Briefly, 100 mg of PLGA-PEG was dissolved in 2 mL of ethyl acetate. 25 mg of memantine was dissolved into 1 mL of water at pH 11. Primary emulsion (w_1/o) was obtained by applying ultrasound energy with an ultrasonic probe for 30 s (38% of amplitude). 2 mL of PVA at 23 mg mL^{-1} was added and ultrasound was applied for 3 min. Finally, 2 mL of poly(vinyl alcohol) (PVA) 0.3% was added dropwise under magnetic stirring and the $w_1/o/w_2$ emulsion was stirred overnight to evaporate the organic solvent.

Characterization of MEM-NP: MEM-NP Z_{av} and PI were determined by photon correlation spectroscopy with a Zetasizer Nano ZS (Malvern Instruments, Malvern, UK) at 25 °C.[39] ZP was evaluated by laser- doppler electrophoresis with M3 PALS system. In all the determinations, the samples were diluted with MilliQ water (1:10). Results represent mean ± SD, $N \geq 3$.

EE was determined indirectly using a Triple Quadrupole LC/MS/MS Mass Spectrometer (Perkin-Elmer Sciex Instruments). Prior to analysis, free drug was separated from nanoparticles by filtration using an Ultra 0.5 centrifugal filter device (Amicon Millipore Corporation, Ireland). EE was calculated using Equation (3)

$$\text{EE}\ (\%) = \frac{\text{Total amount of MEM} - \text{Free MEM}}{\text{Total amount of MEM}} \quad (3)$$

Memantine quantification was performed in multiple reaction monitoring mode of an ion-trap mass spectrophotometer (MS) equipped with an atmospheric pressure electrospray ionization ion source and an Agilent 1100 series HPLC system (Agilent Technologies, USA) coupled with a Brucker Ion Trap SL (Brucker Daltonics GmbH, Germany). Memantine was separated on a reversed phase column (Kinetex of 2.6 μm 50 × 2.1 mm (Phenomenex)) using methanol: 0.1% formic acid in water, 55:45 (v/v) as mobile phase. The flow rate was 1 mL min^{-1} at 45°C.[70]

Preparation of MEM-NP Using a DoE Approach: MEM-NP formulation was optimized by investigating the influence of pH on NP size, dispersity, ZP, and EE (Table 1). The effect of a factor (Ex) was calculated according to Equation (4)

$$\text{Ex} = \frac{\sum_x(+) - \sum_x(-)}{n/2} \quad (4)$$

where $\Sigma_x(+)$ corresponds to the sum of the factors at their highest level (+1) and $\Sigma_x(-)$ to the sum of the factors at their lowest level and $n/2$ for the half of the number of measurements. In addition, interaction between factors was also elucidated by calculating the effect of the first factor at the lowest level of the second factor and subtracting it from the effect of the first factor at the highest level of the second factor.

Morphology Studies: MEM-NP was observed by TEM on a Jeol 1010. To visualize the NP, copper grids were activated with UV light, and samples were placed on the grid surface. Negative staining was performed with uranyl acetate (2% w/v).[28,71]

AFM Studies: AFM analysis was performed in a multimode 8 microscopy with Nanoscope V electronics (Bruker, Germany). The microscope mode used was the peak Force tapping mode with an SNL tip (Bruker). The samples were previously diluted (1:10) and about 5 μL of the solution were dropped to freshly cleaved mica surface and incubated for 5 min. Afterward, the sample was blown off with air.

DSC Studies: DSC was performed in an aluminum pan on a DSC-821 (Mettler Toledo) under nitrogen atmosphere.

^{1}H NMR Studies: ^{1}H-NMR was used to confirm both PLGA-PEG structure on the NP and drug incorporation. MEM-NP were centrifuged and dissolved in D_2O. The spectrum was recorded at 298 K on a Varian Inova 500 MHz spectrometer (Agilent Technologies, Santa Clara, CA, USA).[19]

Stability Studies: MEM-NP stability was assessed by light backscattering by means of a Turbiscan Lab. For this purpose, a glass measurement cell was filled with 20 mL of MEM-NP. The light source, pulsed near infrared light-emitting diode LED (λ = 880 nm), was received by a backscattering detector at an angle of 45° from the incident beam. Readings were carried out every hour for 24 h.[31]

In Vitro *Drug Release*: In vitro release of memantine from MEM-NPs was evaluated using the dialysis bag technique under sink conditions and results compared to free memantine.[63,64] The release medium was composed of a PBS buffer solution (phosphate-buffered saline (PBS) 0.1 M, pH 7.4) and temperature maintained at 32 °C (ocular surface temperature) with stirring. At predetermined time intervals, 1 mL samples were withdrawn from the reaction mixture and replaced with 1 mL of fresh buffer.[72] The memantine content of each aliquot was evaluated using Graphpad Prism v5.0.

Corneal and Scleral Permeation: Ex vivo corneal and scleral permeation experiments were carried out using New Zealand rabbits (male, weighing 2.5–3.0 kg), under veterinary supervision. Rabbits were anesthetized with intramuscular administration of ketamine HCl (35 mg kg^{-1}) and xylazine (5 mg kg^{-1}) and euthanized by an overdose of sodium pentobarbital (100 mg kg^{-1}). The cornea and sclera of the animals were excised and fixed between the donor and receptor compartments of Franz diffusion cells (available permeation area of 0.64 cm^2). The receptor compartment was filled with Bicarbonate Ringer's (BR) solution and kept at 32 and 37 ± 0.5 °C for corneal and scleral permeation respectively. 1 mL of the formulation was placed in the donor compartment and 300 μL were withdrawn from the receptor chamber at fixed time points and immediately replaced by BR. The cumulative drug amount permeated was calculated at each time point from the drug in the receiving medium and plotted as function time.[26,66] All experiments using rabbits were performed according to the Ethics Committee of Animal Experimentation at the University of Barcelona. The amount of memantine retained in the tissues was also determined by extracting the drug from the tissue with methanol: water (75:25, v/v) under sonication for 30 min.[30]

Cytotoxicity Assay: Human retinoblastoma cells (Y-79) and adherent human keratinocyte cells (HaCaT[73]) were purchased from Cell Lines Services (CLS, Eppelheim, Germany) and were maintained in RPMI-1640 and DMEM media respectively. Cell viability was assayed with Alamar Blue (Alfagene, Invitrogene, Portugal) at 24 and 48 h as was previously described.[27,68] Data were analyzed by calculating cell viability through the percentage of Alamar blue reduction compared to the control (untreated cells).[74–76]

Ocular Tolerance Test—HET-CAM and Draize Irritation Test: In order to evaluate the risk of ocular irritation caused by free memantine and MEM-NP administered as eye drops, ocular tolerance tests in vivo and in vitro were conducted. Ocular tolerance was assessed in vitro using the HETCAM test (Figure S4, Supporting Information).[31] Scores of irritation potential were grouped into four categories.[31] Subsequent in vivo ocular tolerance assays were performed using primary eye irritation test of Draize et. al (1994) with New Zealand rabbits (male, 2.5 kg) (n = 3/group).[33] The formulation was instilled in the conjunctival sac of the right eye and a gentle massage was applied. The appearance of irritation was observed at the time of administration and after 1 h, using the left eye as a negative control. The OII was calculated by direct observation of the anterior segment of the eye, noting the possible injury of the conjunctiva, iris, and cornea.[33]

In Vivo *Studies—Therapeutic Efficacy*: Induced glaucoma experimental models such as Morrison model of ocular hypertension were previously validated by our group.[48] Adult male DA rats weighing 150–200 g were treated with procedures approved by the UK Home Office and in compliance with the ARVO Statement for the Use of Animals in Ophthalmic and Vision Research. For the present study 10 rats were used as control without glaucoma induction, and 20 rats underwent surgery to elevate IOP by injection of hypertonic saline solution (1.80 M) into two episcleral veins. The rats undergoing chronic ocular

ADVANCED SCIENCE NEWS
www.advancedsciencenews.com

NANO MICRO
www.small-journal.com

hypertension were divided in two groups (10 rats/group): control group (treated with saline serum) and MEM-NPs group (treated with two drops of MEM-NPs/day). Contralateral unoperated eyes were also used as a control. The IOP of both eyes was measured weekly using a Tonopen XL (Medtronic Solan, Jacksonville, FL).

Histology and RGC Quantification: Animals were sacrificed 3 weeks after OHT induction. Eyes were enucleated and fixed in 4% fresh paraformaldehyde overnight. Whole-mount retinas were stained for the RGC specific nuclear-localized transcription factor Brn3a using a MAB1585 antibody (1:350; Merck Millipore). Immunoreactivity was detected with AlexaFluor 555 donkey antimouse (1:200; Merck Millipore, Darmstadt, Germany). Retinas were mounted and examined under confocal microscopy (LSM 710; Carl Zeiss Micro Imaging GmbH, Jena, Germany) as a tiled z-stack at 10× magnification generating a single plane maximum projection of the RGC layers for subsequent analysis. Image acquisition settings were kept constant for all retinas imaged, allowing comparison of Brn3a expression in each experimental group.[34] Automatic quantification of Brn3a-labeled RGC was achieved using an algorithm previously validated.[34,77] Naïve and OHT only Brn-3a whole retinal counts from DA rats was obtained from our previous work.[34]

Statistical Analysis: Statistical evaluation of data was performed using one-way analysis of variance (ANOVA) with Tukey multiple comparison post hoc test to assess differences between groups and $p < 0.05$ was considered significant.

Supporting Information

Supporting Information is available from the Wiley Online Library or from the author.

Acknowledgements

This work was supported by the Spanish Ministry of Science and Innovation (MAT 2014-59134-R and SAF-2016-33307). M.L.G., A.C.C., M.E., M.A.E., and E.S.L. belong to 2014SGR-1023. The first author, E.S.L., acknowledges the support of the Spanish Ministry for the PhD scholarship FPI-MICINN (BES-2012-056083). The authors want to acknowledge the Portuguese Science and Technology Foundation (FCT/MCT) and European Funds (PRODER/COMPETE) under the projects UID/AGR/04033/2013, M-ERA-NET-0004/2015-PAIRED, and UID/QUI/50006/2013, cofinanced by FEDER, under the partnership Agreement PT2020.

Conflict of Interest

The authors declare no conflict of interest.

Keywords

drug delivery, glaucoma, memantine, nanoparticles, PLGA-PEG

Received: May 30, 2017
Revised: August 10, 2017
Published online:

[1] H. Celiker, N. Yuksel, S. Solakoglu, L. Karabas, F. Aktar, Y. Caglar, *J. Ophthalmic Vis. Res.* **2016**, *11*, 174.
[2] B. M. Davis, L. Crawley, M. Pahlitzsch, F. Javaid, M. F. Cordeiro, *Acta Neuropathol.* **2016**, *132*, 807.
[3] M. Almasieh, A. M. Wilson, B. Morquette, J. L. Cueva Vargas, A. Di Polo, *Prog. Retin. Eye Res.* **2012**, *31*, 152.
[4] D. R. Anderson, *Curr. Opin. Ophthalmol.* **2003**, *14*, 86.
[5] T. Salt, M. Cordeiro, *Eye* **2006**, *20*, 730.
[6] T. Krupin, J. M. Liebmann, D. S. Greenfield, R. Ritch, S. Gardiner, *Am. J. Ophthalmol.* **2011**, *151*, 671.
[7] K. Tian, S. Shibata-Germanos, M. Pahlitzsch, M. F. Cordeiro, S. Shibata-Germanos, M. Pahlitzsch, M. F. Cordeiro, *Clin. Ophthalmol.* **2015**, *9*, 2109.
[8] J. Folch, D. Petrov, M. Ettcheto, S. Abad, E. Sánchez-López, M. L. García, J. Olloquequi, C. Beas-zarate, C. Auladell, A. Camins, *Neural Plast.* **2016**, *2016*, 1.
[9] G. Chidlow, J. P. M. Wood, R. J. Casson, *Drugs* **2007**, *67*, 725.
[10] D. F. Sena, K. Lindsley, *Cochrane Database Syst. Rev.* **2013**, *2*, 1.
[11] N. N. Osborne, *Acta Ophthalmol.* **2009**, *87*, 450.
[12] S. Mcnally, C. J. O. Brien, *Drug Discov. Today Dis. Model.* **2013**, *10*, e207.
[13] E. Prieto, B. Puente, A. Uixera, J. A. Garcia de Jalon, S. Perez, L. Pablo, J. M. Irache, M. A. Garcia, M. A. Bregante, *Ophthalmic Res.* **2012**, *48*, 109.
[14] D. Manickavasagam, M. O. Oyewumi, *J. Drug Deliv.* **2013**, *2013*, 1.
[15] U. B. Kompella, A. C. Amrite, R. Pacha Ravi, S. A. Durazo, *Prog. Retin. Eye Res.* **2013**, *36*, 172.
[16] B. Davis, E. Normando, L. Guo, P. O'Shea, S. Moss, S. Somavarapu, M. Cordeiro, *Small* **2014**, *10*, 1575.
[17] H. Yang, P. Tyagi, R. S. Kadam, C. A. Holden, U. B. Kompella, *ACS Nano* **2012**, *6*, 7595.
[18] G. Singh, T. Kaur, R. Kaur, A. Kaur, *Int. J. Pharmacol. Pharm. Sci.* **2014**, *1*, 30.
[19] A. Vasconcelos, E. Vega, Y. Pérez, M. J. Gómara, M. L. García, I. Haro, *Int. J. Nanomedicine* **2015**, *10*, 609.
[20] E. Prieto, B. Puente, A. Uixera, S. Perez, L. Pablo, J. M. Irache, M. a. Garcia, M. a. Bregante, V. Faculty, V. Faculty, *Opthalmic Res.* **2012**, *48*, 109.
[21] E. Cohen-Sela, M. Chorny, N. Koroukhov, H. D. Danenberg, G. Golomb, *J. Control. Release* **2009**, *133*, 90.
[22] H. Puthussericka, R. Suman, V. Gunjan, *Langmuir* **2015**, *31*, 3.
[23] H. E. Gottlieb, V. Kotlyar, A. Nudelman, *J. Org. Chem.* **1997**, *62*, 7512.
[24] F. J. Mcinnes, N. G. Anthony, R. Kennedy, N. J. Wheate, *Org. Biomol. Chem.* **2010**, *8*, 765.
[25] D. H. Kim, M. Kim, C. Choi, C. Chung, S. H. Ha, C. H. Kim, *Nanoscale Res. Lett.* **2012**, *7*, 1.
[26] Y. Li, Y. Pei, X. Zhang, Z. Gu, H. Zhou, W. Yuan, J. Zhou, J. Zhu, X. Gao, *J. Control. Release* **2001**, *71*, 203.
[27] J. J. Pillai, A. K. T. Thulasidasan, R. J. Anto, N. C. Devika, N. Ashwanikumar, G. S. V. Kumar, *RSC Adv.* **2015**, *5*, 25518.
[28] A. Parra, M. Mallandrich, B. Clares, M. A. Egea, M. Espina, M. L. García, A. C. Calpena, *Colloids Surf. B. Biointerfaces* **2015**, *136*, 935.
[29] M. L. Viger, W. Sheng, C. L. McFearin, M. Y. Berezin, A. Almutair, *J. Control. Release* **2013**, *171*, 308.
[30] G. Abrego, H. Alvarado, E. B. Souto, B. Guevara, L. Halbaut, A. Parra, A. C. Calpena, M. L. García, *Eur. J. Pharm. Biopharm.* **2015**, *231*, 1.
[31] E. Sánchez-López, M. A. Egea, A. Cano, M. Espina, A. C. Calpena, M. Ettcheto, A. Camins, E. B. Souto, A. M. Silva, M. L. García, *Colloids Surfaces B Biointerfaces* **2016**, *145*, 241.
[32] B. McKenzie, G. Kay, K. H. Matthews, R. M. Knott, D. Cairns, *Int. J. Pharm.* **2015**, *490*, 1.
[33] A. M. D. Nóbrega, E. N. Alves, R. D. F. Presgrave, R. N. Costa, I. F. Delgado, *Brazilian Arch. Biol. Technol.* **2012**, *55*, 381.
[34] B. Davis, L. Guo, J. Brenton, L. Langley, E. Normando, M. Cordeiro, *Cell Death Discov.* **2016**, *2*, 1.
[35] R. A. Bouhenni, J. Dunmire, A. Sewell, D. P. Edward, *J. Biomed. Biotechnol.* **2012**, *2012*, 1.
J. Jiang, G. Oberdörster, P. Biswas, *J. Nanoparticle Res.* **2009**, *11*, 77.

[34] G. R. Ramos Yacasi, A. C. Calpena Campmany, M. A. Egea Gras, M. Espina García, M. L. García López, *Drug Dev. Ind. Pharm.* **2017**, *43*, 637.
[35] E. Vega, M. A. Egea, A. C. Calpena, M. Espina, M. L. García, *Int. J. Nanomedicine* **2012**, *7*, 1357.
[36] G. Abrego, H. L. Alvarado, M. A. Egea, E. Gonzalez-Mira, A. C. Calpena, M. L. Garcia, *J. Pharm. Sci.* **2014**, *103*, 3153.
[37] J. Araújo, E. Vega, C. Lopes, M. A. Egea, M. L. Garcia, E. B. Souto, *Colloids Surf. B. Biointerfaces* **2009**, *72*, 48.
[38] M. Vidal-Sanz, M. Salinas-Navarro, F. M. Nadal-Nicolás, L. Alarcón-Martínez, F. J. Valiente-Soriano, J. Miralles de Imperial, M. Avilés-Trigueros, M. Agudo-Barriuso, M. P. Villegas-Pérez, *Prog. Retin. Eye Res.* **2012**, *31*, 1.
[39] C. Galindo-Romero, M. Harun-Or-Rashid, M. Jiménez-López, M. Vidal-Sanz, M. Agudo-Barriuso, F. Hallböök, *PLoS One* **2016**, *11*, 1.
[40] M. J. Pérez de Lara, C. Santano, A. Guzmán-Aránguez, F. J. Valiente-Soriano, M. Avilés-Trigueros, M. Vidal-Sanz, P. de la Villa, J. Pintor, *Exp. Eye Res.* **2014**, *122*, 40.
[41] M. Ishikawa, T. Yoshitomi, C. F. Zorumski, Y. Izumi, *Biomed. Res. Int.* **2015**, *2015*, 1.
[42] P. Boya, L. Esteban-martínez, A. Serrano-puebla, R. Gómez-Sintes, B. Villarejo-zori, *Prog. Retin. Eye Res.* **2016**, *55*, 206.
[43] L. Guo, S. E. Moss, R. A. Alexander, R. R. Ali, F. W. Fitzke, M. F. Cordeiro, *Invest. Ophthalmol. Vis. Sci.* **2005**, *46*, 175.
[44] H.-Y. Li, Y.-W. Ruan, C.-R. Ren, Q. Cui, K.-F. So, *Neural Regen. Res.* **2014**, *9*, 565.
[45] L. Guo, T. E. Salt, A. Maass, V. Luong, S. E. Moss, F. W. Fitzke, M. F. Cordeiro, *Invest. Ophthalmol. Vis. Sci.* **2006**, *47*, 626.
[46] J. W. Johnson, S. E. Kotermanski, *Curr. Opin. Pharmacol.* **2006**, *6*, 61.
[47] G. M. Alley, J. a. Bailey, D. Chen, B. Ray, L. K. Puli, H. Tanila, P. K. Banerjee, D. K. Lahiri, *J. Neurosci. Res.* **2010**, *88*, 143.
[48] B. Ray, P. K. Banerjee, N. H. Greig, D. K. Lahiri, *Neurosci. Lett.* **2010**, *470*, 1.
[49] K. Ito, T. Tatebe, K. Suzuki, T. Hirayama, M. Hayakawa, H. Kubo, T. Tomita, M. Makino, *Eur. J. Pharmacol.* **2017**, *798*, 16.
[50] L. Guo, T. E. Salt, V. Luong, N. Wood, W. Cheung, A. Maass, G. Ferrari, A. M. Sillito, M. E. Cheetham, S. E. Moss, F. W. Fitzke, M. F. Cordeiro, F. Russo-Marie, *Proc. Natl. Acad. Sci. USA* **2007**, *104*, 13444.
[51] Y. Ito, M. Shimazawa, K. Tsuruma, C. Mayama, K. Ishii, H. Onoe, M. Aihara, M. Araie, H. Hara, *Mol. Vis.* **2012**, *18*, 2647.
[52] S. Nizari, L. Guo, B. M. Davis, E. M. Normando, J. Galvao, L. A. Turner, M. Bizrah, M. Dehabadi, K. Tian, M. Francesca Cordeiro, *Cell Death Dis.* **2016**, *7*, e2514.
[53] V. Gupta, V. B. Gupta, N. Chitranshi, S. Gangoda, R. Vander Wall, M. Abbasi, M. Golzan, Y. Dheer, T. Shah, A. Avolio, R. Chung, R. Martins, S. Graham, *Cell. Mol. Life Sci.* **2016**, *73*, 4279.
[54] J. Sivak, *Invest. Opthalmol. Vis. Sci.* **2013**, *54*, 871.
[55] J. A. Ratnayaka, L. C. Serpell, A. J. Lotery, *Eye* **2015**, *29*, 1013.
[56] G. Beidoe, S. A. Mousa, *Clin. Ophthalmol.* **2012**, *6*, 1699.
[57] J. Won-Kyu, K. Keun-Young, M. Angert, K. Duong Polk, J. D. Lindsey, M. H. Ellisman, R. N. Weinreb, *Invest. Ophthalmol. Vis. Sci.* **2009**, *50*, 707.
[58] F. Schuettauf, K. Quinto, R. Naskar, D. Zurakowski, *Vision Res.* **2002**, *42*, 2333.
[59] W. Hare, E. WoldeMussie, R. Lai, H. Ton, G. Ruiz, B. Feldmann, M. Wijono, T. Chun, L. Wheeler, *Surv. Ophthalmol.* **2001**, *45*, S284.
[60] N. N. Osborne, *Vis. Neurosci.* **1999**, *16*, 45.
[61] B. T. Gabelt, C. A. Rasmussen, O. Y. Tektas, C. B. Y. Kim, J. C. Peterson, T. Michael Nork, J. N. ver Hoeve, E. Lütjen-Drecoll, P. L. Kaufman, *Invest. Ophthalmol. Vis. Sci.* **2012**, *53*, 2368.
[62] U. Puangthong, G.-Y. R. Hsiung, *Neuropsych. Dis. Treat.* **2009**, *5*, 553.
[63] P. V. Turner, T. Brabb, C. Pekow, M. a. Vasbinder, *J. Am. Assoc. Lab. Anim. Sci.* **2011**, *50*, 600.
[64] S. Laserra, A. Basit, P. Sozio, L. Marinelli, E. Fornasari, I. Cacciatore, M. Ciulla, H. Türkez, F. Geyikoglu, A. Di, *Int. J. Pharm.* **2015**, *485*, 183.
[65] N. Mittapelly, R. Rachumallu, G. Pandey, S. Sharma, A. Arya, R. S. Bhatta, P. R. Mishra, *Eur. J. Pharm. Biopharm.* **2016**, *101*, 62.
[66] H. Ali, B. Weigmann, E. M. Collnot, S. A. Khan, M. Windbergs, C. M. Lehr, *Pharm. Res.* **2015**, *33*, 1.
[67] A. A. Almeida, D. R. Campos, G. Bernasconi, S. Calafatti, F. A. P. Barros, M. N. Eberlin, E. C. Meurer, E. G. Paris, J. Pedrazzoli, *J. Chromatogr. B. Analyt. Technol. Biomed. Life Sci.* **2007**, *848*, 311.
[68] K. Hu, S. Cao, F. Hu, J. Feng, *Int. J. Nanomedicine* **2012**, *7*, 3537.
[69] M. Teixeira, M. J. Alonso, M. M. M. Pinto, C. M. Barbosa, *Eur. J. Pharm. Biopharm.* **2005**, *59*, 491.
[70] P. Boukamp, P. Rule T, D. Breitkreutz, J. Hornung, A. Markham, N. E. Fusenig, *J. Cell Biol.* **1988**, *106*, 761.
[71] S. Doktorovová, D. L. Santos, I. Costa, T. Andreani, E. B. Souto, A. M. Silva, *Int. J. Pharm.* **2014**, *471*, 18.
[72] C. M. Emnett, L. N. Eisenman, J. Mohan, A. a. Taylor, J. J. Doherty, S. M. Paul, C. F. Zorumski, S. Mennerick, *Br. J. Pharmacol.* **2015**, *172*, 1333.
[73] W. Liu, Z. Xu, T. Yang, B. Xu, Y. Deng, S. Feng, *Mol. Neurobiol.* **2016**, *54*, 5034.
[74] L. Guo, B. Davis, S. Nizari, E. M. Normando, H. Shi, J. Galvao, L. Turner, J. Shi, M. Clements, S. Parrinello, M. F. Cordeiro, *Cell Death Dis.* **2014**, *5*, e1460.

3.4. PEGYLATED PLGA NANOSPHERES OPTIMIZED BY DESIGN OF EXPERIMENTS FOR OCULAR ADMINISTRATION OF DEXIBUPROFEN—*IN VITRO, EX VIVO* AND *IN VIVO* CHARACTERIZATION

Elena Sánchez-López, Maria Antonia Egea, Aamanda Cano, Marta Espina, Ana Cristina Calpena, Miren Ettcheto, Antoni Camins, Eliana B. Souto, Amelia M. Silva, Maria Luisa García

PEGylated PLGA nanospheres optimized by design of experiments for ocular administration of dexibuprofen—in vitro, ex vivo and in vivo characterization

Colloids and Surface B: Biointerfaces. 145 (2016) 241–250

Doi: 10.1016/j.colsurfb.2016.04.054

Colloids and Surfaces B: Biointerfaces 145 (2016) 241–250

Contents lists available at ScienceDirect

Colloids and Surfaces B: Biointerfaces

j ournal homepage: www.elsevier.com/locate/colsurfb

PEGylated PLGA nanospheres optimized by design of experiments for ocular administration of dexibuprofen—*in vitro, ex vivo* and *in vivo* characterization

E. Sánchez-López[a,b], M.A. Egea[a,b], A. Cano[a], M. Espina[a,b], A.C. Calpena[b,c], M. Ettcheto[d,e], A. Camins[d,e], E.B. Souto[f,g], A.M. Silva[h,i], M.L. García[a,b,*]

[a] *Department of Physical Chemistry, Faculty of Pharmacy, University of Barcelona, Barcelona 08028, Spain*
[b] *Institute of Nanoscience and Nanotechnology (IN2UB), Faculty of Pharmacy, University of Barcelona, Barcelona 08028, Spain*
[c] *Department of Biopharmacy and Pharmaceutical Technology, Faculty of Pharmacy, University of Barcelona, Barcelona 08028, Spain*
[d] *Department of Pharmacology and Therapeutic Chemistry, Faculty of Pharmacy, University of Barcelona, Barcelona 08028, Spain*
[e] *Centro de Investigación Biomédica en Red de Enfermedades Neurodegenerativas (CIBERNED), University of Barcelona, Barcelona 08028, Spain*
[f] *Department of Pharmaceutical Technology, Faculty of Pharmacy, University of Coimbra (FFUC), Polo das Ciências da Saúde, Azinhaga de Santa Comba, 3000-548 Coimbra, Portugal*
[g] *REQUIMTE/LAQV, Group of Pharmaceutical Technology, Faculty of Pharmacy, University of Coimbra, Coimbra, Portugal*
[h] *Department of Biology and Environment, School of Life and Environmental Sciences, (ECVA, UTAD), University of Trás-os-Montes and Alto Douro, Quinta de Prados, Vila Real 5001-801, Portugal*
[i] *Centre for the Research and Technology of Agro-Environmental and Biological Sciences, University of Trás-os-Montes and Alto Douro, CITAB-UTAD, Vila-Real 5001-801, Portugal*

a r t i c l e i n f o

Article history:
Received 12 January 2016
Received in revised form 26 April 2016
Accepted 30 April 2016
Available online 3 May 2016

Chemical compounds studied in this article:
Lactic acid (PubChem CID: 612)
Glycolic acid (PubChem CID: 757)
Ethylene glycol (PubChem CID: 174)
Dexibuprofen (PubChem CID: 39912)
Polyvinyl alcohol (PubChem CID: 11199)

Keywords:
Nanospheres
Dexibuprofen
PLGA
PEG
Inflammation
Drug delivery

a b s t r a c t

Dexibuprofen-loaded PEGylated PLGA nanospheres have been developed to improve the biopharmaceutical profile of the anti-inflammatory drug for ocular administration. Dexibuprofen is the active enantiomer of ibuprofen and therefore lower doses may be applied to achieve the same therapeutic level. According to this, two batches of nanospheres of different drug concentrations, 0.5 and 1.0 mg/ml respectively, have been developed (the latter corresponding to the therapeutic ibuprofen concentration for inflammatory eye diseases). Both batches were composed of negatively charged nanospheres (-−14.1 and -−15.9 mV), with a mean particle size below 200 nm, and a high encapsulation efficiency (99%). X-ray, FTIR, and DSC analyses confirmed that the drug was dispersed inside the matrix of the nanospheres. While the *in vitro* release profile was sustained up to 12 h, the *ex vivo* corneal and scleral permeation profile demonstrated higher drug retention and permeation in the corneal tissue rather than in the sclera. These results were also confirmed by the quantification of dexibuprofen in ocular tissues after the *in vivo* administration of drug-loaded nanospheres. Cell viability studies confirmed that PEGylated-PLGA nanospheres were less cytotoxic than free dexibuprofen in the majority of the tested concentrations. Ocular *in vitro* (HET-CAM test) and *invivo* (Draize test) tolerance assays demonstrated the non-irritant character of both nanosphere batches. *In vivo* anti-inflammatory effects were evaluated in albino rabbits before and after inflammation induction. Both batches confirmed to be effective to treat and prevent ocular inflammation.

Abbreviations: NSAIDs, non-steroidal anti-inflammatory drugs; IBU, ibuprofen; DXI, dexibuprofen; GI, gastrointestinal; NPs, nanoparticles; PLGA, poly(lactic-co-glycolic) acid; PEG, poly(ethylene glycol); RES, reticuloendothelial system; NSs, nanospheres; PVA, polyvinyl alcohol; DoE, design of experiments; Z_{av}, average particles size; PI, polydispersity index; ZP, zeta potential; EE, encapsulation efficiency; PCS, photon correlation spectroscopy; HPLC, high performance liquid chromatography; TEM, transmission electron microscopy; DSC, differential scanning calorimetry; XRD, X-Ray diffraction; FTIR, Fourier transformed infrared; PBS, phosphate buffered saline; BR, bicarbonate ringer; CAM, chorioallantoic membrane; SA, sodium arachidonate.

* Corresponding author at: Department of Physical Chemistry, Faculty of Pharmacy, University of Barcelona, 08028, Barcelona, Spain.
E-mail addresses: marisagarcia@ub.edu, rdcm@ub.edu (M.L. García).

1. Introduction

Inflammation is a non-specific response of the body against injuries from the external environment, acting as a defense mechanism to isolate and destroy the triggering agent, as well as to repair the damaged tissues. Ocular inflammation is one of the most prevalent diseases in ophthalmology. It can affect any part of the eye or the surrounding tissues. Corticosteroids are commonly used as anti-inflammatory drugs for the treatment of ocular inflammation, but they induce serious adverse effects when administered continuously [1]. The main alternatives to corticosteroids for the treatment of inflammation are non-steroidal anti-inflammatory drugs (NSAIDs) [2]. In the field of ophthalmology, ibuprofen (IBU) has been receiving particular attention in recent years due to its anti-inflammatory activity, having however a number of adverse effects that limit its use [3,4].

Rapid elimination of NSAIDs administered as eye drops, results in a pre-corneal drug half-life between 1 and 3 min. As a consequence, only a very small amount of the drug (1–5% of the dose) actually penetrates the cornea and is able to reach intraocular tissues. On the other hand, drugs administered onto the ocular mucosa are known to suffer absorption via conjunctiva and nasolacrimal duct, easily reaching the systemic circulation [5,6]. Drugs, such as IBU, may induce adverse side effects that can be minimized by the use of the active enantiomer – dexibuprofen (DXI), which is twice more potent and has less side effects than the former [7]. Gastric and epigastric pain, nausea and vomiting have been the most frequent side effects reported in randomized clinical trials in patients treated with DXI. Effects of DXI in the central nervous system (CNS) were less common than the use of racemic IBU [8]. The racemic mixture was also responsible for a higher gastric toxicity than the S(+) isomer [7]. Moreover, the safety, tolerability and equivalent efficacy between DXI and the double dose of ibuprofen was confirmed by comparing the oral uptake of both drugs for osteoarthritis treatment in a clinical study [8,9].

To protect the drug from inactivation by the enzymes present in the tear film or corneal epithelium, to facilitate its transcorneal penetration prolonging its stay in the precorneal area, and to avoid undesired adverse effects, polymeric nanoparticles (NPs) have been proposed. Biodegradable polymers, including poly(lactic-*co*-glycolic acid) (PLGA) (biopolymer approved by the Food and Drug administration), have been widely used as a biomaterial in medical prostheses and surgical sutures [10]. More recently, PLGA has been used in the development of colloidal carriers for controlled release of drugs, due to its biocompatibility, biodegradability and non-toxicity [11]. Furthermore, compared to natural polymers, these synthetic polymers demonstrate higher reproducibility, are easily formulated and allow the control and prediction of the degradation kinetics [12].

Among other strategies, PEG-coated PLGA NPs offer several advantages. These are firstly attributed to the enhanced contact time of the particles with the corneal surface by the interaction with the mucus layer of the tear film. NPs interact with the mucus layer of the tear film either by electrostatic, hydrophobic and hydrogen bonding, or by their physical retention in the mucin network [13]. Griffiths et al. [13] demonstrated that such retention in the mucin network is dependent on the hydrophobic surface of the particles, which could be overcome by coating them with PEG. On the other hand, the hydrophobic entrapment could be minimized as long as the nanoparticles were adequately surfaced with such hydrophilic PEG layers and depicted negative electrical charge [13]. Therefore, the accumulation of the NPs in the conjunctival sac, as well as the ability of the particles to penetrate in the first layers of the corneal epithelium contribute to enhance drugs bioavailability [14]. In addition, PEGylation contributes to maintain the particles in circulation for a longer time, thus avoiding their recognition by the reticuloendothelial system (RES) [15].

In the present work, we report the development of a new formulation for ocular delivery of dexibuprofen (DXI), based on nanospheres (NSs) composed of poly-l-lactic-co-glycolide (PLGA) surrounded by polyethylene glycol (PEG) chains (DXI-PLGA-PEG NSs). The suitability of DXI-PLGA-PEG NSs to treat and prevent ocular inflammation has been demonstrated. Physicochemical properties and drug-polymer interactions were assessed. *In vitro* and *ex vivo* drug release and short-term stability of DXI NSs were studied. DXI quantification after *in vivo* administration was also performed.

2. Materials and methods

2.1. Materials

Diblock copolymer PLGA-PEG 5% Resomer® was obtained from Evonik Corporation (Birmingham, USA) and the active compound *S*-(+)-Ibuprofen (dexibuprofen) was purchased from Amadis Chemical (Hangzou, China). Polyvinyl alcohol (PVA) and acetone were purchased from Sigma-Aldrich (Madrid, Spain) and Fisher Scientific (Pittsburgh, USA), respectively. Reagents for cell culture were obtained from Gibco (Alfagene, Portugal). Alamar Blue, from Invitrogen Alfagene® (Portugal), was used for cell viability estimation. Water filtered through Millipore® MilliQ system was used for all the experiments and all the other reagents were of analytical grade.

2.2. Methods

2.2.1. Nanospheres preparation

NSs were prepared by solvent displacement method described elsewhere [16]. Briefly, the co-polymer PLGA-PEG and the drug (DXI) were firstly dissolved in acetone. This organic phase was added dropwise, under moderate stirring, into 10 ml of an aqueous solution of PVA (0.33–1.17%) adjusted to the desired pH (3.2–4.8). After that, acetone was evaporated under reduced pressure and the resulting particles were ultracentrifuged, at 15000 r.p.m. for 20 min, in order to remove excess of PVA.

2.2.2. Optimization of nanospheres parameters

Design of experiments (DoE) is frequently used to plan research because it provides maximum information, whilst requiring a minimal number of experiments [17]. A central composite factorial design was developed to analyze the effect of independent variables (pH, DXI and PVA concentrations) on the dependent variables (average particle size (Z_{av}), polydispersity index (PI), zeta potential (ZP) and encapsulation efficiency (EE). The amount of polymer was kept constant for all the assays (90 mg).

According to the composite design matrix generated by Statgraphics Plus 5.1 software, a total of 16 experiments (8 factorial points, 6 axial points and two replicated center points) were required. The experimental responses were the result of the individual influence and the interactions of the three independent variables, as shown in Table 1. The responses were therefore modeled through the full second-order polynomial equation shown in Eq. (1):

$$Y_u = \beta_0 + \beta_1 \times X_1 + \beta_2 \times X_2 + \beta_3 \times X_3 + \beta_{11} \times X_1^2 + \beta_{22} \times X_2^2 + \beta_{33} \times X_3^2 + \beta_{12} \times X_1 \times X_2 + \beta_{13} \times X_1 \times X_3 + \beta_{23} X_2 \times X_3 \quad (1)$$

where Y_u is the measured response, β_0 to $\beta_{2,3}$ are the regression coefficients and X_1, X_2 and X_3 are the studied factors. The effect and the significance level of the factors were evaluated by analysis of variance (ANOVA) [18].

2.2.3. Physicochemical characterization

Z_{av} and PI of NSs were determined by photon correlation spectroscopy (PCS) (after 1:10 dilution) with a Zetasizer Nano

Table 1
Values of the experimental factors according to the matrix designed by 2^3 + star central composite rotatable factorial design parameters and measured responses. Bold values correspond to the optimized formulation of DXI loaded NSs.

	pH		c_{DXI}		c_{PVA}		Z_{av} (nm)	PI	ZP (mV)	EE (%)
	Coded level	pH	Coded level	(mg/ml)	Coded level	(%)				
Factorial points										
F1	**−1**	**3.5**	**−1**	**0.50**	**−1**	**0.50**	**221.4 ± 0.5**	**0.082 ± 0.023**	**−4.17 ± 0.29**	**99.79**
F2	1	4.5	−1	0.50	−1	0.50	219.3 ± 6.6	0.050 ± 0.033	− 11.9 ± 0.19	90.80
F3	−1	3.5	1	1.50	−1	0.50	225.5 ± 3.2	0.072 ± 0.027	− 3.16 ± 0.28	99.20
F4	1	4.5	1	1.50	−1	0.50	201.1 ± 4.6	0.048 ± 0.018	− 5.13 ± 0.55	87.65
F5	−1	3.5	−1	0.50	1	1.00	216.5 ± 2.9	0.068 ± 0.026	− 3.24 ± 0.93	90.72
F6	1	4.5	−1	0.50	1	1.00	216.6 ± 2.1	0.049 ± 0.007	− 5.65 ± 0.26	85.52
F7	−1	3.5	1	1.50	1	1.00	219.0 ± 3.8	0.065 ± 0.009	− 3.53 ± 0.17	89.77
F8	1	4.5	1	1.50	1	1.00	213.3 ± 1.2	0.048 ± 0.029	− 3.15 ± 0.53	89.82
Axial points										
F9	1.68	4.8	0	1.00	0	0.75	229.2 ± 0.7	0.054 ± 0.018	−2.75 ± 0.17	89.87
F10	−1.68	3.2	0	1.00	0	0.75	205.8 ± 2.3	0.063 ± 0.013	−2.53 ± 0.44	92.36
F11	0	4.0	1.68	1.84	0	0.75	223.5 ± 0.6	0.036 ± 0.018	−4.38 ± 0.25	90.90
F12	0	4.0	−1.68	0.16	0	0.75	223.4 ± 1.6	0.052 ± 0.022	− 6.84 ± 0.27	99.10
F13	0	4.0	0	1.00	1.68	1.17	220.4 ± 0.3	0.036 ± 0.007	−5.73 ± 0.13	98.90
F14	0	4.0	0	1.00	−1.68	0.33	203.9 ± 0.4	0.072 ± 0.024	− 8.18 ± 0.23	97.84
Center points										
F15	0	4.0	0	1.00	0	0.75	220.3 ± 6.6	0.046 ± 0.023	−6.01 ± 0.16	90.51
F16	0	4.0	0	1.00	0	0.75	217.3 ± 2.9	0.043 ± 0.030	−6.56 ± 0.93	85.45

ZS (Malvern Instruments, Malvern, UK) at 25 °C using disposable quartz cells and (Malvern Instruments).

NSs surface charge, measured as ZP, was evaluated by using laser-Doppler electrophoresis with M3 PALS system in Zetasizer Nano ZS. ZP indirectly indicates the rate of aggregation of particles. A greater ZP (in absolute value) would induce less aggregation due to repulsion forces between the particles. To calculate this, the Henry equation was used (2):

$$\mu_E = \frac{\zeta ZPF(Ka)}{6g\mu} \quad (2)$$

where μ_E is the electrophoretic mobility, s is the dielectric constant of the medium, ZP is the zeta potential, μ is the viscosity of the medium, K is the Deybye-Hückel parameter and f (Ka) is a correction factor that takes into account the thickness of the elec- trical double layer (1/K) and particle diameter (a). The unit of K is a reciprocal length.

The reported values correspond to the mean ± SD of at least three different batches of each formulation [19].

2.2.4. Evaluation of the encapsulation efficiency

The EE of DXI in the NSs was determined indirectly by measuring the concentration of the free drug in the dispersion medium. The non-encapsulated DXI was separated by a filtration/centrifugation technique (1:10 dilution) by using an Ultracell–100 K (AmiconR Ultra; Millipore Corporation, Massachusetts) centrifugal filter devices at 4 °C and 700*g* for 30 min (Heraeus, Multifuge 3 L-R, Cen- trifuge. Osterode, Germany). The EE was calculated using Eq. (3):

$$EE(\%) \frac{\text{total amount of DXI} - \text{free DXI}}{\text{total amount of DXI}} \times 100 \quad (3)$$

Samples were evaluated by high performance liquid chromatography (HPLC), as described elsewhere [20]. Briefly, samples were quantified using HPLC Waters 2695 separation module and a Kromasil® C_{18} column (5 μm, 150 4.6 mm) with a mobile phase of methanol/phosphoric acid 0.05% (80:20) at a flow rate of 1 ml/min and a wavelength of 220 nm. Standards were pre- pared in methanol:water (90:10) from a stock solution of 500 μg/ml (50–0.5 μg/ml). Data was processed using Empower 3® Software.

2.2.5. Nanospheres characterization and interaction studies

NSs were diluted (1:5) and a morphological study was carried out by transmission electron microscopy (TEM) on a Jeol 1010. To visualize the NSs, copper grids were activated with UV light and samples were placed on the grid surface. Negative staining was performed with uranyl acetate (2%).

X-ray diffraction (XRD) was used to analyze the state (amorphous or crystalline) of the samples (centrifuged NSs or formulation compounds). Compounds were sandwiched between polyester films and exposed to CuK" radiation (45 kV, 40 mA, h = 1.5418 Å) in the range (20) from 2° to 60° with a step size of 0.026° and a measuring time of 200 s per step.

Fourier transform infrared (FTIR) spectra of different samples (NSs formulations or compounds separately) were obtained using a Thermo Scientific Nicolet iZ10 with an ATR diamond and DTGS detector. The scanning range was 525–4000 cm^{-1}.

Thermograms were obtained on a Mettler TA 4000 system (Greifensee, Switzerland) equipped with a DSC 25 cell. Temperature was calibrated by the melting transition point of indium prior to sample analysis. All samples were weighed (Mettler M3 Microbalance) directly in perforated aluminum pans and heated under a nitrogen flow at a rate of 10 °C/min (25–125 °C).

2.2.6. Determination of the in vitro *release profile*

One of the main goals of drug release from the polymer matrix is the possibility to provide an extended release profile over time. *In vitro* release was evaluated using a bulk-equilibrium reverse dialysis bag technique [21]. This technique is based on the dispersion of the colloidal suspension in the dialysis medium accomplishing sink conditions [22]. The release medium was composed of a buffer solution (PBS 0.1 M, pH 7.4). 16 dialysis sacs containing 1 ml of PBS were previously immersed into the release medium. The dialysis sacs were equilibrated with the dissolution medium a few hours prior to the experiments. A volume of 15 ml of free drug in PBS or NSs was added to 285 ml of the dissolution medium. The assay was carried out in triplicate comparing the free drug in PBS against NSs formulations. Release kinetic experiments were performed at a fixed temperature of 32 °C (ocular surface temperature) under constant magnetic stirring (n = 6/group). At predetermined time intervals, the dialysis sacs were withdrawn from the stirred release solution and the volume was replaced by 1 ml of PBS. The content of the

sacs at each time point was evaluated and data were adjusted to the most common kinetic models [19].

2.2.6. Ex vivo corneal and scleral permeation study

Ex vivo corneal and scleral permeation experiments were carried out with New Zealand rabbits (male, weighting 2.5–3.0 kg), under veterinary supervision, and according to the Ethics Committee of Animals Experimentation from the University of Barcelona (CEEA-UB). The rabbits were anesthetized with intramuscu- lar administration of ketamine HCl (35 mg/kg) and xylazine (5 mg/kg) and euthanized by an overdose of sodium pentobar- bital (100 mg/kg) administered through marginal ear vein under deep anesthesia. The cornea and sclera were excised and immedi- ately transported to the laboratory in artificial tear solution. The assay was done using Franz diffusion cells and the tissue was fixed between the donor and receptor compartment. The area available for permeation was 0.64 cm^2. The receptor compartment was filled with freshly prepared Bicarbonate Ringer's (BR) solution. This compartment was kept at 32 0.5±°C and 37 0.5 °C for corneal and scleral permeation, respectively, and stirred continuously. A volume of 1 ml of F (A) NSs or 0.5 mg/ml of DXI was placed in the donor compartment and covered to avoid evaporation. A volume of 300 µl was withdrawn from the receptor compartment at fixed times and replaced by an equivalent volume of fresh BR solution at the same temperature. The cumulative DXI amount permeated was calculated, at each time point, from DXI amount in the receiving medium and plotted as function time (min) [23].

At the end of the study, the cornea was used to determine the amount of drug retained. The tissue was cleaned using a 0.05% solution of sodium lauryl sulfate and washed with distilled water, weighed and treated with methanol under sonication dur- ing 30 min using an ultrasound bath. The amount of DXI permeated and retained through the cornea was determined.

Results are reported as the median±SD of six replicates for the amount of DXI permeated and retained on each tissue, respectively [23].

Lag time, T_L (h), values were calculated by plotting the cumulative DXI permeating the cornea versus time, determining x-intercept by linear regression analysis. The corneal permeability coefficient K_P (cm/h), partition coefficient P_1 (cm) and diffusion coefficient P_2 (h^{-1}) were calculated from the following equations:

$$K_p = P_1 \times P_2 \quad (4)$$

$$P_{F=} \frac{J}{A \times C_0 \times P_2} \quad (5)$$

1

$$P_2 = \frac{}{6 \times T_L} \quad (6)$$

where C_0 is the initial concentration of drug in the donor compartment, A (0.64 cm^2) is the exposed corneal surface [23].

2.2.8. Short-term stability

NSs stability at 4, 25 and 38 °C was assessed by light backscattering by means of a Turbiscan® Lab. For this purpose, a glass measurement cell was filled with the sample for each temperature. The light source, pulsed near infrared light-emitting diode LED (h = 880 nm), was received by a backscattering detector at an angle of 45° from the incident beam. Backscattering data were acquired once a month for 24 h, at 1 h intervals. In addition to this technique, Z_{av}, PI and ZP of NSs were also measured monthly. Temperature studies were carried out by duplicate, and visual observation of the samples was undertaken.

2.2.9. Cytotoxicity assay

Alamar blue assay was carried out in order to investigate the possible toxicity of the developed NSs in comparison to the free DXI. To perform this assay Y-79 (human retinoblastoma) cell line acquired from Cell Lines Service (CLS, Eppelheim, Germany) was used. Y-79 cells were maintained in RPMI-1640, supplemented with 10% (v/v) fetal bovine serum (FBS), 2 mM l-glutamine, and antibiotics (100 U/ml penicillin and 100 µg mL^{-1} of streptomycin) at 37 °C under an atmosphere of 5% CO_2/95% air with controlled humidity (Binder chamber). Cells were centrifuged, re-suspended in FBS-free culture media, counted and seeded, after appropriate dilution, at 1×10^5 cells/ml, in poly-l-lysine pre-coated 96-well plates (100 µl/well). For this study, dilutions of NSs in FBS-free culture media (namely F(A) and F(B), see NSs optimization section), as well as their corresponding free drug were carried out and added to cells 24 h after seeding (100 µl/well). Cell viability was assayed with Alamar Blue (AB, Alfagene, Invitrogen, Portugal), 24 or 48 h after exposure to test compounds, by addition of 100 µl/well of AB solution, 10% (v/v) diluted in FBS-free media, preceded by removal of test solutions. The AB absorbance was determined at h of 570 nm (reduced form) and 620 nm (oxidized form) after 4 h of cell contact. Data were analyzed by calculating the percentage of Alamar blue reduction (according to the manufacture recommendations) and expressed as percentage of control (untreated), as reported before [24].

2.2.10. Ocular tolerance assays: HET-CAM and draize irritation test

To assess the potential risk of ocular irritation caused by NSs, ocular tolerance test by *in vivo* and *in vitro* methods were carried out.

To study the ocular tolerance *in vitro* the HETCAM® test was developed as described in the INVITTOX nº 15 protocol [25]. This test is based on the observation of the irritant effects (bleeding, vasoconstriction and coagulation) in the chorioallantoic membrane (CAM) of an embryonated egg (10 days) induced by application of 300 µl of the studied formulation, during the first 5 min [26]. In the experimental procedure, fertilized and incubated eggs during 10 days were used. These eggs (from the farm G.A.L.L.S.A, Tarragona, Spain) were kept at a temperature of 12 ± 1 °C for at least 24 h before placing them in the incubator with controlled temperature (37.8 °C) and humidity (50–60%) during the incubation days. A series of controls were performed: SDS 1% (positive control for slow irritation), 0.1 N NaOH (positive control for fast irritation), NaCl 0.9% (negative control). Data were analyzed as the media±SD of the time at which the injury occurred (n = 6/group). Scores of irritation potential can be grouped into four categories (see Table A.1 of Supplementary material) [27].

In vivo ocular tolerance assays were performed using primary eye irritation test of Draize et al. [23] using New Zealand albino male rabbits of 2.5 kg middle weight from San Bernardo farm (Navarra). This test was performed according to the Ethical Committee for Animal Experimentation of the UB and current legislation (Decret 214/97, Gencat). The sample was placed in the conjunctival sac of the right eye and a gentle massage was applied to assure the proper sample circulation through the eye. The appearance of irritation was observed at the time of administration and after 1 h, using the left eye as a negative control (n = 6/group). The evaluation was performed by direct observation of the anterior segment of the eye, noting the possible injury of the conjunctiva (inflammation, chemosis, redness or oozing), iris and cornea (opacity and affected surface) (for detailed punctuation see Table A.2 of Supplementary material). Ocular irritation index (OII) was evaluated according to the observed injuries (Table A.1 on Supplementary material).

2.2.11. Inflammatory activity assay

Corneal inflammatory activity of the developed formulations was assessed *in vivo* (n = 6/group). Ocular inflammation was induced administering 50 µl of sodium arachidonate (SA) 0.5%

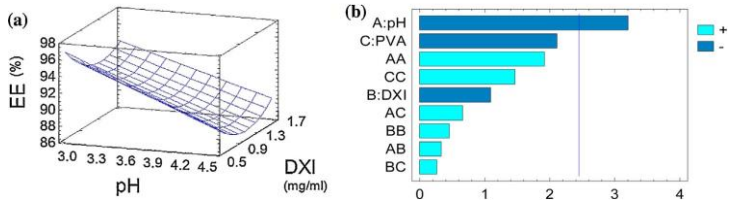

Fig. 1. Optimization of DXI NSs. (a) EE (%) surface response at a fix PVA concentration (0.75%), (b) PI surface response at a fix DXI concentration (0.5 mg/ml).

(w/v) dissolved in PBS (pH 7.4). Inflammation was quantified using a slit lamp at various times, according to a modified Draize scor- ing system [27]. The sum of the inflammation score is expressed by the mean SD ± (detailed punctuations can be found in Table A.2 of Supplementary material).

To assess inflammation prevention, free drug and DXI NSs were instilled (50 µl) in the conjunctival sac, 30 min before induction of ocular inflammation. In order to test the treatment, ocular inflammation was induced and after 30 min, either NSs or free DXI in saline serum were applied.

2.2.11. Ocular drug bioavailability

In order to achieve steady-state concentrations, DXI NSs were administered to New Zealand rabbits (n = 6), every 8 h for two weeks. A volume of 50 µl of each formulation was administered and, at the end of the experiments, animals were scarified and drug amount was quantified in vitreous humor and aqueous humor. Retained DXI on cornea and sclera were also measured [20].

2.2.12. Statistical analysis

All of the data are presented as the mean ± S.D. Two-way ANOVA followed by Tukey post hoc test was used for multi-group comparison. Student's *t*-test was used for two-group comparisons. Statistical significance was set at $p < 0.05$. GraphPad Prism V6.0 InStat (GraphPad Sofware Inc., San Diego, CA, EE.UU.) was used to carry out the analysis.

1. Results and discussion

1.1. Nanospheres optimization

The results obtained from the central composite factorial design are shown in Table 1. EE is greatly influenced by the pH (Fig. 1a) and decreases in alkaline media. Therefore, a low pH value would have to be chosen. Moreover, this acidic media would contribute to obtain a monodisperse population, as the alkaline pH values were shown to increase PI (Fig. 1b). However, acidic pH contributes to sample instability by decreasing the ZP in absolute values (Fig. A.1 of Supplementary material). In order to obtain a balance between the long-term stability of the particles and the physicochemical NSs parameters, a pH of 3.5 was selected (F1, Table 1).

The increase of DXI concentration in the formulations did not have a significant effect on the EE, suggesting that the tested concentrations did not reach polymer-loading capacity. Further studies with F1 particles were carried out, leading to a high EE (99%) using 45 mg of PLGA-PEG. Drug loading capacity depends on the physico- chemical properties of the molecule, as well as on the nanoparticle polymer, and also on the manufacturing process for the nanopar- ticles [28]. In our case, despite the small drug concentration in F1 (0.5 mg/ml), some authors have suggested that DXI is more effec- tive than the racemic counterpart (ibuprofen) in a ratio 1:0.5 [3]. Thus, this concentration would theoretically be enough to treat corneal inflammation. A second formulation, containing an identical drug/polymer ratio but twice the amount of the drug (1 mg/ml), was also developed and characterized for storage stability, inflammation and irritation assays. Both formulations have been studied: F(A) for NSs containing DXI 0.5 mg/ml, and 45 mg of polymer and F(B) for NSs containing 1 mg/ml DXI and 90 mg of polymer.

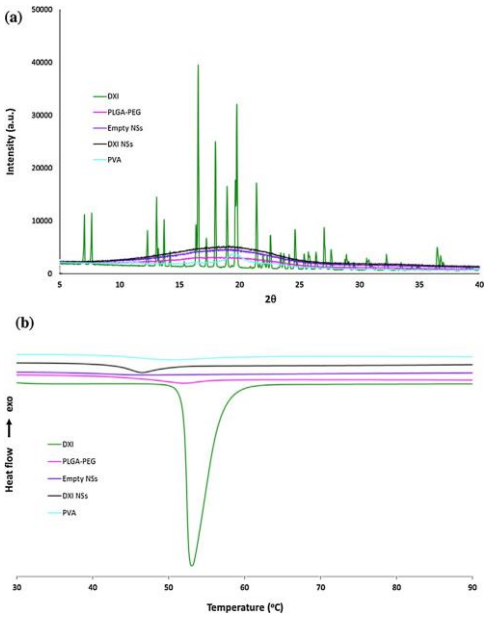

Fig. 2. Physical characterization of DXI-PLGA-PEG NSs, empty PLGA-PEG NSs and NSs compound separately. (a) X-ray diffraction patterns, (b) Differential scanning calorimetry.

1.2. Nanospheres characterization and interaction studies

NSs parameters after ultracentrifugation are summarized in Table A.3 (Supplementary material). Both formulations presented a monodisperse population (PI < 0.1) and a mean size below 200 nm, suitable for ocular administration. Superficial charge was negative (around 15 mV) due to polymer carboxylic chains [29]. The observed decrease on the ZP values, compared to those reported for PLGA-NPs by Vega et al. [27] (higher than −20 mV), were attributed to the presence of PEG layer, which reduces the negative surface charge characteristic of PLGA-NPs. The carboxylic groups of PLGA were masked by PEG, due to the use the solvent displacement technique for the production of the nanoparticles. In this method, a

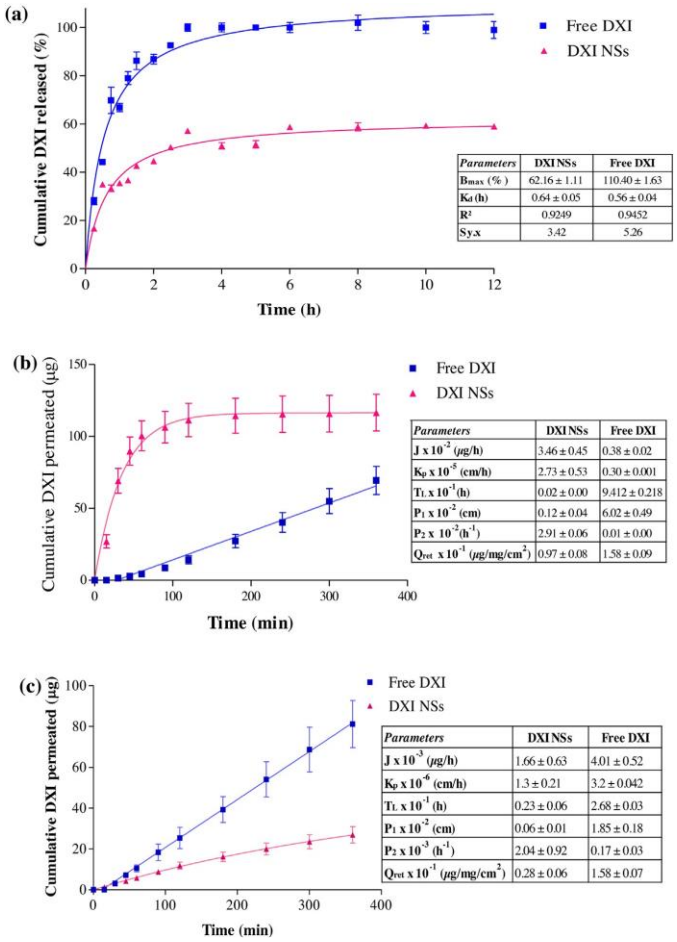

Fig. 3. Release profiles of free DXI against DXI-PLGA-PEG NSs (n=6/group). (a) *in vitro* release, (b) *Ex vivo* corneal permeation, (c) *Ex vivo* scleral permeation.

microphase separation occurs because of the mutual immiscibility between PLGA and PEG. PLGA backbone would collapse easily in water (non-solvent for PLGA), leaving the PEG chains toward the external surface of the emulsion droplets facing the aqueous phase (good solvent for PEG) [30].

TEM images (Fig. A.2, Supplementary material) reveal that the optimized NSs showed spherical shape without signals of aggregation phenomena. The mean NSs size was similar to that obtained by PCS (<200 nm).

In order to study interactions between drug and NSs, XRD, spectroscopic analysis and DSC studies were carried out.

XRD profiles of DXI (Fig. 2a) show intense sharp peaks of crystallinity, whereas the polymer diffracted an amorphous pattern. PVA exhibits a peak at 2θ = 20° due to its semi-crystalline state. Empty NSs, drug-loaded NSs and PLGA-PEG showed similar profiles. The peaks corresponding to the drug were not detected in the drug-loaded particles. This may indicate that the drug was present mainly in the dissolved state (molecular dispersion) [31].

FTIR analysis was used to study the interactions between the drug and polymer. There was no evidence of strong bonds between DXI and PLGA-PEG or between NSs and the polymer (Fig. A.3, Supplementary material). DXI presents a peak at 1697 cm^{-1} due to C O stretching, some small peaks corresponding to C C stretching (1403, 1461 and 1504 cm^{-1}) and C O (1277 cm^{-1}) and finally a peak at 777 cm^{-1} corresponding to OH bending [32]. PLGA-PEG exhibits intense bands at 2907 and 2950 cm^{-1} corresponding to the C H stretching, also present in NSs dispersions. An intense peak at 1743 cm^{-1} is shown by the polymer and by the NSs dispersions, this corresponding to the C O stretching vibration of the carbonyl groups present in the two monomers that form the polymer matrix. Bands obtained 1077, 1199 and 1305 cm^{-1} in the NSs dispersions and in the PLGA-PEG profile are attributed to stretching vibrations of the OH group [33]. The pattern displayed by both empty and drug-loaded NSs correspond to the polymer bands, but their absorbance increases due to the DXI present in the DXI-PLGA-PEG NSs. It is worth to remark that neither empty

nor DXI NSs showed the characteristic peak corresponding to PVA (at 3300 cm^{-1}), indicating an effective reduction of the surfactant amount by centrifugation process [16].

DSC profiles of DXI (Fig. 2b) show a sharp endotherm corresponding to its melting transition, characterized by a OH = 86.35 J/g and a T_{max} = 53.06 °C, which was not detected in DXI-PLGA-PEG NSs [32]. This fact suggests that DXI formulated in PLGA-PEG NSs are in an amorphous or disordered crystalline phase of a molecular dispersion or a solid solution state in the polymer matrix [27]. These results are in agreement to those obtained by other authors [5]. The polymer presented the onset of the glass transition (T_g) at 43.50 °C, whereas the NSs presented the onset at 42.50 °C, due to drug-polymer interaction. The slight decrease of NSs T_g against polymer T_g has been attributed to the effect of the acidic drug due to weak interactions with PLGA [34,35]. PVA showed a peak at 193.55 °C which was not present in the developed formulations (data not shown).

1.1. In vitro *drug release*

The release profiles of free DXI and DXI loaded NSs are shown in Fig. 3a. As expected, free DXI showed faster release kinetics than the drug-loaded particles. After three hours, the free drug achieved 100% release, whereas after 12 h the NSs released 55% of the initial amount [36]. This assay confirms that NSs could release the drug at a faster rate during the first 3 h followed by a slower diffusion (Fig. 3a, triangle symbols), which would assure a prolonged effect by a slower drug release. Some authors describe that the drug can be released from PLGA matrix either via diffusion, polymer erosion or by a combination of both mechanisms. But if drug diffusion is faster than matrix degradation, drug release occurs mainly by dif- fusion [5,27]. In our case, a burst effect was observed, due to the fraction of DXI, which is absorbed or weakly bound to the large surface area of the NSs. The second part of the profile corresponds to a sustained release behaviour, where the loaded DXI slowly dif- fuses from the polymeric matrix to the release medium. In order to ascertain the kinetic model that better fits for DXI release, data were adjusted to the most common kinetic models [37]. The most appropriate release profile corresponds to a hyperbola equation. NSs K_d was higher than the free drug, this confirms the slower DXI release from the particle matrix. These results indicate that the developed formulations could offer a prolonged release of DXI from the polymeric matrix where it is dispersed [27].

1.2. Ex vivo *corneal and scleral permeation study*

An *ex vivo* corneal and scleral permeation study, comparing NSs dispersion with the free DXI, was carried out for 6 h. Results and permeation parameters are summarized in Fig. 3b and c. J and Kp values in the cornea and the sclera are both similar in free DXI, whereas DXI NSs present high corneal permeation and accumulation in the cornea than in the sclera. This fact could be useful to justify the effect of DXI on the cornea and aqueous humor. Moreover, the amount of drug released through the cornea was higher in DXI NSs than in free DXI and the opposite effect was found for the sclera. This study shows that DXI NSs may deliver the drug effectively to the specified area by releasing DXI slowly across the corneal tissue, which would be useful for the treatment of inflammatory process such as that induced by cataract surgery. T_L values corresponding to DXI NSs on the cornea and sclera are smaller than that obtained with free DXI, which translates the capacity of NSs for sustained release of DXI in the studied tissues.

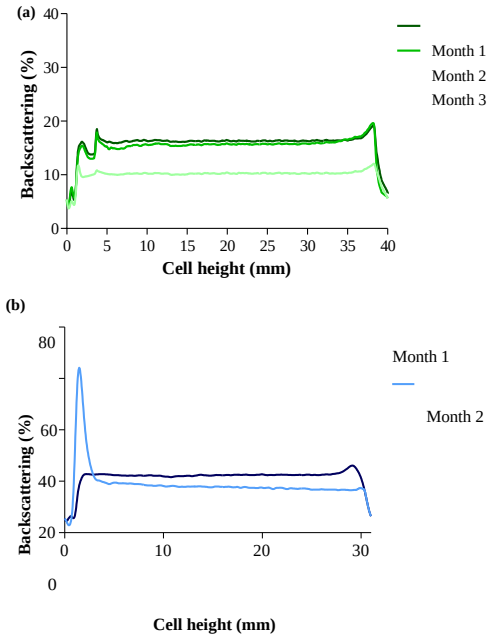

Fig. 4. DXI-PLGA-PEG NSs backscattering profile. (a) F(A), (b) F(B).

1.3. *Short-term stability*

Fig. 4 shows the evolution of the backscattering (BS) profile of DXI loaded NSs during the first months of storage. The obtained profiles translate the instability of the particles, affecting the homogeneity of the dispersion (fluctuations in BS signals, lower than 10%) in the third month of storage for F(A). The particles showed a significant decrease of the surface charge in the third month, in agreement with backscattering results (Table A.4, Supplementary material). Due to the aggregation phenomena, F(B) was shown to be unstable at the end of the second month of storage (Fig. 4b), decreasing the ZP and increasing the mean particle size. The limited stability of polymeric NPs in aqueous suspension is well known and these results confirm that in order to improve long-term stability, the removal of water from the solution (either by freeze-drying or by spray-drying) is necessary [22]. Taking into account the fact that the expiration date of collyria is limited to one month after opening the bottle, the stability of freeze-dried samples, reconstituted before application, would be more suitable for ocular administration.

1.4. *Cytotoxicity assay*

Evaluation of cell viability is important to ensure the safety of the developed NSs and avoid cell cytotoxicity. Our results demonstrate that, in the first 24 h, F(A) NSs are safer than the free drug, in all the tested concentrations (Fig. 5a). NSs with a concentration of 50 µg/ml slightly decreased cell viability (15% decrease). Although cell viability of the free DXI was lower than the obtained with the F(A) NSs at 24 h, both exhibit cell viability above 80%. After 48 h, cells exposed to free DXI showed more than 90% survival, attributed to the DXI metabolism by the cytochrome P450. This could be due to metabolite formation, namely 2-[4-(2-hydroxy-2- methylpropyl)phenyl] propionic acid and 2-[3-(2-carboxypropyl)phenyl] propionic acid within 48 h of contact, which is not toxic for the cells [38].

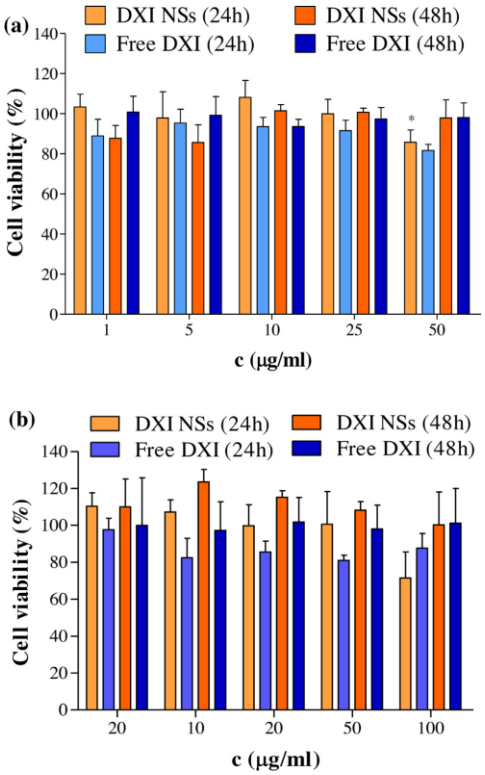

Fig. 5. Alamar Blue cytotoxicity of DXI NSs against free DXI. (a) F(A) DXI-PLGA-PEG NSs at different concentrations, (b) F(B) DXI-PLGA-PEG NSs at different concentrations.
Values are expressed as mean ± SD; $^{*}p < 0.05$, significantly lower than the same formulation at different time of exposure.

The results from cell viability studies corresponding to F(B) NSs are shown in Fig. 5b. Cells exposed to the concentration of 100 μg/ml of NSs showed 70% cell viability in the first 24 h, whereas after 48 h the same concentration did not show cytotoxic effects, attributed to a drug degradation mechanism. Regarding the other concentrations, NSs were safer and produced higher rates of cell survival than the free drug. No statistically significant differences were detected when comparing free drug and the NSs for F(A) and F(B).

1.1. In vitro *ocular tolerance*

In vitro ocular tolerance was studied using the HET-CAM test. An addition of 0.9% saline solution to the healthy membranes produced no visual response over a five minutes period. In contrast, 1 M NaOH produced severe, hemorrhage, which increased over five minutes grading this solution as severe irritant. Application of 300 μl of the samples (F(A), F(B) or PBS solution containing 0.5 or 1 mg/ml DXI) into the chorioallantoic membrane, revealed optimal ocular tolerance in the first 5 min of application (Fig. A.4, Supplementary material) [39]. OII for all tested samples show a non-irritant reaction (Table A.5, Supplementary material). These results are in

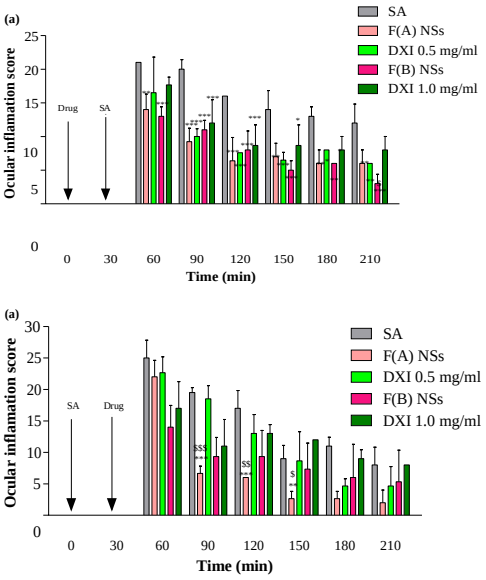

Fig. 6. Comparison of ocular anti-inflammatory efficacy of F(A), F(B) and the free DXI. (a) Inflammation treatment, (b) inflammation prevention.
Values are expressed as mean SD; $^{*}p < 0.05$, $^{**}p < 0.01$ and $^{***}p < 0.001$ significantly lower than the inflammatory effect induced by SA; $^{\$}p < 0.05$, $^{\$\$}p < 0.01$ and $^{\$\$\$}p < 0.001$ significantly lower than the inflammatory effect induced by the corresponding free drug.

agreement to those obtained by other authors loading NSAIDs into PLGA NSs for ocular applications [16,40].

3.8. In vivo *ocular tolerance*

A single *in vitro* test could not properly mimic the entire situation *in vivo*, therefore, tolerance assays in male albino rabbits were performed. The OII obtained for both F(A) and F(B) and for free DXI was null (Fig. A.5, Supplementary material), being the NSs classified as non-irritant (Table A.5, Supplementary material). These results are in agreement to those obtained with the HET-CAM test, confirming the suitability of the *in vitro* method for the assessment of the ocular tolerance of the particles, and their non-irritant properties, adequate for ocular administration [27,39,41].

3.9. *Inhibition of the inflammation*

Two studies were performed to determine the anti-inflammatory efficacy of the developed NSs, in order to confirm their usefulness for preventing and treating inflammation.

F(A) NSs prevent inflammation showing significant differences regarding positive control within the first 30 min after SA administration ($p < 0.01$) (Fig. 6a). As described elsewhere, this correlates with the amount of drug retained in the cornea [16]. In addition, free DXI at 0.5 mg/ml also prevents inflammation compared to the control which shows significant differences after 1 h of testing. This demonstrates that reduced DXI doses are an effective strategy for the prevention of ocular inflammation. In addition, encapsu- lation in polymeric NSs, increases drug effect. These results show that F(A) would be adequate to prevent ocular inflammation. F(B) also significantly reduced inflammation after 30 min of applica- tion ($p < 0.001$). In general, PLGA-PEG nanoparticles enhance ocular bioavailability of drugs due to the especial behaviour of PEG that facilitates the drug-mucin interactions [13,42].

Conjunctival inflammation with significant hyperemia was induced by SA after 30 min of exposure. At this time, the drug was applied to the conjunctival sac and degree of inflammation was measured accurately. Formulations containing 1 mg/ml of DXI, F(B) and the corresponding free drug, reduced the inflammation faster (Fig. 6b), making it adequate for high rates of inflammation which need an emergency treatment. However, F(A) demonstrated to reduce the inflammatory response more effectively than the con- trol after 1 h of application ($p < 0.001$). The differences observed in degrees of inflammation and the prevention and treatment of this pathology could be related to the different absorption of NSs in healthy and inflamed tissues. Indeed, the instillation of SA prior to the administration of the particles lead to enhanced lacrimation, increasing precorneal loss and clearance of NSs [43]. F(A) would be adequate for the prevention of inflammatory injuries (e.g. cataract surgery) reducing inflammation and providing less adverse sys- temic effects than the free drug or F(B) NSs [43].

The results obtained in this study are in agreement to published data, such as studies carried out by Buccolo et al. [44] and also by Musumeci et al. [30] with melatonin-loaded PLGA-PEG, which show a higher prolonged lowering of IOP in rabbits for melatonin-PLGA-PEG nanoparticles, than that observed without drug-loading particles. In PLGA-PEG nanoparticles, mucoadhesion can be related to the PEG crown which allows a better and longer interaction between the particles and the eye [45]. Similar results were obtained for acyclovir-loaded PEG-PLA nanospheres [46].

Globally, F(A) would be a satisfactory treatment in the prevention of inflammation and the treatment of medium-low inflammation pathologies. In the case of rescue treatment, both slight free DXI at 1 mg/ml and F(B) would be suitable, representing the NSs an improvement in reducing corneal inflammation lev- els. The NSs improvement during the first hour could be due to NSs corneal preference. As demonstrated by the ocular permeation studies, free DXI is distributed and retained in the cornea and the sclera indistinctively, whereas DXI NSs provide higher drug levels in the cornea, as well a higher drug penetration to achieve aqueous humor.

3.9. *Ocular drug bioavailability*

In order to elucidate NSs amount into eye structures, F(A) was administered *in vivo* and DXI amount was quantified 2 h after the last administration. DXI amount in the cornea (3.08 μg/ml) was higher in comparison to every other tissue, including the sclera (1.28 μg/ml). These results are in agreement to those obtained in *ex vivo* corneal and scleral permeation study. As reported by other authors [44], a certain amount of drug was also measured in the aqueous humor (in our case, 0.32 μg/ml), but no DXI was found in the vitreous humor. These results demonstrate that DXI NSs remained retained in the first structures of the eye and released the drug slowly to inner tissues, such as the aqueous humor. More- over, it has been demonstrated that, with small amount of drug, the active enantiomer loaded within NSs achieves an effective ocular anti-inflammatory activity, thus leading to a potential reduction of the adverse effects.

1. Conclusions

Ocular administration for the treatment of pathological eye tis- sues offers the advantage of delivering the drug directly to the site of action, whilst providing high drug concentration. In this study PLGA-PEG NSs were developed for topical delivery of DXI.

The DoE approach shows that pH was one of the most influential parameters on the preparation of the nanoparticles. The optimized formulations of NSs were shown to be monodisperse ($PI < 0.1$), with a mean particle size smaller than 200 nm, with a negative surface charge and high EE. DSC studies showed that DXI was distributed as a molecular dispersion inside the polymeric matrix. XRD showed evidence of the drug loaded within the NSs. FTIR studies showed that there was no evidence of chemical interaction or strong bond formation between the NSs compounds. F(A) NSs showed stability at 25 °C for three months, whereas F(B) NSs showed a sedimentation process in the second month possibly due to an increase in polymer and drug concentration that, in addition, contributed to their interactions. DXI *in vitro* release from the polymeric matrix was slower than the release of free drug. *Ex vivo* and *in vivo* studies confirmed that NSs permeate better through corneal tissue than free DXI. The opposite effect was observed for the sclera, thus confirming that NSs were appropriate for the treatment of corneal inflammation. Cytotoxicity studies show that NSs do not significantly reduce cell viability with respect to the free drug. Both presented high survival percentages. HET-CAM assay results correlate with Draize test, both showing good ocular tolerance for the developed colloidal systems. *In vivo* assays with F(A) showed therapeutic effects on prevention and inflammation treatment.

Our study demonstrates the advantages of using DXI-loaded PLGA nanospheres coated with PEG for prophylaxis of eye inflammation and/or for the treatment of non-severe inflammatory processes. The results obtained from the pharmacokinetic studies confirm the capacity of the developed PLGA-PEG NSs to achieve a sustained release of DXI, therefore reducing its systemic absorption and associated side effects.

Acknowledgments

This work was supported by the Spanish Ministry of Science and Innovation (MAT 2014-59134-R project). MLG, ACC, ME, MAE and ESL belong to 2014SGR-1023 and AC and ME belong to 2014SGR 525. The first author, ESL, acknowledges the support of the Spanish Ministry for the PhD scholarship FPI-MICINN (BES-2012-056083). We also acknowledge FCT – Portuguese Foundation for Science and Technology, under the project UID/AGR/04033/2013. This work was also financed through project UID/QUI/50006/2013, receiv- ing financial support from FCT/MEC through national funds, and co-financed by FEDER, under the Partnership Agreement PT2020.

Appendix A. Supplementary data

Supplementary data associated with this article can be found, in the online version, at http://dx.doi.org/10.1016/j.colsurfb.2016.04.054.

References

[1] F.E. Silverstein, G. Faich, J.L. Goldstein, L.S. Simon, T. Pincus, A. Whelton, et al., Gastrointestinal toxicity with celecoxib vs nonsteroidal anti-inflammatory drugs for osteoarthritis and rheumatoid arthritis, Am. Med. Assoc. 284 (2000) 1247–1255.
[2] E.B. Souto, S. Doktorovova, E. Gonzalez-Mira, M.A. Egea, M.L. Garcia, Feasibility of lipid nanoparticles for ocular delivery of anti-inflammatory drugs, Curr. Eye Res. 35 (2010) 537–552, http://dx.doi.org/10.3109/02713681003760168.
[3] S.T. Kaehler, W. Phleps, E. Hesse, Dexibuprofen: pharmacology, therapeutic uses and safety, Inflammopharmacology 11 (2003) 371–383, http://dx.doi.org/10.1017/CBO9781107415324.004.
[4] R. Pignatello, C. Bucolo, P. Ferrara, A. Maltese, A. Puleo, G. Puglisi, Eudragit RS100® nanosuspensions for the ophthalmic controlled delivery of ibuprofen, Eur. J. Pharm. Sci. 16 (2002) 53–61, http://dx.doi.org/10.1016/S0928-0987(02)00057-X.
[5] E. Vega, F. Gamisans, M.L. García, A. Chauvet, F. Lacoulonche, M.A. Egea, PLGA nanospheres for the ocular delivery of flurbiprofen: drug release and interactions, J. Pharm. Sci. 97 (2008) 5306–5317, http://dx.doi.org/10.1002/jps.
[6] R.C. Nagarwal, S. Kant, P.N. Singh, P. Maiti, J.K. Pandit, Polymeric nanoparticulate system: a potential approach for ocular drug delivery, J. Control Release 136 (2009) 2–13, http://dx.doi.org/10.1016/j.jconrel.2008.12.018.

[1] A. Bonabello, M.R. Galmozzi, R. Canaparo, G.C. Isaia, L. Serpe, E. Muntoni, et al., Dexibuprofen (S(+)-isomer ibuprofen) reduces gastric damage and improves analgesic and antiinflammatory effects in rodents, Anesth. Pharmacol. 97 (2003) 402–408, http://dx.doi.org/10.1213/01.ANE.0000073349.04610.42.

[2] W. Phleps, Overview on clinical data of dexibuprofen, Clin. Rheumatol. 20 (2001) S15–21.

[3] O. Zamani, E. Böttcher, J.D. Rieger, J. Mitterhuber, R. Hawel, S. Stallinger, et al., Comparison of safety, efficacy and tolerability of dexibuprofen and ibuprofen in the treatment of osteoarthritis of the hip or knee, Wien. Klin. Wochenschr. 126 (2014) 368–375, http://dx.doi.org/10.1007/s00508-014-0544-2.

[4] S.A. Salem, N.M. Hwei, A. Bin Saim, C.C.K. Ho, I. Sagap, R. Singh, et al., Polylactic-co-glycolic acid mesh coated with fibrin or collagen and biological adhesive substance as a prefabricated, degradable, biocompatible, and functional scaffold for regeneration of the urinary bladder wall, J. Biomed. Mater. Res. — Part A 101 A (2013) 2237–2247, http://dx.doi.org/10.1002/jbm.a.34518.

[5] N. Graf, D.R. Bielenberg, N. Kolishetti, C. Muus, J. Banyard, O.C. Farokhzad, et al., avβ3 Integrin-targeted PLGA-PEG nanoparticles for enhanced anti-tumor efficacy of a Pt(IV) prodrug, ACS Nano 6 (2012) 4530–4539.

[6] J.M. Anderson, M.S. Shive, Biodegradation and biocompatibility of PLA and PLGA microspheres, Adv. Drug Deliv. Rev. 64 (2012) 72–82, http://dx.doi.org/10.1016/j.addr.2012.09.004.

[7] P.C. Griffiths, B. Cattoz, M.S. Ibrahim, J.C. Anuonye, Probing the interaction of nanoparticles with mucin for drug delivery applications using dynamic light scattering, Eur. J. Pharm. Biopharm. 97 (2015) 218–222, http://dx.doi.org/10.1016/j.ejpb.2015.05.004.

[8] S. Akhter, F. Ramazani, M.Z. Ahmad, F.J. Ahmad, Z. Rahman, A. Bhatnagar, et al., Ocular pharmacoscintigraphic and aqueous humoral drug availability of ganciclovir-loaded mucoadhesive nanoparticles in rabbits, Eur. J. Nanomed. 5 (2013) 159–167, http://dx.doi.org/10.1515/ejnm-2013-0012.

[9] N.M. Khalil, T.C.F. do Nascimento, D.M. Casa, L.F. Dalmolin, A.C. de Mattos, I. Hoss, et al., Pharmacokinetics of curcumin-loaded PLGA and PLGA-PEG blend nanoparticles after oral administration in rats, Colloids Surf. B Biointerfaces 101 (2013) 353–360, http://dx.doi.org/10.1016/j.colsurfb.2012.06.024.

[10] G. Abrego, H.L. Alvarado, M.A. Egea, E. Gonzalez-Mira, A.C. Calpena, M.L. Garcia, Design of nanosuspensions and freeze-dried PLGA nanoparticles as a novel approach for ophthalmic delivery of pranoprofen, J. Pharm. Sci. 103 (2014) 3153–3164, http://dx.doi.org/10.1002/jps.24101.

[11] J.F. Fangueiro, T. Andreani, M.A. Egea, M.L. Garcia, S.B. Souto, A.M. Silva, et al., Design of cationic lipid nanoparticles for ocular delivery: development, characterization and cytotoxicity, Int. J. Pharm. 461 (2014) 64–73, http://dx.doi.org/10.1016/j.ijpharm.2013.11.025.

[12] D. Cun, D.K. Jensen, M.J. Maltesen, M. Bunker, P. Whiteside, D. Scurr, et al., High loading efficiency and sustained release of siRNA encapsulated in PLGA nanoparticles: quality by design optimization and characterization, Eur. J. Pharm. Biopharm. 77 (2011) 26–35, http://dx.doi.org/10.1016/j.ejpb.2010.11.008.

[13] E. Gonzalez-Mira, S. Nikolic, A.C. Calpena, M.A. Egea, E.B. Souto, M.L. García, Improved and safe transcorneal delivery of flurbiprofen by NLC and NLC-based hydrogels, J. Pharm. Sci. 101 (2012) 707–725, http://dx.doi.org/10.1002/jps.

[14] M. Ganesan, K.S. Rauthan, Y. Pandey, P. Tripathi, Determination of ibuprofen in human plasma with minimal sample, Int. J. Pharm. Sci. Res. 1 (2010) 120–127.

[15] J.-X. Wang, X. Sun, Z.-R. Zhang, Enhanced brain targeting by synthesis of 3′,5′-dioctanoyl-5-fluoro-2′-deoxyuridine and incorporation into solid lipid nanoparticles, Eur. J. Pharm. Biopharm. 54 (2002) 285–290, http://dx.doi.org/10.1016/S0939-6411(02)00083-8.

[16] M. Teixeira, M.J. Alonso, M.M.M. Pinto, C.M. Barbosa, Development and characterization of PLGA nanospheres and nanocapsules containing xanthone and 3-methoxyxanthone, Eur. J. Pharm. Biopharm. 59 (2005) 491–500, http://dx.doi.org/10.1016/j.ejpb.2004.09.002.

[17] G. Abrego, H. Alvarado, E.B. Souto, B. Guevara, L. Halbaut, A. Parra, et al., Biopharmaceutical profile of pranoprofen-loaded PLGA nanoparticles containing hydrogels for ocular administration, Eur. J. Pharm. Biopharm. 231 (2015) 1–10, http://dx.doi.org/10.1016/j.ejpb.2015.01.026.

[18] S. Doktorovová, D.L. Santos, I. Costa, T. Andreani, E.B. Souto, A.M. Silva, Cationic solid lipid nanoparticles interfere with the activity of antioxidant enzymes in hepatocellular carcinoma cells, Int. J. Pharm. 471 (2014) 18–27, http://dx.doi.org/10.1016/j.ijpharm.2014.05.011.

[19] M. Warren, K. Atkinson, S. Steer, INVITTOX: The ERGATT/FRAME data bank of in vitro techniques in toxicology, Toxicol. Vitro 4 (1990) 707–710, http://dx.doi.org/10.1016/0887-2333(90)90148-M.

[20] D. Jírová, K. Kejlová, S. Janoušek, H. Bendová, M. Malý, H. Kolářová, et al., Eye irritation hazard of chemicals and formulations assessed by methods in vitro, Neuroendocrinol. Lett. 35 (2014) 133–140.

[21] E. Vega, M.A. Egea, A.C. Calpena, M. Espina, M.L. García, Role of hydroxypropyl-β −cyclodextrin on freeze-dried and gamma-irradiated PLGA and PLGA-PEG diblock copolymer nanospheres for ophthalmic flurbiprofen delivery, Int. J. Nanomed. 7 (2012) 1357–1371.

[22] C. Bucolo, F. Drago, S. Salomone, Ocular drug delivery: a clue from nanotechnology, Front. Pharmacol. 3 (2012) 1–3, http://dx.doi.org/10.3389/fphar.2012.00188.

[23] G. Ma, C. Zhang, L. Zhang, H. Sun, C. Song, C. Wang, et al., Doxorubicin-loaded micelles based on multiarm star-shaped PLGA–PEG block copolymers: influence of arm numbers on drug delivery, J. Mater. Sci. Mater. Med. 27 (2016) 1–15, http://dx.doi.org/10.1007/s10856-015-5610-4.

[24] T. Musumeci, C. Bucolo, C. Carbone, R. Pignatello, F. Drago, G. Puglisi, Polymeric nanoparticles augment the ocular hypotensive effect of melatonin in rabbits, Int. J. Pharm. 440 (2013) 135–140, http://dx.doi.org/10.1016/j.ijpharm.2012.10.014.

[25] E. Vega, M.A. Egea, M.L. Garduño-Ramírez, M.L. Garcia, E. Sánchez, M. Espina, et al., Flurbiprofen PLGA-PEG nanospheres: role of hydroxy-þ-cyclodextrin on ex vivo human skin permeation and in vivo topical anti-inflammatory efficacy, Colloids Surf. B Biointerfaces 110 (2013) 339–346, http://dx.doi.org/10.1016/j.colsurfb.2013.04.045.

[26] B.M. El-Houssieny, E.Z. El-Dein, H.M. El-Messiry, Enhancement of solubility of dexibuprofen applying mixed hydrotropic solubilization technique, Drug Discov. Ther. 8 (2014) 178–184, http://dx.doi.org/10.5582/ddt.2014.01019.

[27] R. Singh, P. Kesharwani, N.K. Mehra, S. Singh, S. Banerjee, N.K. Jain, Development and characterization of folate anchored Saquinavir entrapped PLGA nanoparticles for anti-tumor activity, Drug Dev. Ind. Pharm. 41 (2015) 1888–1901, http://dx.doi.org/10.3109/03639045.2015.1019355.

[28] F. Alexis, Factors affecting the degradation and drug-release mechanism of poly(lactic acid) and poly[(lactic acid)-co-(glycolic acid)], Polym. Int. 54 (2005) 36–46, http://dx.doi.org/10.1002/pi.1697.

[29] M. Miyajima, A. Koshika, J. Okada, M. Ikeda, Mechanism of drug release from poly(l-lactic acid) matrix containing acidic or neutral drugs, J. Control Release 60 (1999) 199–209, http://dx.doi.org/10.1016/S0168-3659(99)00083-8.

[30] S. Muralidharan, S.N. Meyyanathan, K. Krishnaraj, S. Rajan, Development of oral sustained release dosage form for low melting chiral compound Dexibuprofen and it's in vitro-in vivo evaluation, Int. J. Drug Deliv. 3 (2011) 492–502.

[31] P. Costa, J.M. Sousa Lobo, Modeling and comparison of dissolution profiles, Eur. J. Pharm. Sci. 13 (2001) 123–133, http://dx.doi.org/10.1016/S0928-0987(01)00095-1.

[32] N.M. Davies, Clinical pharmacokinetics of ibuprofen the first 30 years, Drug Diisposition 34 (1998) 101–154.

[33] A.M.D. Nóbrega, E.N. Alves, R.D.F. Presgrave, R.N. Costa, I.F. Delgado, Determination of eye irritation potential of low-irritant products: comparison of in vitro results with the in vivo draize rabbit test, Braz. Arch. Biol. Technol. 55 (2012) 381–388 http://www.scielo.br/scielo.php?pid=S1516-89132012000300008&script=sci_arttext.

[34] J. Araújo, E. Vega, C. Lopes, M.A. Egea, M.L. Garcia, E.B. Souto, Effect of polymer viscosity on physicochemical properties and ocular tolerance of FB-loaded PLGA nanospheres, Colloids Surf. B. Biointerfaces 72 (2009) 48–56, http://dx.doi.org/10.1016/j.colsurfb.2009.03.028.

[35] B. McKenzie, G. Kay, K.H. Matthews, R.M. Knott, D. Cairns, The hen's egg chorioallantoic membrane (HET-CAM) test to predict the ophthalmic irritation potential of a cysteamine-containing gel: quantification using Photoshop® and ImageJ, Int. J. Pharm. 490 (2015) 1–8, http://dx.doi.org/10.1016/j.ijpharm.2015.05.023.

[36] T. Andreani, L. Miziara, E.N. Lorenzón, A.L.R. De Souza, C.P. Kiill, J.F. Fangueiro, et al., Effect of mucoadhesive polymers on the in vitro performance of insulin-loaded silica nanoparticles: interactions with mucin and biomembrane models, Eur. J. Pharm. Biopharm. 93 (2015) 118–126, http://dx.doi.org/10.1016/j.ejpb.2015.03.027.

[37] A. Vasconcelos, E. Vega, Y. Pérez, M.J. Gómara, M.L. García, I. Haro, Conjugation of cell-penetrating peptides with poly(lactic-co-glycolic acid)-polyethylene glycol nanoparticles improves ocular drug delivery, Int. J. Nanomed. 10 (2015) 609–631, http://dx.doi.org/10.2147/IJN.S71198.

[38] C. Bucolo, A. Maltese, G. Puglisi, R. Pignatello, Enhanced ocular anti-inflammatory activity of ibuprofen carried by an Eudragit RS100 nanoparticle suspension, Opthalmic Res. 34 (2002) 319–323, http://dx.doi.org/10.1159/000065608.

[39] A. Ludwig, The use of mucoadhesive polymers in ocular drug delivery, Adv. Drug Deliv. Rev. 57 (2005) 1595–1639, http://dx.doi.org/10.1016/j.addr.2005.07.005.

C. Giannavola, C. Bucolo, A. Maltese, D. Paolino, M.A. Vandelli, G. Puglisi, et al., Influence of preparation conditions on acyclovir-loaded poly-d,l-lactic acid nanospheres and effect of PEG coating on ocular drug bioavailability, Pharm. Res. 20 (2003) 584–590, http://dx.doi.org/10.1023/A:1023290514575.

4. DISCUSSION

4. DISCUSSION

The aim of the current study was to design biodegradable polymeric nanoparticles and explore their possibilities as nanocarriers of pharmaceutical compounds for different applications such as inflammation and neurodegeneration. In this sense, formulations of MEM-PLGA-PEG and PLGA-PEG-DXI NPs were developed. The formulations were optimized and assessed for its efficacy against ocular inflammation, glaucoma and Alzheimer's disease.

4.1 DESIGN AND CHARACTERISATION OF POLYMERIC NANOPARTICLES

The NPs were prepared by two different methods according to the chemical characteristics of each of the encapsulated drugs. The solvent-displacement method is a well-known proedure in order to entrap hydrophobic compounds such as DXI. On the other hand, due to the hydrophilic character of Memantine Hydrochloride, the solvent-displacement method is not suitable and, for this reason, NPs were prepared by using the double emulsion method (118).

MEM is a highly hydrophilic compound, which makes this drug more difficult to encapsulate into biodegradable NPs (119), (120). A second drawback of this compound is that it does not absorb on the UV or visible wavelength and is neither fluorescent (121). For this reason, a mass-spectrometry method coupled with HPLC was used in order to quantify the amount of drug loaded into NPs based on the ionization of the amine group. MEM-PLGA-PEG NPs were prepared using the double emulsion method, typically used for proteins or gene material, and ethyl acetate was chosen as the organic solvent due to

its increased safety rather than the widely used methylene chloride (122). In addition, as previously reported by Cohen-Sela et al. (118), smaller NPs are obtained when a water-miscible solvent is used. As previously reported by other authors, several conditions of the NPs prepared by double emulsion should be optimized (123). Therefore, MEM-PLGA-PEG NPs were optimized through several steps by using the design of experiments (DoE) approach. Firstly, sonication parameters were studied, namely wave amplitude sonication time, and afterwards the concentrations of each compound were optimized. Finally, the suitable pH of the two different aqueous phases, namely inner water phase (w_1) and external water phase (w_2) were optimized in order to maximize the encapsulation efficiency of the hydrophilic drug due to the fact that this is one of the main drawbacks of hydrophilic compound encapsulation. Two formulations were obtained and assessed for Alzheimer's disease and glaucoma, respectively. In agreement with other authors, the surfactant used was polyvinyl alcohol (PVA) and it was eliminated afterwards by ultracentrifugation methods (124).

On the other hand, PEG-PLGA-DXI NPs were obtained by applying the solvent-displacement method described by Fessi et al. (125). The organic solvent used was acetone due to its relative safety compared with other solvent and it was evaporated under reduced pressure. DoE was used to optimize each of the formulation compounds (PLGA-PEG, DXI and PVA) as well as the pH of the water phase. A slightly acid pH similar to the drug pK_a was the one providing higher encapsulation efficacy, probably due to the fact that DXI was not protonated and this fact facilitates it's entrapment avoiding it's fast release from the NPs matrix. Due to the low water solubility of DXI a dilution prior to filtration-centrifugation in order to avoid insoluble DXI was carried out and the drug content on the supernatant was measured by HPLC in order to evaluate the encapsulation

efficiency (EE). Two colloidal formulations were obtained, for DXI delivery as eye-drops for corneal inflammation and for oral administration for AD.

For ocular drug delivery on the anterior segment, a smaller amount of drug was used because their direct application as eye-drops on the anterior eye segment guarantees a higher DXI amount on the target site than the formulations design to arrive to the retina. However, since PEGylated DXI delivery systems were designed for oral drug delivery and it is described that they undergone under a certain first hepatic loss, an increased amount of drug was entrapped on the formulation. On the other hand, for MEM entrapment, both formulations of MEM PLGA-PEG were designed to cross several barriers, either for oral administration and posterior brain delivery or for retinal administration in order to cross the BRB.

All the developed nanoparticles were observed by dynamic light scattering as fast and easy routine technique (126). In this sense, all the formulations show an average diameter of 200 nm and a PI < 0.1, characteristic of the monodisperse systems. As previously reported by other authors encapsulating NSAIDs into polymeric NPs, mean average size ranged between 150 and 200 nm is confirmed to be suitable for ocular drug delivery and high drug entrapment values are achieved (104). However, several publications with NPs size around 400 nm have been proved to successfully deliver drugs to the ocular tissues without causing corneal irritation (111). Some controversy is still around the ideal NPs size to cross the BBB since some authors reported efficient delivery NPs mean size of less than 200 nm (127) with a negative surface charge (128) while others have successfully deliver nanosystems with an average size of 350 nm (129). NPs surface charge charge was negative due to the acid character of the polymer, which was the main compound in all the cases. This negative charge increased after centrifuging the NPs due

to the surfactant elimination. PEG chains increase NPs hydrophilicity and stability and also avoid the rapid elimination of these systems (128). In addition, centrifuged NPs were observed under transmission electron microscopy (TEM) under negative staining confirming the mean diameter smaller than 200 nm of the DLS measurements and a round and smooth surface of the systems (112). In all the cases, due to the fact that DLS measures the hydrodynamic diameter of the NPs, the images obtained with TEM confirmed a slightly smaller diameter than the DLS. Thermal characterisation was carried out observing the glass transition temperature (T_g) of the centrifuged NPs compared with the polymer and the physical mixture of the compounds using differential scanning calorimetry technique. No peak corresponding to drug decomposition was observed, thus meaning that the drug was entrapped on the polymeric matrix. The thermal profile of the NPs was observed and compared with the polymer profile. In the case of MEM loaded PLGA-PEG NPs, the encapsulated drug increased the T_g of the polymer due to its highly hydrophilic character and high decomposition temperature (316.05 ^{o}C) whereas in the case of DXI the opposite phenomena was observed due to its hydrophobic nature and lower T_g temperature (55.5 ^{o}C) (130), (131).

X-Ray diffraction (XRD) pattern of the developed formulations confirmed that the main compound on the NPs was the polymer and small bands corresponding to the entrapped drug were observed since this technique provides information about the while structure of the NPs. No peaks of the surfactant were present, thus meaning that the PVA was almost completely eliminated from the formulation. FTIR was also carried out in order to observe the bands corresponding to the polymer and the encapsulated drug.

Stability of the developed NPs at different temperatures (4ºC, 25ºC and 38ºC) was also monitored. Samples stored at 38ºC were completely transparent and unstable by the end

of the first month because of the degradation of the polymer induced by higher temperatures. However, the formulations stored at 4 and 25 ºC showed a good short-term stability. Interestingly, in the case of MEM-PLGA-PEG NPs, the mean size, PI and ZP remain unchanged for the first six months but a slight decrease of the backscattering profile was observed at the end of the last month for samples stored at room temperature thus meaning that, for these systems, the preferential storage temperature would be 4 ºC. These results, compared with the three months stability of DXI-PLGA-PEG NPs could be due to the fact that the preparation method influences their stability favouring the double emulsion an increased stability. However, in all the cases, the possibility of freeze-drying and sterilization by γ-radiation reported by other authors such as Ramos et al. (104)was explored and the NPs were successfully freeze dried (data not shown).

4.2 BIOPHARMACEUTICAL BEHAVIOUR

In vitro drug release was carried out for all the optimized formulations showing a sustained release preceded by a burst release also reported by other authors as a drug fraction which is absorbed on the NPs size and not entrapped on the polymeric matrix (122). This initial fast kinetics was probably due to the fact that a small amount of drug was retained between PEG surface chains. Afterwards, a sustained release of the drug from the NPs was obtained. Different kinetic models were used to fit the experimental data obtained from drug release experiments (104). In this case, the best fit an hyperbola equation demonstrating an slow release of the drug from the polymeric matrix. Regarding DXI, the solvent displacement method achieve high entrapment inside the polymeric matrix. In contrast, MEM NPs, due to the difficulty of hydrophilic compounds encapsulation, it was found that the majority of the compound was entrapped on the

surface or first layers of the nanosphere and only a small amount of drug was internalized. Despite this fact, the amount of drug encapsulated was higher than the concentration achieved by other authors with the same drug (132), (133).

In order to study NPs for ocular applications, permeation parameters of the NPs across corneal and the scleral tissues were assessed and compared with the corresponding free drug. The encapsulated drug show a certain degree of corneal tropism, previously reported by other authors, being this fact beneficial for corneal drug delivery (112). Also a slower release trough the sclera was also observed and here we hypothesised that when administered in a proper dose, this can be beneficial for retinal drug delivery since it was highly probable that the nanoparticles were able to cross the BRB due to PEG chains.

4.3 CELL CULTURE EXPERIMENTS AND OCULAR TOLERANCE

In the recent years, toxicity of drug delivery compounds has gained increased attention, especially in concern to neurotoxicity issues (134). Cytotoxicity assessments were carried out with the widely used Alamar blue technique, based on the reduction potential of metabolically active cells after their contact with different compounds that might be toxic (135), (136). In order to perform the experiment, different cell lines according to each application of the NPs were employed. In this sense, to ensure safety across ocular drug delivery, keratinocytes and retinoblastoma cells lines were used. In the case of DXI neither the free drug nor the DXI-PLGA-PEG NPs were cytotoxic obtaining cell viability values higher than 80% in all the assessed concentrations. MEM free showed to be toxic and MEM-PLGA-PEG NPs provide an increased safety due to the slow drug release protecting the cells with the polymeric matrix. NPs for brain delivery were also assessed

in astrocytes, bEnd.3 (brain endothelial cells) and PC12 cell lines in order to ensure it's safety. Using the first two cell lines, their transport across the BBB, also similar to the BRB, was assessed in order to ensure their suitability to arrive to the target site. Both DXI and MEM PLGA-PEG nanosystems confirmed to overcome the BBB *in vitro* probably due to the PEG chains which increases their transport across this barrier. In this way, it has been reported that small hydrophilic drugs can enter to the brain trough paracellular pathway and, in the case of NPs, with their small size, they can enhance cell uptake by adsortive mediated transcytosis (129).

In order to assess the potential irritation of the developed formulations, an *in vitro* test (HET-CAM) was carried out. Neither DXI nor DXI NPs were irritant whereas MEM free demonstrated to be slightly irritant, but this effect was not present in MEM-PLGA-PEG formulations. After the *in vitro* experiments, the *in vivo* Draize irritation test was carried out and the eyes were examined immediately, after 30 minutes and after 1 hour of the administration of the eye-drops. The results were similar to those obtained on the *in vitro* test meaning that only MEM free showed slightly-irritant potential. Due to this fact, DXI free was compared with DXI-PLGA-PEG NPs in order to assess the inflammatory efficacy but free MEM was not assessed for glaucoma experiments and just MEM-PLGA-PEG eye drops were applied in order to demonstrate their effectivity.

4.4 *IN VIVO* MODELS TO ASSESS THE EFFECTIVITY OF PLGA-PEG NANOPARTICLES FOR NEURODEGENERATIVE AND OCULAR DISEASES

Brain disorders affect about a quarter of the population worldwide being more than 600 disorders characterized by CNS dysfunctions. Among all, neurodegenerative diseases and, specially AD, is one of the most common (137). For these reason, both DXI and MEM drug delivery systems were assessed using transgenic mice (APPswe/PS1De9, APP/PS1) which secrete an elevated amount of the human Aβ peptide. The groups were compared with their non-transgenic littermates (C57Bl6). Behavioral tests such as morris water maze (MWM) and novel object recognition (NORT) demonstrate that both systems were able to effectively deliver the drug and also that inflammation and excitotoxicity were implicated on AD. Immunohistochemical assays of Aβ-plaque development showed a decrease of these plaques using both drug delivery systems although the MEM NPs were more evident. Interestingly, MEM NPs also decrease brain inflammation although DXI NPs decreased the inflammatory process more effectively.

In order to asses MEM-PLGA-PEG NPs for glaucoma purposes, the Morrison's ocular hypertension model in Dark Agouti rats was assessed by administering two eye-drops of MEM-NP daily for three weeks (138). This treatment induces an increase on the IOP which peak its observed 1 day after surgery. The IOP profile was comparable between MEM-NP and OHT control groups thus suggesting that MEM-NP administered as eye-drops did not affect IOP decreasing, which is currently the only symptom treated in glaucoma patients. In addition, surviving RGCs were visualised histologically in retinal flat mounts and quantification of RGC populations was completed using a previously published automated script in order to avoid biased results (139). Global RGC density

was significantly diminished in the untreated OHT group versus naïve controls ($p < 0.001$) thus confirming the model suitability. Although not affecting the IOP, the treatment with MEM-NP was found to significantly protect against OHT induced RGC injury in this model ($p<0.001$), suggesting that it was neuroprotective in a non-IOP-dependent manner. As such, several authors have previously used Brn3a as a marker to quantify RGC density in several rodent and mammalian glaucoma models (140), (141). Twice-daily topical administration of MEM-NPs for three weeks was found to significantly protect RGC from injury in this model in an IOP independent manner, suggestive of a neuroprotective effect.

RGC loss in the rodent model of ocular hypertension is reported to occur via a combination of primary and secondary degenerative processes (139). Where, primary degeneration of RGC occurs as a result of injury and secondary degeneration describes the loss of RGC as a consequence of the primary insult, for example as a result of oxidative stress, inflammation or excitotoxicity (142). Glutamate excitotoxicity has previously been reported to play a role in RGC loss in the OHT model (143). An attractive explanation for the neuroprotective effect of topically administered MEM-PLGA-PEG NPs in the OHT model could therefore be due to the well documented NMDA receptor antagonism of this agent (26). Therefore, the designed NPs were able to arrive and deliver the drug effectively on the retina showing benefits for glaucoma confirming the recent studies that define glaucoma as a neurodegenerative disease.

Since glaucoma has been also associated to a certain degree of inflammation (144), in further studies it would be worth to design drug delivery systems encapsulating both DXI, MEM and using mannitol as a crioprotectant in order to decrease inflammation, the excitotoxicity and also address the IOP within the same formulation.

Anti-inflammatory efficacy of DXI-PLGA-PEG NPs administered as eye-drops on to the rabbit eye was assessed in order to test the NPs for prevention and treatment of the inflammatory disorders. Eye-drops have been reported to be a comfortable route for the patients rather than other routes such as intravitreal injections. The developed formulation was compared with DXI and IBU free drug and IBU-PLGA-PEG NPs developed for comparative purposes. DXI-PLGA-PEG NPs demonstrated to be a suitable strategy useful to prevent corneal inflammation, which can be used after surgery or any invasive ocular procedure. For fast inflammation treatment, due to the rapid drug effect needed, although the NPs demonstrated to be useful, the systems had not proven additional benefits against the free drug. By contrast, other author such as Vega et al. (110), developed NSAIDs PLGA NPs for ocular inflammation increasing the mucoadhesivity avoiding the rapid drug corneal loss suffered by the free drug. Despite this fact, here we suggest the use of this systems for the prevention of inflammation secondary to cataract surgery or other procedures associated with inflammation (110). If DXI NPs were used as a prevention, adverse side effects of NSAIDs such as gastric inflammation would be reduced due to the combination of the active enantiomer and the slow drug release from the polymeric matrix. In addition, patients compliance would increase as well as drug effectivity due to the maintenance between the therapeutic limits on the target site.

5. CONCLUSIONS

5. CONCLUSIONS

In this work, polymeric nanoparticles for sustained delivery of Dexibuprofen and Memantine, were designed for the treatment of ocular and neurodegenerative diseases.

5.1 Memantine nanoparticles prepared by the double emulsion method and optimized by DoE, confirmed to be suitable for ocular drug delivery as eye-drops (193.1 nm) and for brain delivery (152.6 nm) being admistered as eye-drops and oral solution, respectively.

5.2 Optimized Dexibuprofen nanoparticles were made by solvent-displacement technique with an average size suitable for their administration as eye-drops (221.4 nm) for corneal inflammation and as oral solution (195 nm) being able to overcome the blood brain barrier.

5.3 Polymeric nanoparticles were characterised by spectroscopic (FTIR, X-Ray) and thermal (DSC) methods confirming that the drug was encapsulated in the polymeric matrix and the surfactant was eliminated by the centrifugation process.

5.4 Both formulations demonstrated a sustained release, against the free drug, adjusted to a hyperbola equation with an initial burst effect followed by a slow drug release.

5.5 The optimized nanoparticles demonstrated to be non-cytotoxic neither in ocular (retinoblastoma cell line) nor in brain cells (PC12, astrocytes and Bend3).

5.6 Dexibuprofen and Memantine nanoparticles were assessed for Alzheimer's disease in an in vivo model (APP/PS1 mice). Memantine nanoparticles demonstrated to treat efficiently AD whereas Dexibuprofen nanoparticles were suitable for disease prevention. Both formulations decreased the number of plaques and the inflammation associated.

5.7 Memantine nanoparticles were assessed in a rat model of glaucoma. They did not show any effect on the intraocular pressure (IOP) but they significantly decreased the apoptotic processes of the retinal ganglion cells of the retina after administering the nanoparticles for 3 weeks.

5.8 Dexibuprofen nanoparticles assesed *in vivo* for ocular inflammation are suitable to prevent ocular inflammation.

Therefore, in this work, efficient nanoparticles encapsulating Memantine and Dexibuprofen were designed for ocular and bran delivery in order to treat ocular inflammation, glaucoma and Alzheimer's disease.

6. REFERENCES

6. REFERENCES

1. Baldacci F, Lista S, Garaci F, Bonuccelli U, Toschi N, Hampel H. Biomarker-guided classification scheme of neurodegenerative diseases. J Sport Heal Sci. 2016;5(4):383–7.

2. Fiest KM, Roberts JI, Maxwell CJ, Hogan DB, Smith EE, Frolkis A, et al. The prevalence and incidence of dementia: a systematic review and meta-analysis. Can J Neurol Sci. 2016;43:S51–82.

3. Folch J, Petrov D, Ettcheto M, Abad S, Sánchez-López E, García ML, et al. Current research therapeutic strategies for Alzheimer' s disease treatment. Neural Plast. 2016;2016:1–15.

4. Cordeiro MF, Levin LA. Clinical evidence for neuroprotection in glaucoma. Am J Ophthalmol. 2011;152(5):715–6.

5. London A, Benhar I, Schwartz M. The retina as a window to the brain - from eye research to CNS disorders. Nat Rev Neurol. 2013;9(1):44–53.

6. Townsend KP, Praticò D. Novel therapeutic opportunities for Alzheimer's disease: focus on nonsteroidal anti-inflammatory drugs. FASEB J. 2005;19(12):1592–601.

7. Nieuwenhuys R, Donkelaar HJ Ten, Nicholson C. The central nervous system of vertebrates. 2014. 2-13 p.

8. Mc Carthy DJ, Malhotra M, O'Mahony AM, Cryan JF, O'Driscoll CM. Nanoparticles and the blood-brain barrier: advancing from in-vitro models towards therapeutic significance. Pharm Res. 2015;32(4):1161–85.

9. Pardridge WM. Blood-brain barrier delivery. Drug Discov Today. 2007;12(2):54–61.

10. Reichel A. Addressing central nervous system (CNS) penetration in drug discovery: Basics and implications of the evolving new concept. Chem Biodivers. 2009;6(11):2030–49.

11. Alfonso E, González Beatriz G. Barrera hematoencefálica. Neurobiología, implicaciones clínicas y efectos del estrés sobre su desarrollo. Rev Mex Neurocienc. 2008;9(5)(5):395–405.

12. Pathan SA, Iqbal Z, Zaidi SMA, Talegaonkar S, Vohra D, Jain GK, et al. CNS drug delivery systems: novel approaches. Recent Pat Drug Deliv Formul. 2009;3(1):71–89.

13. Grabrucker AM, Ruozi B, Belletti D, Pederzoli F, Forni F, Vandelli MA, et al. Nanoparticle transport across the blood brain barrier. Tissue Barriers. 2016;4(1):e1153568.

14. Veszelka S, Bocsik A, Walter FR, Hantosi D, Deli MA. Blood-brain barrier co-culture models to study nanoparticle penetration: Focus on co-culture systems. Acta Biol Szeged. 2015;59:157–68.

15. Van Rooy I, Cakir-Tascioglu S, Hennink WE, Storm G, Schiffelers RM, Mastrobattista E. In vivo methods to study uptake of nanoparticles into the brain. Pharm Res. 2011;28(3):456–71.

16. Maurer K, Volk S, Gerbaldo H. Auguste D and Alzheimer ’s disease. Lancet. 1997;349:1906–9.

17. Singh M, Kaur M, Kukreja H, Chugh R, Silakari O, Singh D. Acetylcholinesterase inhibitors as Alzheimer therapy: From nerve toxins to neuroprotection. Eur J Med Chem. 2013;70:165–88.

18. Haass C, Kaether C, Thinakaran G, Sisodia S. Trafficking and proteolytic processing of APP. Cold Spring Harb Perspect Med. 2012;2(5):1–25.

19. Anand P, Singh B. A review on cholinesterase inhibitors for Alzheimer’s disease. Arch Pharm Res. 2013;36(4):375–99.

20. Wen MM, El-Salamouni NS, El-Refaie WM, Hazzah HA, Ali MM, Tosi G, et al. Nanotechnology-based drug delivery systems for Alzheimer's disease management: technical, industrial, and clinical challenges. J Control Release. 2017;245:95–107.

21. Reisberg B, Doody R, Stoffler A, Schmitt F, Ferris S, Mobius HJ. Memantine in moderate-to-severe Alzheimer's disease. N Engl J Med. 2003;348(14):1333–41.

22. van Marum R. Update on the use of memantine in Alzheimer's disease. Neuropsychiatr Dis Treat. 2009;5:237–47.

23. Wilkinson D. A review of the effects of memantine on clinical progression in Alzheimer's disease. Int J Geriatr Psychiatry. 2012;27(8):769–76.

24. Wu TY, Chen CP. Dual action of Memantine in Alzheimer Disease: a hypothesis. Taiwan J Obstet Gynecol. 2009;48(3):273–7.

25. Danysz W, Parsons CG, Mobius HJ, Stoffler A, Quack G. Neuroprotective and symptomatological action of memantine relevant for Alzheimer's disease - A unified glutamatergic hypothesis on the mechanism of action. Neurotox Res. 2000;2:85–97.

26. Johnson JW, Kotermanski SE. Mechanism of action of memantine. Curr Opin Pharmacol. 2006;6:61–7.

27. Parsons CG, Stöffler A, Danysz W. Memantine: a NMDA receptor antagonist that improves memory by restoration of homeostasis in the glutamatergic system - too little activation is bad, too much is even worse. Neuropharmacology. 2007;53:699–723.

28. Jin D-Q, Sung J-Y, Hwang YK, Kwon KJ, Han S-H, Min SS, et al. Dexibuprofen (S(+)-isomer ibuprofen) reduces microglial activation and impairments of spatial working memory induced by chronic lipopolysaccharide infusion. Pharmacol Biochem Behav. 2008;89(3):404–11.

29. Tabet N, Feldmand H. Ibuprofen for Alzheimer's disease. Cochrane Database Syst. 2003;2:1465–858.

30. Kaehler ST, Phleps W, Hesse E. Dexibuprofen: pharmacology, therapeutic uses and safety. Inflammopharmacology. 2003;11(4):371–83.

31. Bonabello A, Galmozzi MR, Canaparo R, Isaia GC, Serpe L, Muntoni E, et al. Dexibuprofen (S(+)-Isomer Ibuprofen) reduces gastric damage and improves analgesic and antiinflammatory effects in rodents. Anesth Pharmacol. 2003;97(2):402–8.

32. Phleps W. Overview on clinical data of dexibuprofen. Clin Rheumatol. 2001;20(1):S15-21.

33. El-Houssieny BM, El-Dein EZ, El-Messiry HM. Enhancement of solubility of dexibuprofen applying mixed hydrotropic solubilization technique. Drug Discov Ther. 2014;8(4):178–84.

34. Kim YC, Chiang B, Wu X, Prausnitz MR. Ocular delivery of macromolecules. J Control Release. 2014;190:172–81.

35. Forrester J V, Dick AD, McMenamin PG, Roberts F, Pearlman E. The eye. Basic sciences in practice. Elsevier Health Sciences. 2015. 1-103 p.

36. Perez VL, Saeed AM, Tan Y, Urbieta M, Cruz-Guilloty F. The eye: A window to the soul of the immune system. J Autoimmun. 2013;45:7–14.

37. R. Kanwar J, Zhou S-F. Toll like receptors play a role in general immunity, eye infection and inflammation: TLRs for nanodelivery. J Clin Cell Immunol. 2011;2(4):1–10.

38. Kronfeld PK. The eye. Vegetative physiology and biochemistry. University College of London. 1962. 1-62 p.

39. Cholkar K, Dassari SR, Pal D, Mitra A. Eye: anatomy, phisiology and barrier to drug delivery. In: Ocular Transporters and Receptors: Their Role in Drug Delivery. 2012. p. 2–28.

40. Sánchez-López E, Espina M, Doktorovova S, Souto EB, García ML. Lipid nanoparticles (SLN, NLC): Overcoming the anatomical and physiological barriers of the eye – Part I – Barriers and determining factors in ocular delivery. Eur J Pharm Biopharm. 2017;110:58–69.

41. Celiker H, Yuksel N, Solakoglu S, Karabas L, Aktar F, Caglar Y. Neuroprotective effects of memantine in the retina of glaucomatous rats: An electron microscopic study. J Ophthalmic Vis Res. 2016;11(2):174.

42. Benhar I, London A, Schwartz M. The privileged immunity of immune privileged organs: the case of the eye. Front Immunol. 2012;3:1–6.

43. Davis BM, Crawley L, Pahlitzsch M, Javaid F, Cordeiro MF. Glaucoma: the retina and beyond. Acta Neuropathol. 2016;132(6):807–26.

44. Almasieh M, Wilson AM, Morquette B, Cueva Vargas JL, Di Polo A. The molecular basis of retinal ganglion cell death in glaucoma. Prog Retin Eye Res. 2012;31(2):152–81.

45. Salt T, Cordeiro M. Glutamate excitotoxicity in glaucoma: throwing the baby out with the bathwater? Eye. 2006;20(6):730–2.

46. Krupin T, Liebmann JM, Greenfield DS, Ritch R, Gardiner S. A randomized trial of brimonidine versus timolol in preserving visual function: results from the Low-Pressure Glaucoma Treatment Study. Am J Ophthalmol. 2011;151(4):671–81.

47. Tian K, Shibata- S, Pahlitzsch M, Cordeiro MF, Shibata-Germanos S, Pahlitzsch M, et al. Current perspective of neuroprotection and glaucoma. Clin Ophthalmol. 2015;9:2109–18.

48. Chidlow G, Wood JPM, Casson RJ. Pharmacological neuroprotection for glaucoma. Drugs. 2007;67(5):725–59.

49. Sena DF, Lindsley K. Neuroprotection for treatment of glaucoma in adults. Cochrane database Syst Rev. 2013;(2):1–30.

50. Osborne NN. Recent clinical findings with memantine should not mean that the idea of neuroprotection in glaucoma is abandoned. Acta Ophthalmol. 2009;87(4):450–4.

51. Mcnally S, Brien CJO. Models for eye disorders Drug discovery in glaucoma and the role of animal models. Drug Discov Today Dis Model. 2013;10(4):e207–14.

52. Chen VH, Lipton SA. The chemical biology of clinically tolerated NMDA receptor antagonists. J Neurochem. 2006;97:1611–26.

53. Gabelt BT, Rasmussen CA, Tektas OY, Kim CBY, Peterson JC, Michael Nork T, et al. Structure/function studies and the effects of memantine in monkeys with experimental glaucoma. Investig Ophthalmol Vis Sci. 2012;53(4):2368–76.

54. Hare WA, WoldeMussie E, Weinreb RN, Ton H, Ruiz G, Wijono M, et al. Efficacy and safety of memantine treatment for reduction of changes associated with experimental glaucoma in monkey, II: Structural measures. Investig Ophthalmol Vis Sci. 2004;45(8):2640–51.

55. Hare W, WoldeMussie E, Lai R, Ton H, Ruiz G, Feldmann B, et al. Efficacy and safety of Memantine, an NMDA-type open-channel blocker, for reduction of retinal injury associated with experimental glaucoma in rat and monkey. Surv Ophthalmol. 2001;45:S284–9.

56. Yücel YH, Gupta N, Zhang Q, Mizisin AP, Kalichman MW, Weinreb RN. Memantine protects neurons from shrinkage in the lateral geniculate nucleus in experimental glaucoma. Arch Ophthalmol. 2006;124(2):217–25.

57. Hare WA, WoldeMussie E, Lai RK, Ton H, Ruiz G, Chun T, et al. Efficacy and Safety of Memantine Treatment for Reduction of Changes Associated with Experimental Glaucoma in Monkey, I: Functional Measures. Investig Opthalmology Vis Sci. 2004;45(8):2625.

58. Casson RJ. Possible role of excitotoxicity in the pathogenesis of glaucoma. Clin Exp Ophthalmol. 2006;34(1):54–63.

59. Ahuja M, Dhake AS, Sharma SK, Majumdar DK. Topical ocular delivery of NSAIDs. AAPS J. 2008;10(2):229–41.

60. Silverstein FE, Faich G, Goldstein JL, Simon LS, Pincus T, Whelton A, et al. Gastrointestinal toxicity with celecoxib vs nonsteroidal anti-inflammatory drugs for osteoarthritis and rheumatoid arthritis. Am Med Assoc. 2000;284(10):1247–55.

61. Souto EB, Doktorovova S, Gonzalez-Mira E, Egea MA, Garcia ML. Feasibility of lipid nanoparticles for ocular delivery of anti-inflammatory drugs. Curr Eye Res. 2010;35(7):537–52.

62. Vega E, Gamisans F, García ML, Chauvet A, Lacoulonche F, Egea MA. PLGA nanospheres for the ocular delivery of flurbiprofen: drug release and interactions. 2008;97(12):5306–17.

63. Nagarwal RC, Kant S, Singh PN, Maiti P, Pandit JK. Polymeric nanoparticulate system: a potential approach for ocular drug delivery. J Control Release. 2009;136(1):2–13.

64. Zamani O, Böttcher E, Rieger JD, Mitterhuber J, Hawel R, Stallinger S, et al. Comparison of safety, efficacy and tolerability of dexibuprofen and ibuprofen in the treatment of osteoarthritis of the hip or knee. Wien Klin Wochenschr. 2014;126(11–12):368–75.

65. London A, Benhar I, Schwartz M. The retina as a window to the brain-from eye research to CNS disorders. Nat Rev Neurol. 2013;9(1):44–53.

66. Hart NJ, Koronyo Y, Black KL, Koronyo-Hamaoui M. Ocular indicators of Alzheimer's: exploring disease in the retina. Acta Neuropathol. 2016;132(6):767–87.

67. Gupta VK, Chitranshi N, Gupta VB, Golzan M, Dheer Y, Wall R Vander, et al. Amyloid β accumulation and inner retinal degenerative changes in Alzheimer's disease transgenic mouse. Neurosci Lett. 2016;623:52–6.

68. Chiu K, Chan TF, Wu A, Leung IYP, So KF, Chang RCC. Neurodegeneration of the retina in mouse models of Alzheimer's disease: What can we learn from the retina? Age (Omaha). 2012;34(3):633–49.

69. Suffredini G, East JE, Levy LM. New applications of nanotechnology for neuroimaging. Am J Neuroradiol. 2014;35(7):1246–53.

70. Salem SA, Hwei NM, Saim A Bin, Ho CCK, Sagap I, Singh R, et al. Polylactic-co-glycolic acid mesh coated with fibrin or collagen and biological adhesive substance as a prefabricated, degradable, biocompatible, and functional scaffold for regeneration of the urinary bladder wall. J Biomed Mater Res - A. 2013;101 A(8):2237–47.

71. Graf N, Bielenberg DR, Kolishetti N, Muus C, Banyard J, Farokhzad OC, et al. αvβ3 Integrin-targeted PLGA-PEG nanoparticles for enhanced anti-tumor efficacy of a Pt(IV) prodrug. ACS Nano. 2012;6(5):4530–9.

72. Anderson JM, Shive MS. Biodegradation and biocompatibility of PLA and PLGA microspheres. Adv Drug Deliv Rev. 2012;64:72–82.

73. Liu L, Guo K, Lu J, Venkatraman SS, Luo D, Chye K, et al. Biologically active core/shell nanoparticles self-assembled from cholesterol-terminated PEG-TAT for drug delivery across the blood-brain barrier. Biomaterials. 2008;29:1509–17.

74. Vega E, Egea MA, Garduño-Ramírez ML, Garcia ML, Sánchez E, Espina M, et al. Flurbiprofen PLGA-PEG nanospheres: role of hydroxy-β-cyclodextrin on ex vivo human skin permeation and in vivo topical anti-inflammatory efficacy. Colloids Surfaces B Biointerfaces. 2013;110:339–46.

75. Griffiths PC, Cattoz B, Ibrahim MS, Anuonye JC. Probing the interaction of nanoparticles with mucin for drug delivery applications using dynamic light scattering. Eur J Pharm Biopharm. 2015;97:218–22.

76. Akhter S, Ramazani F, Ahmad MZ, Ahmad FJ, Rahman Z, Bhatnagar A, et al. Ocular pharmacoscintigraphic and aqueous humoral drug availability of ganciclovir-loaded mucoadhesive nanoparticles in rabbits. Eur J Nanomedicine. 2013;5(3):159–67.

77. Khalil NM, Nascimento TCF, Casa DM, Dalmolin LF, Mattos AC de, Hoss I, et al. Pharmacokinetics of curcumin-loaded PLGA and PLGA-PEG blend nanoparticles after oral administration in rats. Colloids Surfaces B Biointerfaces. 2013;101:353–60.

78. Al-Halafi AM. Nanocarriers of nanotechnology in retinal diseases. Saudi J Ophthalmol Off J Saudi Ophthalmol Soc. 2014;28(4):304–9.

79. Novack GD. Ophthalmic drug delivery: development and regulatory considerations. Clin Pharmacol Ther. 2009 May;85(5):539–43.

80. Kim NJ, Harris A, Gerber A, Tobe LA, Amireskandari A, Huck A, et al. Nanotechnology and glaucoma: a review of the potential implications of glaucoma nanomedicine. Br J Ophthalmol. 2014;98(4):427–31.

81. Pinto Reis C, Neufeld RJ, Ribeiro AJ, Veiga F. Nanoencapsulation I. Methods for preparation of drug-loaded polymeric nanoparticles. Nanomedicine Nanotechnology, Biol Med. 2006;2(1):8–21.

82. Ahlin Grabnar P, Kristl J. The manufacturing techniques of drug-loaded polymeric nanoparticles from preformed polymers. J Microencapsul. 2011;28(4):323–35.

83. Kuo Y-C, Rajesh R. A critical overview of therapeutic strategy and advancement for Alzheimer's disease treatment. J Taiwan Inst Chem Eng. 2017;77:92–105.

84. De Rosa G, Salzano G, Caraglia M, Abbruzzese A. Nanotechnologies: A Strategy to Overcome Blood-Brain Barrier. Curr Drug Metab. 2012;13(1):61–9.

85. Kreuter J. Drug delivery to the central nervous system by polymeric nanoparticles: what do we know? Adv Drug Deliv Rev. 2014;71:2–14.

86. Luppi B, Bigucci F, Corace G, Delucca A, Cerchiara T, Sorrenti M, et al. Albumin nanoparticles carrying cyclodextrins for nasal delivery of the anti-Alzheimer drug tacrine. Eur J Pharm Sci. 2011;44(4):559–65.

87. Wilson B, Samanta MK, Santhi K, Kumar KPS, Ramasamy M, Suresh B. Chitosan nanoparticles as a new delivery system for the anti-Alzheimer drug tacrine. Nanomedicine. 2010;6(1):144–52.

88. Baysal I, Ucar G, Gultekinoglu M, Ulubayram K, Yabanoglu-Ciftci S. Donepezil loaded PLGA-b-PEG nanoparticles: their ability to induce destabilization of amyloid fibrils and to cross blood brain barrier in vitro. J Neural Transm. 2017;124:33–45.

89. Shadab B, Mushir A, Sanjula B, Jasjeet KS, Bhatnagar A, Javed A. Preparation, characterization, in vivo biodistribution and pharmacokinetic studies of donepezil-loaded PLGA nanoparticles for brain targeting. Drug Dev Ind Pharm. 2014;40:278–87.

90. Ali M, Ali R, Bhatnagar A, Baboota S, Ali J. Donepezil nanosuspension intended for nose to brain targeting: In vitro and in vivo safety evaluation. Int J Biol Macromol. 2014;67:418–25.

91. Joshi SA, Chavhan SS, Sawant KK. Rivastigmine-loaded PLGA and PBCA nanoparticles: Preparation, optimization, characterization, in vitro and pharmacodynamic studies. Eur J Pharm Biopharm. 2010;76:189–99.

92. Fazil M, Sadab M, Haque S, Kumar M, Baboota S, Sahni J kaur. Development and evaluation of rivastigmine loaded chitosan nanoparticles for brain targeting. Eur J Pharm Sci. 2012;47:6–15.

93. Khemariya RP, Khemariya PS. New-fangled approach in the management of Alzheimer by formulation of polysorbate 80 coated chitosan nanoparticles of rivastigmine for brain delivery and their in vivo evaluation. Int J Curr Res Med Sci. 2016;2:18–29.

94. Fornaguera C, Feiner-Garcia N, Calderó G, García-Celma MJ, Solans C. Galantamine-loaded PLGA nanoparticles, from nano-emulsion templating, as novel advanced drug delivery systems to treat neurodegenerative diseases. R Soc Chem. 2015;7:12076–84.

95. Hanafy AS, Farid RM, ElGamal SS. Complexation as an approach to entrap cationic drugs into cationic nanoparticles administered intranasally for Alzheimer's disease management: preparation and detection in rat brain. Drug Dev Ind Pharm. 2015;41:2055–68.

96. Kurakhmaeva KB, Djindjikhashvili IA, Petrov VE, Balabanyan VU, Voronina TA, Trofimov SS, et al. Brain targeting of nerve growth factor using poly(butyl cyanoacrylate) nanoparticles. J Drug Target. 2009;17:564–74.

97. Liu Z, Gao X, Kang T, Jiang M, Miao D, Gu G, et al. B6 peptide-modified PEG-PLA nanoparticles for enhanced brain delivery of neuroprotective peptide. Bioconjug Chem. 2013;24:997–1007.

98. Wang ZH, Wang ZY, Sun CS, Wang CY, Jiang TY, Wang SL. Trimethylated chitosan-conjugated PLGA nanoparticles for the delivery of drugs to the brain. Biomaterials. 2010;31:908–15.

99. Mathew A, Aravind A, Brahatheeswaran D, Fukuda T, Nagaoka Y, Hasumura T, et al. Amyloid-binding aptamer conjugated curcumin-PLGA nanoparticle for potential use in Alzheimer's disease. BioNanoSci. 2012;2:83–93.

100. Muntimadugu E, Dhommati R, Jain A, Gopala V, Challa S, Khan W. Intranasal delivery of nanoparticle encapsulated tarenflurbil: a potential brain targeting strategy for Alzheimer's disease. Eur J Pharm Sci. 2016;92:224–34.

101. Sun D, Li N, Zhang W, Zhao Z, Mou Z, Huang D, et al. Design of PLGA-functionalized quercetin nanoparticles for potential use in Alzheimer's disease. Colloids Surfaces B Biointerfaces [Internet]. 2016;148:116–29. Available from: http://dx.doi.org/10.1016/j.colsurfb.2016.08.052

102. Vandervoort J, Ludwig A. Preparation and evaluation of drug-loaded gelatin nanoparticles for topical ophthalmic use. Eurpean J Pharm Biopharm. 2004;57:251–61.

103. Ramos GR, Calpena AC, Egea MA, Espina M, García ML. Freeze drying optimization of polymeric nanoparticles for ocular flurbiprofen delivery: effect of protectant agents and critical process parameters on long-term stability. Drug Dev Ind Pharm. 2017;43(4):637–51.

104. Ramos GR, Coca AP, Calpena AC. Influence of freeze-drying and γ -irradiation in preclinical studies of flurbiprofen polymeric nanoparticles for ocular delivery using d-(+)-trehalose and polyethylene glycol. Int J Nanomedicine. 2016;11:4093–106.

105. Adibkia K, Omidi Y, Siahi MR, Javadzadeh AR, Barzegar-jalali M, Barar J, et al. Inhibition of Endotoxin-Induced Uveitis by Methylprednisolone Acetate Nanosuspension in Rabbits. J Pharmacol Ther. 2007;23(5):421–32.

106. Li VHK, Wood RW, Kreuter J, Harmia T, Robinson JR, Li VHK, et al. Ocular drug delivery of progesterone using nanoparticles. J Microencapsul. 1986;3(3):213–8.

107. Papadimitriou S, Bikiaris D, Avgoustakis K. Chitosan nanoparticles loaded with dorzolamide and pramipexole. Carbohydr Polym. 2008;73:44–54.

108. Motwani SK, Chopra S, Talegaonkar S, Kohli K, Ahmad FJ, Khar RK. Chitosan – sodium alginate nanoparticles as submicroscopic reservoirs for ocular delivery : Formulation, optimisation and in vitro characterisation. Eur J Pharm Biopharm. 2008;68:513–25.

109. Pignatello R, Ricupero N, Bucolo C, Maugeri F, Maltese A, Puglisi G, et al. Preparation and characterization of Eudragit retard nanosuspensions for the ocular delivery of cloricromene. AAPS PharmSciTech. 2006;7(1):1–7.

110. Vasconcelos A, Vega E, Pérez Y, Gómara MJ, García ML, Haro I. Conjugation of cell-penetrating peptides with poly(lactic-co-glycolic acid)-polyethylene glycol nanoparticles improves ocular drug delivery. Int J Nanomedicine. 2015;10:609–31.

111. Abrego G, Alvarado HL, Egea MA, Gonzalez-Mira E, Calpena AC, Garcia ML. Design of nanosuspensions and freeze-dried PLGA nanoparticles as a novel approach for ophthalmic delivery of pranoprofen. J Pharm Sci. 2014;103(10):3153–64.

112. Parra A, Mallandrich M, Clares B, Egea MA, Espina M, García ML, et al. Design and elaboration of freeze-dried PLGA nanoparticles for the transcorneal permeation of carprofen: Ocular anti-inflammatory applications. Colloids Surf B Biointerfaces. 2015;136:935–43.

113. Alvarado HL, Abrego G, Garduño-Ramirez ML, Clares B, Calpena AC, García ML. Design and optimization of oleanolic/ursolic acid-loaded nanoplatforms for ocular anti-inflammatory applications. Nanomedicine Nanotechnology, Biol Med. 2015;11(3):521–30.

114. Musumeci T, Bucolo C, Carbone C, Pignatello R, Drago F, Puglisi G. Polymeric nanoparticles augment the ocular hypotensive effect of melatonin in rabbits. Int J Pharm. 2013;440(2):135–40.

115. Lamprecht A, Ubrich N, Hombreiro Pérez M, Lehr C-M, Hoffman M, Maincent P. Influences of process parameters on nanoparticle preparation performed by a double emulsion pressure homogenization technique. Int J Pharm [Internet]. 2000 Mar [cited 2015 Oct 5];196(2):177–82. Available from: 8517399004226

116. Sonkusare SK, Kaul CL, Ramarao P. Dementia of Alzheimer's disease and other neurodegenerative disorders--memantine, a new hope. Pharmacol Res. 2005 Jan;51(1):1–17.

117. Hesselink MB, De Boer BG, Breimer DD, Danysz W. Brain penetration and in vivo recovery of NMDA receptor antagonists amantadine and memantine: a quantittative microdialysis study. Pharm Res. 1999;16(5):637–42.

118. Cohen-Sela E, Chorny M, Koroukhov N, Danenberg HD, Golomb G. A new double emulsion solvent diffusion technique for encapsulating hydrophilic molecules in PLGA nanoparticles. J Control release. 2009;133(2):90–5.

119. Bilati U, Allémann E, Doelker E. Poly(D,L-lactide-co-glycolide) protein-loaded nanoparticles prepared by the double emulsion method--processing and formulation issues for enhanced entrapment efficiency. J Microencapsul. 2005;22(2):205–14.

120. Giri TK, Choudhary C, Alexander A, Badwaik H, Tripathi DK. Prospects of pharmaceuticals and biopharmaceuticals loaded microparticles prepared by double emulsion technique for controlled delivery. Saudi Pharm J. 2013;21(2):125–41.

121. Almeida AA, Campos DR, Bernasconi G, Calafatti S, Barros FAP, Eberlin MN, et al. Determination of memantine in human plasma by liquid chromatography-electrospray tandem mass spectrometry: application to a bioequivalence study. J Chromatogr B. 2007;848(2):311–6.

122. Meng FT, Ma GH, Qiu W, Su ZG. W/O/W double emulsion technique using ethyl acetate as organic solvent: Effects of its diffusion rate on the characteristics of microparticles. J Control Release. 2003;91(3):407–16.

123. Zambaux M. Influence of experimental parameters on the characteristics of poly(lactic acid) nanoparticles prepared by a double emulsion method. J Control Release. 1998;50(1–3):31–40.

124. Bilati U, Allémann E, Doelker E. Sonication parameters for the preparation of biodegradable nanocapsules of controlled size by the double emulsion method. Pharm Dev Technol. 2003;8(1):1–9.

125. Fessi H, Puisieux F, Devissaguet JP, Ammoury N, Benita S. Nanocapsule formation by interfacial polymer deposition following solvent displacement. Int J Pharm. 1989;55:R1–4.

126. Abrego G, Alvarado H, Souto EB, Guevara B, Halbaut L, Parra A, et al. Biopharmaceutical profile of pranoprofen-loaded PLGA nanoparticles containing hydrogels for ocular administration. Eur J Pharm Biopharm. 2015;231:1–10.

127. Wilson B, Samanta MK, Santhi K, Kumar KPS, Paramakrishnan N, Suresh B. Poly(n-butylcyanoacrylate) nanoparticles coated with polysorbate 80 for the targeted delivery of rivastigmine into the brain to treat Alzheimer's disease. Brain Res. 2008;1200:159–68.

128. Zhang C, Wan X, Zheng X, Shao X, Liu Q, Zhang Q, et al. Dual-functional nanoparticles targeting amyloid plaques in the brains of Alzheimer's disease mice. Biomaterials. 2014;35(1):456–65.

129. Kirby BP, Pabari R, Chen CN, Al Baharna M, Walsh J, Ramtoola Z. Comparative evaluation of the degree of pegylation of poly(lactic-co- glycolic acid) nanoparticles in enhancing central nervous system delivery of loperamide. J Pharm Pharmacol. 2013;65(10):1473–81.

130. Achim M, Vlase L, Tomută I, Muntean D, Iuga C, Georgescu R, et al. Preformulation studies for parenteral solution of memantine. Farmcia. 2011;59(5):636–46.

131. Manjanna KM, Rajesg KS, Pramos Kumar TM. Formulation and evaluation of Dexibuprofen matrix tablets for oral controlled drug delivery. World J Pharm Res. 2015;4(4):591–613.

132. Prieto E, Puente B, Uixera A, Perez S, Pablo L, Irache JM, et al. Gantrez AN nanoparticles for ocular delivery of Memantine: in vitro release evaluation in albino rabbits. Opthalmic Res. 2012;48:109–17.

133. Laserra S, Basit A, Sozio P, Marinelli L, Fornasari E, Cacciatore I, et al. Solid lipid nanoparticles loaded with lipoyl–memantine codrug: preparation and characterization. Int J Pharm. 2015;485:183–91.

134. Gao H. Progress and perspectives on targeting nanoparticles for brain drug delivery. Acta Pharm Sin B. 2016;6(4):268–86.

135. Gliga AR, Skoglund S, Wallinder IO, Fadeel B, Karlsson HL. Size-dependent cytotoxicity of silver nanoparticles in human lung cells: the role of cellular uptake, agglomeration and Ag release. Part Fibre Toxicol. 2014;11(1):11.

136. Kim CS, Mout R, Zhao Y, Yeh YC, Tang R, Jeong Y, et al. Co-Delivery of protein and small molecule therapeutics using nanoparticle-stabilized nanocapsules. Bioconjug Chem. 2015;26(5):950–4.

137. Barbu E, Molnàr É, Tsibouklis J, Górecki DC. The potential for nanoparticle-based drug delivery to the brain: overcoming the blood–brain barrier. Expert Opin Drug Deliv. 2009;6(6):553–65.

138. Cordeiro MF, Guo L, Luong V, Harding G, Wang W, Jones HE, et al. Real-time imaging of single nerve cell apoptosis in retinal neurodegeneration. PNAS. 2004;101(36):13352–6.

139. Davis B, Guo L, Brenton J, Langley L, Normando E, Cordeiro M. Automatic quantitative analysis of experimental primary and secondary retinal neurodegeneration: implications for optic neuropathies. Cell Death Discov. 2016;2(16031):1–11.

140. Galindo-Romero C, Harun-Or-Rashid M, Jiménez-López M, Vidal-Sanz M, Agudo-Barriuso M, Hallböök F. Neuroprotection by α2-adrenergic receptor stimulation after excitotoxic retinal injury: a study of the total population of retinal ganglion cells and their distribution in the chicken retina. PLoS One. 2016;11(9):1–21.

141. Pérez MJ, Santano C, Guzmán-Aránguez A, Valiente-Soriano FJ, Avilés-Trigueros M, Vidal-Sanz M, et al. Assessment of inner retina dysfunction and progressive ganglion cell loss in a mouse model of glaucoma. Exp Eye Res. 2014;122:40–9.

142. Li H-Y, Ruan Y-W, Ren C-R, Cui Q, So K-F. Mechanisms of secondary degeneration after partial optic nerve transection. Neural Regen Res. 2014;9(6):565–74.

143. Guo L, Salt TE, Maass A, Luong V, Moss SE, Fitzke FW, et al. Assessment of neuroprotective effects of glutamate modulation on glaucoma-related retinal ganglion cell apoptosis invivo. Invest Ophthalmol Vis Sci. 2006;47(2):626–33.

144. Zhou X, Li F, Kong L, Tomita H, Li C, Cao W. Involvement of inflammation, degradation, and apoptosis in a mouse model of glaucoma. J Biol Chem. 2005;280(35):31240–8.